Concepts in Coalmine Ventilation and Development of the VamTurBurner© for Extraction of Thermal Energy from Underground Ventilation Air Methane

Submitted by

Daniel L. Cluff P.Phys, P.Eng., C.Eng.
B.A., Hon. B.Sc., M.Sc., M.Eng.

To
The University of Exeter,
College of Engineering, Mathematics and Physical Sciences,
Camborne School of Mines

As a dissertation for the degree of
Doctor of Philosophy in Mining and Minerals Engineering
In May 2014

I certify that all material in this dissertation, which is not my own work, has been identified and that no material has previously been submitted and approved for the award of a degree by this or any other University.

Signature: 

Abstract

Climate change is emerging as a significant challenge in terms of the response needed to mitigate or adapt to the predicted global changes. Severe impacts due to rising sea-level, seasonal shifts, increased frequency and intensity of extreme weather events such as storms, floods or droughts have become accepted by the scientific community as a real and present threat to civilisation. The most significant impacts are expected in the Arctic, the Asian mega-deltas, Small Island Developing States (SIDS) and sub-Saharan Africa (IPCC 2007). There are two approaches to global climate change either mitigation or adaptation.

This dissertation aims to provide the initial design concepts for a system to mitigate methane, a significant Greenhouse Gas (GHG), emitted from coalmines by ventilation air circulated through the underground workings. The VamTurBurner©, a Ventilation Air Methane (VAM) gas turbine based methane burning system, is proposed as a method of extracting the thermal energy from the VAM. A key aspect of the problem responsible for the difficulty in extracting the energy from VAM is the low concentration of methane in the high volume ventilation airflow. This approach recasts the concepts of combustion dynamics of a premixed fuel flow to that expected for VAM to ascertain the conditions conducive to combustion or oxidation of the methane in the ventilation air. A numerical model using Large Eddy Simulation (LES) to study the combustion dynamics revealed that the temperature of the incoming ventilation air is a key variable related to the concentration of the VAM. Computational Fluid Dynamics modeling was used to study the design features needed to engineer a system capable of providing the required temperature of the incoming ventilation air.

Applications for the available thermal energy are discussed in terms of the potential to generate electricity with steam turbines, provide space heating, produce hot water for many uses, and use the heat for industrial drying or as desired. The efficiency of the energy system is enhanced when the output from the amount of natural gas or electricity purchased is compared to the output enhanced by the addition of methane, considered as free. The VamTurBurner© concept, as described in this dissertation, appears to be a viable method of mitigating atmospheric methane in the pursuit greenhouse gas reduction.

Acknowledgements

I would like thank the following for their assistance, participation and patience:

The University of Exeter, College of Engineering, Mathematics and Physical Sciences, Camborne School of Mines for the financial support scholarship provided for the period of study without which I would not have been able to proceed.

Dr. Gareth A. Kennedy and Dr. Patrick J. Foster, my first and second supervisors respectively for their assistance with initiating the project, bringing the project to a conclusion and their wisdom as the work proceeded.

My son Adric and daughter Kathern for their assistance proofreading the manuscript and wife Myrna for her support and patience through the times I was obsessed with another simulation.

Finally the academic and support staff at The Camborne School of Mines for their assistance and for making my stay at CSM enjoyable and productive.

Dedication

This work is dedicated to the memory of my Grandfather, Albert Godin, a miner by trade and a kind and gentle man.

Sincerely,

Daniel L. Cluff

Table of Contents

List of Figures

List of Tables

List of nomenclature variables and constants

CH_4	Methane
$CO\ or\ CO_2$	Carbon monoxide or carbon dioxide
aN_2	Nitrogen times “a” the fractional amount of nitrogen in air
ν'_F	Fractional amount of fuel
$\nu'_k\ \nu''_k$	Fractional amount of a species as either a mass or a molar fraction
F	Fuel
ν'_o	Fractional amount of oxygen
P	Combustion products
H or H_2	Hydrogen or hydrogen gas
$O\ or\ O_2$	Oxygen or Oxygen gas
W_i	Atomic weight of species i
S	Stoichiometric ratio
Y_k	Mass fraction of species k
m_i	Mass of species i
ϕ	Equivalence ratio
ρ_k	Density of species k
R	Rydberg’s constant
P_k	Pressure or partial pressure of species k
T	Temperature usually in Kelvin
T^0	Temperature at the enthalpy of formation either 0 K or 298.15 K
C_{pk}^m	Specific heat capacity at constant pressure for species k, or the molar C^m
h_k	Enthalpy of species k
$\Delta H_{f,k}^0$	Enthalpy of formation
Δh	Specific enthalpy or enthalpy/mass
M_k	Molar mass of species k
N_k	Number of moles of species k
W	Mean atomic weight of a mixture
N	Total number of molecules in a mixture
X_k	Molar fraction of species k in a mixture
$V_{k,i}$	Diffusion of species k through species i
$\dot{w}_k$	Reaction rate of species k
$-T_a$	Activation temperature
M_k	Generic symbol for species k

$\mathbb{V}$	Flow velocity of VAM
$\mathbb{Y}$	Reduced mass fraction
$\boldsymbol{\theta}$	Reduced temperature
$\boldsymbol{M}$	Mach number
$\mathbf{v}_s$	Velocity of sound
$\mathbf{v}_f$	Velocity of fluid flow
$\boldsymbol{\gamma}$	Gamma the ratio of specific heat capacities
$\dot{\boldsymbol{m}}$	Rate of change of mass per unit time
$\mathbf{A}^*$	The cross sectional area of the choked flow state when the flow is at Mach-One
$\boldsymbol{A_e}$	Turbine exit area
$\boldsymbol{V_e}$	Turbine exit velocity
$\boldsymbol{P_e}$	Turbine exit pressure
$\boldsymbol{T_{04}}$	Inlet temperature
RPM	Revolutions per minute

1. Introduction

Methane is a greenhouse gas with a global warming potential of about 21 times that of carbon dioxide over a one hundred year timeframe (IPCC, 1996). The impact of methane in the atmosphere is second only to carbon dioxide in terms of the global warming potential. The amount of methane released to the atmosphere from coalmining operations represents about 8% to 10% of the anthropogenic methane and of that, the ventilation air methane (VAM) is the main source representing about 70% of the total released by the mining operations. Since VAM represents about 7% of anthropogenic methane, it is a valid target for mitigation. This dissertation proposes the initial design parameters for a methane mitigation system called the VamTurBurner©. To put the effect of methane related to mining into a context, slightly more than half of current CH_4 emissions are anthropogenic (IPCC, 2001), mining accounts for 5% so VAM is approximately 4% of all emissions.

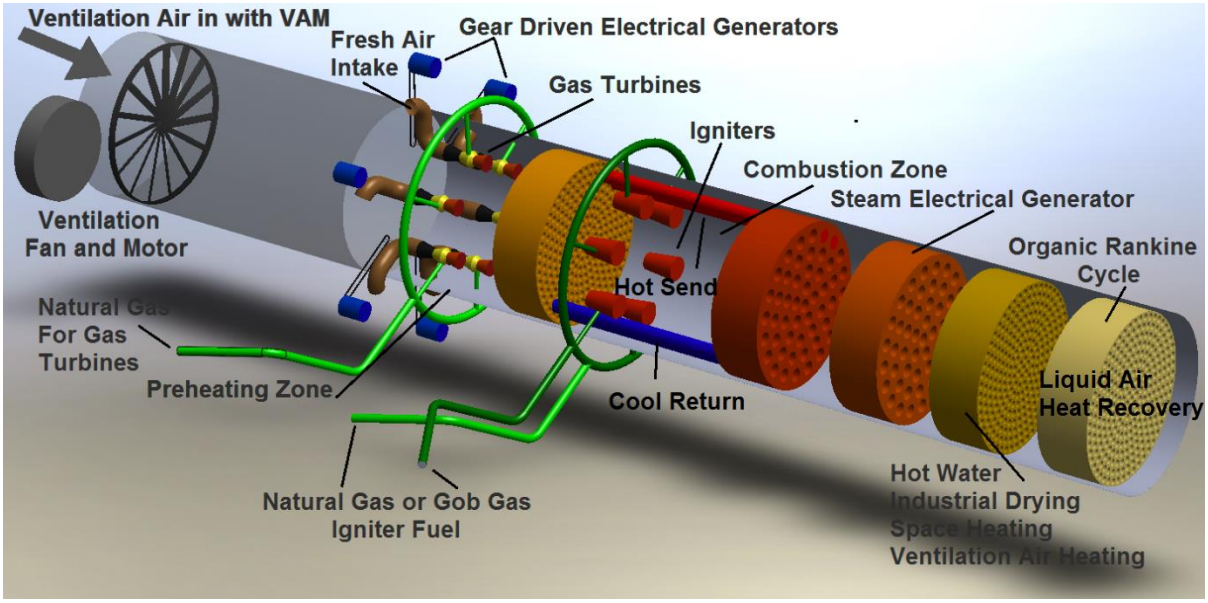

Figure 1.1.1 A conceptual design of the VamTurBurner©

The VamTurBurner© design evolved from an attempt to consider flowing mine ventilation air containing the varying amounts of methane and mine dust through a gas turbine as a supplementary fuel. It was realized at an early stage that the concept was flawed, which lead to the conceptualization of the VamTurBurner©. The computational fluid dynamics, modeling of thermal flow and combustion dynamics studies in this dissertation demonstrate the feasibility of the design.

1.1. Aims of this work

The aim of this work is to provide a proof of concept and the initial design parameters of a methane mitigation strategy capable of capturing the energy from methane that would otherwise be atmospherically released through the ventilation systems of coalmining operations. The amount of energy available depends on the concentration of methane in the ventilation air or the VAM, but is essentially a free energy source if it can be captured. The current state of the art offers two methods of VAM mitigation where the methane is either the primary fuel or a secondary fuel or supplement. The primary fuel option oxidises methane in flow reactors by bringing the airflow containing the methane in contact with a bed of media, ceramic beads or stone, at a high enough temperature to oxidize the methane. The secondary fuel option uses the airflow containing the methane as part or all of the intake air for a standard combustion based engine such as diesel. The drawback of the primary fuel method is that a significant fraction of the heat produced from the oxidation of the methane is used to maintain the heat in the media; thus, it is not available for use as a thermal product. The drawback of the secondary or supplemental fuel method is that gas turbines are too sensitive and the amount of air intake of diesel or internal combustion engines is typically quite small compared to the amount of ventilation air exhausting from the mine. The VamTurBurner© system is anticipated to be able to use all the ventilation flow and use all of the heat generated by the combustion of the methane without losses due to maintaining the media heat profile.

1.2. Structure and outline

The first section of Chapter 2 endeavours to present a discussion outlining the emerging methane situation in the Arctic and the global impact that the release of methane from the permafrost may have upon melting. Arguments are presented pertaining to the rate of decrease of the Arctic ice, the cost to the global economy and that the current atmospheric modeling suggests that the effect of the current and expected impact of atmospheric methane on global warming and climate change are comparable to that of carbon dioxide. Since coalmining accounts for about 10% of anthropogenic methane, the impact of mining is global and the issue of methane release in the Arctic brings the issue into clear focus. Data from satellite observations and extracts from the IPCC, NOAA, PIOMASS, US EPA and the British

Meteorological Office are used to make a strong case that it is urgent and necessary to consider atmospheric methane as a significant factor in the global climate change scenario and a valid target for more robust mitigation efforts.

The second section of Chapter 2 presents the case for the mitigation of VAM. Coal mining represents a significant component of the energy supply system on a global scale. It is argued that methane abatement programs from coalmines are significant enough, within the context of the larger scale of global emissions, to be considered as a significant part of a meaningful GHG reduction effort.

A review of existing VAM mitigation technologies is presented in Chapter 3 to further justify the need for a robust mitigation technology capable of extracting the energy available in the VAM. There are two basic methods to oxidize VAM, primary and secondary fuel usage. In primary fuel system applications such as Thermal Flow Reverse Reactors (TFRR), Catalytic Flow Reverse Reactors (CFRR), lean burn Gas Turbines, recuperative gas turbines or Regenerative Thermal Oxidation (RTO) the VAM is the main fuel source. When VAM is used as a secondary fuel, the VAM replaces a usual air source, at the expected flow rates, in a combustion process such as in gas turbines, internal combustion engines, rotary kilns or even a coal-fired power station. The VAM present in the airflow is burnt in the normal combustion process of the unit with the associated decrease in the required fuel inflow as a result of the ingress of fuel in the inlet air.

Primary systems of note are the VOCSIDIZER© systems, first demonstrated in 1994 at the Thoresby Mine in Nottinghamshire, United Kingdom, operated by MEGTEC and the VAMCAT™ developed by the Commonwealth Scientific and Industrial Research Organization (CSIRO) of Australia. The Appin Colliery and Tower Colliery where Caterpillar 3516LE generators are used to burn the VAM in the intake air best illustrate secondary systems.

The main difficulty with the systems using VAM as a primary fuel is that the heat available for use as an energy product is reduced because of the amount of energy needed simply to sustain the reaction. This is the case for systems such as the CANMET catalytic flow-reversal reactors (CFRR), EDL recuperative gas turbine, CSIRO lean burn catalytic turbine and CSIRO catalytic combustor. The main limitation of TFRR and CFRR systems is that it is difficult to extract useful energy for

power generation, so they are merely mitigating the greenhouse impact of the methane, by oxidizing to carbon dioxide, with the expectation that the economics will be supported by carbon credit trading. The CSIRO catalytic turbine powered with one percent methane is more of a prospective technology rather than one expected to both mitigate the methane and generate electricity. From this discussion, it becomes evident that if an economical mitigation technology is proposed it must be capable of using the energy available for the production of electricity, motive force, cooling or in general, a useable energy product made available to the company, industrial site or the community.

The combustion dynamics of a methane air mixture are considered in Chapter 4 and analytical analysis of the adiabatic flame temperature and flame speed for the methane concentrations expected in ventilation air are developed. The analysis is constructed with an understanding that the safety expected and required for the implementation of such a system is paramount. The recent Tragedy at the Pike River Coal Mine in 2012 is discussed to illustrate that point (Royal Commission on the Pike River Coal Mine Tragedy, 2012) The evidence contained in the report establishes the need for stringent regulations and the absolute adherence to regulations by proponents given the potential for catastrophic outcomes.

In Chapter 5, the combustion dynamics were studied using the procedure of Large Eddy Simulation (LES) to carry out the numerical modelling of the combustion dynamics of a VAM air mixture containing small percentages of methane as a function of the preheating conditioning and interaction with a flame igniter. LES solves for the large-scale turbulent structures, but at some point, selected to be computationally expedient, the system is modeled rather than solved explicitly. For the purposes of this numerical model the chemical kinetics are simulated by the four-step model, derived for the oxidation of methane by Jones and Lindstedt (1988). This is a well-known chemical scheme and it is considered to be sufficiently accurate, but allows for a significant reduction in computing time compared to that required if the entire spectrum of species and reactions were used and yields a good and sufficient result. In this model, the four reversible chemical reactions are comprised of seven species (CH_4, CO_2, O_2, CO, H_2O, H_2 and N_2). This LES numerical modelling advances the concepts developed in Chapter 4, especially in

terms of the level of complexity from the point of view that a four-step model is used rather than a global single step reaction model.

Having shown that the energetics of the proposed VamTurBurner© system are feasible a design is needed to demonstrate the operational principles. The VamTurBurner© system is similar in nature to a combined heat and power CHP system or a trigeneration system when cooling is added. In that respect, it becomes desirable to discuss the notion of distributed power generation. It is the opinion of this author that distributed energy generation coupled with a robust storage scheme is the way forward if the desired outcome is a robust power grid.

In Chapter 6 the design features of the VamTurBurner© are outlined such as the separate air intake system for the gas turbines protruding from the ventilation system ducting, which circumvents any mine ventilation air from entering the microturbine combustion system. The decision to keep the ventilation air from entering the microturbines ensures the expected operating conditions are adhered to so as not to hinder the expected reliability and availability specifications of the chosen microturbine. The efficiency of any system is defined as the (work out)/(energy in). The “work out” is regarded as the useful work directed toward the intended purpose while the “energy in” is any energy consumed toward producing that intended work. The energy input to the VamTurBurner© arises from three separate fuel sources, the heat from the microturbine exhaust, the fuel consumed by the igniters, and the VAM. Considering the input energy consists of only that purchased for purpose the additional VAM serves to increase the efficiency, that is, the energy contained in the VAM is free, which improves the overall efficiency of the system.

Considerable effort to develop a design tool, based on the operation of a gas turbine and computational flow dynamics of the internal workings of the system, is described throughout the remainder of the chapter. The interaction between the VamTurBurner© and the gas turbine is influenced by matching a compressor to a turbine. A MATLAB computer program was written to determine the gas turbine characteristics best suited to the design and has the capability to provide outputs including the compressor/turbine maps, fuel air ratios and mass flow rates for a given set of input parameters such as the Mach number, ambient conditions and conversion efficiencies.

The first iteration of design characteristics are summarized by assuming an 80% thermal conversion efficiency. A cluster of six 250 kW microturbines generates 1.5 MW_e at a 20% efficiency from an input of 0.207 kg/s of fuel at a caloric value of 38 MJ/kg. The power available from the VAM is 19.25 MW_{th}, with 6.29 MW_{th} available from the microturbines and 4.44 MW_{th} from the igniters, collectively the total power available for use by the heat exchanger systems is 29.98 MW_{th}; thus, for an 80% thermal conversion efficiency the output available is 23.98 MW_{th}. Since the purchased power only represents 35.7% of the total the coefficient of performance could be defined to be (Heat delivered)/(Purchased delivered) = 20.98/10.73 = 2.24.

A study of the computational fluid dynamics CFD of various proposed models, presented in Chapter 7, to assess the interaction of the hot exhaust air from the gas turbines with the incoming ventilation air in terms of the temperature increase and turbulent mixing. Further modeling was performed to determine the methodology and design best suited to preheating the mixture to a value near the result determined by the LES modeling in Chapter 5 of 500 K. CFD models including several heat exchanger configurations and recirculation scenarios were constructed and studied to determine the most efficient and least expensive method of preheating the incoming ventilation air. It was found that by recirculating a fraction of the hot air from the combustion zone to the preheating zone and mixing the two flows that sufficient heat is available to raise the temperature and allow an ongoing stream for conversion to electricity and other thermal products. The CFD modelling illustrates that the system is indeed a viable design option for the proposed mode of operation. Although a single gas turbine was selected for a cluster, there is no reason to insist that all the gas turbines are the same size; thus, a combination of various electrical outputs and independent CHP systems is possible. In the remaining chapters, the possibilities of using the energy to provide a spectrum of energy products such as electrical generation, space heating, water heating, industrial drying or ventilation air-cooling are considered.

Chapter 9 contains the conclusion and recommendations for future work.

1.3. Published works related to this dissertation.

There are two refereed journal papers, two refereed conference papers, one conference presentation and a master's dissertation based on the results of this

dissertation. The first paper was presented in person at the World Mining Congress at Montreal in August 2013 and subsequently was chosen as one of ten from the Congress to be published in the Journal of Applied Thermodynamics special edition on Energy in Mining.

Cluff D. L. Kennedy G. A and Bennett J. G., (2013). Capturing Energy from Ventilation Air Methane at Operating Coal Mines. In *23rd World Mining Congress 2013 Proceedings*. Montreal, Canada; ISBN 978-1-926872-15-5. 1 (Track 8 - Energy & Mines, Lowering Cost and Energy with Improved Mine Ventilation and Refrigeration), paper 582.

Collaboration with colleagues from The University of Lancaster allowed for the Large Eddy Simulation of the combustion dynamics using the software developed at Lancaster. The paper below has been published in the journal *Fuel.*

Mira-Martinez, D., Cluff D. L., Jiang X., (2014). Numerical Investigation of the Burning Characteristics of Ventilation Air Methane in a Combustion Based Mitigation System. *Fuel*. 133 (1), 182 - 193.

A third paper was written and presented, during the study period, at the American Society of Civil Engineers conference on Arctic Sustainability at Anchorage Alaska in June 2013, which indirectly relates to this work, but pertains to this authors passion for the Arctic. The paper is referenced in Chapter 2 as an example of a strategy to reduce Greenhouse Gas.

Cluff, D.L. and Kazakidis V.N., (2013). Opportunities and Constraints of Engineering Frozen Backfill for Underground Mining Applications in Permafrost. *In ISCORD 2013: Planning for Sustainable Cold Regions*. Anchorage, Alaska, June 2013. Proceedings of the 10th International Symposium on Cold Regions Development (Frozen ground and permafrost: American Soceity of Civil Engineers. 175 - 191.

This author presented this work at the Canadian Association of Physicists Congress, 15-20 June 2014. The presentation argued that methane is a significant greenhouse gas with potential to seriously affect the Arctic in a positive feedback loop, discussed the LES work and included results of computational flow dynamics modelling for the design of the VamTurBurner© Multigeneration system.

Cluff, D.L., Mira-Martinez, D., and Jiang X (2014). A numerical investigation using Large scale eddy simulation of the burning characteristics of ultralow methane concentration flows. *In Canadian Association of Physicists Congress June 16 - 20 2014*. Laurentian University, Sudbury, Ontario, June 18, 2013. Ottawa, Canada: Canadian Association of Physicists. 1 - 60.

This author was the principle supervisor for a master's dissertation project based on this work. In the project, Roderick Griffin worked on a prototype system at the CSM test mine and achieved a grade above 70%; a summary appears in the appendix.

2. Atmospherically dispersed methane

2.1. Implications of atmospherically dispersed methane

"It's not enough that we do our best; sometimes we have to do what's required"
Sir Winston Churchill (1874 – 1965)

Methane is a greenhouse gas (GHG) having a global warming potential (GWP) of about 21 times that of carbon dioxide over a one hundred year timeframe (IPCC, 1996). The significance of methane as a GHG is best understood by the fact that the radiative forcing factor is second only to carbon dioxide (Forster et al., 2007). Slightly more than half of current CH_4 emissions are anthropogenic (IPCC, 2001). These two attributes are of great concern when considering the impact of methane emissions on the near term global temperature and the impact of a potential methane feedback loop that might occur due to the release of methane sequestered in the permafrost if it abruptly melts.

According to the long-term modeling, of global temperature increase due to carbon dioxide forcing, the temperature increases are not globally uniform. The northern regions are more inclined to experience higher marginal increases in temperature than the southern hemisphere due to the moderating influence of the oceans in the south and the global redistribution of heat from the equator to the poles. An increase of temperature in the northern region has the potential to create a catastrophic methane feedback loop if the methane contained in the permafrost is abruptly released atmospherically when the permafrost melts (BBC, 2006). Table 2.1-1, shows permafrost records from as early as 1910 up to 2003, the various zones have all suffered an increase in temperature (Lemke et al, 2007).

The countries with the highest methane emissions are clearly those with the strongest potential for economic mitigation of methane. The top five producers account for over 75% of global production; these countries are in order of highest to fifth: China, the United States, India, Ukraine, Russia and Australia. These are obvious target countries for the development of methane abatement technology, but may need to develop the political will to intervene appropriately with a sensible approach to this situation.

Table 2.1-1 Recent trends in permafrost temperature (IPCC 2007)

Region	Depth (m)* approximate	Period of Record	Permafrost temperature change
United States			
Northern Alaska	*1	1910 to 1950	2 to 4
Northern Alaska	20	1983 to 2000	2 to 3
Interior of Alaska	20	1953 to 2000	0.5 to 1.5
Canada			
Alert, Nunavut	15	1995 to 2000	0.6
Northern Mackenzie Valley	20 to 30	1990 to 2002	0.3 to 0.6
Central Mackenzie Valley	10 to 20	1980's to 2003	0.5
Southern Mackenzie Valley & Southern Yukon Territory	*20	1980's to 2003	0
Northern Quebec	10	1980's to 1990's	<-1
Northern Quebec	10	1996 to 2001	1
Lake Hazen	2.5	1994 to 2000	1
Iqaluit, Eastern Canada Arctic	5	1993 to 2000	2
Russia			
East Siberia	1.6 to 0.2	1960 to 2002	-1.3
Northern West Siberia	10	1950 to 1990	0.3 to 0.7
European north of Russia continuous permafrost zone	0	1973 to 1992	1.6 to 2.6
Northern European Russia	0	1970 to 1995	1.2 to 2.6
Europe			
Juvvashoe, Southern Norway	*3	past 30 to 40 yrs	0.5 to 1.0
Jenssonhaaaugen, Svaltbad	*2	past 60 to 80 yrs	1 to 2
Murtel, Corvatch	11.5	1987 to 2001	1
China			
Tibetan Plateau	*10	1970's to 1990's	0.2 to 0.5
Qinghai-Xizang Highway	3 to 5	1995 to 2002	up to 0.5
Tianshan Mountains	16 to 20	1973 to 2002	0.2 to 0.4
Da Hinggan Mountains, Northern China	*2	1973 to 1991	0.7 to 1.5

An excerpt from the EPA presentation to the Arctic Council Task Force (Gunning, 2008).

1. *The science on methane is clear - it is a critical part of the climate solution, offering tremendous opportunities for rapid mitigation to avoid near term impacts or tipping points.*

2. *Growing urgency to accelerate methane reduction efforts due to impacts in the Arctic. Methane reductions can be cost-effective and achievable with existing technology*

3. *Reductions can also offer important co-benefits*
    a. *Air quality – ozone*
    b. *Human health*
    c. *Water quality*
    d. *Industrial Safety*
    e. *Clean Energy*

4. *Finance alone is not enough—a need remains for training, technology transfer, and capacity building to get projects into the pipeline.*

5. *A Global Methane Initiative is needed to accelerate reductions – providing a strong infrastructure to build capacity and facilitate project development that fully supports country efforts and commitments under the UNFCCC*

This dissertation recommends a focus on the utilization or transformation of coalmine methane emissions to energy. A number of significant co-benefits will be realized such as providing a local source of energy, which can be used by industry, a community or sold to the grid. The subsequent improvements in air quality would be noticeable on a global scale. The effect of a reduction methane on global climate

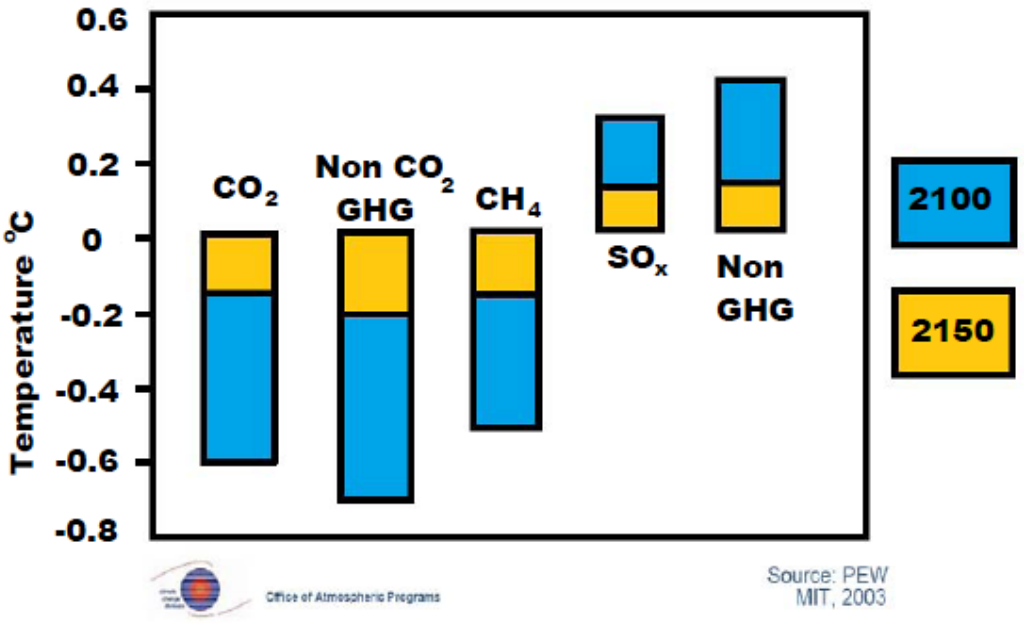

Figure 2.1.1 Global mean temperature effect of a 50% reduction in greenhouse emissions between 2000 and 2050, maintained through to 2100. Reducing methane has nearly the same climate benefits as reducing carbon dioxide emissions (Source, Office of Atmospheric Programs, image in public domain)

compared to a reduction in carbon dioxide is shown in Figure 2.1.1. It is clear that the current atmospheric modeling suggests that the effect of methane on the global climate is comparable to that of carbon dioxide.

In Figure 2.1.2, the expected distribution of marginal temperature increase based on the SRES A1B scenario is shown. Clearly, the warming is greater over continents than oceans, but it is largest at high latitudes of the Northern Hemisphere. These results are from the GFDL CM2.1 model (NOAA, 2011), but are consistent with a broad consensus of modelling results such as the HadCM3 climate model used at the Hadley center in the UK. The highest increases in temperature are expected in the upper northern Arctic. These increases have been modeled without including the increased effect of methane in the Arctic due to releases from the permafrost, bioactivity and ocean sediment. Atmospheric concentrations of GHG have continually increased since the onset of the industrial age; carbon dioxide is currently 0.04% of the earth's atmosphere, an increase of 31% since 1750. Methane has increased by 149% with more than two-thirds of this increase attributed to human activities (IPCC, 2001). According to some researchers, a major difference between the two gases is that carbon dioxide levels continue to climb drastically

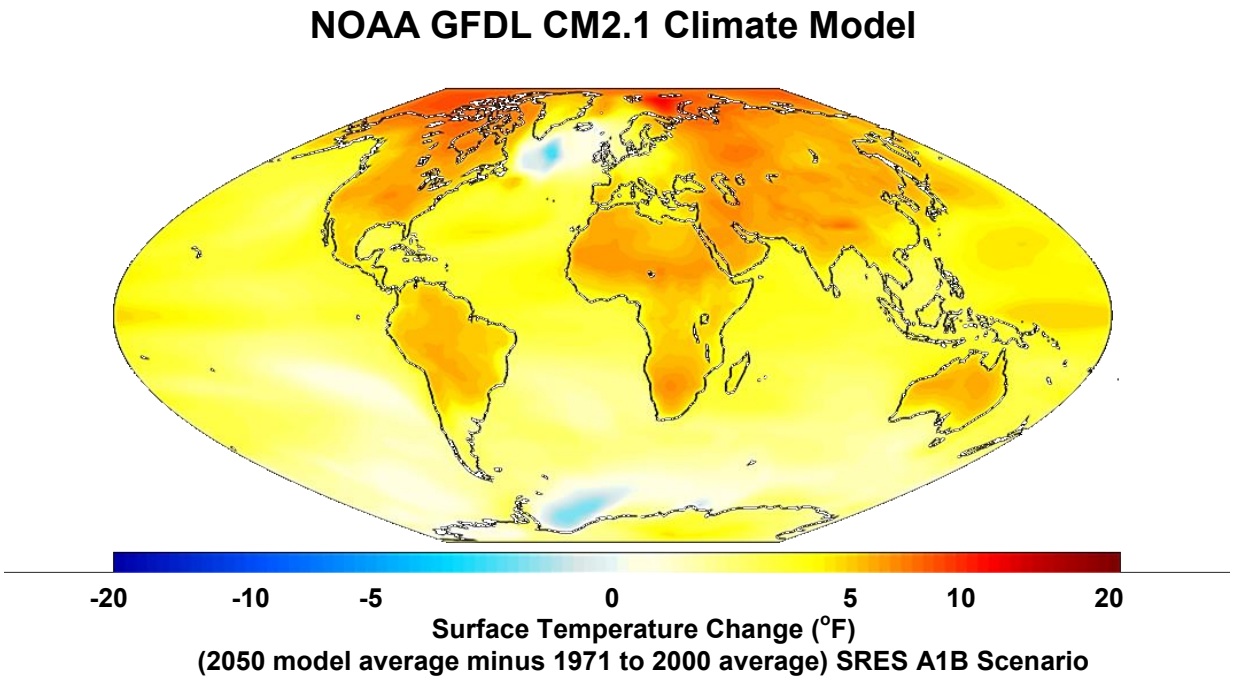

Figure 2.1.2 Modeled annual mean surface air temperature (1971-2000 average) to (2051-2060 average). Caused by increasing GHG and aerosols. This scenario is denoted as IPCC SRES A1B [reference: IPCC, 2000]. (Courtesy, NOAA, image in public domain)

each year, while methane concentrations are leveling off (Simpson et al, 2006), this may have been a premature assessment. At present the average atmospheric concentration of methane is about 1750 ppb, which is quite an abundance in the atmosphere compared to values a few centuries ago (IPCC, 2001), but only a fraction of the abundance in the Earth's early history. The ancient Earth may have had 600 times the amount of atmospheric methane as the current concentrations (Kasting, 2004). Some recent arguments suggesting that atmospheric methane is actually stabilizing (Simpson et al, 2006), based on the observation that the global average appeared to be leveling off over a few years, note the plateau from about 1998 to 2002 in Figure 2.1.3. The effect of atmospheric methane emissions becomes apparent almost immediately after release, methane has a high radiative forcing factor; thus, a reduction anywhere globally leads to an immediate reduction of Arctic temperature.

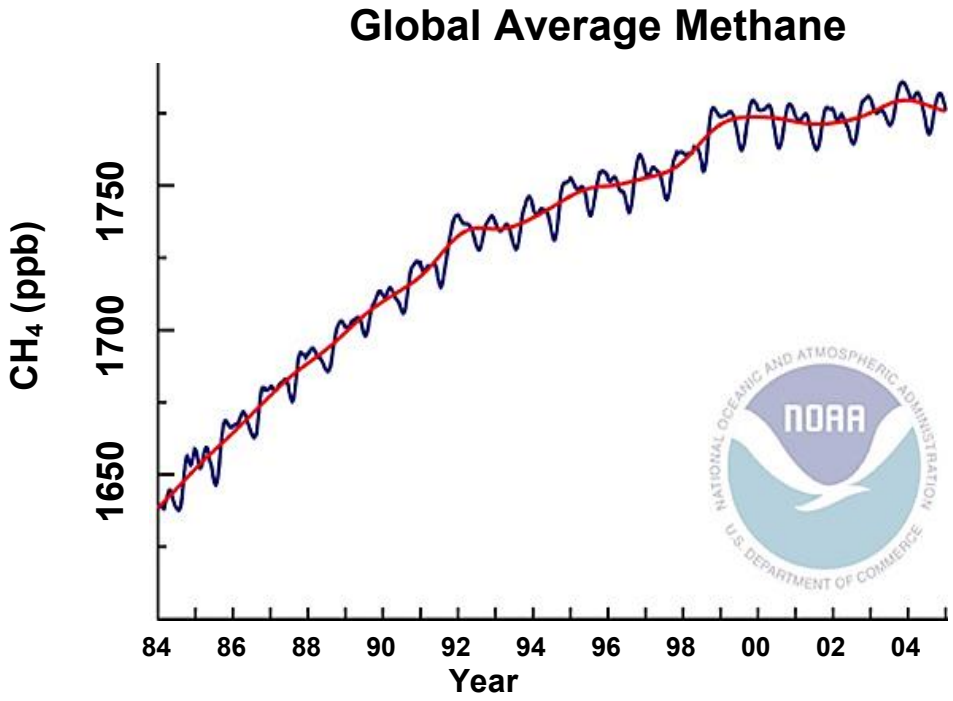

Figure 2.1.3 Global average methane concentrations since 1984, with an apparent leveling off appearing from about the year 1998 to 2005. (Courtesy NOAA, image is in public domain)

"If one really tightens emissions, the amount of methane in the atmosphere ten years from now could be less than it is today. We will gain some ground on global warming if methane is not as large a contributor in the future as it has been in the past century." (Simpson et al, 2006).

The variation in concentrations of methane found in the atmosphere as a function of season and latitude are shown in Figure 2.1.4. The five years of leveling that prompted the idea that the methane may be leveling off is clear at all latitudes;

however, the increase in atmospheric methane concentration in the polar region is pronounced and about 200 ppm greater than that at the equator.

This is evidence that not only is the methane content increasing, but that the effect in the Arctic is clearly increasing at a faster rate than other areas of the globe as is seen in Figure 2.1.5, (a, b and c). The average Arctic methane levels increased in Aug 2012 by about 10 ppb since Aug 2011 and 20 ppb since 2008.

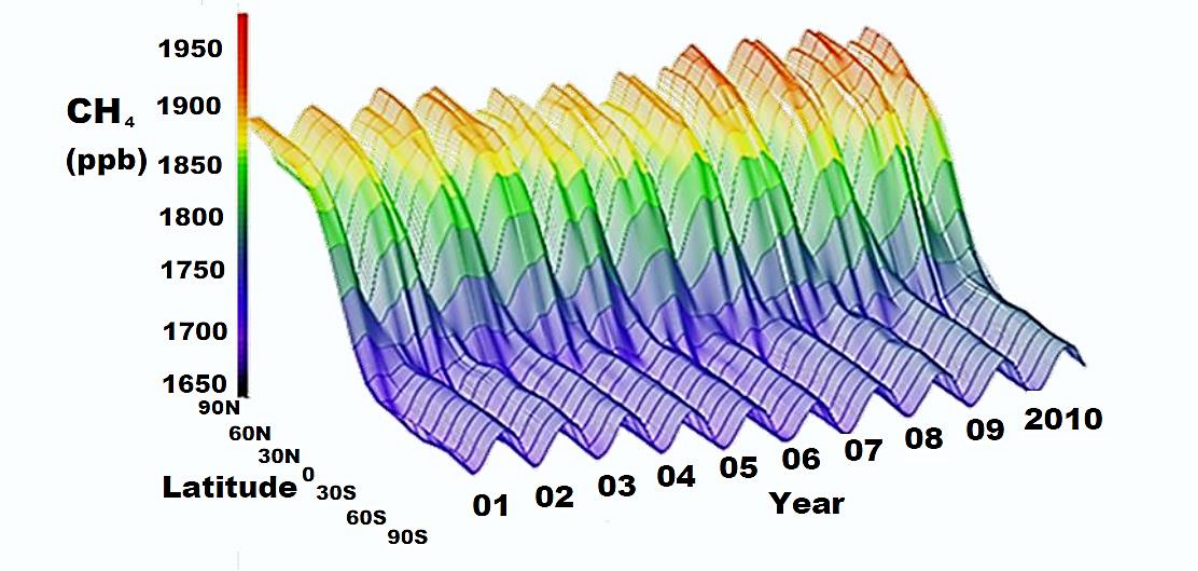

Figure 2.1.4 Three dimensional plot of the global atmospheric methane distribution seasonal variations and latitudinal variation over the last decade and from the equator to the North Pole (source, Dlugokencky (2012) image in public domain).

Arctic methane levels during August have ranged between 1840 and 1860 ppb in 2012 compared to 1830 to 1850 ppb in 2011 and 1820 to 1840 ppb in 2003 (Yurganov, Xiaozhen and Wofsy, 2012). This is striking evidence of what appears to be a pressing scenario with respect to the potential for an Arctic methane radiative forcing feedback loop. The increase in Arctic temperatures that results could possibly accelerate melting of the permafrost and Arctic ice, and may be capable of affecting the global temperature with the predicted unfortunate consequences like higher sea levels.

Radiative forcing is an expedient method used to compare different effects of the various components capable of changing the climate system. Estimations are made independently for the various components. For example, the insolation effect is simply the change in the average amount of solar energy absorbed per square meter at the Earth's surface. The insolation is multiplied by the fraction of incident

sunlight that is absorbed, F = (1 - R), where R is the reflectivity, or albedo, of the Earth. The average global albedo of the Earth is approximately 0.3, so F is approximately equal to 0.7. Consequently, a change in the Earth's albedo, due to a change in the amount of atmospheric aerosols or the reflectivity of the surface will produce a change in the solar forcing. The radiative forcing of the atmospheric gasses is the difference between the incoming solar electromagnetic radiation and the outgoing infrared radiation or the so-called "greenhouse effect".

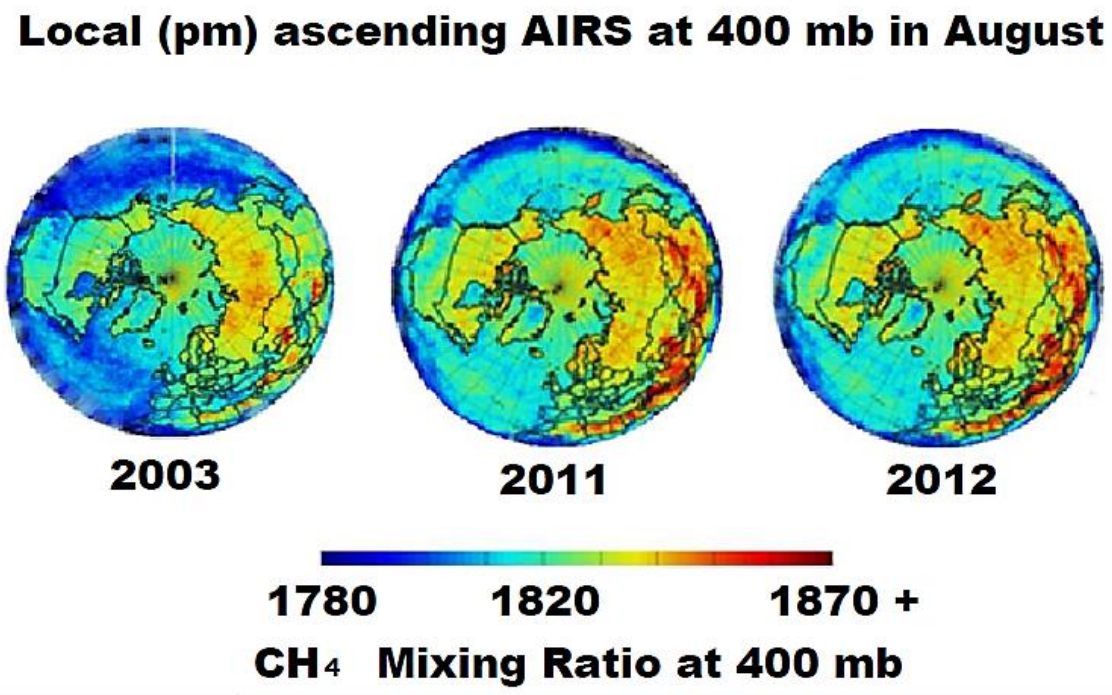

Figure 2.1.5 The average global methane concentration determined from Satellite observations during a campaign initiated by the University of Maryland, the baseline measurement (a) in 2003 "strong increases in Arctic methane concentration from August 2011 (b) and 2012 (c) (source, Scribbler, (2012)).

Calculating the radiative forcing effect follows the relationship in Eqn.2.1.

Eqn. 2.1. $$F = A\ln(C/C_o)$$

Where:

A is a constant pertaining to the gas in question,

C is the current concentration,

C_o is the reference concentration, and

F is the value of the radiative forcing.

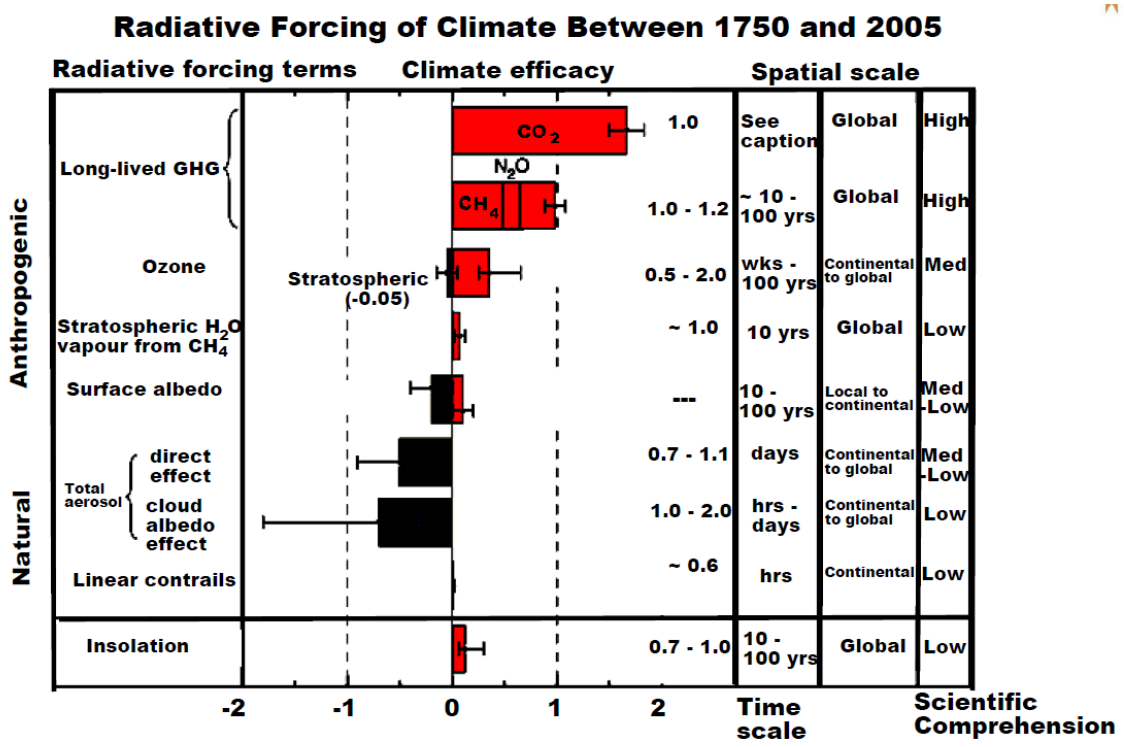

Figure 2.1.6 Radiative forcing 1750, the start of the industrial era, to 2005 (Forster et al, 2007)

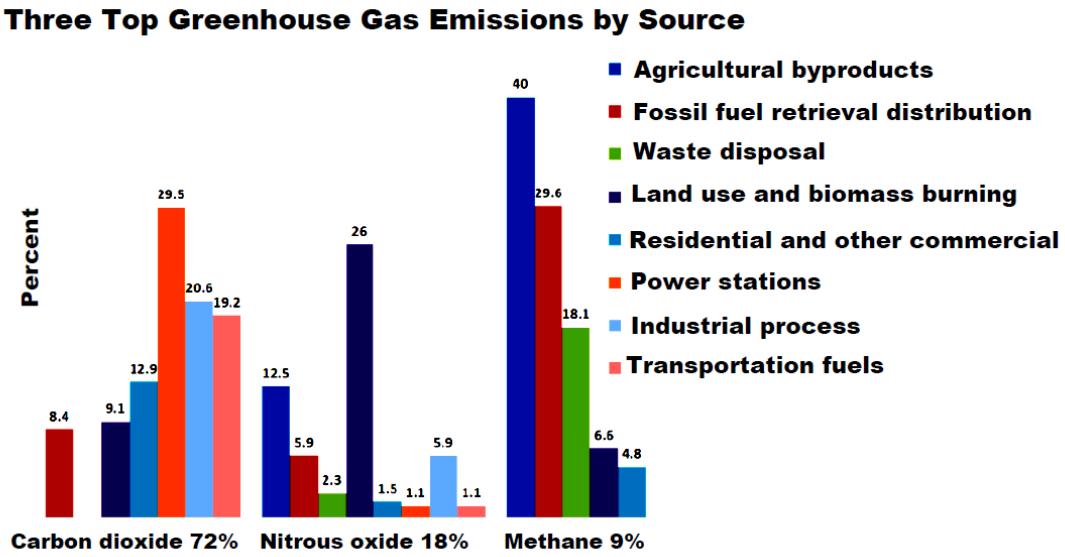

Figure 2.1.7 Annual greenhouse gas emissions by source, (derived from Edgar, (2013))

A summary of the radiative forcing effects that affect the climate, associated with human activities or natural processes is shown in Figure 2.1.6. This data is relative to the start of the industrial era in 1750, the positive radiative forcing factors, such as atmospherically distributed GHG or an increase in insolation lead to

warming and the negative forcing factors like atmospheric aerosols or an increase in the surface reflectivity lead to cooling (Forster et al, 2007).

In Figure 2.1.7 the distribution of the three top GHG, carbon dioxide, methane and nitrous oxide are shown separately by their sector source; methane accounts for 18% of the total GHG emissions. Considering the global effect on average temperature, as shown in Figure 2.1.2, the predictions of the distribution of temperature change due to global warming suggest that the northern regions have the highest temperature increases (USEPA, 2013). There is an expectation that methane will play a significant role in the Arctic temperature increase due to the high level of short term radiative forcing.

The Second Assessment Report of the Inter-Governmental Panel on Climate Change (IPCC, 1996), suggested that atmospheric methane concentrations appear to adjust to changes in anthropogenic emissions in a nine to fifteen year timeframe. In addition, if the current annual methane emissions were abruptly reduced by about eight per cent, the atmospheric methane concentrations would actually remain at constant levels. Considering the scenario in the opposite direction, with increasing atmospheric methane, the increase in temperature known to be concentrated in the northern Arctic, accelerates the Arctic methane emissions; thus, a methane-driven Arctic temperature increase feedback loop ensues (BBC, 2006).

The average global methane concentration determined from Satellite observations during a campaign initiated by the University of Maryland show strong increases in Arctic methane concentration between August 2011 and August 2012 (Yurganov, Xiaozhen and Wofsy, 2012). The satellite observations demonstrate a trend of increasing methane concentrations in the Arctic from Aug 2003, the baseline measurement year. The methane increase in the Arctic provides an additional heating component and when coupled with the expectation that the northern regions will sustain higher increases than the remainder of the globe as a result of the carbon dioxide forcing, again is evidence that a feedback loop could be follow on effect. The rate of methane increase in the Arctic for 2011 to 2012 is equivalent to about 0.25 to 1 ppm carbon dioxide corresponding to a 12% to 50% increase in carbon dioxide for the same period. This author has developed the concern that a local increase in methane may rapidly influence the Arctic environment resulting in a local temperature increase especially in view of the recent increase from 2011 to

2012, which is equivalent to the entire increase of the eight previous years spanning 2003-2011. Coupling this effect with the decrease in reflectivity, due to a loss of ice cover, the change in albedo compounds the effect resulting in greatly increased Arctic heating along with a number of worsening extreme weather and glacial melting events far exceeding the impacts we see today.

In 2007, the Arctic sea ice volume reached the lowest levels ever recorded, a level far below the 1979-2001 average, see Figure 2.1.8, when the sea ice volume was reduced by 20% of the total summer coverage of the previous year. Since that time, Arctic sea ice volume has failed to recover with 2011 showing the second lowest volume on record at summers end, very close to the unprecedented 2007 record low. The 2010 September ice volume anomaly did in fact exceed the previous 2007 minimum by a large enough margin to declare it a new record (Schweiger et al, 2011). In the graph shown in Figure 2.1.8, the mean trend projection, minimum projection and maximum trend projection, obtained by projecting the curve fitting equations to future years, suggest the Arctic ice will be completely absent sometime between 2017 and 2040 with 2027 the most probable

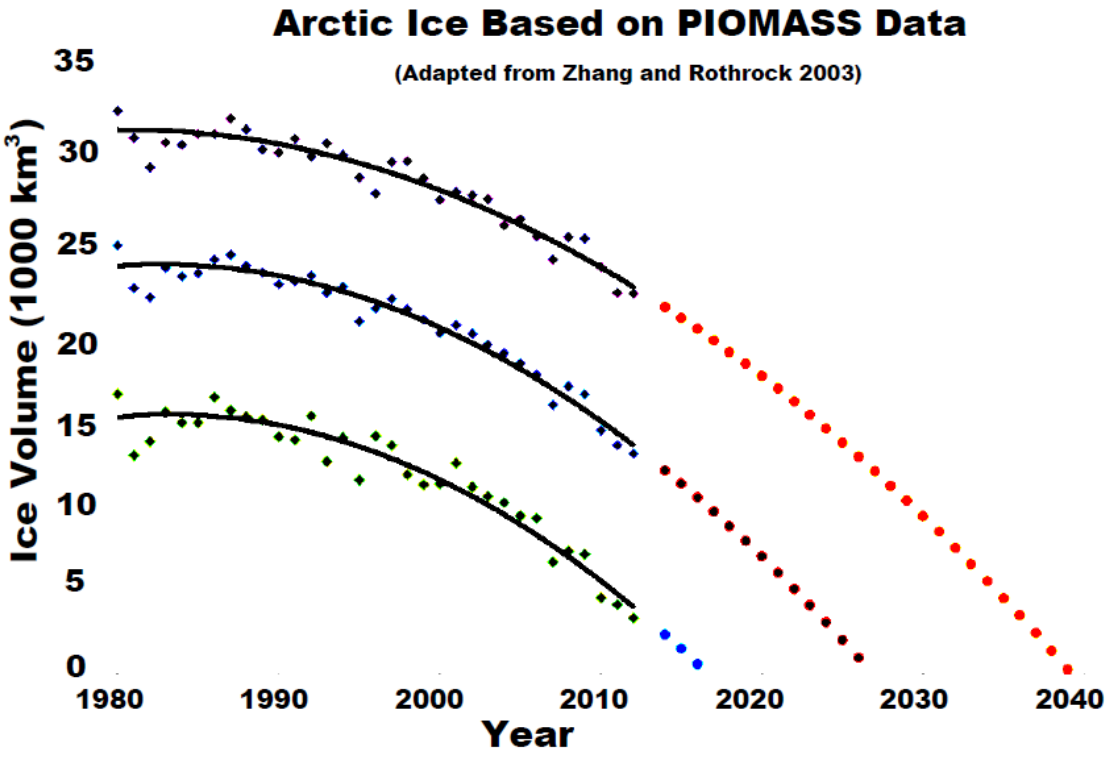

Figure 2.1.8 Measured Arctic ice volumes (Adapted from Zhang and Rothrock 2003, using PIOMAS data) Mean trend R^2 = 0.9465, Min trend R^2 = 0.9222 and Max trend R^2 = 0.9222

year. Given the current trends in temperature and the outcomes of most climate models, it is unlikely that the temperature will suddenly decrease, which suggests that in the next generation there will be a drastic decrease in the Arctic ice volumes reaching zero in that timeframe. The methane contained within the permafrost will also be completely released; recently an estimate of the global cost of methane released in the Arctic due to melting permafrost is $US 60 trillion (Whiteman, Hope and Wadhams, 2013)

> "*Scientific climate projections do not currently account for carbon emissions from permafrost, but the study concludes that the effect is "strong enough to warrant inclusion in all projections of future climate." (NOAA, 2011).*

The GHG effects of methane are not as recognized or discussed as frequently as carbon dioxide. Although both are a GHG, the effect of methane is a short term high effect forcer, which means that a small amount of methane has a large effect over a shorter period of time (USEPA, 2012). When we consider the evidence of ice loss and methane concentration increases and that these effects may compound to cause further methane releases in the Arctic indicates that an urgency for methane mitigation programs is evident. Recent recommendations to the Arctic Council below to bring the point into focus (Gunning, 2008).

AMAP Recommendations 2008.

> *"Methane reductions anywhere on the globe will benefit the Arctic Methane mitigation a "no-regrets" measure: both well understood science AND mitigation".*

Recommendation to Senior Arctic Officials from September 2008 AMAP Workshop.

> *"Arctic Council ministers should consider a commitment to undertake maximum feasible reductions of methane within Arctic nations and globally in the near term for the purpose of achieving rapid Arctic climate benefits. Focus should include methane sources of significance…. and emphasize both additional national action and international cooperation such as active participation in the Methane-to-Markets Partnership, the Clean Development Mechanism, and Joint Implementation."*

Tromso Declaration, April 2009 Office of Atmospheric Programs.

> *"Urge implementation of early actions where possible on methane and other short-lived climate forcers, and encourage collaboration with the Methane to 3 Markets Partnership and other relevant international bodies taking action to reduce methane and other short-lived forcers."*

In Figure 2.1.8, the trend of the ice volumes, which directly relates to the ice thickness in the Arctic, is a further indication of the difficulty faced in the region due to global warming. The projection is that there will be little or no ice in the year 2027,

but when the tundra melts the water contained in the permafrost will often reside on the surface forming new temporary lakes. Ignition by lightning can result in can result in immense fires over the tundra that can burn gigantic areas of the Arctic. One such tundra fire in Alaska recently burned an area the size of Cape Cod. To some extent, the benefit of burning the methane is offset because the burning of substantial volumes of biological matter creates carbon dioxide, which provides an additional source of carbon dioxide over and above that which would be produced by the combustion of the methane alone. A graphic demonstration of the effect of the contained methane, seen in Figure 2.1.9 is a rather compelling example of how much methane is contained and can be emitted from the permafrost.

Figure 2.1.9 Flaring methane from a hole in the Arctic permafrost a rather graphic representation of the methane that will be released as the permafrost melts (Source, National Geographic, 2012, photo by Mark Thiessen)

A number of factors are coalescing to contribute to an unsustainable situation in the Arctic. As the Arctic albedo changes and the waters begin to absorb electromagnetic radiation from the sun causing the Arctic to warm and the permafrost melts the changes will be more dramatic. In this author's opinion, the change is more likely to be rapid and chaotic rather than slow and smooth, weather events such as large hurricanes or cyclones and Arctic outpourings of cold air,

guided by the jet stream, are the type of events that a chaotic system would undergo while moving from one set point to another. Fluctuations in the jet stream amplitude could result from a change in these heat flows, which could cause remarkable alterations to the northern microclimate and increased turbulence in the global climate. The global interaction involving heat movement from the equator to the poles or the Hadley cell circulation may also be dramatically affected. These changes have the potential to contribute to climate change on a Global scale.

One other area of research this author has pursued to reduce GHG in the Arctic is the use of Frozen Backfill for mining operations in permafrost conditions. Frozen backfill, patent pending (Cluff and Kazakidis, 2013), does not use cement as a binder; thus, has the benefit of reducing the GHG release in general due to the reduction of the GHG associated with cement production. In addition, the cement would normally have to be delivered to the Arctic mine sites by Diesel truck transport, often along the ice roads over a short period while the season permits, would not be required. As the temperatures increase the transportation season decreases; thus, the intensity of transport trucking would have to increase to meet the needs of the Arctic industrial complex, which may result in a sudden perturbation of GHG increase to the Arctic system. Reducing the transport and production of cement would substantially decrease the GHG impact on the Arctic.

The focus on the Arctic methane issue is intended to bring the concept of methane feedback loop into focus and is a specific methane related problem that demonstrates the urgency to consider methane as a significant greenhouse gas. Since the usual greenhouse gas discussion tends to be centered on carbon dioxide, it is instructive to bring the methane situation to the forefront as a target for mitigation technologies. The large amount of methane contained in the Arctic permafrost and sediments may make use of mitigation strategies similar to the concepts proposed in this dissertation or in some manner linked to the methods proposed.

2.2. Ventilation air methane (VAM) mitigation. reducing global climate change while providing an energy source

Of the 8% to 10% of atmospheric anthropogenic methane produced associated with coal mining, see Table 2.2-1, about 70% is contained in the ventilation air. Therefore, it follows that methods to mitigate the Ventilation Air

Methane (VAM) are both desirable from a Global Climate perspective and could be economical if the heat generated can be captured. Since methane is a GHG target for mitigation, VAM from coal mining operations is an obvious candidate.

Table 2.2-1 Global anthropogenic methane by sector in 2000; total methane emissions of 282.6 Tg, (sources, IEA CCC 2005, M2M 2006, and US EPA 2006).

Agency/ Source	IEA CCC 2005 (%)	M2M 2006 (%)	US EPA 2006 (%)
Natural Gas	15	16	17
Coal	8	8	6
Oil	1	1	1
Solid Waste	13	14	12
Waste Water	10	11	9
Fuel	1	1	1
Biofuel	4	4	--
Other	--	--	7
Biomass	5	--	3
Fermentation	28	29	30
Manure	4	4	4
Rice	11	12	10

Since methane has an initial global warming potential higher than that of carbon dioxide, the effect of atmospheric methane emissions can be quite abrupt and in turn cause more rapid climactic changes. The reduction of ventilation air methane emitted to the atmosphere is a significant because of the significance of methane as a GHG.

A typical gassy coalmine has five sources of methane.

i. *Degasification or drainage systems at underground coal mines. Vertical and/or horizontal holes are used to recover methane in pre-mining or after mining from the gob or goaf.*

ii. *Ventilation air containing dilute methane concentrations or VAM.*

iii. *Nonoperational mines from vent holes or through fissures.*

iv. *Open pits are directly exposed to the atmosphere.*

v. *Post-mining operations where the coal emits methane during storage or transportation.*

VAM is the low methane concentration high volumetric flow case while the others are high concentration low volume opportunities or not possible to capture. Ultimately, VAM accounts for approximately two thirds of all coalmine methane emissions; however, because of the low methane concentration and high airflow volume, it is the most difficult to capture and exploit.

twenty-one is a major benefit according to the current climate models.

Energy demand is not expected to diminish in any projection by any authority and coal plays a large part in the future energy supply in the largest economies of China, India and The United States. Regardless of whether technologies evolve to provide a cleaner coal burning plant, it is clear that the coal will have to be mined. Currently China produces seventy-one percent of its energy from coal (Somers and Burklin, 2012). As the demand for coal continues, the surface deposits will become less of the total and deeper mines will be required to satisfy the requisite coal demand. As the mining activities are carried out at deeper levels the in-situ stress increases; thus, the methane contained in coal increases due to pressure confinement.

The relationship between depth and methane contained in the coal as depth increases, displayed in the Figure 2.2.1 plot with a linear regression, shows that coal mined at fifteen hundred meters contains approximately five times the methane of that mined at five hundred meters. The pressure increases as the depth of the mine does, which reduces the level of permeability. The increased pressure with reduced permeability causes the methane to be more tightly bound to the coal and surrounding rock strata compared to surface mining methane. Because of this underground mining produces more methane than surface mining. At the current tonnage, needed to meet the expected energy demand and with the expected future increase demand there are already deeper projects planned and the current mines are reaching deeper as well. This trend will undoubtedly increase the anthropogenic emissions of methane due to increased coal mining at depth and the need to keep the methane dilute will lead to an increase in VAM emissions.

The five countries accounting for over seventy-five percent of the global coal production are presented in Figure 2.2.2 (Somers and Burklin, 2012). Somers estimates the quantities of VAM emissions associated with these production quantities suggests that the world market for VAM destruction technologies has a potential value of several billion dollars. Over the last decade, China and Indonesia have essentially doubled their production and although the US has reduced their production somewhat India has recently started to grow at a more rapid pace, which carries with it the expectation that their coal use will also increase.

Table 2.2-2 USA Methane emissions by coal mining activity source (U.S. Environmental Protection Agency, 2012)

	Average 1990–2009		2010	
Mining activity	bcf	%	bcf	%
Post mining	19	10.06	18.87	9.86
Surface mines	31.9	16.90	32.64	17.06
Abandoned mines	13.6	7.20	12.32	6.44
Drained gas	---	---	9.49	4.96
Degasification vented from UG	9.4	4.98	---	---
VAM	114.9	60.86	118	61.68
Total bcf	188.8	---	191.32	---

As an example, the methane emissions from mines in The United States are presented in Table 2.2-2, and are considered similar to the typical emissions of global mines; the VAM emissions from US coalmine ventilation systems are about sixty- two percent of the total coal mine related methane emissions. Some estimates for the global VAM emissions are as high as seventy percent (Warmuziński, 2008) while other researchers set the value at sixty-four percent (Su and Beath, 2005). These estimates place VAM in the high priority category for mitigation because it is released directly to the atmosphere and the energy content has potential for economic return.

Ventilation Air Methane or VAM is dilute in the ventilation air from coalmines mainly due to the need for safety in the workings of the mine. When the monitoring system detects changes in the methane content in the ventilation air there are prescribed legislated actions. The legislation is similar for most countries with minor variations; as such, the details of the US regulations are a good example (Kissell 2006).

Mines with a history of gas emissions are usually already on notice that they have a methane problem. The U.S. regulatory standards have very specific monitoring requirements and actions to be taken depending on the category of mine and its methane history. These measures are intended to provide commonsense approach to methane monitoring and control and are representative to international standards. Non-coalmines that liberate significant quantities of gas must monitor for it each shift in a pre-shift examination similar to that for coalmines. No testing is mandated for those mines where methane is not expected to be present, but there

are action levels and prescribed actions when gas is detected at certain levels, as follows:

i. *Actions at 0.25% methane: If the mine had never before measured 0.25% or more or never had an ignition, then changes must be made to improve ventilation, and MSHA must be notified immediately.*

ii. *Actions at 0.5% methane: Ventilation changes are required to reduce methane below 0.5%. In the meantime, depending on the category of mine, one or more of the following are necessary: electrical power must be de-energized, diesel equipment must be shut off or removed, and/or work must stop.*

iii. *Actions at 1.0% methane: Ventilation changes are required to reduce the methane. In the meantime, depending on the category of mine, one or more of the following are necessary: all workers from the affected areas must be withdrawn except those needed to make the ventilation changes, electrical power must be de-energized, and/or diesel equipment must be shut off or removed.*

iv. *All persons must be withdrawn from the mine if the 1.0% accumulation results from a main fan failure or if 1.0% is measured at a main exhaust fan.*

v. *Actions at 2.0% methane: Ventilation changes are required to reduce the methane, and all persons must be withdrawn except those necessary to make the ventilation changes. Depending on the category of mine, one or more of the following are necessary: MSHA must be informed, the methane must be reduced to below 0.5%, and/or the methane must be reduced to below 1.0%.*

vi. *For all of the above scenarios, the mine category also impacts*

- ***a.*** *The frequency and location of methane testing,*
- ***b.*** *The use of atmospheric monitoring systems*
- ***c.*** *The use of methane monitors on mining equipment, and*
- ***d.*** *Whether explosion-proof electrical equipment is used, among other factors.*

Typically, ventilation air methane is in the neighborhood of 0.2% to 1% on a volume-volume basis, but varies in concentration as the atmospheric pressure changes, as the underground operations change, in the event of seismic activity or as the mining proceeds deeper. Although these concentrations are kept low, mainly for safety reasons (Mallett and Su, 2004), the high volume of ventilation air from a

coalmine can easily be 100 m^3/s and can be as high as 300 m^3/s, representing a very large quantity of methane emitted into the atmosphere. Using a density for methane of 0.68 kg/m^3 and a calorific value of 55.5 MJ/kg, Table 2.2-3 shows the thermal power available for typical methane concentrations and ventilation flows.

Table 2.2-3 Power available and carbon dioxide equivalents for mitigation of various typical methane concentrations in typical coal mine ventilation flows. (Cluff, Kennedy and Bennett, 2013)

Ventilation Flow Rate (m^3/s)	Methane Concentration (%)	Methane Mass Flow kg/s	Methane Tonnes/yr	Conversion Methane to Carbon Dioxide Tonnes/yr	21 times Equivalent Carbon Dioxide Tonnes/yr	Power (MWth)
50	0.2	0.068	2,144	5,897	39,136	3.77
150	0.5	0.51	16,083	44,289	293,521	28.30
300	1.0	2.04	64,333	176,917	1,174,085	113.22

It becomes clear from the calculations presented in Table 2.2-3 that the economic benefit of converting the fugitive methane emissions contained in VAM could provide a significant enhancement to any engineering project undertaken to mitigate the VAM provided the thermal energy can be captured and converted to various products. Essentially the VAM is considered as a free energy source if combined with other energy or operational systems' waste heat and collected through a heat exchanger to create steam for electricity production or various other energy outputs. In effect a system that oxidizes the VAM would produce heat and carbon dioxide, the collection of the heat becomes the obvious task to provide an economic advantage and the mitigation of a GHG with carbon dioxide equivalence of

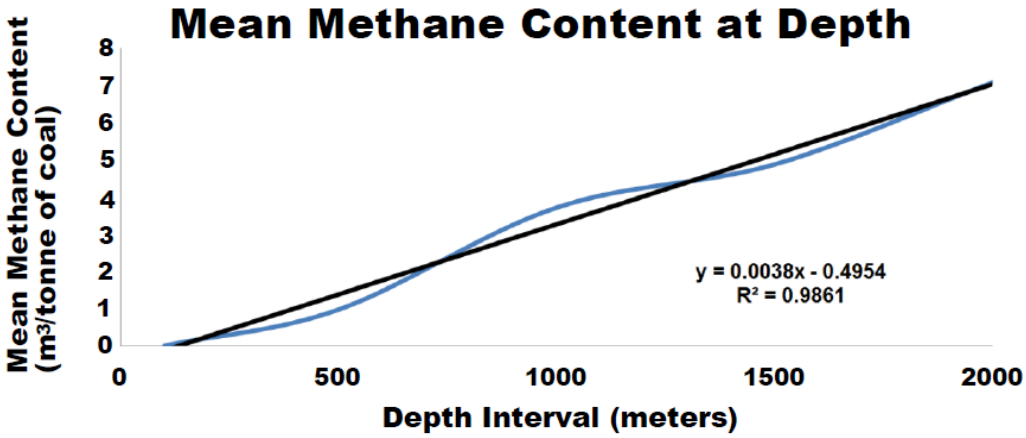

Figure 2.2.1 Mean methane content with increasing depth, a linear regression with the R2 = 0.9861 indicates a very high level of correlation. (source, *IEA CCC, 2005)*

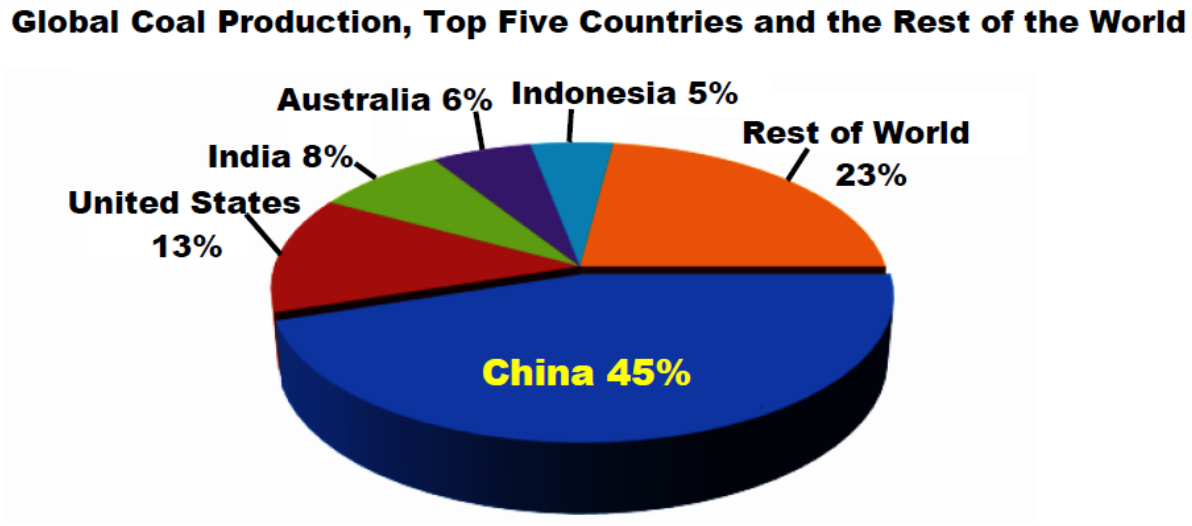

Figure 2.2.2 Percent distribution of coal production for the top 5 producers and the rest of the world (Source: U.S. Energy Information Administration, International Energy Statistics, 2010).

Emission of methane causes similar global warming to carbon dioxide and is a climate warming forcer with significant implications for the Arctic regions. Although methane emissions are of global concern it appears there is a concentration and perhaps a reaction to that the interaction with the Arctic that may accelerate the release of existing stores of methane locked in the permafrost and Arctic ice. This could result in rising sea levels and an alteration in the way of life for the coastal populations and wildlife on a global scale. Methane abatement programs from coalmines are significant enough within the context of the larger scale of global emissions to be considered an important part of a meaningful GHG reduction effort. A quote by this author, from an interview August 23, 2005 regarding the impending hurricane Katrina as it formed over the Atlantic (Bradely, 2005), is a statement that puts the potential increase in coal mining activity from two of the current world leaders in coal production. The ensuing methane associated with expansion of these economies is a target for mitigation by the VamTurBurner© technology.

The increase in the rate of change of these climatic changes, the temperature rises for example and the damage they indirectly cause through storms is alarming. If rising temperatures, caused in part by burning fossil fuels, do feed this destruction, then what happens when highly populated countries like China and India industrialize?

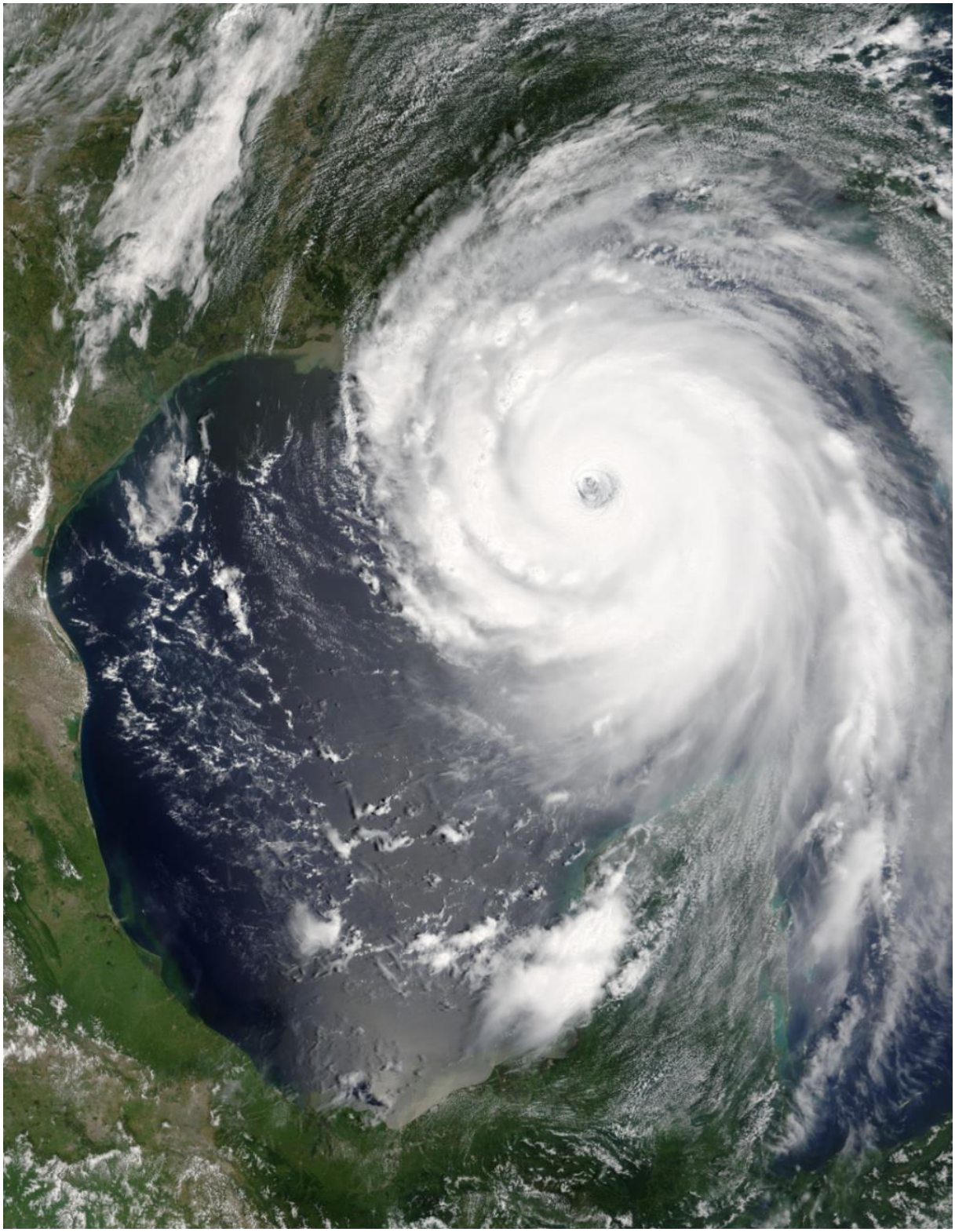

Figure 2.2.3 Hurricane Katrina (Courtesy NASA, Public Domain)

3. A review of VAM mitigation projects

A number of technologies either developed or currently in operation to mitigate VAM. There are two basic methods employed to burn VAM. Used as a secondary fuel, the VAM replaces a usual air source, at the expected flow rates, in a combustion process such as in gas turbines, internal combustion engines, rotary kilns or even a coal-fired power station. In primary fuel system applications such as Thermal Flow Reverse Reactors (TFRR), Catalytic Flow Reverse Reactors (CFRR), lean burn Gas Turbines, recuperative gas turbines or Regenerative Thermal Oxidation (RTO) the VAM is the main fuel source. Higher concentrations of methane such as drained sources can often be used to supplement the VAM to raise the methane concentration, but are often flared or sold to market if the quality of the gas is sufficient. A technology for concentrating methane is desirable, but not commercially available; some researchers propose the development of a nano-membrane technology to extract methane from the ventilation flow. The available technologies are based on the direct or catalytic combustion or oxidation of methane even at the very low concentrations found in VAM.

3.1. VAM as a primary fuel

The Commonwealth Scientific and Industrial Research Organization (CSIRO) has built and tested a 1.2 MW rotary kiln system, Figure 3.1.1 where waste coal and

Figure 3.1.1 EESTech Inc. rotary kiln VAM/coal system, (by permission of EESTech Inc.)

VAM are burned in a rotating kiln to generate electricity by using externally fired steam turbine system (Pyper, 2003; Somers and Schultz, 2010 and Schultz, 2003). EESTech Inc. acquired the rotary kiln system technology and they are currently

attempting to design 10 MW and 30 MW systems. Although the company is actively seeking the commercialization of the technology in China and India, to date no evidence exists to suggest the 10 MW plant was designed or developed further.

CSIRO has also supported the development of the VAMCAT™ a lean burn catalytic gas turbine custom-built for VAM. The VAMCAT™ can operate on a fuel source as low as 0.8% methane using an innovative catalytic combustion gas turbine system to oxidize methane to carbon dioxide and water while generating electricity (Somers and Schultz, 2010). A 25kWe power generator demonstration unit was commissioned at an underground coalmine of the Huainan Coal Mining Group, China in November 2011. The current design is shown in Figure 3.1.2 and a proposed 1 MW design was reported, but has not yet been completed (Somers and Schultz, 2010).

The current state of the VAMCAT™ technology, see Figure 3.1.2, is that it provides 25 kW_e of electricity. At this electrical generation rate, the gas flow through the combustor would be in the neighborhood of 0.25 m^3/s to 0.3 m^3/s; thus, for a VAM flow of 100 m^3/s about 334 to 400 VAMCAT™ units would be required to accommodate the VAM flow from a single ventilation shaft. Although it is of scientific interest and valid precursor research for the development of larger systems this is not currently a realistic solution to the actual ventilation flows encountered at real mines and the lead time required to engineer a 1 MW gas turbine suggests there will

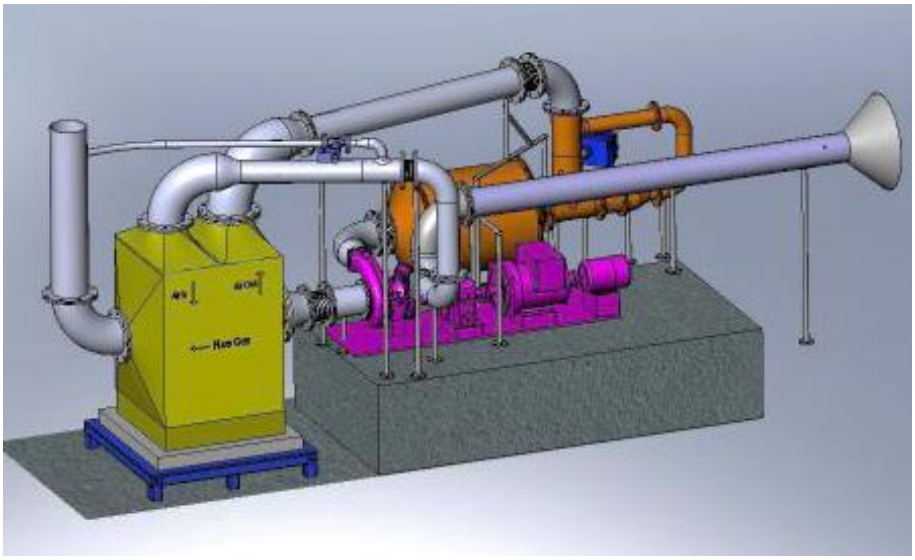

Figure 3.1.2 Representation of the VAMCAT™ (source: Mallett and Su, 2004)

be a considerable lag time until such technology is developed.

MEGTEC has a longer history in the mitigation of VAM and more projects in operation than any other supplier does. The MEGTEC VOCSIDIZER™ in Figure 3.1.3, actually began as a system for the destruction of volatile organic compounds and has carried that history on through in the current name for the technology. The technology is based on a regenerative thermal oxidizer (RTO) and can supply a superheated steam if the methane content is 0.9% (Kosmack, Winschel and Zak, 2007). The steam can be used to drive an ordinary steam turbine to generate

Figure 3.1.3 The MEGTEC VOCSIDIZER™, (printed by permission of MEGTEC)

electrical power for the grid or the company, which falls under the category of basic engineering design and is also one of the aspects of the VamTurBurner© system. The VOCSIDIZER™ was first demonstrated in 1994 at the Thoresby Mine in Nottinghamshire, United Kingdom (Somers and Schultz, 2010; Kosmack, Winschel and Zak 2007). The result of that demonstration proved the VOCSIDIZER's™ capability to maintain an oxidation reaction at the low concentrations and variations of methane found in a typical coalmine ventilation system.

Subsequent to the positive results from the Thoresby Mine, continued and scaled up testing was performed in 2001-2002 at the Appin Colliery in New South Wales, which included an internal heat exchanger to capture the heat of combustion. The project operated over a 12-month period, a robust demonstration of the

technology, which proved that even when confronted with the variations in VAM flow typical at active underground coalmines the installation was successful (Somers and Schultz, 2010). This project confirmed that a TFRR with a heat exchanger can provide energy for an assortment of potential applications, such as hot water for the company or the community, hot air for space heating, industrial drying, cooling using low grade heat with an absorption chiller or electricity generation. MEGTEC and BHP Billiton installed a large-scale electrical power generation project at the West Cliff Colliery in New South Wales (Somers J.M. and Schultz H.L., 2009). The West Cliff VAM Project or WestVAMP, seen in Figure 3.1.4, is the world's first commercial scale VAM project, which began operation in West Cliff Mine in April 2007.

Figure 3.1.4 The West Cliff VAM Project or WestVAMP VOCSIDIZER™, (Courtesy of MEGTEC)

WestVAMP oxidizes 70 m^3/s of 0.9 percent methane. The concentration is maintained at a constant flow rate by mixing drainage gas with the ventilation exhaust airflow. Heat collected from the VOCSIDIZER™ units is used to provide superheated steam to conventional steam turbines producing electrical power. The 6 MW_e generated by a conventional steam turbine is used by the West Cliff colliery.

> *"Four VOCSIDIZERs are up-and-running at West Cliff Colliery, BHP Billiton, Australia. MEGTEC Development Manager Ake Kallstrand reports that, for more than one year, these systems have been converting the energy of the coal mine's 0.9% VAM concentration into electrical power. Actually, Kallstrand explains, the VOCSIDIZER turns VAM into high grade, superheated steam that operates a 6 MW (Megawatt) conventional steam turbine. The electricity generated by the plant is fed into the local area power grid." (MEGTEC Systems news release, 2008)*

Apart from the projects in the UK and Australia, MEGTEC has also demonstrated their VOCSIDIZER technology in the US, at the CONSOL Energy Windsor Coal Mine, a closed mine in West Liberty, West Virginia (Kosmack,

Winschel and Zak, 2007). The project operated for 20 months to demonstrate the reliability of VAM conversion.

> *"The abandoned mine gas was injected into a fresh air flow in order to simulate VAM at various concentrations. After 18 months of demonstration and evaluation, CONSOL Energy is planning to relocate the VAM Vocsidizer® to an operating mine"*

The VAM was simulated at a 0.6 percent concentration and flow rate of 14 m^3/s using drained methane from the closed workings, and to determine the available energy that can be extracted from the system (Kosmack, Winschel and Zak 2007).

The Windsor project, Figure 3.1.5, provided hands-on U.S. experience in operating a VAM oxidizer and verified the VAM destruction efficiency, system operational safety, and reliable operation of the system under U.S. field conditions.

Figure 3.1.5 Windsor Mine Project (printed by permission of MEGTEC)

This test verified the ability to convert the low concentration methane typical of underground coal mine exhausts to carbon dioxide, an insight into the cost of deploying this technology at U.S. coal mines and estimates of the amount of useful energy that TFRR's can produce (Somers et al, 2010 and Kosmack, Winschel and Zak, 2007).

Zhengzhou Coal Mining Group in China operates a system based on the MEGTEC VOCSIDIZER™ for VAM abatement and energy recovery in the form of hot water for local use commissioned in October 2008. It has a system capacity of

18 m^3/s while operating on a nominal VAM concentration of 0.3% to 0.7%, but often less than 0.3%. This was the first VAM mitigation project to be officially approved by the UNFCCC for allocation of Kyoto related Carbon Credits or CER's (Coalbed Methane Outreach Program, 2011).

The installation at the Zhengzhou mine is generating hot water used for heating and showers. The heat recovery, using an air-to-water heat exchanger installed between the VOCSIDIZER™ and its exhaust stack, recovers the energy in the hot exhaust air. The amount of energy that can be recovered by secondary heat exchange on the exhaust depends on the VAM concentration and on the water temperature to be achieved. See Figure 6.3.1 for a plot of the percentage recoverable energy from TFRR and CFRR technologies at various VAM concentrations. Notice the need for the sustaining energy, which uses the lower concentration at about 0.2% VAM to maintain the oxidation reaction for the VOCSIDIZER™.

3.2. VAM as a supplemental fuel in the air intake

Using VAM as a supplemental fuel, by drawing the VAM through the standard air supply system, was began in 1996 at the Appin Colliery. Internal combustion engines only require a medium quality gas, so they are an appropriate choice for using ambient air containing VAM to support the combustion processes. Diesel engines are routinely used to provide electricity to mines in remote locations. Mining companies are well informed as to the capital cost and operating costs of these power plants, which can also be used to reduce the VAM emissions provided the installation is designed to avoid costs associated with transportation of the VAM. (Karakurt, Aydin and Aydiner 2011)

The 54 internal combustion engines that are powering the electricity generation project at the Appin Colliery in New South Wales, Australia are comprised of 1 MW units. The VAM/CMM driven internal combustion engines can produce up to 55.6 MW of electricity for the mine (Bibler and Carothers, 2003) and 40 more at the Tower location, Figure 3.2.1, provides a combined output of 97 MW from 94 Caterpillar 3516LE generators. In this case, VAM represents a supplemental fuel, which contributes a portion of the fuel input to the IC engines and all the drained gas from the mine is also used (Mallett and Su, 2003; EPA-CMOP, 2009). The VAM

supplies between four to ten percent of the required engine fuel and uses about twenty percent of the ventilation emitted from the mine. The total output of about 654 GWH_e each year is enough to power approximately 60,000 homes according to the owner of the project Energy Developments (Energy Developments, 2011).

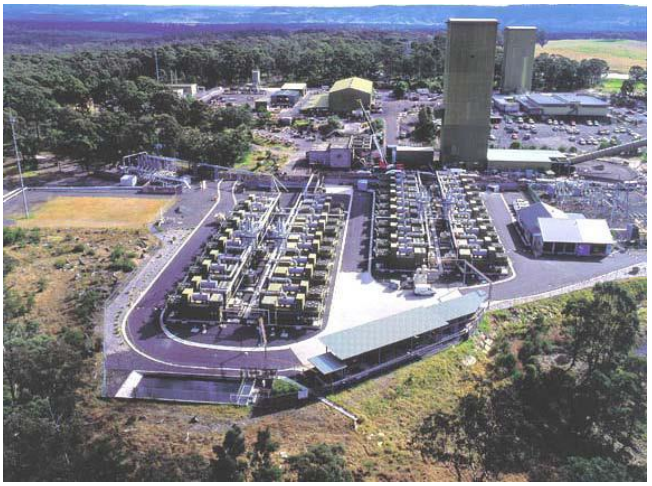

Figure 3.2.1 Tower Colliery Caterpillar 3516LE generators installation (source, USEPA, (2004) image in public domain)

A pilot-scale study was performed at the Vales Point Power Station to determine the feasibility of using VAM as combustion airflow when the coalmine and power station are conveniently proximal. A full-scale demonstration of this technique at this power station was planned with the support of an Australian federal government program in 2003. In this project, the VAM flow rate of about 220 m^3/s routed to the intake of the power station. Total air consumption for the two 660 MW pulverized coal fired boilers at the power station is approximately 1200 m^3/s. Using ventilation exhaust as combustion air in large boilers requires that the plant and the mine be located within reasonable distances to limit transportation issues so the possibilities are limited while the more flexible internal combustion engines are routinely installed at remote locations.

A gas turbine can be placed near the evasé of the ventilation system fan to draw ventilation air and would be so situated to use the VAM as combustion air. A scrubber located in the air duct to remove any particulates that could damage the internal components of the turbine and air monitoring and fuel-mixing controls will also be required. The variable quality of the methane in the air requires a control system to adjust the fuel flows in order to maintain proper operation of the gas

turbine (Johnson et al, 1998). Gas turbines use a fraction of the incoming air for cooling and the remainder for combustion. A difficulty involving the use of VAM as the cooling air is that the moisture and methane can react at the temperatures found within the gas turbine, to form small amounts of hydrogen, which could lead to hydrogen brittalization (Johnson et al, 1998). The shaft of the turbine can drive an electrical generator to provide power to the local utility grid or the mine, but the design implications involving the turbine metallurgy could be a major drawback. This concept has been determined to be unfeasible resulting the VamTurBurner© design.

Carbureted gas turbines use an external combustor where the reaction is at a lower temperature than standard turbines (Schultz, Mattus and Carothers, 2005). VAM is at too low a methane concentration so a supplemental fuel, which could be gob gas, is used to enrich the fuel to the operating requirement of 1.6 percent by volume. The gas flow is compressed and heated in an exhaust gas recuperator. The typical VAM has a methane concentration well below one percent; thus supplemental fuel will be required during any normal operating of the system.

In 2004, a demonstration project was undertaken at the Appin Colliery Mine. The amount of combustion air required by a gas turbine depends on the ideal fuel air ratio, the flow rate through the compressor-turbine system and the temperatures at various points in the flow. The typical combustion air required to operate a simple cycle gas turbine is approximately 0.003 m^3/s-kW of installed turbine capacity (US EPA 6202J, 2004), so for a 250 kW microturbine the airflow is about 0.7 m^3/s while the more complex combined cycle plants require slightly lower air flows. A 2.5 MW Solar Centaur 3000R turbine was modified to use inlet airflow of about 1.6% methane (Mallett and Su, 2004). These trials were suspended because of technical challenges pertaining to the operation of the gas turbine operation, the gas turbine suffered a failure to start suspected to be on account of the variations in composition of the inlet air, Figure 3.2.2 (Cummings, 2004).

These systems operate at higher levels of fuel concentration, near 4.8 percent, at higher power outputs and only idle at the lower levels of methane quoted, consequently these flows are insufficient to be able to efficiently mitigate methane from an operating mine. Further difficulties arose with the contamination of the mine air having an effect on the operation and stability of the gas turbine, the project was

suspended due to the combustor heat exchange tubing over-heating and failing during start-up.

Figure 3.2.2 Appin collery turbine installation (source, Cummings, 2004)

Estimates have determined that VAM with a 0.5% methane concentration could provide from 4% to 12% of the fuel needed to operate a gas turbine. The operation of the gas turbine of course is dependent on the operating pressures, temperatures, manufacturer selected, ambient conditions and moisture content of the air. Northwest Fuel Development, Inc. demonstrated the technique in the early 1990's, using an air mixture of 0.5% to 1.5% methane in the combustion air. This work formed the basis of further gas turbine experiments.

The FlexEnergy Microturbine was adapted, with a catalytic combustor, to operate on a wide range of fuels, including VAM. The FlexEnergy unit can achieve full power with fuel as low as 1.5% methane or lower at less than full power. The compressor and combustor are contained within a compact turbine module and the hot compressed gases are allowed to expand in the turbine to power the generator (Global Methane Initiative, 2011). A FlexEnergy turbine has been installed at the DCOR oilfield near Santa Barbara, California, to consume oilfield gas at concentrations ranging from 1.5 to 4.2 percent, and another is running on coal process waste gas at the Western Research Institute in Laramie, Wyoming.

Catalytic monolith reactor technology is comprised of a honeycomb shaped monolithic reactor. By virtue of the geometry exceptional flow profiles are realized at a low pressure drop, due to low flow resistance and high mechanical strength. Monoliths consist of a structure of parallel channels with walls coated by a porous support containing catalytically active particles. The methane in the flow is oxidized as it comes in contact with the catalyst media on the substrate of the monolith. Sindicatum acquired the global rights except for Japan until 2019 to use the "CH4MIN" catalytic oxidation technology, see Figure 3.2.3, developed by the Centre for Mineral and Energy Technology (CANMET), a Canadian government energy research organization that is part of Natural Resources Canada (NRCan). Sindicatum performed full-scale testing of this technology during 2008 and 2009 at a location in the US to facilitate the design of a commercial regenerative catalytic oxidizer the first one of which is installed at Duerping coal mine, Shanxi, China.

Figure 3.2.3 The CH4MIN pilot model at CANMET (Courtesy Hristo Sapoundjiev CANMET)

"Ventilation shafts are the largest source of methane emissions from the global coal industry and our technology converts the methane into less harmful carbon dioxide to reduce the climate change impact of the mining operations. The project is currently at the validation stage of the UNFCCC approval process, and is expected to generate 2 million CERs over its life".

There are two separate phases to the project, Phase I is a 2-Can Regenerative Thermal Oxidizer ("RTO") from MEGTEC with a flow rate of 35 m^3/s and a 20 m^3/s CH4MIN Regenerative Catalytic Oxidizer ("RCO") also built by MEGTEC. Two more MEGTEC RTO's are to be installed in phase II. (Sindicatum, 2012).

The project was registered with the UNFCCC in March 2009, and is expected to generate 3.1 million CER's over its life. This is more a case of the CMM use; however, it is discussed as an example of the use of CMM, which would be very useful for use in the proposed VamTurBurner as a supplemental or igniter fuel.

HEL-East Ltd., a world leader in RTO technology based in the United Kingdom, designed constructed and installed a full-scale operational RTO unit on a UK Colliery; the design in Figure 3.2.4 forms the basis of what is anticipated to be the world's largest VAM abatement project expected to be installed in Shanxi, China.

Figure 3.2.4 Hel East VAM abatement RTO design (Courtesy HEL-East)

Biothermica has developed the VAMOX® technology, which oxidizes VAM using the familiar principle of regenerative thermal oxidation (RTO). The BIOTOX® system, which was first commercialized in 1991, is based on the cyclic reversal of the airflow through multiple vessels filled with heat absorbing media to minimize heat losses during the oxidation process, provided the basis of the operating principle for the VAMOX®. According to Biothermica: (Biothermica, 2010)

> *"each ton of methane oxidized by the VAMOX® reduces GHG emissions by approximately 18 tCO_2e. In addition, whenever the VAM concentration is above 0.25%, heat can be recovered as hot water, low grade steam or electricity can be produced from superheated steam".*

This aspect of the technology is in fact similar to the other flow reversal technologies currently on the market. The operational requirement that the methane concentration be at least 0.25% before any heat can be removed is approximately between the lower values and higher values quoted for other CFRR and TFRR systems.

Figure 3.2.5 Biothermica VAMOX® technology (Courtesy, Biothermica 2013)

A VAMOX® system, Figure 3.2.5, has been operational since March 2009 at Walter Energy's Mine in Brookwood, Alabama. This VAMOX® project represents the first VAM abatement initiative at an active mine in America. After four years, the amount of methane mitigated is equivalent to 80,766 tonnes of carbon dioxide.

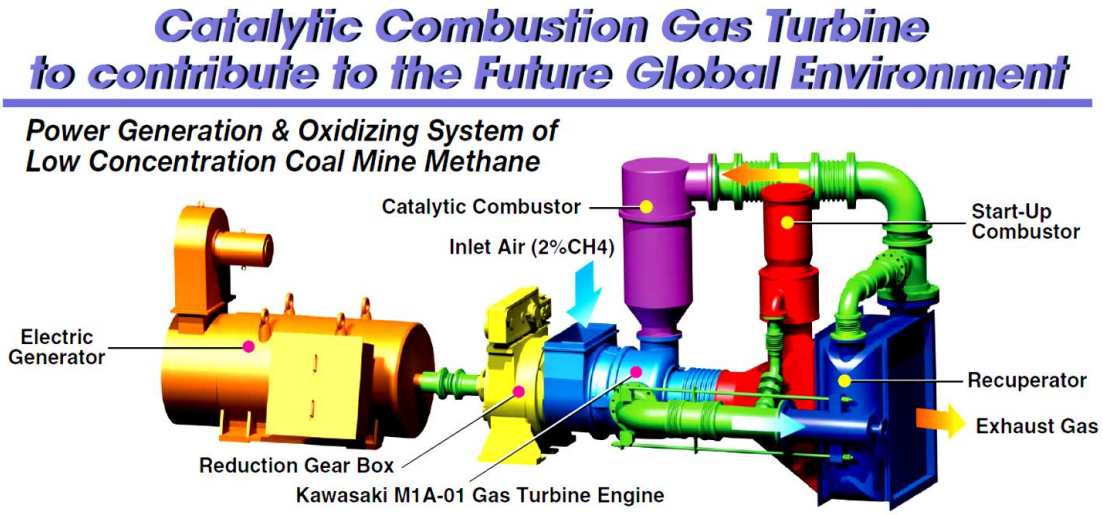

Figure 3.2.6 Kawasaki M1A-01 Gas Turbine Engine KHI System (source, Kawasaki, 2011)

A recently developed technology from Kawasaki, Figure 3.2.6 above, has similarities to the VamTurBurner©, but uses a catalytic combustor. The VAM is preheated through a recuperator before enhancement to 2% methane by the addition of coalmine methane extracted from the seam.

3.3. Comparing existing technologies to the VamTurBurner©.

The main difficulty with the systems using VAM as a primary fuel is the amount of heat available for use as a product is reduced by the percentage needed to sustain the reaction. This is the case for systems such as the CANMET catalytic flow-reversal reactors, the EDL recuperative gas turbine, the CSIRO lean burn catalytic turbine and CSIRO catalytic combustor. Provided there is enough methane available, typically due to the supplementation of the VAM as primary fuel, any of these systems could be combined with ancillary equipment to provide coal drying, heating of water or cooling possibly with an adsorption chiller.

The main limitation of TFRR and CFRR systems is that it is difficult to extract useful energy for power generation, so they generally tend to merely mitigate most of the greenhouse impact of the methane, by oxidizing to carbon dioxide, with the expectation that the economics will be supported by carbon credit trading. The CSIRO catalytic turbine powered with one percent methane is more of a prospective technology rather than one expected to both mitigate the methane and generate electricity. A concentration of one percent or more methane can usually be obtained by combining mine ventilation air methane and drainage gas if it is available at a gassy mine.

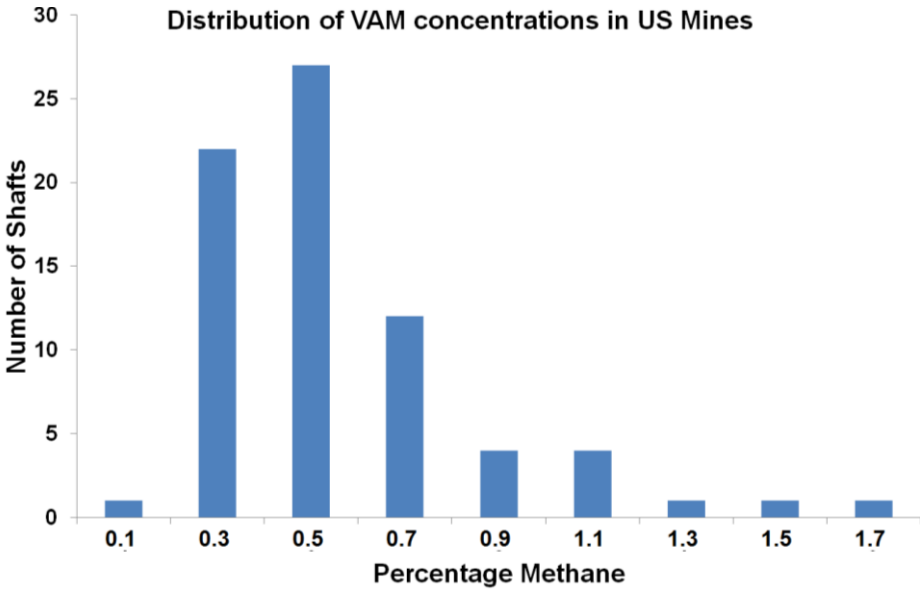

Figure 3.3.1 The CH_4 concentration in VAM for US coalmine shafts (source, USEPA, 2010)

The distribution of the concentration of methane in VAM is shown in Figure 3.3.1 for U.S. underground mines. It is a lognormal distribution with a mode of 0.375 at 25.67

shafts, which shows that about 70% of the US underground mine shafts have methane concentrations above about 0.4 percent. Taking 0.4 to 0.5 as a base level and including the concept of supplementation to target concentrations of 0.9 percent methane is completely reasonable and proven in many projects. The West Cliff technology is demonstrating the use of supplemental CMM to maintain sufficient heat output to generate electric power. WestVAMP oxidizes 70 m^3/s of 0.9 percent methane, maintained at a constant flow rate while mixing drainage gas with the ventilation exhaust airflow. A concentration of 0.2 percent methane is required in order to maintain the system in self-sustaining oxidation mode; therefore, the energy of VAM concentrations exceeding this level can be recovered as thermal energy in the form of hot water or steam. Experience shows that when the VAM concentration in the ventilation air being used by the Vocsidizer™ installation is lower than 0.2 %, the system automatically stops (Zhengzhou Coal Industry (Group) Co., Ltd. 2009).

The VAM/CMM driven internal combustion engine project at the Appin Colliery is representative of the instance where VAM is a supplemental fuel, in both the VAMCAT and FlexEnergy lean-fuel technologies, VAM is the principal fuel, but drained CMM is used as a supplement (Somers and Schultz, 2008). The Centaur 3000R system can operate on a total fuel demand of 1.6% methane in the air entering the turbine, again. It is a mixture of coalmine ventilation air plus methane from other sources such as coal seam drainage. The Kawasaki KHI catalytic combustor system uses a two percent methane concentration, which is attained by mixing available methane or importation of natural gas with the ventilation air.

In virtually all cases, the VAM is supplemented to reach an operational concentration or practical level. When the ventilation air methane used as a primary fuel is often only burned to mitigate the methane and gain carbon credits to be a viable enterprise. This could have consequences as the carbon credit market suffers instability. In the case of VAM, as a secondary fuel, in systems such as at the Appin Colliery or in rotating kiln systems the impact of the addition of extra fuel energy to the system is obvious. For the purposes of this work there may also be a requirement that a supplemental fuel be added to the system; however, these examples are presented as a case for the argument that it is an expectation due to the nature of the ventilation air methane, which is a high airflow rate flow with low methane concentration.

4. Combustion dynamics model for VAM

An analytical model is developed so a straightforward calculation of the temperatures that are required to render the ventilation air methane (VAM) susceptible to ignition along with a calculated value for the temperatures of the reaction products. These calculations enable the determination of the amount of heat required to bring the VAM to the point of ignition and the amount of heat generated by the combustion at the values of methane content in air found in typical VAM.

If it is considered that the rudimentary combustion scenario; fuel is mixed with air and an applied heat flux ignites the mixture immediately thereafter, it could be anything from a campfire to a rocket engine. It is well known that it is quite dangerous to store a fuel premixed with an oxidizer close to or at stoichiometry anywhere, because all it needs to ignite is a spark, like your typical gas barbeque. The solution to this dangerous aspect of combustion is to mix the fuel and oxidizer at the last minute just before ignition so the risk of combustion, in areas where it may be dangerous or difficult to control, is substantially reduced. This is called a diffusion flame, the safety factor is higher but the complexity is increased while the efficiency is reduced. The trick is to be able to mix the fuel and air as fast as possible; thus, a major amount of work has been done on the design of combustion chambers. Since it is proposed that what essentially amounts to a combustion chamber on the end of the ventilation system it must be demonstrated that the safety of the personnel and the mine has been duly considered. Since the concentrations of VAM are legislated to be kept below the flammability limit, one of the essential features of the ventilation design is to provide a ventilation system with the capacity to reduce methane concentrations within the mine to well below the flammability limit for all potential scenarios. However, in some cases when there is a catastrophic failure underground, the system capacity may be exceeded. Ventilation air methane (VAM) is a premixed fuel in the strictest sense using the terminology of combustion engineering, but is usually kept at low enough concentrations to prevent auto-ignition, spark ignition or explosion. The VamTurBurner© design calls for preheating of the methane in advance of the combustion chamber so the notion that a potential

for a flashback may arise or become a concern to the mine ventilation engineer, mine manager or workers from the point of view of the safety of the system. Apart from incompetence during the engineering of the system or blatant disregard of standards, the methane concentration in the ventilation air can vary under normal operation. Potential episodes than can cause increased methane concentration are: a change in atmospheric pressure, a sudden seismic event, unexpected penetration of a previously unknown pocket of gas, ventilation system failure or significant breakdown, alteration of the ventilation airflow or changes in the mining activities. These possible changes are reason for continued vigilance, monitoring and readiness for active intervention of the ventilation system; such that, the system is able to respond in a timely manner should a hazard arise.

An excerpt from The Royal Commission on the Pike River Coal Mine Tragedy

> *"On Friday 19 November 2010, at 3:45pm, the mine exploded. Twenty-nine men underground died immediately, or shortly afterwards, from the blast or from the toxic atmosphere. Two men in the stone drift, some distance from the mine workings, managed to escape.*
>
> *Over the next nine days the mine exploded three more times before it was sealed. There is currently no access to the mine.*
>
> *The commission is satisfied that the immediate cause of the first explosion was the ignition of a substantial volume of methane gas. The commission's report identifies a number of possible explanations for the source of that accumulation of methane, and the circumstances in which it was ignited.*
>
> *Methane gas, which is found naturally in coal, is explosive when it comprises 5 to 15 percent in volume of air. In that range it is easily ignited. Methane control is therefore a crucial requirement in all underground coal mines. Control is maintained by effective ventilation, draining methane from the coal seam before mining if necessary, and by constant monitoring of the mine's atmosphere.*
>
> *The mine was new and the owner, Pike River Coal Ltd (Pike), had not completed the systems and infrastructure necessary to safely produce coal. Its health and safety systems were inadequate. Pike's ventilation and methane drainage systems could not cope with everything the company was trying to do: driving roadways through coal, drilling ahead into the coal seam and extracting coal by hydro mining, a method known to produce large quantities of methane.*
>
> *There were numerous warnings of a potential catastrophe at Pike River. One source of these was the reports made by the underground deputies and workers. For months they had reported incidents of excess methane (and many other health and safety problems). In the last 48 days before the explosion there were 21 reports of methane levels reaching explosive volumes, and 27 reports of lesser, but potentially dangerous, volumes. The reports of excess methane continued up to the very morning of the tragedy. The warnings were not heeded."*

In order for the possibility of a flashback or explosion to occur, defined here as an ignition of methane at the surface by the oxidation system, which propagates back to the workings through the ventilation system, a few variables must conspire to create the dangerous condition. Once the temperature of the VAM has been raised

to a value near the auto-ignition temperature the state of the mixture is changed from a safe flow of low concentration methane to that of a premixed fuel capable of ignition in the presence of a sufficient heat source or spark.

Conditions that create an unsafe circumstance in the ventilation system are:

i. The amount of fuel in the ventilation air must remain at a high enough level to maintain combustion.
ii. The flow rate of the ventilation air bringing the fuel to the combustion zone must be slow enough to allow the flame speed, which would move in the opposite direction, to overcome the flow velocity and propagate back down to the workings.
iii. The variation in the methane concentration must increase enough to cause a significant change in the ignition characteristics of the ventilation.
iv. A design flaw in the flow dynamics could be responsible for a flashback if the design does not provide the dilution required to render the VAM safe.

The proposed VamTurBurner© system is designed to operate in stages, where the premixed VAM enters the system, is subjected to a preheating sequence, mixed with more fuel and burned in a combustion chamber. It is the endeavor of this work to include a discussion on the incorporation of failsafe systems and designs to prevent the system from being susceptible to the flashback event that could occur when a sudden increase in methane concentration, but not the goal of the work, mainly because this is preliminary design. The main causes of sudden flashback in coalmine ventilation system would be due to a large amount of high concentration methane in the upcast of the ventilation air, which would require a larger scale event such as a microseismic event or a sudden release of gas from a confined pocket. Under normal circumstances, the notion of a flame speed associated with VAM would be considered as impossible, but this system produces conditions, which are outside of the normal safety limits of a ventilation system, but are completely safe in the context of the system. In Chapter 2, numerous examples of oxidation systems, all having high temperatures and safely coupled to the ventilation systems are outlined. To appreciate the issues involved with elevating the temperature of the VAM the flame speed for various concentrations of VAM were calculated, based on the combustion theory presented in this chapter, which provides a straightforward analytical solution.

Another aspect of combustion is the potential for acoustic oscillations, which could either disrupt or prevent the system from operating. Some acoustic coupling to the combustion of a flow is by design, as in the case of pulsed rocket engines, or arises through a design failure as in the case of the Alstrom gas turbine, which almost bankrupted the company. Since the components of the ventilation system on the surface are mainly comprised of tubes, the system may be susceptible to sympathetic vibrations in the same way that a church organ produces a sound. In the worst-case scenario, the development of combustion related acoustic vibrations could conceivably destroy the system of tubular devices on the surface or in the least case could become a source of continued acoustic irritation to workers even to the point of being the cause of a work stoppage. It is not within the purview of this work to examine the potential effects that may arise as a result of such combustion interactions, but a reference to the potential for such a problem is made for the sake of completeness. A brief explanation of the process is found in the work of Khanna (2001), the acoustic oscillations occur because instabilities in the heat release rate of the flame can cause pressure fluctuations, which could be in phase with the acoustic pressure fluctuations of the combustor. If this is the case, the amplification of the acoustic pressure oscillations proportionately increases the oscillation in the mass flow rate of the product gasses. A closed loop system occurs with the oscillation in the heat release. The sympathetic oscillations reinforce themselves in amplitude until some friction in the system opposes the growth or the oscillation reaches a limiting value, such as destruction of the tubing, which prevents any further growth. This aspect of the design is better studied as the development of prototypes or full-scale systems are developed.

4.1. Analytical solution for temperature changes

In general, a global reaction is a reaction between an amount of fuel $\boldsymbol{\nu'_F}$ and an amount of oxygen $\boldsymbol{\nu'_o}$ to give combustion products **P** in a single reaction step, represented by the following equation.

Eqn. 4.1. $\boldsymbol{\nu'_F F + \nu'_o O = P}$ *for example;* $\boldsymbol{H_2 + \frac{1}{2}O_2 \rightarrow H_2O}$

The stoichiometric ratio **S**, is that ratio at which all the reactants are consumed. This means that the amount of oxidant present in the reaction is just enough to completely burn the fuel (Khanna, 2001). Air consists of about 21%

oxygen and 79% nitrogen by volume, ignoring argon and trace gasses for the purpose of this point, the equation for a stoichiometric reaction of an air-methane mixture on a molar basis is found in Eqn. 4.10, for a = 3.76 (Khanna, 2001). We use the atomic weights $\boldsymbol{W_i}$ to express the stoichiometric ratio, in the example eight times the amount of oxygen by mass is needed than the amount of fuel for a complete burning with no excess oxygen.

Eqn. 4.2. $$S = \frac{\nu_O' W_O}{\nu_F' W_F}, \textit{ for example, } H_2,\ S_{H_2} = \frac{\frac{1}{2}(32)}{2} = 8, \textit{ for } CH_4,\ S_{CH_4} = \frac{2(32)}{16} = 4$$

For the mass fraction $\boldsymbol{Y_k}$ of a given species **k**, $\boldsymbol{m_k}$ is the amount of mass of **k** divided by the total mass $\boldsymbol{m}$ and it is self-evident that the sum of all mass fractions is unity.

Eqn. 4.3. $$Y_k = \frac{m_k}{m} \quad where; \quad m = \sum_1^k m_k \quad and; \quad \sum_1^n Y_k = 1$$

In a mixture at stoichiometry, the ratio of the mass fractions or the ratio of the fuel to oxygen is $\frac{1}{S}$ so the ratio in the example for the mass of hydrogen to oxygen is ⅛ and for methane ¼. For combustion to occur where all the reactants are completely reacted, to form products, eight and four times as much hydrogen and methane respectively would be needed as oxygen (Turns, 2000).

Eqn. 4.4. $$\left(\frac{Y_F}{Y_O}\right)_S = \frac{1}{S}$$

It is often the case, in a combustion situation, that it is not completely verifiable the mixture is near enough to stoichiometry to efficiently burn, especially in the case of VAM with the further complication of fluctuations in the fuel concentration in the flow. We use the equivalence ratio **ϕ** to resolve this problem. The equivalence ratio is a ratio of ratios; the ratio of the actual fuel to oxidizer ratio to the fuel to oxidizer ratio at stoichiometry. (Bibrzycki and Poinsot, 2010)

Eqn. 4.5. $$\left(\frac{Y_F}{Y_O}\right) / \left(\frac{Y_F}{Y_O}\right)_S = S\left(\frac{Y_F}{Y_O}\right) = \phi$$

In the actual case of a VAM flow, the oxygen is delivered as a fraction of air. We use the fact that nitrogen is generally non-reactive and that the number of moles of nitrogen in air remains constant, **a** = 3.76. For the equivalence ratio **ϕ** the mass fractions and the ratio of the mass fractions are equivalent to the ratio of the molecular weights where 3.76 is the multiplier of the amount of nitrogen in air:

Eqn. 4.6. $$Y_{H_2} + Y_{O_2} + Y_{N_2} = 1$$

Eqn. 4.7. $$\phi = S\frac{Y_{H_2}}{Y_{O_2}}$$

Eqn. 4.8. $$\frac{Y_{N_2}}{Y_{O_2}} = a\frac{W_{N_2}}{W_{O_2}}$$

The mass fractions can then be expressed as functions of the stoichiometric ratio, equivalence ratio and the atomic weights.

Eqn. 4.9. $$Y_{H_2} = \frac{1}{1+\frac{S}{\phi}\left(1+\frac{aW_{N_2}}{W_{O_2}}\right)} \qquad Y_{O_2} = \frac{1}{\frac{\phi}{S}+1+\frac{aW_{N_2}}{W_{O_2}}}$$

Now to apply the concept to a VAM mixture, taking the view that the interest is the concentration of methane, which is not exactly stoichiometric, consequently is not normally a mixture of best ignition potential; however, if the safety protocols are neither in place nor adhered to the consequences can be devastating (Panckhurst Hon Justice, Bell and Henry 2012).

The concern is that will be the temperature conditioning of a premixed flow of methane entering a combustion chamber have any potential for a flashback down the ventilation system. The balanced first order combustion equation or global reaction is shown below.

Eqn. 4.10. $$CH_4 + 2(O_2 + aN_2) \rightarrow CO_2 + 2H_2O + 2aN_2$$

Eqn. 4.11. $$Y_{CH_4} = \frac{1}{1+\frac{S}{\phi}\left(1+\frac{aW_{N_2}}{W_{O_2}}\right)} = 5.5\%$$

Calculation of the mass fraction of methane at stoichiometry for **S** = 4 and $\phi = 1$, obtain a methane concentration of 5.5% mass fraction is obtained or 9.52% volumetrically. This means that for methane in air the perfect stoichiometric ratio exists when a mixture contains 5.5% CH_4 that is the methane concentration in air where the slightest spark would ignite the mixture. The behaviour of the mixture at stoichiometry is the concentration of concern for a flashback down the ventilation system. A mixture with 5.5% methane could possibly occur under rare conditions such as an air blast or seismic event and would need to be detected prior to reaching the combustion system. According to the UK The Coal Mining History Resource Center, there have been an estimated 164,356 UK coal mine accident related deaths, from 1700 to 2000, which illustrates the seriousness of the need for an

understanding of the methane at the mine and the control of methane concentrations in the mine and ventilation systems.

To proceed with the thermodynamic calculations it is instructive to note it is assumed that ideal gasses are expected. For circumstances which dictate otherwise the gas must be at very high temperatures (>5000 K) the regime of plasmas or very high pressures (>100 bar) the regime of supercritical flow. These are the domain of devices such as rockets or high temperature plasma cutting apparatus. Since it is expected that in gas turbines the constriction that the temperatures and pressures are commensurate with maintaining the flow stability and within ranges amenable to the materials remaining structurally sound, it is reasonable to make the ideal gas assumption.

There are a number of species in any combustion scenario, those at the start, those created as the reaction proceeds and the resultants. As the combustion proceeds, the number of species is dependent on physical variables such as the temperature and pressure during the reaction; thus, are different for the same starting species depending on whether the reaction is confined or in a free space. Most fuels are multispecies for example gasoline or kerosene contains in the neighborhood of at least 300 species. Generally speaking, it is a multispecies of ideal gasses so the thermodynamic constants such as the specific heat capacity and thermal conductivity are often considered as constants; however, they must be considered as variables in the temperature range of interest because these values are used in all calculations.

The main species of interest in combustion are H_2, O_2, C and N_2, although they may start as CH_4, the molecules are dissociated heat of the reaction increases and often undergo ancillary reactions as individual diatomic gasses, but will also undergo reactions as compounds. The reactions that occur during a combustion sequence are also often reversible; thus, a species partial pressure or concentration can vary in a nonlinear fashion as the sequence proceeds to completion. This can lead to very complicated modeling involving tens to hundreds of equations. Considering the complexity of such situations and the computing power required to solve a sequence, approximations are often made to solve a sequence to a reasonable degree of accuracy, for example the a 4-step chemical kinetic

mechanism listed in Eqn. 4.12, Eqn. 4.13, Eqn. 4.14 and Eqn.4. 12, is frequently used in combustion modeling (Jones and Lindstedt, 1988).

Eqn. 4.12. $C_nH_{2n} + {}^{n}/_{2}\,O_2 \rightleftharpoons nCO + (n+1)H_2 \quad \rightarrow \quad CH_4 + {}^{1}/_{2}\,O_2 \rightleftharpoons CO + 2H_2$

Eqn. 4.13. $C_nH_{2n} + nH_2O \rightleftharpoons nCO + (2n+1)H_2 \quad \rightarrow \quad CH_4 + H_2O \rightleftharpoons CO + 3H_2$

Eqn. 4.14. $H_2 + {}^{1}/_{2}\,O_2 \rightleftharpoons H_2O$

Eqn. 4.15. $CO + H_2O \rightleftharpoons CO_2 + H_2$

For each species, the atomic weight W_k is specified in kg/mole and the partial density $\rho_k = \rho Y_k$ or the mass fraction Y_k is the partial density over the total density ρ_k / ρ. So since gas is considered as an ideal gas the partial pressure is given by the ideal gas equation $P_k = \rho_k(R/W_k)T$ and clearly the value of $(R/W_k) = r_k$ is unique for each species. Consideration of the specific heat capacity can be made for each species by looking at the molar heat capacity $C_{pk}^m = C_{pk}W_k$, and since it is usually a diatomic gas the $C_{pk}^m = \frac{7R}{2} = 28.8$, for low temperatures, so for our typical gasses the value of the specific heat capacity is calculated for oxygen having a molar mass of 0.032 kg/mole.

Eqn. 4.16. $C_{pk} = {}^{C_{pk}^m}/_{W_k} = {}^{28.8}/_{.032} = 900\frac{J}{mole}K$

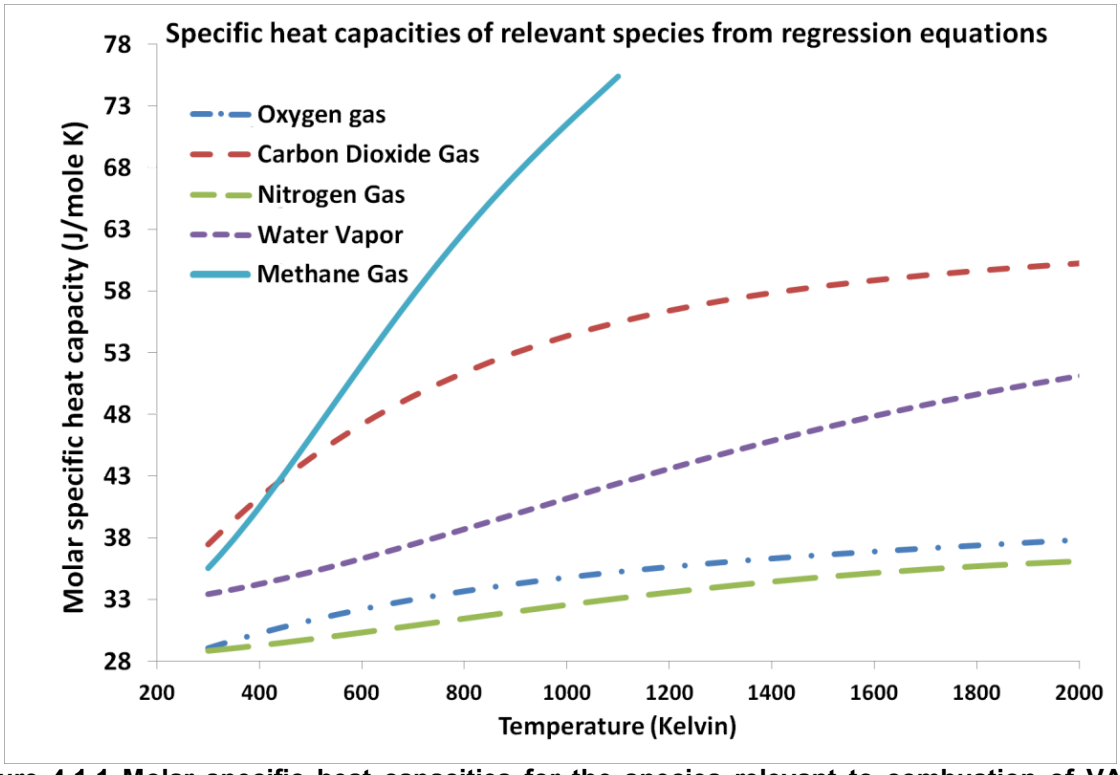

Figure 4.1.1 Molar specific heat capacities for the species relevant to combustion of VAM, adapted from JANAF tables.

The calculated values give the specific heat capacity at the initial Kelvin temperature and are only valid for low temperatures. The issue that arises in calculating the adiabatic flame temperature of combustion sequences is that the specific heat capacity and enthalpy are not constant. The reactants dissociate to multiple species and form other species not present in the reactants or in the combustion products. The specific heat capacity variation with temperature is shown in Figure 4.1.1 over the temperature range from a typical initial temperature of 300 K up to 6000 K or the temperature range of interest in the combustion dynamics expected in the oxidation of VAM. It is important to note that the increase in dissociation of diatomic gasses over 1500 K becomes significant and affects the specific heat in such a manner as to become a combination of diatomic and monatomic gasses, eventually progressing to predominantly monatomic species at temperatures that are higher than relevant to these calculations. In Figure 4.1.1 the specific heat capacities for the temperature ranges of interest used to determine the values used in the model were derived from the polynomial regression curves for oxygen, nitrogen, water vapour, carbon dioxide and methane.

The polynomials are sixth order and the coefficients are 30 digit accuracy, this was required to yield a near perfect statistical fit to the data. A lesser degree polynomial may be used, but does not provide the accuracy desired, even the parabolic version has an R^2- value of 0.9988. However, the high level of confidence attached to the higher degree function is practical over the larger temperature ranges for all the species except for methane, which only includes data up to 1100 K since the auto-ignition temperature of methane combustion is 810 K (Robinson and Smith, 1984). The equations may now be used to represent the specific heat capacity at a given temperature in further calculations where the need to account for the variation of C_{pk} over a temperature range is justified.

These are also the subject of advanced modeling codes, which are necessary for calculating details of the species interactions during the reaction, but not required when using a global or single reaction concept for the calculation. The analytical model developed for this work is a straightforward calculation of the adiabatic flame temperature, resulting from the various degrees of pre-heating required to produce reaction products, at the values of methane content typically found in ventilation air.

The enthalpy in elementary physics is often written simply as $\Delta h = C_p \Delta T$, but in combustion analysis the enthalpy is comprised of two components (i) the energy required to create a complex molecule, or the enthalpy of formation, and (ii) the sensible enthalpy due to the change in temperature of the species. The enthalpy of formation is evaluated at $\mathbf{T^0}$, which is either specified at 0 K or 298.15 K by definition. The generalized enthalpy, in terms of the two components, is written in Eqn. 4.17, (Poinsot and Veynante, 2005) including the molar enthalpy or the enthalpy for one mole of a substance, which is simply $\boldsymbol{h_k W_k}$, the enthalpy multiplied by the molar mass. The enthalpy of formation for diatomic species is defined as zero.

Eqn. 4.17. $$h_k = \Delta H^0_{f,k} + \int_{T^0}^{T} C_{pk}\, dT \; ; \; h^m_k = h_k W_k = \Delta H^0_{f,k} W_k + \int_{T^0}^{T} C_{pk}\, W_k dT$$

In combustion sequences, there may be a distribution of temperatures throughout the mixture as the combustion proceeds through the system of species. To simplify the calculations it is reasonable and within the bounds of observations over the scales of this combustion system to assume that, the temperature at any given time is constant throughout the domain of the problem. This is an acceptable assumption for situations of less complexity as is the case for VAM and leads to the following relationship, see Eqn. 4.18, for the mean atomic weight of the mixture. The mass fraction $\boldsymbol{Y_k}$ and the molar fraction $\boldsymbol{M_k}$ for the individual species are linked; the mass fraction can be written as seen in Eqn. 4.18 where the mean atomic weight of the mixture **W** is not a constant. This is because **W** is one value in the fresh mixture and becomes a different value as the mixture is burned, because the concentration of the various species changes as the reaction proceeds (Poinsot and Veynante, 2011).

Eqn. 4.18. $$Y_k = \frac{M_k N_k}{WN} = \frac{W_k}{W} X_k \; ; \; \sum Y_k = 1, \; so, \; \sum \frac{W_k X_k}{W} = 1 \; \therefore W = \sum_1^n W_k X_k$$

Since the mean atomic weight depends on the concentration or distribution of species, which is changing as the reaction proceeds, the mean atomic weight also changes as the reaction proceeds.

4.2. Mixtures

For a mixture such as VAM, the pressures, densities and temperatures are defined by the ideal gas law, the plural is used to indicate that in the general case

the mixture contains a distribution of these physical variables. Since the gas mixture is an ideal gas composed of ideal gasses, the total values as the sum of the partial values for pressure **P**, and density $\boldsymbol{\rho}$ can be expressed as in Eqn. 4.19, but continue to follow the assumption that the temperature is singular for all species in the mixture.

Eqn. 4.19. $\boldsymbol{\rho = \sum_1^n \rho_k \; and \; P = \sum_1^n P_k \; and \; T = constant}$

It is often convenient to perform calculations using the mass fraction instead of the molar fractions, consequently the expression for the sum of the partial pressures is written below in Eqn. 4.20 and when the ideal gas law **P = ρrT** is used the following expression for the molecular weight of the mixture is obtained in terms of the mass fractions.

Eqn. 4.20. $\boldsymbol{\sum P_k = \sum \rho_k \frac{R}{W_k} T \; where \; \rho_k = \rho Y_k}$

Eqn. 4.21. $\boldsymbol{\frac{1}{W} = \sum_1^n \frac{Y_k}{W_k}}$

The data in Table 4.2-1 are useful values of the enthalpy of formation and atomic weights for relevant species of interest in the burning of VAM. Although the ventilation air from the mine would contain various other constituents, such as: ethane, butane and coal dust all of which are combustible the main component is methane.

To calculate the adiabatic flame temperature, a global reaction is used for an initial mass of $\boldsymbol{M_k}$, with a methane concentration of $\boldsymbol{Y_k^1}$ at $\boldsymbol{T_1}$. The mass remains constant, but the constituents become $\boldsymbol{Y_k^2}$ the new concentration after burning and the mixture will have attained a temperature of $\boldsymbol{T_2}$, the adiabatic flame temperature. The initial temperature is of great significance, because the ignition of the mixture is strongly influenced by the initial temperature of the mixture and will be discussed in more detail as this dissertation unfolds.

A flame proceeds as a front or membrane where the chemical kinetics occurs. In the initial stage are the fresh gasses, the intermediate species are where the reactions take place and the final stage is where the products reside. The speed of the reaction is a direct consequence of the chemical kinetics of the reaction while the thermo chemistry deals with the initial and final states, which as mentioned earlier is the global reaction approach taken in this chapter.

Table 4.2-1 Enthalpy of formation and atomic weights for relevant species of interest in the burning of VAM (Poinsot and Veynante, 2011)

Species	W_k	$\Delta H_{f,k}^{0}\left({}^{KJ}/_{Kg}\right)$	$\Delta H_{f,k}^{0,m}\left({}^{KJ}/_{mole}\right)$
CH_4	0.016	-4675	-74.8
H_2O	0.018	-13433	-241.8
O_2	0.032	0	0
H_2	0.002	0	0
CO_2	0.046	-8554.54	–393.509

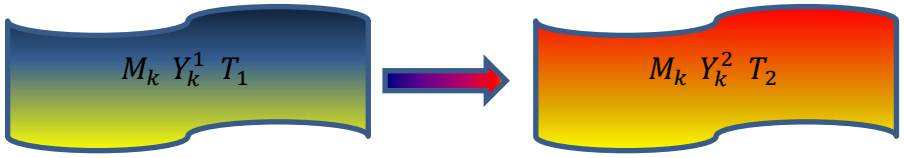

Figure 4.2.1 A diagrammatic representation of a fresh gas reacting to become the product gas.

For example, it is normal to heat up the mixture before combustion in a combustion engine or gas turbine, the temperatures of the pre-mixture could be from 300 K to 900 K. To perform the calculation an accounting of the species is required in order to use the global reaction concept, employed here for simplicity, which leads to the result that all the species in the pre-mixture are converted to the new species through a single reaction. All the species at $\boldsymbol{v_k'}$ and $\mathbf{T_1}$ in the fresh gasses react to produce the gasses $\boldsymbol{v_k''}$ at $\mathbf{T_2}$ in the burned mixture.

Eqn. 4.22. $\sum \boldsymbol{v_k' M_k} \rightarrow \sum \boldsymbol{v_k'' M_k}$

A new variable is defined for computational convenience, $\boldsymbol{v_k} = \boldsymbol{v_k''} - \boldsymbol{v_k'}$ is used to indicate the molar or mass balance of the reaction equation, it is tabulated for the reaction in Eqn. 4.10; note the values for the non-reacting nitrogen remain constant.

To compute the temperature $\mathbf{T_2}$ it is assumed that the pressure is constant, as such the total enthalpy is conserved. Even though the fresh gas species at $\mathbf{T_1}$ evolve to different species in the products at $\mathbf{T_2}$ the conservation of enthalpy $\mathbf{H(T_1) = H(T_2)}$ occurs because it is assumed that the reaction is at constant pressure (Poinsot and Veynante, 2005). The reaction is very sensitive to the initial temperature of the reactants, which is the reason why the fuel mixture in a gas turbine or internal combustion engine is pre-heated and then compressed just prior to ignition. The

equations for molar enthalpies include the enthalpy of formation for the species or products and the integral of the specific heat capacity from $\mathbf{T_1}$ to $\mathbf{T_2}$. It is helpful to remind the reader that in most physics calculations this is simply the familiar $\mathbf{Q = mC_p\Delta T}$, the enthalpy of formation is ignored because it is the same for both states i.e., the only change is the temperature, sometimes including a phase change, but with no change in species so the calculation is a straightforward heat balance. The following set of equations appears somewhat more complex, but can be equated due to the conservation of enthalpy and because the reaction is carried out at constant pressure, the $\boldsymbol{C_{pk}^m}$ are also assumed to be constant.

Table 4.2-2 Molar balance for the global methane oxidation reaction

	CH_4	O_2	N_2	CO_2	H_2O
$\upsilon_k'(T_1)$	1	2	2a	0	0
$\upsilon_k''(T_2)$	0	0	2a	1	2
υ_k	-1	-2	0	1	2

Eqn. 4.23. $$\boldsymbol{H(T_1) = \sum_1^n \nu_k' \left(\Delta H_{f,k}^{0,m} + \int_{T^0}^{T_1} C_{pk}^m dT\right) = H(T_2) = \sum_1^n \nu_k'' \left(\Delta H_{f,k}^{0,m} + \int_{T^0}^{T_2} C_{pk}^m dT\right)}$$

The only unknown in Eqn. 4.23 is $\mathbf{T_2}$, taking into account that the individual species have enthalpies of formation and that the reactions have a heat of reaction, which is a function of the enthalpies of reaction for all the species involved in the reaction. Then by assuming constant $\boldsymbol{C_{pk}^m}$ is a function of temperature and rearranging Eqn. 4.23, the solution for the final temperature is given as Eqn. 4.24, below where $\boldsymbol{Q^m}$ is the molar heat of the reaction. The molar heat of reaction is due to the all the species involved in the global reaction, see Table 4.2-1 for selected molar heat of reaction pertinent to this work. It is important to distinguish between the heat of reaction, which is the heat due to the entire reaction whereas the species have enthalpies of formation.

This method of calculating the adiabatic flame temperature assumes constant values for the molar specific heat capacities at constant pressure and a fuel oxidizer mixture of stoichiometry. The reactants and products exist at different temperatures at the start, during and at the completion of the reaction. The values for the specific heat capacities over a range of 300 K to 6000 K except that the range for methane is only from 300 K to 1100 K were used to determine the regression equations used in

the spreadsheet calculations, shown graphically in Figure 4.1.1 for the range of interest 300 K to 2000 K. The range of temperatures expected for the reactant species or fresh gas could vary from 300 K to nearly 900 K depending on the amount of energy added during the preheating phase. The value of the temperature used to determine the molar specific heat capacity, required in the model for the reaction products, could vary from the initial temperature of the reactant species 300 K to the final adiabatic flame temperature. However, it has been found by comparison to the results obtained using advanced numerical modeling that an intermediate value provides the best estimate of the adiabatic flame temperature to be determined. The appropriate value for the specific heat capacity of the reactant species is of course the initial temperature. Initial temperatures for the reaction in Figure 4.2.2 range from 300k, the initial temperature for no preheating, to 1100 K an overheated value. Using Eqn. 4.24, the adiabatic flame temperature for the expected VAM mixtures is expanded in Eqn. 4.25 to include the specific species of the global reaction described in Eqn. 4.10.

Eqn. 4.24. $$T_2 = T_0 + \frac{\sum_1^k \nu_k' C_{p,k}^m (T_1 - T_0) + Q^m}{\sum_1^k \nu_k'' C_{p,k}^m} \; ; \; Q^m = \sum_1^k (\upsilon_k' - \upsilon_k'') \Delta H_{f,k}^{0,m} = \sum_1^k \upsilon_k \Delta H_{f,k}^{0,m}$$

Table 4.2-3 Example of the convergence of the calculated adiabatic flame temperature to the final value of temperature corresponding to that used to calculate the specific heat capacity. The final temperature of 1788.077 K is the temperature the model converges to as the temperature of the final products is increased

Species		H_2O	O_2	CH_4	CO_2	N_2	
molar specific heat capacity at							
T_1 = 300 K	$C_p^m(T_1)$	33.430	29.055	35.5404	37.186	28.840	J/mole K
T_2 = 1788.077 K	$C_p^m(T_F)$	49.526	37.349	75.389	59.539	35.665	J/mole K

Eqn. 4.25. $$T_2 = T_0 + \frac{\left(C_p^m(CH_4) + 2C_p^m(O_2) + 2aC_p^m(N_2)\right)(T_1 - T_0) + Q^m}{\left(C_p^m(H_2O) + C_p^m(CO_2) + 2aC_p^m(N_2)\right)}$$

The adiabatic flame temperature, calculated for a range of pre-heating temperatures using this model, is presented as a family of curves in Figure 4.2.2 for the initial fresh gas temperatures ranging from 300 K up to 1100 K. The values of the molar specific heat capacities, were calculated at the initial temperature of the fresh gasses. The values of the molar specific heat capacities of the product gasses were varied from the initial temperature of the fresh gasses to the temperature at which the evaluation temperature being considered converged to the same value as

the adiabatic flame temperature. For example, in Table 4.2-3 below are values used to plot the curve for the initial temperature of 300 K; the molar specific heat capacities of fresh gasses are calculated at $\mathbf{T_1}$ and remain constant throughout the remainder of the calculation. The value at $\mathbf{T_2}$ is determined by performing an iteration of the difference between the calculated temperature and the evaluation temperature until the difference converges to zero, then the evaluation temperature and the adiabatic flame temperature are identical.

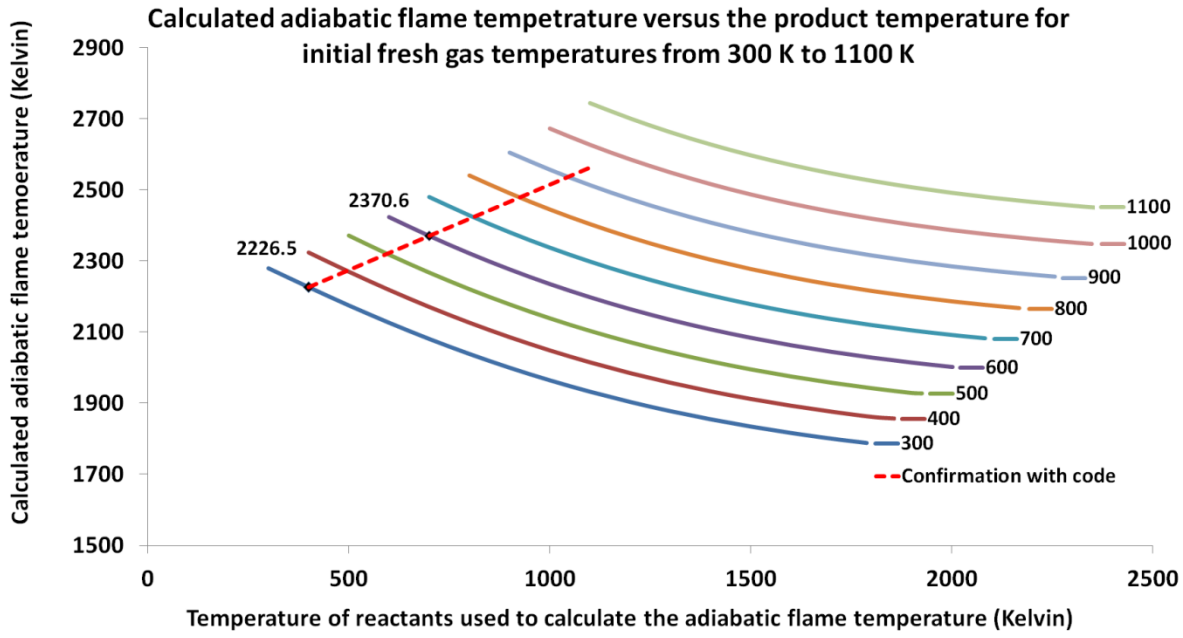

Figure 4.2.2 Adiabatic flame temperature calculated using the molar specific heat capacities for the fresh gasses, evaluated at the initial temperature of the fresh gasses versus the temperature at which specific heat capacities of the product gasses were evaluated.

In Figure 4.2.2, the two values used to define the dashed line are the calculated adiabatic flame temperature of 2226.5 K on the 300 K curve and 2370.6 K on the 600 K curve. These correspond well to the values of 2225 K for an initial temperature of 298.15 K and 2367 for 600 K (Frenklach et al, 1995) obtained by calculating the adiabatic flame temperature of stoichiometric methane-air flames using an equilibrium code, EQUIL of the CHEMKIN package, and all species of GRI Mechanism. The intersection of the dashed line with the family of curves at each initial temperature provides the temperature at which the specific heat capacity that is used to obtain the best estimate for the adiabatic flame temperature over the full range of initial temperatures.

The GRI Mechanism contains significantly more species than the model used in the calculations performed with the model in this work; however, the agreement is encouraging given the simplicity of the model used here compared to the complexity of the numerical code used in the calculations by Frenklach et. al, provided the value of the specific heat capacity used in the calculation is evaluated at the temperature near the dashed line spanning the curves in Figure 4.2.2. Observing the intersection of the linear extrapolation for these values extending to intersect the remaining curves suggests the simple supposition that the best values of the adiabatic flame temperature are calculated using the molar specific heat capacity of the product species approximately 100 K above the initial fresh gas temperature.

4.3. An argument for pre-heating of the VAM flow

To establish a framework for the expected concentrations encountered in VAM and consider using the model to predict preheating temperatures capable of yielding a fresh gas state amenable to oxidation the model must be recast in terms of the equivalence ratio. Taking Eqn. 4.25 for $\mathbf{T_2}$, the adiabatic flame temperature and introducing the equivalence ratio $\boldsymbol{\phi}$ from Eqn. 4.7, the adiabatic flame temperature is developed for the case of mixtures at less than stoichiometry or $\boldsymbol{\phi} < 1$.

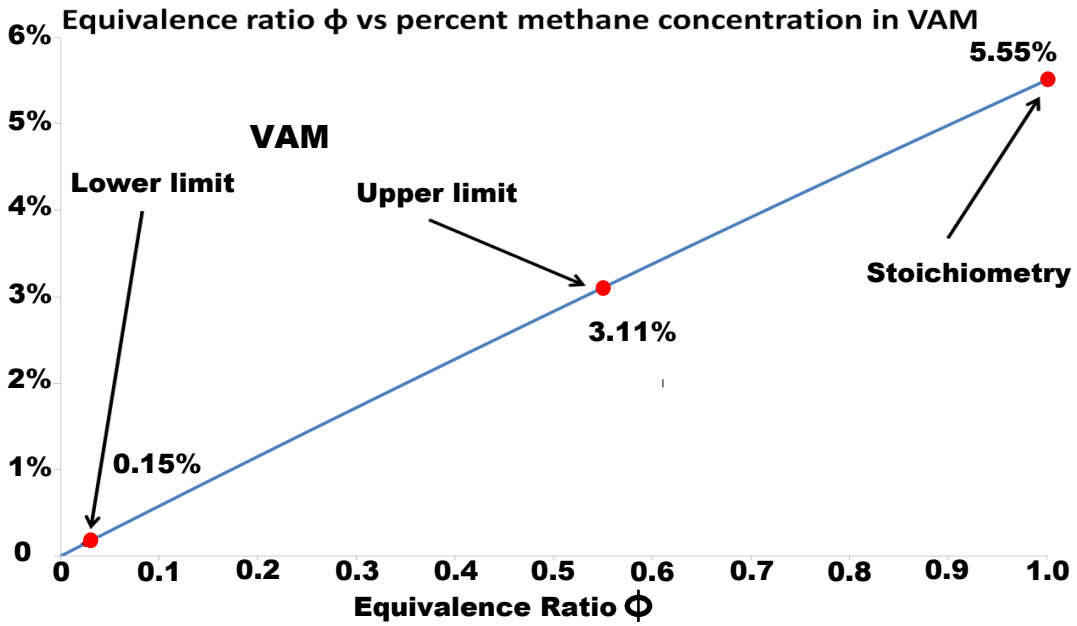

Figure 4.3.1 The zone of potential VAM available to the VamTurBurner © expressed as the equivalence ratio for ϕ from zero to unity

Eqn. 4.26. $$T_2 = T_0 + \frac{(\phi C_p^m(CH_4) + 2C_p^m(O_2) + 2aC_p^m(N_2))(T_1 - T_0) + \phi Q^m}{\left(2\phi C_p^m(H_2O) + \phi C_p^m(CO_2) + 2aC_p^m(N_2) + 2(1-\phi)C_p^m(O_2)\right)}$$

The values of the methane concentration for VAM under consideration are from 0.15%, corresponding to ϕ =0.025, to 3% an upper limit corresponding to ϕ, =0.6, which is actually encountered occasionally in mines today. The legislated limits for maximum methane concentrations for Germany, the UK, France, Spain and the USA are; 1.0%, 1.25%, 2.0%, 2.5% and 3.0% respectively (Noack, 1998). The region of equivalence ratio for the percentage concentrations of methane in VAM is shown in Figure 4.3.1. With these ranges and the formulation of Eqn. 4.26, the family of curves for the fresh gas pre-heating temperatures from 300 K to 900 K versus the equivalence ratio is constructed. The data in Figure 4.3.1 establishes the boundaries of viability for the VamTurBurner©. Large eddy simulation (LES) numerical modeling, described in Chapter 5, is used to establish the pre-heating temperature needed for the system operational parameters. The amount of pre-heating required to produce an adiabatic flame temperature, near the auto-ignition temperature of methane, is dependent on the equivalence ratio and taken as a guide for the system design. From the data in Figure 4.3.2 it can be seen that an auto-ignition temperature is reached for the 300 K initial fresh gas temperature at an equivalence ratio of about 0.3 and that if fresh gas is preheated to a temperature of 900 K. The adiabatic flame temperature near the auto-ignition temperature is achieved at an equivalence ratio of about 0.025. These results are promising and suggest that the more advanced LES modeling will determine the combustion dynamics of pre-heated VAM auto-ignition. The amount of thermal energy available from the system is dependent on both the methane concentration and the energy per unit mass, or calorific value of for methane. These values are used to obtain the power of a combustion system, by establishing a flow rate it is found by the product of the calorific value and the flow rate or $\boldsymbol{P(MJ) = Q\dot{m}}$.

At typical flow rates and some selected methane concentrations, the available power added to the operating power of a cogeneration system coupled to a combustion chamber, is calculated. Using a density of 0.68 kg/m^3 and the value of 55.64 MJ/kg as the calorific value for methane the potential thermal energy available and equivalent conversion mitigation, calculated for some typical VAM

concentrations at some typical ventilation flow rates, for a coalmine ventilation system.

Eqn. 4.27. $$Q = {Q^m}/{W_F} = -\sum_1^k \nu_k \Delta H_{f,k}^{0,m};\ so,\ \frac{\{-2(-285.8)+1(393.509))-1(-74.8)\}}{0.016} = 55.64 \frac{MJ}{kg}$$

It becomes quite clear, from the calculations in Table 4.3-1 that although a challenging undertaking the benefit of utilizing the energy contained in VAM would be economically beneficial. The VAM mitigation systems available today depend on the use of reverse flow reactors to burn all the VAM or internal combustion engines to partially burn the VAM. These systems have their drawbacks, which are expected to be overcome using the VamTurBurner© technology.

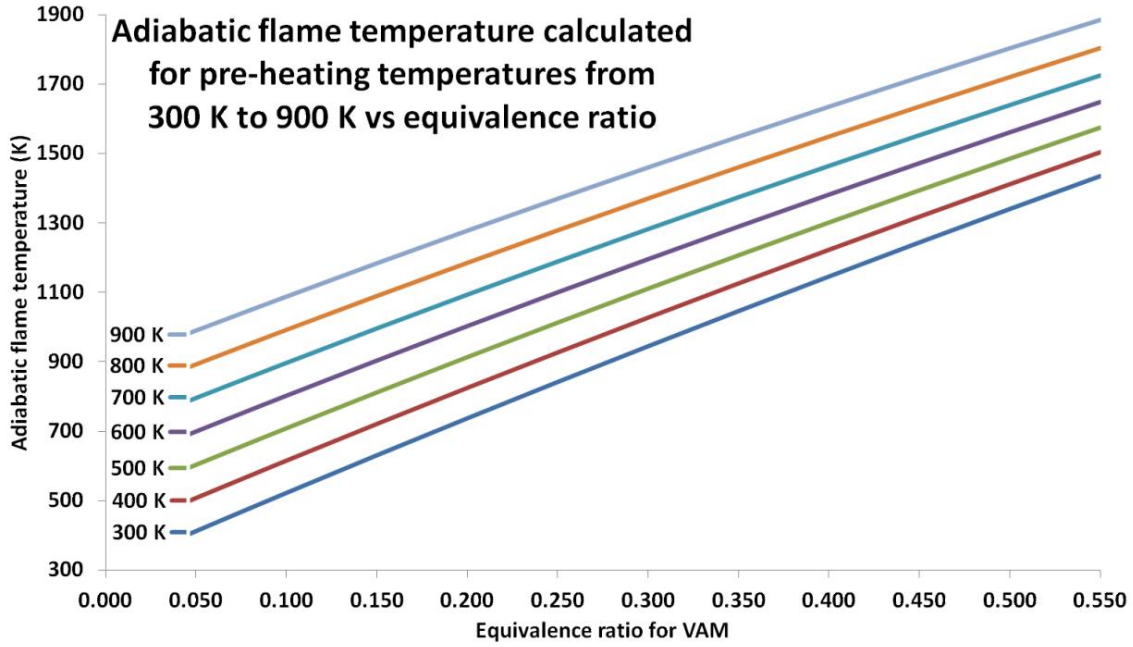

Figure 4.3.2 Adiabatic flame temperature calculated for the equivalence ratio of methane expected in ventilation air and for a range of pre-heating temperatures of the fresh gasses of 300 K to 900 K

The problem of ignition of a low concentration methane air mixture and the pre-heating required to accomplish it are the elements that determine if a system such as the proposed VamTurBurner© is feasible. A variable of interest is the ignition time as a function of the preheat temperature. The ignition time of the premixed methane-air system depends quite heavily on the temperature of the fresh gas compared to the activation temperature. The activation temperature of methane is given as 840 K (Robinson and Smith, 1984). The heat flux is calculated by taking the mass flow of methane calculated from the ventilation flow and VAM

concentration with the calorific value as calculated in Eqn. 4.27. The relationship defining the ignition time t_{ig} is based on assuming a sphere of premixed fuel and oxidizer has a heat flux incident on the mixture. The diffusion of heat into the volume of premixed fuel and oxidizer raises the temperature and once the ignition temperature is attained combustion occurs; thus, the relationship involves the thermodynamic properties of a methane-air mixture such as the thermal conductivity, density and specific heat capacity. These values were calculated for the case of a 100 m^3/s flow at 0.5% VAM.

Table 4.3-1 Power available and carbon dioxide equivalence for mitigation of various typical methane concentrations in typical ventilation flows of a coal mine (Cluff, Kennedy and Bennett 2013)

Ventilation flow rate (m^3/s)	Methane concentration (%)	Methane mass flow kg/s	Methane tonnes/yr	Conversion to carbon dioxide tonnes/yr	21 times equivalent carbon dioxide tonnes/yr	Power (MW)
50	0.2	0.068	2144	5897	39136	3.77
100	0.5	0.34	10722	29486	195681	18.87
150	0.5	0.51	16083	44289	293521	28.30
300	1.0	2.04	64333	176917	1174085	113.22

Eqn. 4.28. $$t_{ig} = {}^{\pi}/_{4}\ \kappa\rho C_P \left(\frac{T_{ig} - T_o}{q}\right)^2$$

The ignition times indicate that the delay encountered for ignition is of the order of microseconds. These times suggest that at the ventilation air flow rates of nominally 1.8 m/s the VAM flow would not extend beyond the fiducial volume of the igniters prior to the mixture undergoing the required ignition.

The relation in Eqn. 4.29 is a generalized reaction for species reacting in a combustion scheme to create reaction products; the reversibility is most often related to the temperature, but can be dependent on catalysis.

Eqn. 4.29. $$\sum_{k=1}^{n} v' k_j M_k \rightleftarrows \sum_{k=1}^{n} v'' k_j M_k$$

The nature of combustion modeling is very complex because it combines the concepts of computational fluid dynamics (CFD), accounting for five equations with five unknowns with the chemical kinetics, which may account for upwards of 300 equations. The five equations involving CFD include the continuity equation, the three momentum equations and an energy equation. Considering that the continuity

equation in Eqn. 4.30, which also appears in the large eddy simulation discussed later, is usually a simple statement of the conservation of mass, but in combustion, the composition or mass fraction of all the components in the gas is taken into account this is known as the species equation (Poinsot and Veynante, 2011).

Eqn. 4.30. $$\frac{\partial \rho Y_k}{\partial t} + \frac{\partial}{\partial x_i}\left(\rho\left(u_i + V_{k,i}\right)Y_k\right) = \dot{w}_k \; where \; \sum_{k=1}^{n} \dot{w}_k = 0$$

The first term describes how the mass of the key species is changing, followed by the flux due to convection, the diffusion velocity of species k and finally the reaction rate of species k. Therefore, it is seen that in combustion the continuity equation takes into account the reactions, species creation and destruction, as well as the transport of species. So in the case of VAM, the methane mixture comes in at one end, combustion is forced due to the addition of a heat flux, carbon dioxide and water comes out the exit at higher temperatures, which is all described through the reaction rate. The totality of the species reduces to the continuity equation, which is summed over all species and so is the same whether combustion is involved or not as it is simply the mass flow.

Eqn. 4.31 is essentially a statement of the velocities of the species and again is not any different whether combustion is present or not, so the momentum accounts for three equations or the velocity in three dimensions (Poinsot and Veynante, 2011).

Eqn. 4.31. $$\frac{\partial \rho u_i}{\partial t} + \frac{\partial \left(\rho u_i u_j\right)}{\partial x_j} + \frac{\partial \rho}{\partial x_i} = \frac{\partial \tau_{ij}}{\partial x_i} \quad for\, i = 1, 2, 3$$

In general, a combustion reaction will contain many species and reactions, which are occurring and reversing amongst these species, the reactions range from molecular creation and destruction to dissociations, a generalized reaction is written as Eqn. 4.29 to represent that the reaction can occur in either direction often depending on the temperature and reaction rate $\dot{w}_k$.

Since the generalized concepts of combustion can lead to very large systems of equations, it becomes necessary to determine what level of complexity is required for the task. Since only the basic design features are being considered, a simplified model is desired for the calculations and propositions at this stage; however, it is instructive to elucidate the reader to the complexity involved by describing the terms in Eqn. 4.32.

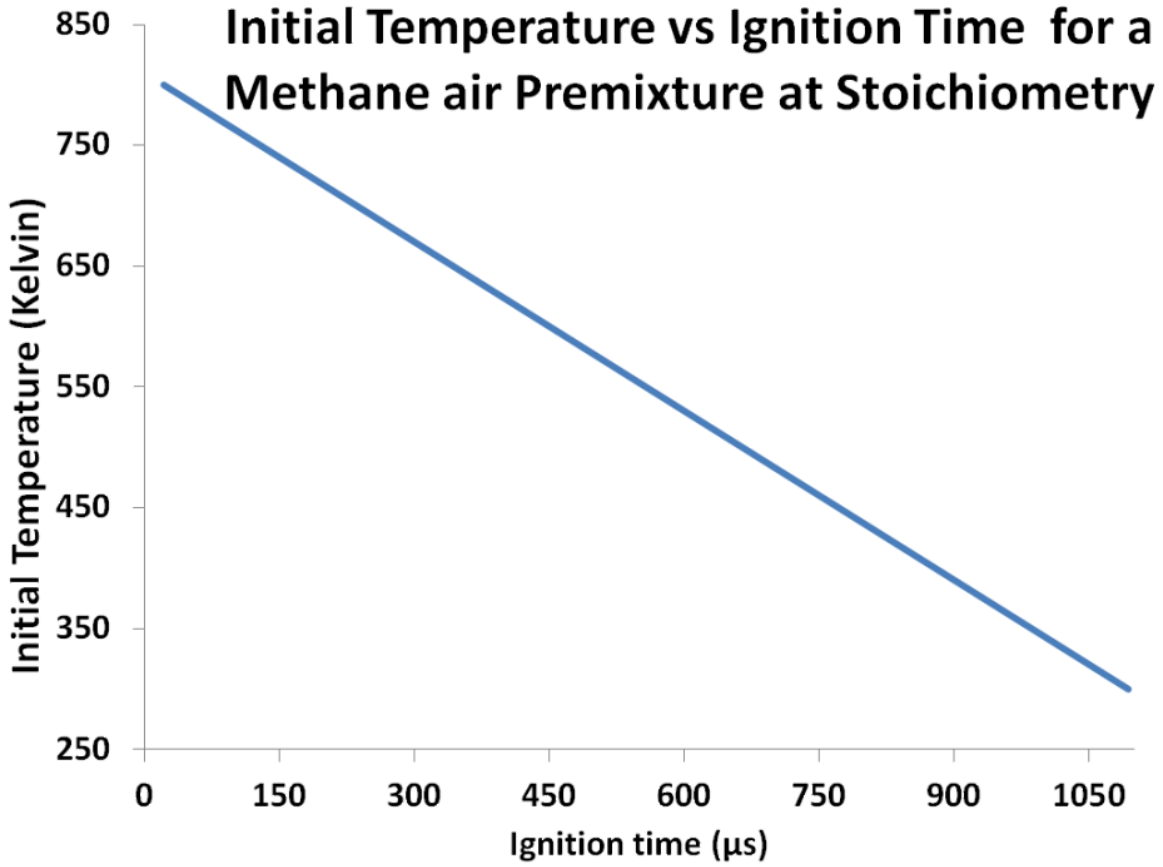

Figure 4.3.3 Based on Eqn. 4.28, the ignition time for methane pre-mixture is calculated for pre-heating temperatures of the fresh gas from 300 K to 800 K

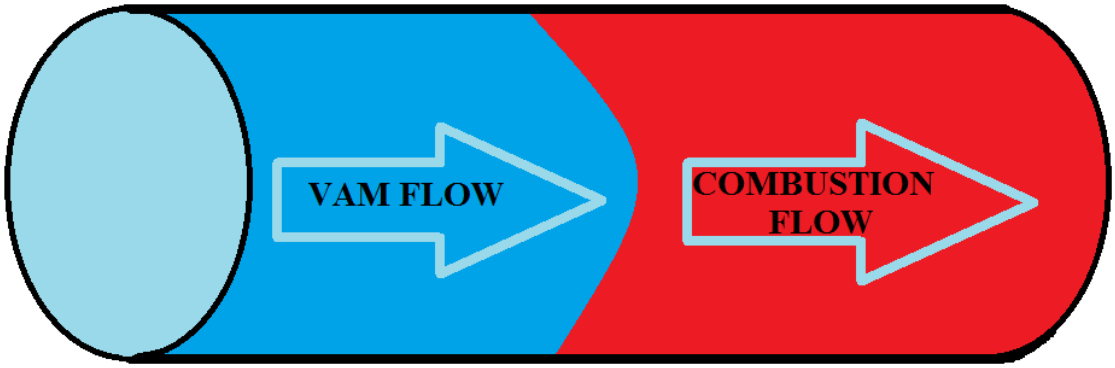

Figure 4.3.4 representation of VAM flowing to the combustion zone.

Eqn. 4.32. $$\rho C_p \frac{Dt}{Dt} = \frac{\partial}{\partial x_i}\left(\lambda \frac{\partial T}{\partial x_i}\right) + \frac{DP}{\partial t} + \tau_{ij}\frac{\partial u_i}{\partial x_j} - \frac{\partial T}{\partial x_i}\rho \sum v\, k_i Y_k C_{pk} + \dot{\omega}_T$$

A verbal description of the mathematical terms in Eqn. 4.32, the general equation for the temperature of any flame, (Poinsot and Veynante, 2005) states that:

The Increase of temperature = Temperature increase due to heat flux created by diffusion + Temperature change due a change pressure + Temperature change due to viscous stress tensor – Temperature change due to diffusion velocities + Heat of reaction released.

The simplifications introduced for the case of deflagration significantly simplify Eqn. 4.32. Since the Mach number or speed of the flow is low, the temperature change due to diffusion velocities is negligible, the pressure is almost constant, so the pressure differential is zero and the viscous stresses are negligible; thus, the power generated by the viscous stress tensor term is reduced zero.

4.4. Flame Speed Approximation

The notion of a flashback occurring is only a real possibility when a pre-mixed fuel source is coupled a to combustion system with some intervening gap between the combustion zone and the premixing. Simply put, a premixed fuel capable of ignition, such as a stoichiometric mixture, encounters a flame. Although the VAM is intentionally kept at low concentrations for safety reasons, it can spontaneously vary in concentration resulting in unplanned changes in the system operational parameters. It is important to understand these parameters from an operational and prototype viewpoint; therefore, the intent of this section is to provide an analytical model sufficient to establish design parameters and proceed with the advanced numerical modeling of combustion process. For the purpose of this problem, the flame speed is calculated analytically following a straightforward model.

To model the system flame speed a tube is assumed to have a VAM flow of velocity $\mathbb{V}$ entering the combustion volume and an equivalence ratio commensurate with Figure 4.3.1. For a premixed flame at constant temperature, a single step lean reaction is used such that the amount of fuel in the mixture is the driver of the single step reaction. All the heat capacities are constant and the Lewis number is unity, so the diffusion flow and heat flow are approximately equivalent and Fick's law is an excellent approximation for the diffusion velocities (Poinsot and Veynante, 2011). To solve for the velocity based on the equivalence ratio, go directly to the linearized equation, based on the following two differential equations outlined in Eqn 4.33.

Eqn. 4.33. $\rho_1 S_L \frac{dY_F}{dx} = \frac{d}{dx}\left(\rho D \frac{dY_F}{dx}\right) + \dot{\omega}_F \; and \; \rho_1 S_L C_p \frac{dT}{dx} = \frac{d}{dx}\left(\lambda \frac{dT}{dx}\right) + Q\dot{\omega}_F$

The introduction of a number of standard variable changes are needed to linearize the system and to eliminate the source terms $\dot{\omega}_F$ from the differential equations. The basis for this analysis as was accomplished in the seminal work by Zeldovich in 1940. After making some change of variable substitutions, making use of the equivalence of heat flow by both transport and the diffusion effect, so the Lewis number $\lambda/C_p = 1$, introducing the reduced temperature θ and the reduced mass fraction $\mathbb{Y}$, given below in Eqn. 4.34, and defining $Z = \theta + \mathbb{Y} = 1$ everywhere, the relations developed by Zeldovich 1940, are presented in Eqn. 4.35.

Eqn. 4.34. $\theta = {(T - T_1)}/{(T_2 - T_1)} \; and \; \mathbb{Y} = {Y_F}/{Y_F^1}$

Eqn. 4.35. $\rho_1 S_L \frac{d\theta}{dx} = \frac{d}{dx}\left(\rho D \frac{d\theta}{dx}\right) + A\rho(1 - \theta)e^{-T_a/T}$ (Zeldovich,1940)

The point of view taken is in the frame of reference of the flame; therefore, the position $x = 0$ is the position of the actual flame. If a flow is arriving from the left at the speed of the ventilation flow S_V and if the speed of the flame S_L is less than the speed of the ventilation flow then the flame will not propagate backward or flashback down the ventilation system to the workings in the mine. This is a condition, which is only expected under defined operating conditions, not for the case where the methane content of the flow meets or exceeds stoichiometry or resides in the explosive range. By applying the simplifications and variable substitutions above, the following linear result is obtained for the source term; that is, the non-differential term at the far right hand side of Eqn. 4.35.

The source term has become quite a complicated function of the temperature making the integration difficult; however, when the form of the equation is examined, the source term, isolated below in Eqn. 4.36, can be plotted independently to determine the critical temperature at which the combustion starts (Poinsot and Veynante, 2011).

Eqn. 4.36. $A\rho(1-\theta)e^{\left(-\frac{\beta}{\alpha}\right)} \frac{e^{\left(-\beta\frac{1-\theta}{1-\alpha(1-\theta)}\right)}}{1+\alpha\frac{\theta}{1-\theta}}$

The critical temperature is the temperature at which combustion is inevitable. Examples of the meaning of the critical temperature and the effect of reaching the

critical temperature on a system can be found in situations such as the spontaneous combustion of a compost pile. Spontaneity is not quite the proper description, but rather inevitability would be more appropriately descriptive. The process occurs because of a temperature increase, which has retained internal heat generated by exothermic reactions due to the size of the pile to the point the temperature is high enough for the fuel to ignite.

Looking at the temperature profile for typical combustion of pre-mixed fuels in Figure 4.4.1 the critical temperature is the boundary between the pre-heating zone and the combustion zone. Once combustion has initiated, the diffusion of heat, back to the pre-heating zone, encourages continued combustion provided the fuel and oxidizer are continuously supplied.

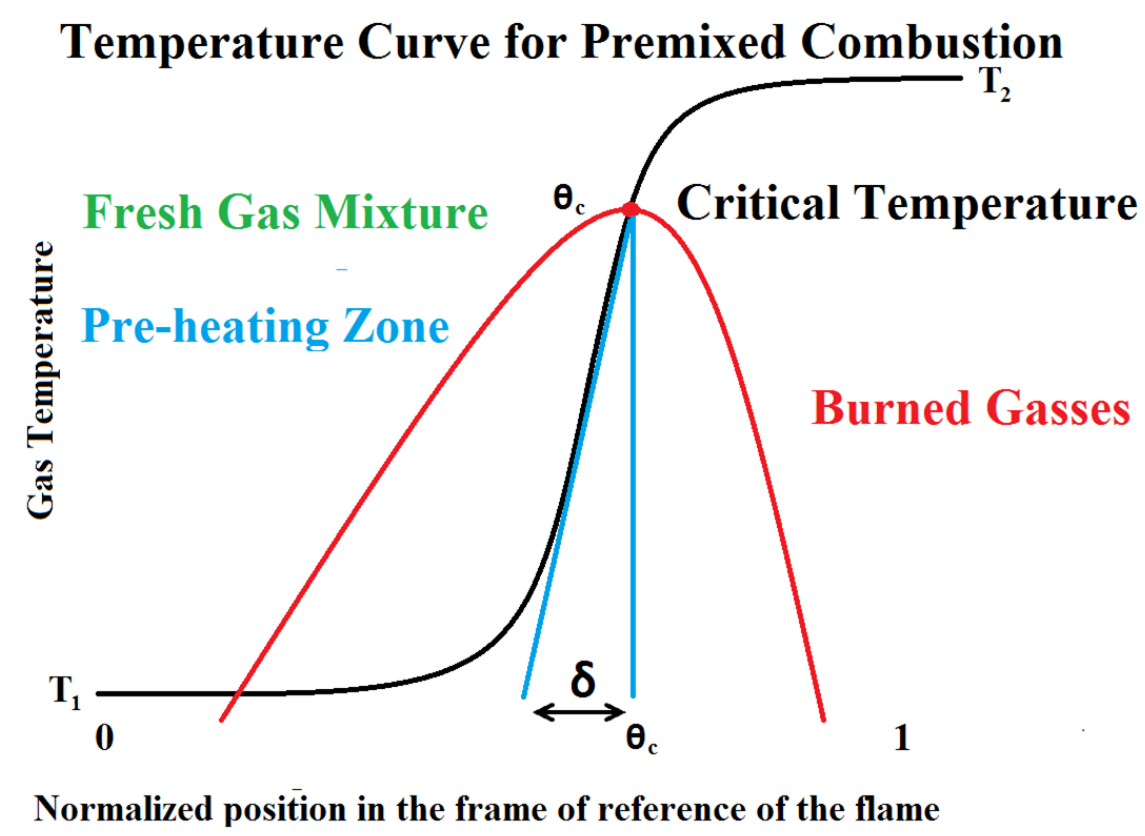

Figure 4.4.1 Temperature profile for a pre-mixed fuel in the frame of reference of the flame. The fresh gas is flowing from the pre-heating zone on the left to the combustion zone on the right. Combustion starts at the critical temperature θc and the flame width is δ.

Plotting the relation in Eqn. 4.36, for various initial temperatures of the fresh gasses, the critical temperature was determined for a normalized reaction rate at the reduced temperature. Once the reduced critical temperature is determined, Eqn. 4.34 can be used to calculate the value of the temperature given that the values for

the initial temperature or pre-heated temperature and the adiabatic flame temperature or final temperature of the flame at combustion are all known.

The family of curves in Figure 4.2.2 redefines the shape of the generic temperature curve of Figure 4.4.1 by shifting the critical temperature and the initial fresh gas T_1 and adiabatic flame temperatures $T_{2;}$ the plateaus shown at the left and right hand sides of the diagram. The critical temperature θ_c is determined by finding the maximum value of the normalized reaction rate curve. This was done using excel functions to find the maximum value of the normalized reaction rate and the corresponding value for θ_c, which was taken from the tabulated data for each curve. The θ_c values were plotted at the maximum values for each initial temperature on the normalized reaction rate versus reduced temperature curve in Figure 4.2.2 to create a curve for the critical temperature as a function of initial temperature. The critical temperature was also be determined analytically by taking the derivative of Eqn. 4.36 with respect to **θ** and applying the standard maxim-minimum techniques of differential calculus. In Table 4.4-1 and Figure 4.3.3 the values of the calculated critical temperature are based on an adiabatic flame temperature of 2226.5 K and an activation temperature of 840 K.

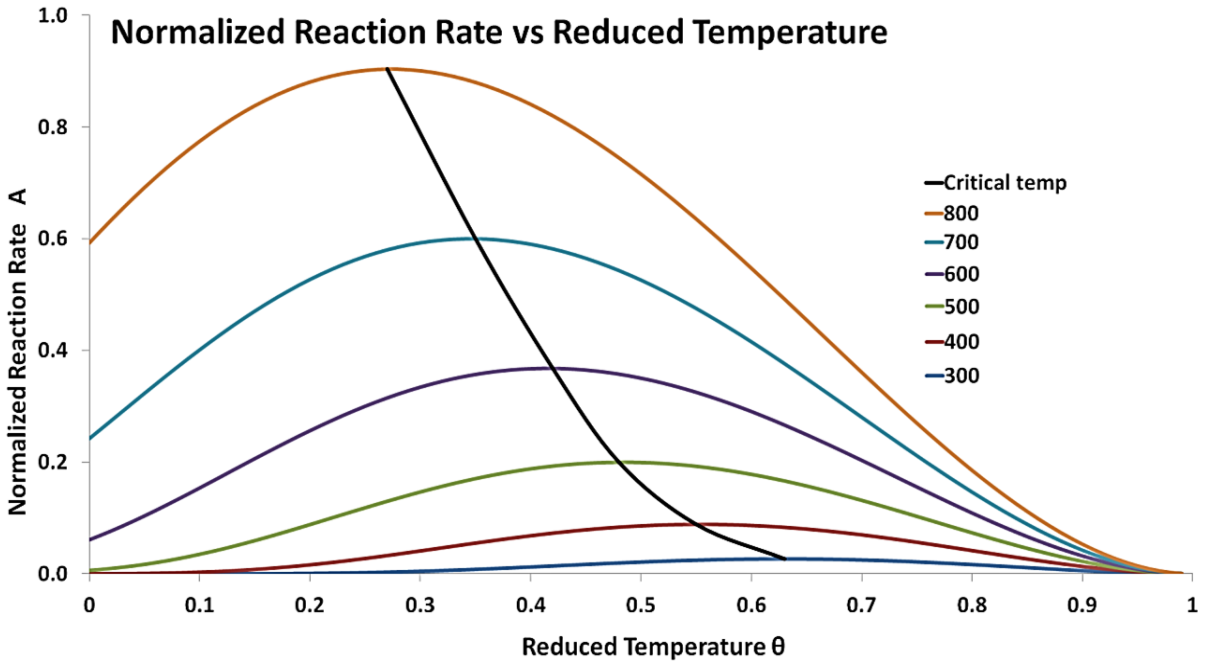

Figure 4.4.2 The normalized reaction rate versus the reduced temperature for a methane VAM flow entering the pre-heating zone, as shown in Figure 4.4.1 and Figure 4.4.6 undergoing combustion when the temperature reaches θc the critical temperature follows the maximum reaction rate based on the source term in Eqn. 4.20

Given the reaction rates in Table 4.4-1 it can be seen that as the temperature increases, see Figure 4.2.2, the rate of the reaction also increases; however, there is no increase in the amount of fuel, so the increase in reaction rate is taken up entirely by the increase in ignition time as seen in Figure 4.2.2. When the concepts of reaction rate are introduced, being zero before combustion or $\theta < \theta_c$ and is $\rho_1 R(1 - \theta)$ after combustion starts for $\theta > \theta_c$, then the Eqn. 4.35 reduces to the linearized form in Eqn. 4.37.

Eqn. 4.37. $$\rho_1 S_L \theta' = \rho_1 D\theta'' \; and \; \rho_1 S_L \theta' = \rho_1 D\theta'' + \rho_1 R(1-\theta)$$

Table 4.4-1 Normalized reaction rates compared to expected ignition times at the fresh gas initial temperatures corresponding to the critical temperatures.

Fresh Gas Temperature	300	400	500	600	700	800
Normalized Reaction Rate	0.0267	0.0885	0.1997	0.3676	0.5995	0.9031
Critical Temperature-spreadsheet	0.63	0.55	0.48	0.42	0.35	0.27
Critical Temperature-analytical	0.6958	0.6067	0.5187	0.4295	0.3369	0.2385
Corresponding Ignition time (μs)	1093	879	665	450	236	21
Averaged Ignition temperature (K)	1542	1456	1362	1290	1223	1162

Solving Eqn. 4.37 for the flame speed S_L, the following relationship Eqn. 4.38, which depends on both the reaction rate and diffusion rate. This confirms that the diffusion of the heat and reaction rate work together to provide combustion, see

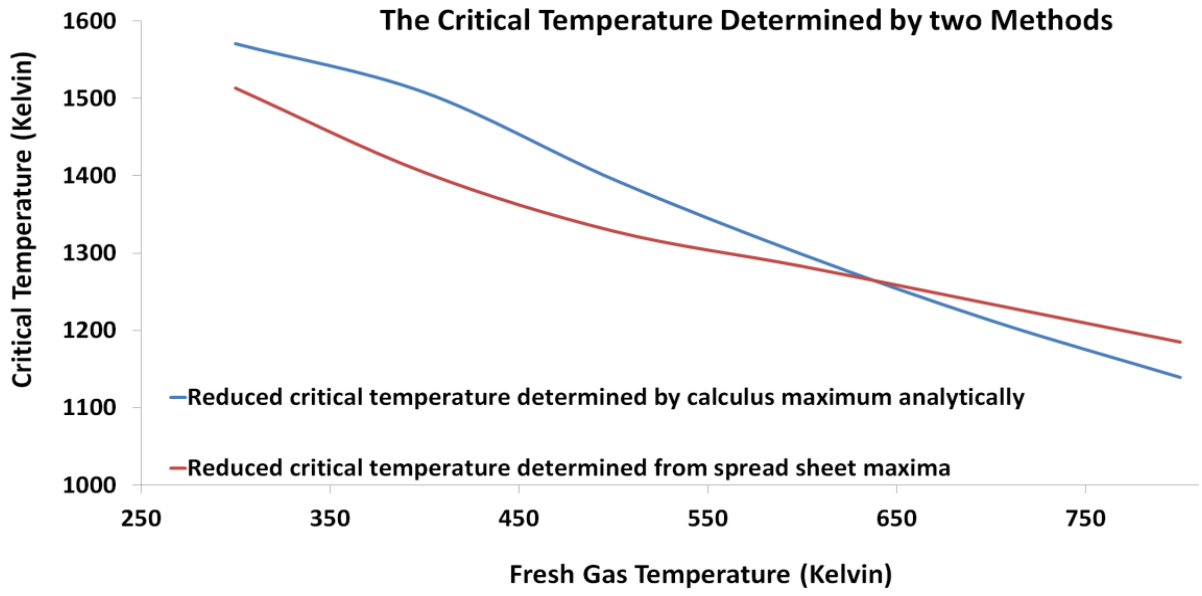

Figure 4.4.3 The critical temperature determined analytically and by taking the maximum values from the spreadsheet plots from Figure 4.4.2.

Figure 4.4.1, where the heat is diffusing back from the combustion zone to the pre-heating zone separated by the flame thickness, which is associated with the critical temperature $\boldsymbol{\theta_c}$. This is the essence of how the flame moves or acquires a velocity, where the reaction rate depends on the chemical kinetics and the diffusion rate depends on the thermochemistry. The value of the reaction rate depends on the amount of fuel in the mixture, typically in a gas turbine or internal combustion engine the fuel ratio would only change to move the engine from one operating point to another. In this case, the VAM is considered as the fuel source, where the VAM concentration could change spontaneously; however, it is still at quite a low equivalence ratio, see Figure 4.3.1.

Eqn. 4.38. $S_L = \sqrt{\frac{RD}{\beta(\beta-1)}}$ and the flame thickness δ is related by $\frac{S_L \delta}{D} = 1$

The diffusivity is exponentially proportional to the temperature where the exponential factor is $\boldsymbol{\gamma}$ and inversely proportional to the pressure, so the diffusivity is written as Eqn. 4.39.

Eqn. 4.39. $D = \frac{T^{\gamma}}{P} \Rightarrow \left(\frac{P_0}{P_1}\right)^{1/2} \left(\frac{T_1}{T_0}\right)^{\gamma/2}$.

The value of $\boldsymbol{\gamma}$ is to some extent a question to be resolved, because the experimentally determined values for the exponents are not in numerical agreement, but have the correct directional agreement (Poinsot and Veynante, 2011). A simple discussion of the value of $\boldsymbol{\gamma}$ is only provided to slightly increase the level of clarity on this point. Typically $\boldsymbol{\gamma}$ is 1.4 for most calculations, based on the gas constant concept of degrees of freedom $\boldsymbol{\gamma} = 1 + 2/\boldsymbol{f}$ where $\boldsymbol{f}$, the number of degrees of freedom, is three for a monatomic gas or five for a diatomic gas, so $\boldsymbol{\gamma} = 1.4\ to\ 1.67$ respectively. Although these values would lead to 0.7 to 0.835 for the exponent in Eqn. 4.39, the experimentally determined values are higher. Because of this, an alternate approach is taken for the determination of the flame velocity.

Using the empirical formula for the flame thickness developed by (Heravi et al, 2007) detailed in Eqn. 4.40, and the ignition times calculated for the expected initial fresh gas temperatures of the VAM, shown in Eqn. 4.28, a flame speed can be constructed. The flame speed inferred by the ignition times and flame thickness, depicted on Figure 4.4.1 as $\boldsymbol{\delta}$, is calculated for the case of a 100 m^3/s flow and a 0.5% VAM concentration, which results in a heat flux of about 300,000 W/m^2, based

on the size of the combustion chamber. The heat flux is determined by the area of the combustion zone and the amount of fuel contained in a volume corresponding to the flame thickness releasing its energy across that area. The concept employed is that the dimensionality of the thickness of the flame, in the frame of reference of the flame, is the distance over which the ignition time is taken as the traversal time; otherwise the flame would not remain stationary in its frame of reference.

Eqn. 4.40. $$\delta = 0.2643\left(T/300\right)^{-0.85} P^{-0.58} = S_L/t_{ig}$$

The plot in Figure 4.4.5, of flame speed versus initial temperature of the fresh gasses in the preheating zone shows that the flame speed does not exceed the expected ventilation flow speed coming from the mine. The velocity at low fresh gas temperatures for stoichiometric mixtures, calculated by this method is estimated to be only about 0.2 m/s for the low temperature near 300 K and up to 0.6 m/s for the temperatures up to 750 K, which is considered to be a high preheating temperature.

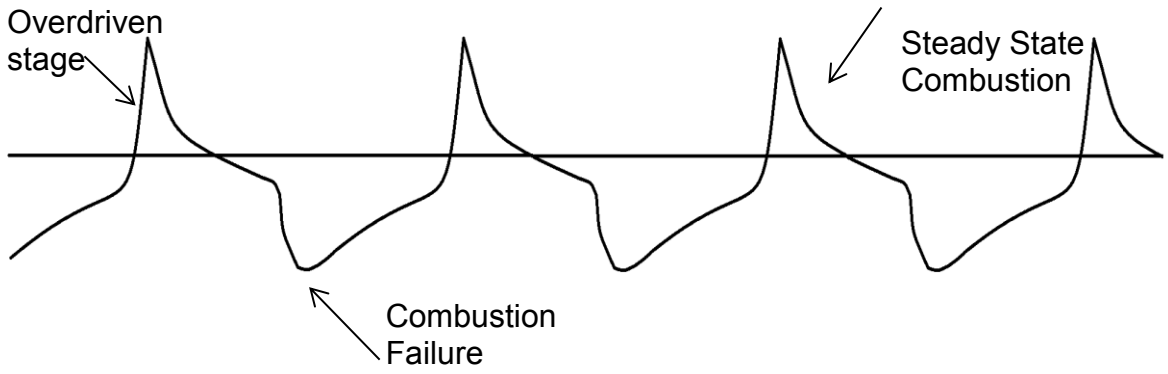

Figure 4.4.4 Galloping detonation. In the overdriven phase, the methane is rapidly burned followed by a state of steady detonation until it fails, the fuel builds up and the cycle repeats.

The flame width **δ** depicted in Figure 4.4.1 and in Figure 4.4.6 is more sensitive to temperature changes than pressure changes, for the purposes of these calculations the pressure is considered to be constant; thus, only the change in temperature from 300 K to 750 K is considered. The critical temperature decreases as the temperature of the fresh gasses or preheating temperature increases. These calculations suggest that a pre-heating temperature of up to 600 K would be safe, since the spontaneous ignition temperature would be near 1280 K to 1300 K. These temperatures also suggest that the values will be easily obtained in the igniter section of the VamTurBurner© and that diffusion of heat from the flame zone should

not be of significant concern since the ventilation flow is 1.8 m/s while the flame propagation speed is only about 0.2 to 0.6 m/s as shown in Figure 4.4.5. As can be seen from Figure 4.4.5 the flame speed substantially increases at fresh gas temperatures above 750 K. Since the change in ignition time is linear over the temperature range of interest, the rapid upswing in flame speed evident in Figure 4.4.5 is due predominantly to the exponentially sharp drop in the flame thickness **δ** as the temperature increases. This is indicative of the galloping detonation as described by Oakley and Thomas (2004), where they describe a transition from deflagration to detonation leading to an overdriven detonation that decays to a steady detonation, which subsequently fails whereupon the sequence is repeated. These transitions between the two states can occur with remarkable consistency over a large number of cycles as seen in Figure 4.4.4. Such an event can lead to severe damage at each of the locations where transition to the overdriven phase occurs.

A schematic depiction of the ventilation VAM flowing in from the left and the flame speed moving toward the right is shown in Figure 4.4.6. The heat flux is due to the VAM fuel burning and diffusing heat back to the preheating zone as would be

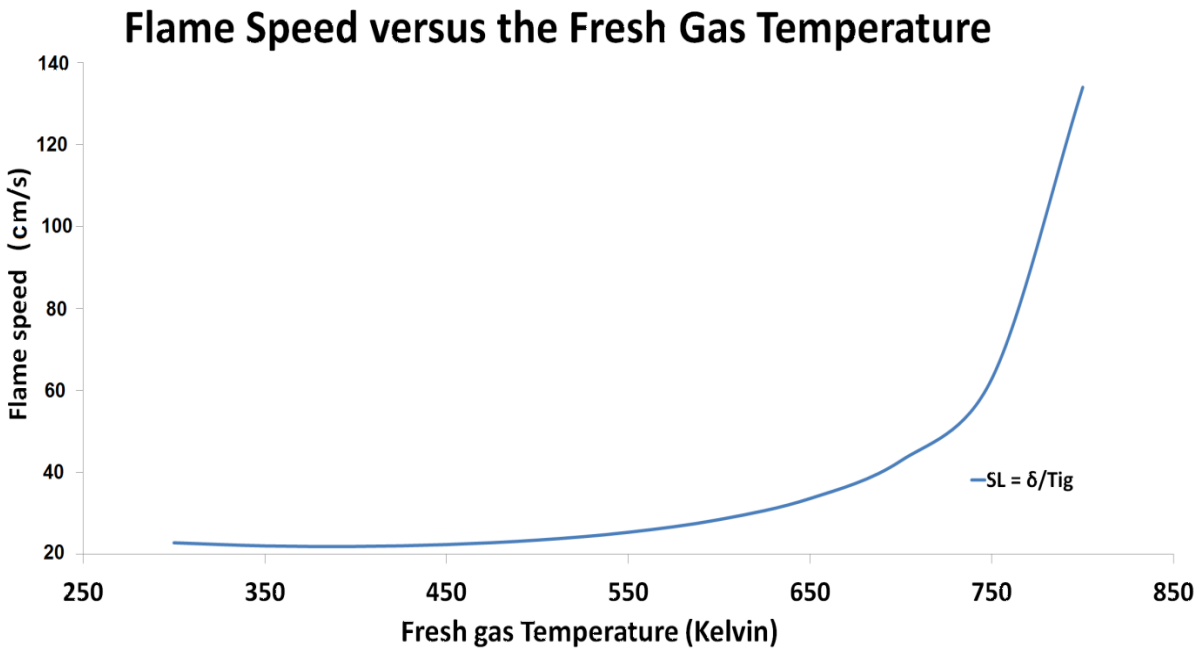

Figure 4.4.5 Flame speed for a methane air mixture at stoichiometry vs the fresh gas temperature in the pre-heating zone.

the case with a typical flame. The combustion zone also contains igniters, which are a flame burner or flaring system connected to a separate source of fuel, which could

contain drained methane, natural gas or a combination thereof. The fuel arriving at the igniters is controllable; thus, can be varied to accommodate changes in the VAM concentration and temperature if required. The control of the fuel to the igniters is also a means of allowing for the heat moving from the igniter section or combustion zone back to the preheating zone to be built up at the onset of operation. As the system temperature increases from start-up it is expected that the amount of fuel required for the igniters can be reduced because the heat flow circulating to the preheater will be recirculated in the VAM flow back to the combustion zone.

The calculation by this technique is compared to the values of the flame speeds of methane mixtures determined by numerical modeling methods, using advanced numerical modeling codes, the direct calculation of flame speeds in Figure 4.4.8. The plot shows flame speeds, with an equivalence ratio near the lean end of a typical VAM flow, for fresh gas temperatures of 298.15; the temperature normally used for characterizing the enthalpy of formation, which is standard to combustion modeling (Vagelopoulos and Egolfopoulos 1997).

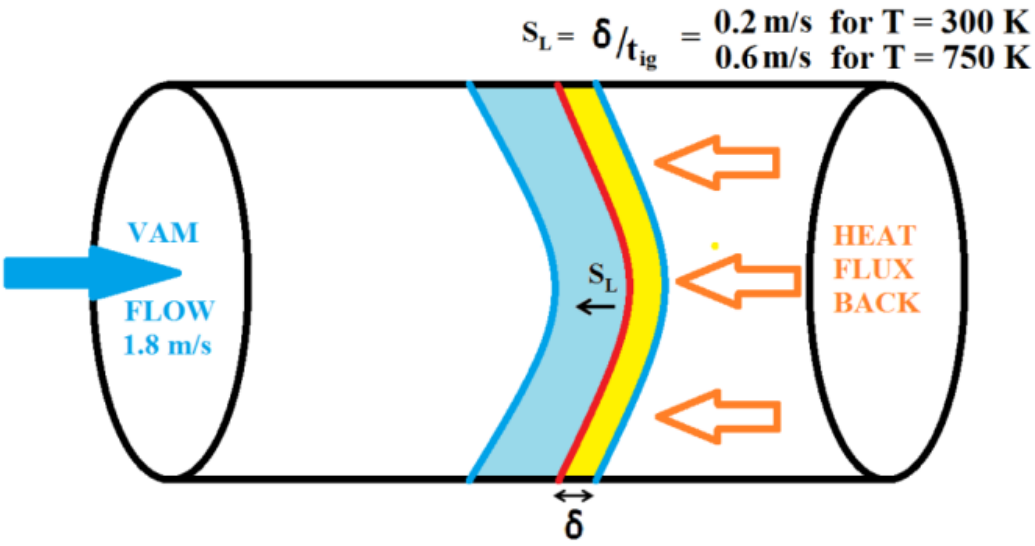

Figure 4.4.6 Depiction of a VAM flow at a typical ventilation speed of 1.8 m/s opposing a flame speed of 0.2 to 0.6 m/s predicted for fresh gas temperatures of 300 K and 750 K respectively

Notice the flame speed is a maximum, at mixtures that are just slightly greater than stoichiometric. The distribution of speed is quite symmetrical on either the lean or the rich side of the equivalence ratio, but on the rich side at the higher equivalence ratio, the lower speed is due to quenching by an overabundance of fuel

and on the lean side, it is due to an absence of fuel. The plot of flame speed versus temperature in Figure 4.4.5, at a constant equivalence ratio over the temperature range of interest for this study, shows a significant increase in flame speed as the initial temperature approaches the auto-ignition temperature. This is mainly due to the sudden rapid burning of the methane, which leads to a galloping type of combustion at the higher region of the pre-heating temperatures. The speed of 40 cm/s, often quoted as the flame speed of a stoichiometric mixture of methane, occurs for a fresh gas temperature of about 700 K. Comparing the values obtained by Frenklach et al. 1995, in Figure 4.4.8 to the speeds obtained by the method used to produce Figure 4.4.5 it is clear that the flame speed values calculated analytically compared to those arrived at by numerical methods are commensurate with the equivalence ratio expected for VAM. The minimum equivalence ratio in Figure 4.4.7 is near the maximum equivalence ratio expected for VAM.

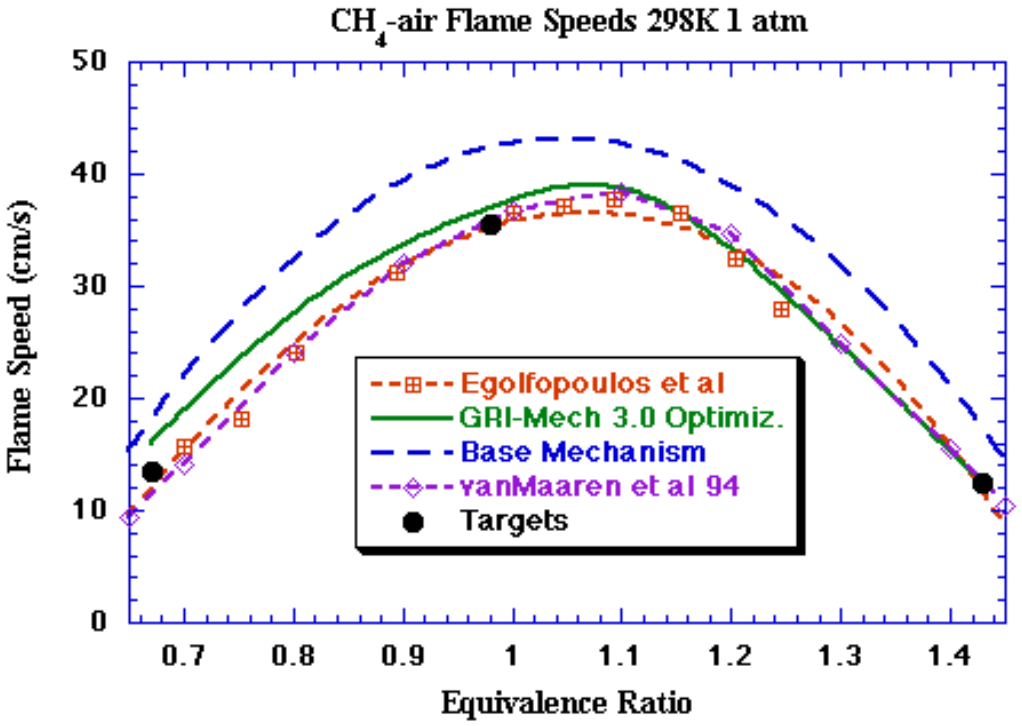

Figure 4.4.7 Flame speeds of methane mixtures determined at 298 K, by a number of methods from the direct calculation of flame speeds (Vagelopoulos and Egolfopoulos, 1997)

Observation of the trend of the curves suggests that the values obtained in Figure 4.4.5 are acceptable and comparable to those obtained by the advanced GRI-Mech 3.0 combustion code that Vagelopoulos and Egolfopoulos used to obtain the speeds

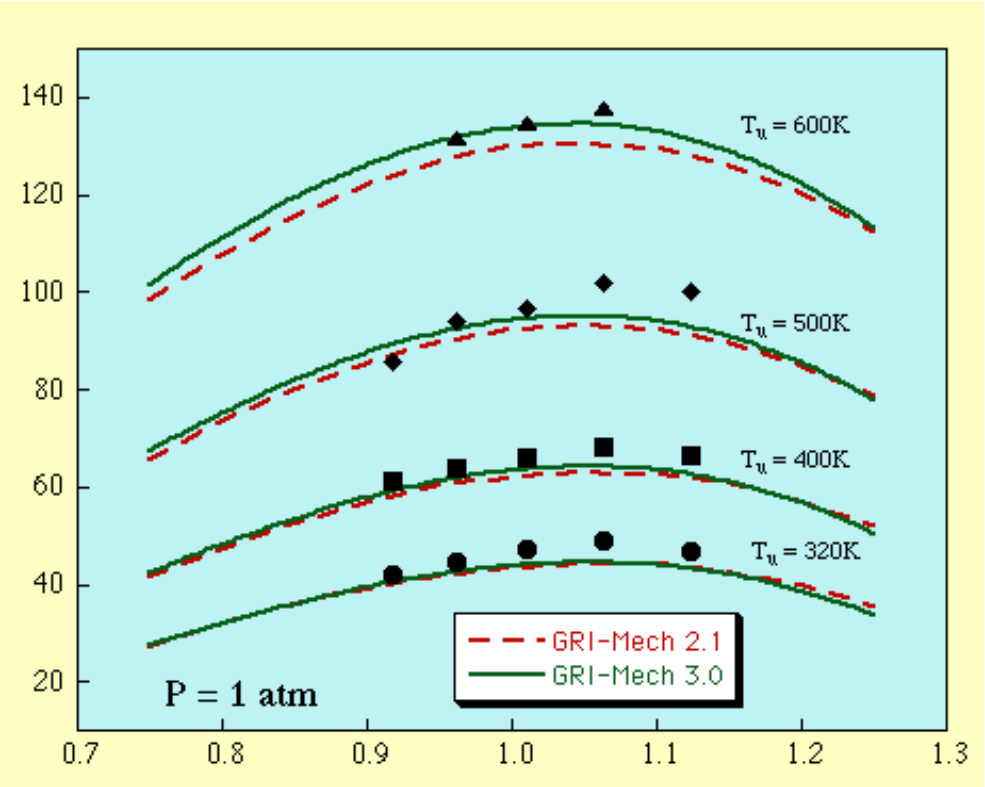

Figure 4.4.8 Flame speed at fresh gas temperatures from 320 K to 600 K (Frenklach et al. 1995)

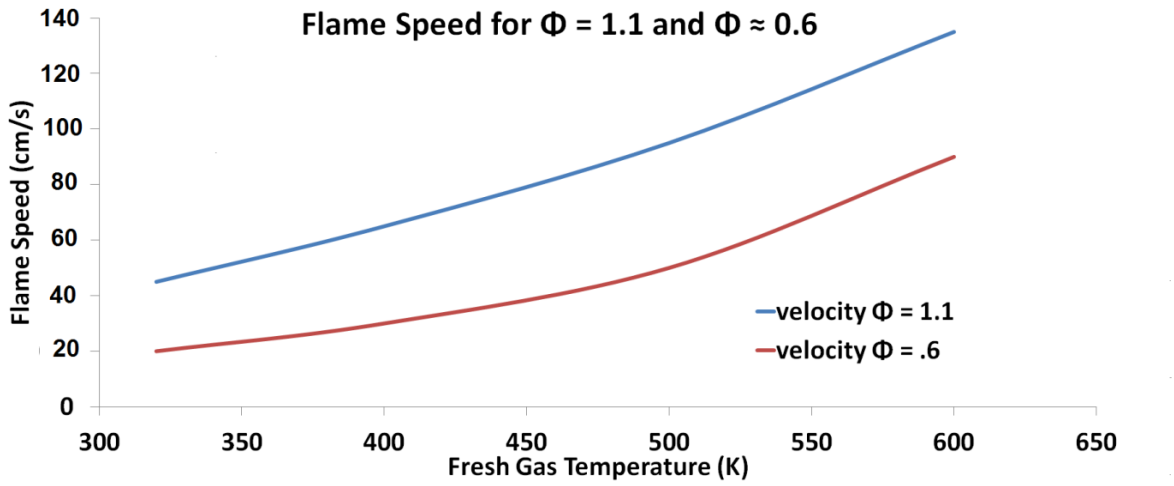

Figure 4.4.9 Flame speed for fresh gas temperatures from 320 K to 600 K and equivalence ratio Φ ≈ 0.6 and Φ ≈ 1.1 (adapted from Frenklach et al., 1995 seen in Figure 4.4.8)

In Figure 4.4.7 for temperatures in the range expected for the VamTurBurner©. Extrapolating for the values of **Φ ≈ 0.6** and reading the values of flame speed for **Φ ≈ 1.1** from Figure 4.4.7 the graph shown in Figure 4.4.9 was prepared to provide an improved comparison to the values for the flame speed calculated and shown in Figure 4.4.5. It appears that there is a consistency between the simple analytical calculations used here and the values obtained using advanced numerical modeling.

Although the data available from the modeling only covers temperatures up to 600 K, the trend and values are consistent in the temperature range available. This suggests that using the simple model developed for the calculation of the flame speed is appropriate for the work carried out in this phase of design.

4.5. Summary

The intent of this chapter is to develop the ideas of a VAM combustion system without having to resort to the use of intensive and expensive numerical modeling for routine design changes by developing a simple analytical model, which can be readily applied. The elementary descriptive analysis needed to develop an analytical combustion dynamics model was developed. The adiabatic flame temperature model arrived at in Eqn. 4.26 is predictive and adequate for the range of equivalence ratio expected for typical VAM concentrations. The flame speed S_L corresponding to the adiabatic flame temperature was evaluated using a simple model that assumes the distance traversed δ is the flame thickness and the time taken t_{ig} is the ignition time resulting in the simple relation $\delta = {S_L}/{t_{ig}}$.

This flame speed model suggests that at the higher initial fresh gas temperatures rapid burning of the methane occurs in what is referred to as galloping combustion. The conditions that can potentially cause a flashback are explored, based on the expected flame speed and mode of combustion in order to provide the safety boundaries for the initial design of the Vanturburner© system. It was determined that for the rate of flow of the ventilation air nominally at 1.8 m/s the flame speed is not sufficient to move the flame in the direction of the incoming fuel faster than the speed of incoming ventilation air. It is also expected that due to the notion that galloping combustion will be the dominant combustion mode at the higher temperatures the methane is rapidly consumed and as such extinguishes the flame until the fuel need is replaced. In a prototype or for a full-scale design, safety systems would be in place, such as explosion diffusion and flame arrestors, to prevent the propagation of hazardous situations should they occur.

5. Determination of the combustion dynamics of ventilation air methane using large eddy simulation

5.1 Turbulence

The procedure of Large Eddy Simulation is used to carry out the numerical modeling of the combustion dynamics of a ventilation air mixture containing small percentages of methane. The modelling of preheating conditioning and subsequent interaction with a flame igniter must be predicated by a short discussion on turbulence.

Turbulence is a complex problem, which will be described for the purpose of this dissertation as the superposition of a spectrum of velocity fluctuations causing eddies to be nested within a mean velocity flow. These eddies vary in physical size; thus, have a distribution of velocities, vorticities and pressure gradients. Therefore, a turbulent flow is comprised of a continuum of eddies within a range of length scales determined by the size of the containment. The range of length scales can be defined by the energy spectrum or the kinetic energy contained in the velocity fluctuations of the eddies at each of the eddy size fractions in question. The scale of the energy cascade, the transfer of energy from the larger sizes to the smaller scales, is generally uncontrollable and highly non-symmetric or chaotic. The size of the eddies covers the entire length spectrum, that is, there exist eddies at every size from the largest to the smallest possible size at one location or another in space or time during the existence of the flow. However, at the smaller scales, friction effects due to viscous forces serve to eradicate the existence of the small scale eddies; thus, there is a constant state of eddy creation and dissipation at the smaller scale. This is a reflection of the notion that a turbulent flow is inherently chaotic, but can be split into distinct scale driven regimes.

Lorenz discovered the famous *Lorentz Equations*, a chaotic system based on some rather innocent looking differential equations, in 1963 while studying atmospheric turbulence. These differential equations gave rise to the familiar butterfly pattern commonly referred to as a strange attractor. The Lorenz equations below were used in a Maple16 routine to create two representations, a *DEplot* in real space or Cartesian Coordinates and a *phaseportrait* in the phase space of the attractor. It is instructive to observe that the DEplot clearly shows the non-periodicity

for these simple equations yet the phaseportrait shows there exist two points of attraction or *set points* for the system.

Eqn. 5.1 $\frac{d}{dt}x(t) = -9x(t) + 9y(t);$

Eqn. 5.2 $\frac{d}{dt}y(t) = 28x(t) - y(t) - x(t)z(t);$

Eqn. 5.3 $\frac{d}{dt}z(t) \ -\frac{8}{3}z(t) + x(t)y(t)$

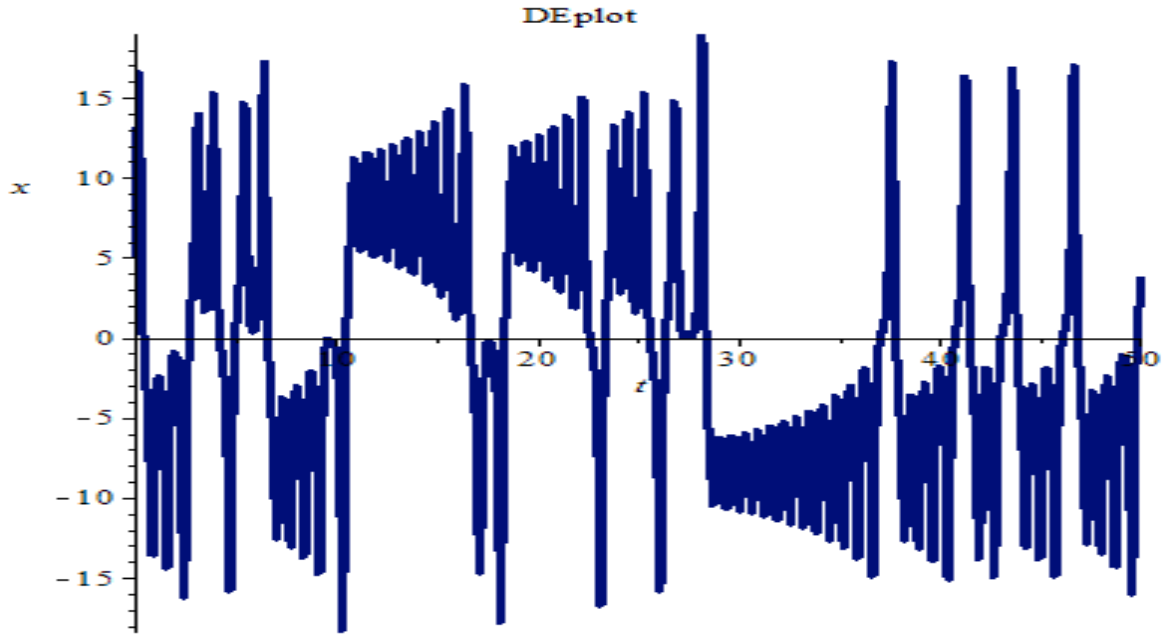

Figure 5.1.1 Lorentz equations in Cartesian Coordinates demonstrates the non-periodicity.

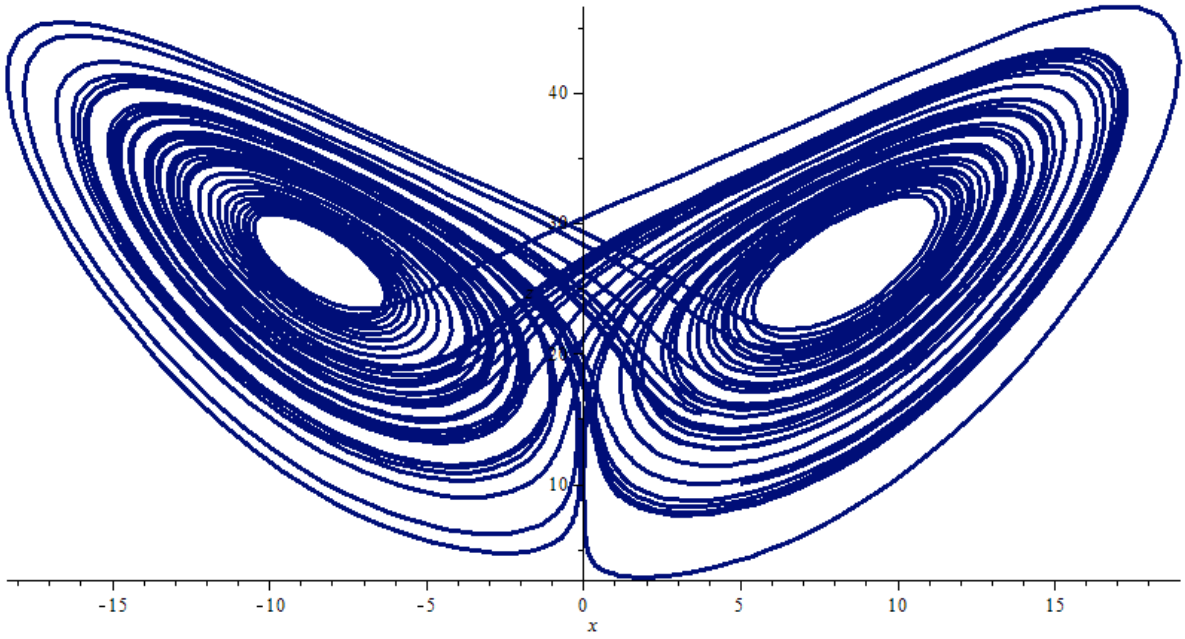

Figure 5.1.2Phase portrait for the Lorenz equations shows two distinct attractive set points.

Lorentz discusses the notion of small-scale dissipation in the following quote

> *"In any real hydrodynamical system, viscous dissipation is always occurring, unless the system is moving as a solid, and thermal dissipation is always occurring, unless the system is at constant temperature." (Lorenz, 1963).*

Despite the inherent complexity, turbulence is often defined quite simply as that regime of flow in a pipe that occurs when the Reynolds number is higher than about 4000. The Reynolds number is the ratio of inertial forces to viscous forces; thus, a dimensionless index (Stokes, 1851). The Reynolds number is the primary index used to distinguish between laminar flows, which occur at lower Reynolds numbers and turbulent flows that occur at higher Reynolds numbers. At the lower Reynolds numbers, the viscous forces are the principle forces governing the dynamics of the flow commonly regarded as a smooth or a constant fluid motion. The turbulent flows occurring at higher Reynolds numbers are governed by the inertial forces and are commonly referred to as chaotic with eddies and vortices, which induce significant flow instabilities. It is generally accepted from experimental observations of flow under varying conditions that laminar flow occurs when the Reynolds number is less than 2300 and turbulent flow occurs when the Reynolds number is greater than 4000 (Holman, 2010). Transitional flows occur when the Reynolds number lies between 2300 and 4000. Both laminar and turbulent flows are possible in the transition regime or within the critical Reynolds numbers, which was the subject of the work by Reynolds in 1883. A common descriptive observation is that of the rising column of smoke, like that seen from a cigarette in stationary air. The column rises as a laminar flow, but as the velocity increases, suddenly there is a clear transition point at which the stream breaks the smooth flow becoming turbulent. The same observation is also seen in large-scale plumes from smoke stacks and volcanoes. The scale is dependent on the energy contained in the flow, which is a direct consequence of the velocity of the flow.

5.2 Large Eddy Simulation

Large eddy simulation (LES) is a technique used in the computational fluid dynamics modeling of turbulence. It was initially suggested by Smagorinsky in 1963, while studying the simulation and the study of the dynamics of the atmosphere's general circulation, the same year as Lorentz discovered the chaotic behaviour of atmospheric turbulence. Deardorff expanded the concept by studying the details

pertaining specifically to LES. Deardorff advanced and developed the concepts of sub-grid scale effects simulated with eddy coefficients proportional to the local velocity deformation (Deardorff, 1970). LES is a mathematical technique useful for solving problems in combustion dynamics, but is also applicable to other fields of computational physics.

LES puts controls or limits on the Navier–Stokes equations in order to select the appropriate range of length scales for the solution, this is a critical element in the computation because the goal is a reduction of computational cost, which allows for larger scale and more simulations. A simplified version of the Navier-Stokes equations, shown below in Eqn. 5.4, is essentially an expression of Newton's second law of motion for a fluid, for a detailed derivation the reader is referred to *An Introduction to Fluid Dynamics* by Batchelor, (1967).

Eqn. 5.4 $$\boldsymbol{F_{gravity} + F_{pressure} + F_{viscous} = ma}$$

The key point is that a large eddy simulation is fundamentally a low-pass filtering operation not dissimilar to a frequency filter used to split the treble and bass on an audio speaker system. A low pass filter reduces the computational extent by avoiding the computations pertaining to the small scale eddies or the high frequencies. The significance of this approach rests in the decision as to where the cut-off point is selected. This is the size scale or wave number associated with the small scale eddies or sub-grid scale effects, typically the point where the viscous forces dominate; thus, when LES is used to control the behaviour of the Navier–Stokes equations the small scale eddies are eliminated from the computation, but modeled in the solution.

To establish a sensible cut-off point, assumptions regarding the cascade of energy from the larger scale eddies in the flow to the next smaller scale is required. It is expected that this energy transfer is achieved without a loss of kinetic energy to viscous forces. This is equivalent to stating that the energy dissipation is due solely to the inertial term, which is nonlinear in the Navier-Stokes equations or the energy dissipation $\boldsymbol{\epsilon = \nu k_o^3 |\nabla u(x,t)|^2}$ is constant over the spatial and temporal existence of the flow (Foias et al, 2008). The second somewhat obvious, but equally important assumption is that the amount of energy flowing from the larger scale to the smaller scale is consistent with the conservation of energy; thus, the amount of energy flowing from the larger scale equals the amount of energy arriving at the smaller

scale. The governing Navier-Stokes equations are recast to base the solution on the simple filtering of the velocity field, that is, the length and time scales eliminated from being resolved in the solution are selected according to turbulence theory and available computational resources (Pope, 2000).

Direct Numerical Simulation is certainly capable of providing a solution with superior accuracy because every scale is computed to an arbitrarily small error determined solely by the number of terms in the Taylor expansion shown in Eqn. 5.5. The last term in the expansion is the term that determines the size of the error in the calculation or the level of resolution (Arfken, 1985).

Eqn. 5.5 $$f(x) = \sum_{n=0}^{\infty} \frac{f^n(a)}{n!}(x-a)$$

A commonly quoted application of the Taylor expansion, solving for the value of the natural logarithmic base e, is instructive, $\frac{de^x}{dx} = e^x; so\ e^x = c_0 + c_1 x + c_2 \frac{x^2}{2!} + c_3 \frac{x^3}{3!}$. By successive differentiation, $c_0 = 1,\ c_1 = 1,\ c_2 = {}^1/_{2!}\ ,\ c_3\ {}^1/_{3!},\ c_4 = {}^1/_{4!},$ when evaluated at **x = 0**, note that as terms are added the accuracy of the solution is improved. An exact solution to a turbulence or combustion problem could conceivably be achieved if an infinite amount of computer computation is available and the Direct Numerical Simulation has an error commensurate with the Plank length scale or in the neighborhood of 1.616252×10^{-35} m.

Large eddy simulation resolves large scales of the flow field solution, but only models the smallest or most computationally expensive scales of the solution, so they are not actually resolved as would be the case with a DNS solution. This allows applied engineering problems with turbulent flow configurations or complex geometry to be economically computed, nonetheless these calculations still require supercomputers to perform a simulation, as such, calculations are not possible on laptops or even larger systems. Large eddy simulations require more computer time than Reynolds averaged approaches, but in certain cases, such as combustion dynamics, which requires calculation of both the turbulent flows and the species interactions like the case under consideration here, the Reynolds averaged approaches fail to predict important statistical aspects of the flow (Oliveira, Miserda and Cunha, 2007). Alternatively, DNS resolves every scale of the solution, which makes it exorbitantly expensive even for the simplest turbulent flows or any systems with some geometrical complexity.

5.3 Combustion dynamics of ventilation air mixtures

The combustion dynamics of ventilation air mixtures was described analytically and sufficiently for the design of a VamTurBurner© system in chapter 4. The LES modelling of ventilation airflows, containing 0.5% to 3% methane composition were studied to establish the feasibility of the combustion conditions. The large-scale structures of the flow were resolved by the LES governing equations and the small-scale structures were modelled using closure rules (Pitsch, 2006). The flow field is filtered in space using a box filter given by $\Delta = V^{1/3}$ where V is the cell volume. The complexity of the system was reduced by filtering the variables that have density variations, using the well-known Favre-averaged filtering technique (Oliveira, Miserda and Cunha, 2007). The filtering process, described by $\tilde{f} = \overline{\rho f}/\overline{\rho}$

where the bar represents space-filtered quantities and the tilde is used for the Favre-averaged variables (Favre, 1983). The process needed to arrive at the averaging equations is found by considering a generic flow property that can be regarded as a function of either or both space and time $\emptyset(\boldsymbol{x},\boldsymbol{t})$ where the spatial average, commonly represented by $\overline{\emptyset}(\boldsymbol{x},\boldsymbol{t})$, is found by taking the integral over the volume

Eqn. 5.6 $$\overline{\emptyset}(\boldsymbol{x},\boldsymbol{t}) = \int_{\xi} \emptyset(\boldsymbol{r},\boldsymbol{t})\boldsymbol{G}(\boldsymbol{x}-\boldsymbol{r})\boldsymbol{dr}$$

where **x** is the position vector, **r** is the displacement vector with respect to **x**, and $\boldsymbol{\xi}$ represents the volume in **r**-space over which the integral is taken, that is the volume defined by a radial distance of **r**, from a position **x** in the space occupied by the flow. The function $\boldsymbol{G}(\boldsymbol{x}-\boldsymbol{r})$ is a filtering function, but a density-weighted average process is more suitable for compressible models. The averaged mass and momentum balance equations are written using index notation in the three-dimensional system.

The LES governing equations for multi-species reacting compressible flows are presented in (Mira-Martinez, Cluff and Jiang, 2014), which are comprised of the continuity equation or conservation of mass, conservation equations for both momentum and energy and the species equations, refer also to Eqn. 4.30, Eqn. 4.31, Eqn. 4.32 & Eqn. 4.33. The filtered stress tensor $\overline{\tau_{ij}}$ is obtained neglecting the effect of the unresolved field (Menon and Calhoon, 1996) and is given by:

Eqn. 5.7 $$\overline{\tau_{ij}} = \overline{\bar{\mu}\left\{\frac{\partial \tilde{u}_i}{\partial x_j} + \frac{\partial \tilde{u}_j}{\partial x_i} - \frac{2\partial \tilde{u}_k}{3\partial x_k}\delta_{ij}\right\}}$$

Where $\bar{\mu}$ represents the averaged dynamic viscosity and δ_{ij} is the Kronecker delta, which is unity for $i = j$ and zero for $i \neq j$.

Eqn. 5.8 $$\bar{q}_j = -\overline{\bar{K}\frac{\partial \widetilde{T_i}}{\partial x_j}} + \bar{\rho}\sum_{m=1}^{N}\widetilde{h_m}\,\overline{\bar{D}_m\frac{\partial \widetilde{Y_m}}{\partial x_j}}$$

Where $\bar{K}, \widetilde{T}, \bar{D}_m$ and $\widetilde{h}_m$ are the filtered thermal conductivity, temperature, diffusion coefficient and enthalpy of species m respectively. The thermal conductivity is obtained by using a constant Prandtl number, set to 0.7, for each species contained in the flow field, $\bar{K} = \frac{\mu c_p}{Pr}$. The Prandtl number is the dimensionless ratio of the viscous diffusion rate to the thermal diffusion rate and is typically 0.7 to 0.8 for air and most other gasses (Mira-Martinez, 2013). The heat capacity at constant pressure c_p is obtained from the National Institute of Standards and Technology JANAF thermochemical tables for a multi-component mixture (Chase et al, 1985), while the equivalent diffusion coefficient of the m_{th} species, released or created in the mixture D_m used in the calculations, is obtained from the relation in Eqn. 5.9.

Eqn. 5.9 $$D_m = \frac{1 - Y_m}{\sum_{k\neq m}^{N} X_k / D_{km}}$$ (Poinsot, Veynante and Edwards,2005)

Where X_k is the species mole fraction of the kth species, see Eqn. 4.9.

The subgrid scale terms $\tau_{ij}^{sgs}, h_j^{sgs}, \Theta^{sgs}$ and Φ_{jm}^{sgs} represent the unresolved components of momentum transport and heat flux, the subgrid scale dissipation and species mass flux respectively. The velocity-pressure gradient correlation term and the subgrid scale diffusive mass flux are both neglected, in the energy equations, because of their insignificant contribution to the energy. The filtered reaction rates are given in Arrhenius form, Arrhenius was the first scientist to correlate the rise of CO_2 to a rise in temperature through the greenhouse effect, and were modelled without distinguishing between the resolved and unresolved scales. Despite the limitations of this approach, the results are expected to provide good estimations of the scalar fields that can be further improved by using a more precise reaction rate filtering approach. However, for the objectives of this study, these predictions are sufficient to allow the comparison of and distinction between the flame dynamics for the selected VAM concentration at the selected temperature cases.

The chemical kinetics are governed by the four step model, see Eqns. 4.12, Eqn. 4.13, Eqn. 4.14 and Eqn. 4.15 for the detailed description, derived for the oxidation of methane (Jones and Lindstedt, 1988), which is a well-known chemical scheme and it is considered as sufficiently accurate for the purpose of the current numerical simulation. The four reversible chemical reactions are comprised of seven species (CH_4, CO_2, O_2, CO, H_2O, H_2 and N_2). The use of a four-step mechanism allows for a significant reduction in computing time compared to that required if the entire spectrum of species and reactions was used, but yields a good and sufficient result.

5.4 Temperature profiles of the LES combustion dynamics simulations necessary to characterize the expected VAM concentrations to determine the initial temperatures required for sustained combustion of the incoming VAM.

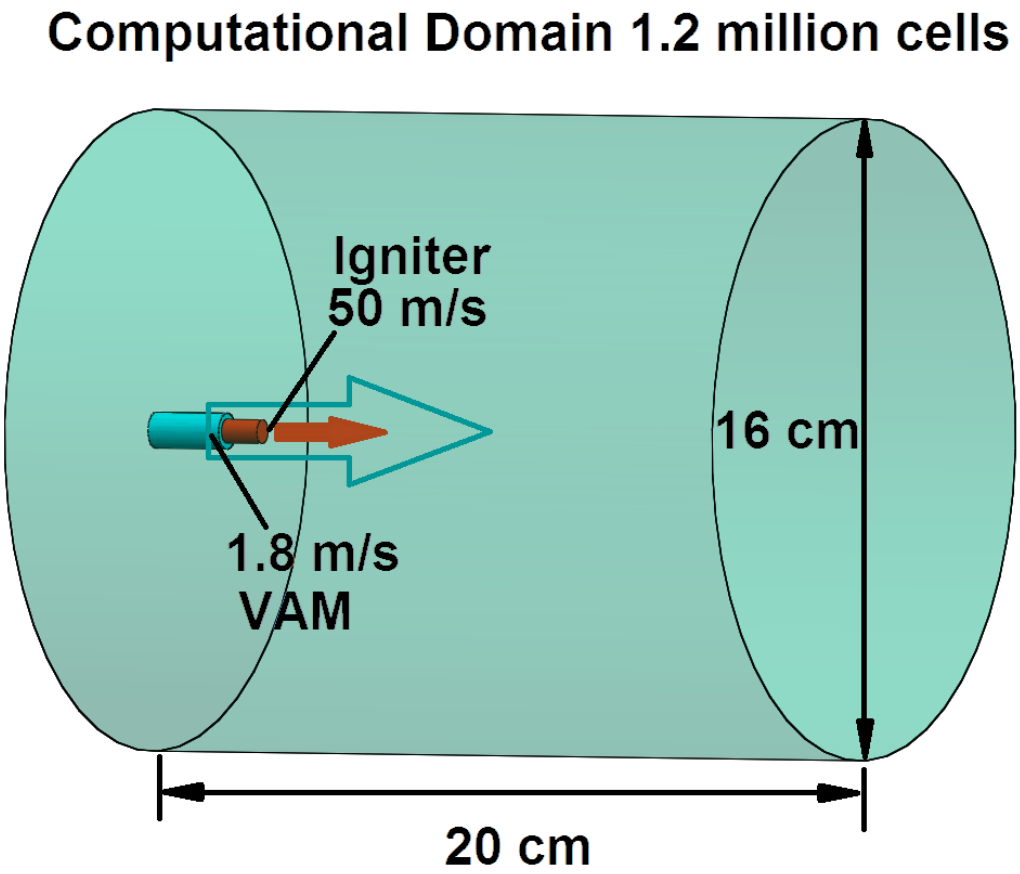

Figure 5.4.1 Dimensions and co flow characteristics used in the LES model

The scale of the computation is quite small, but contains 1.2 million cells. This allows computations to be performed in reasonable timeframes while providing

detailed and realistically high-resolution information on the combustion dynamics. The computational domain was designed to simulate the igniter by defining a well-established simple jet flame configuration surrounded by the incoming VAM co-flow. The computational domain with annular injector is shown in Figure 5.4.1, and an expanded view, of the igniter flame 0.03 m in diameter with the injected VAM surrounding the injector flame by a 0.045 m annulus, is shown in Figure 5.4.2. This configuration reduces the edge effect turbulence while bringing the VAM and igniter flame into contact. The computational domain contains VAM at the same concentration as that surrounding the igniter.

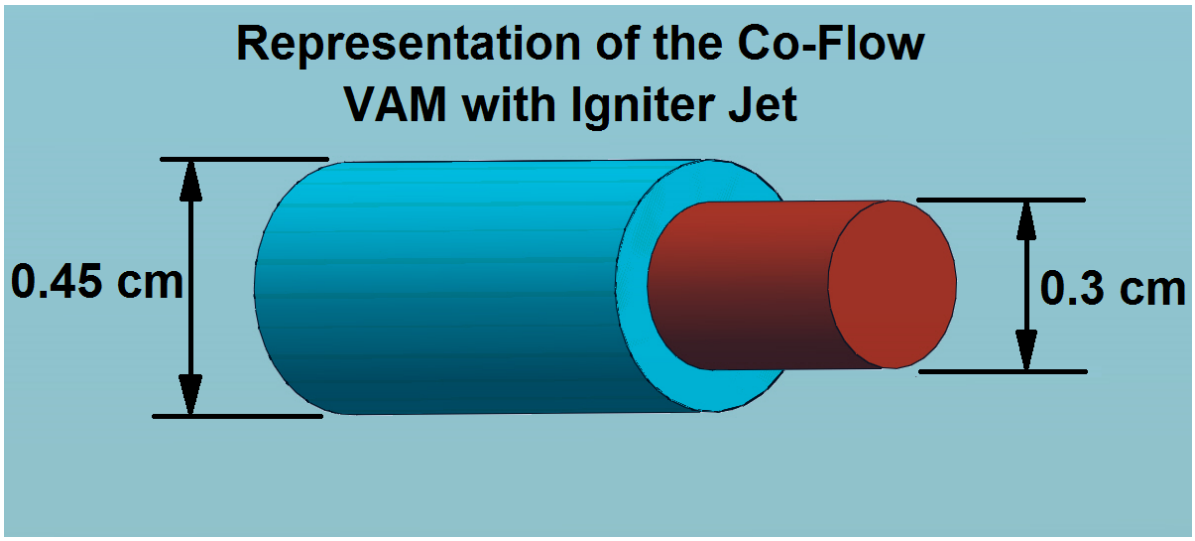

Figure 5.4.2 Representation of VAM igniter co-flow

The concentrations studied are from 0.5% to 3% VAM and the temperature range is from 300 K to 500 K, the instances modeled are presented in Table 5.4-1. A control simulation was performed to establish the flow patterns of a co-flow comprised of a 3000 K flow, representing the injector flame, and a 300 K VAM flow. This is a purely computational flow dynamics simulation without any combustion interaction calculations.

Table 5.4-1 The eight combinations of VAM concentration and temperatures in the study.

Simulation Instance	Temperature (K) of the incoming VAM	VAM Concentration volume%
Control	300	0.5
Simulation 1	300	1.0
Simulation 2	300	2.0
Simulation 3	400	1.0

Simulation 4	400	2.0
Simulation 5	400	3.0
Simulation 6	500	0.5
Simulation 7	500	1.0
Simulation 8	500	2.0

This simulation provides a benchmark flow profile for contrast with the profiles obtained when combustion dynamics are included in the computation. The co-flow was comprised of air with a 0.5% VAM concentration at 1.8 m/s and a 3000 K air jet at 50 m/s. As can be seen from Figure 5.4.3 the jet traverses the same computational domain as all simulations. The interaction between the jet and the incoming VAM does not exhibit any of the characteristic turbulence that a combustion system exhibits. The control simulation was designed and executed with Solidworks.

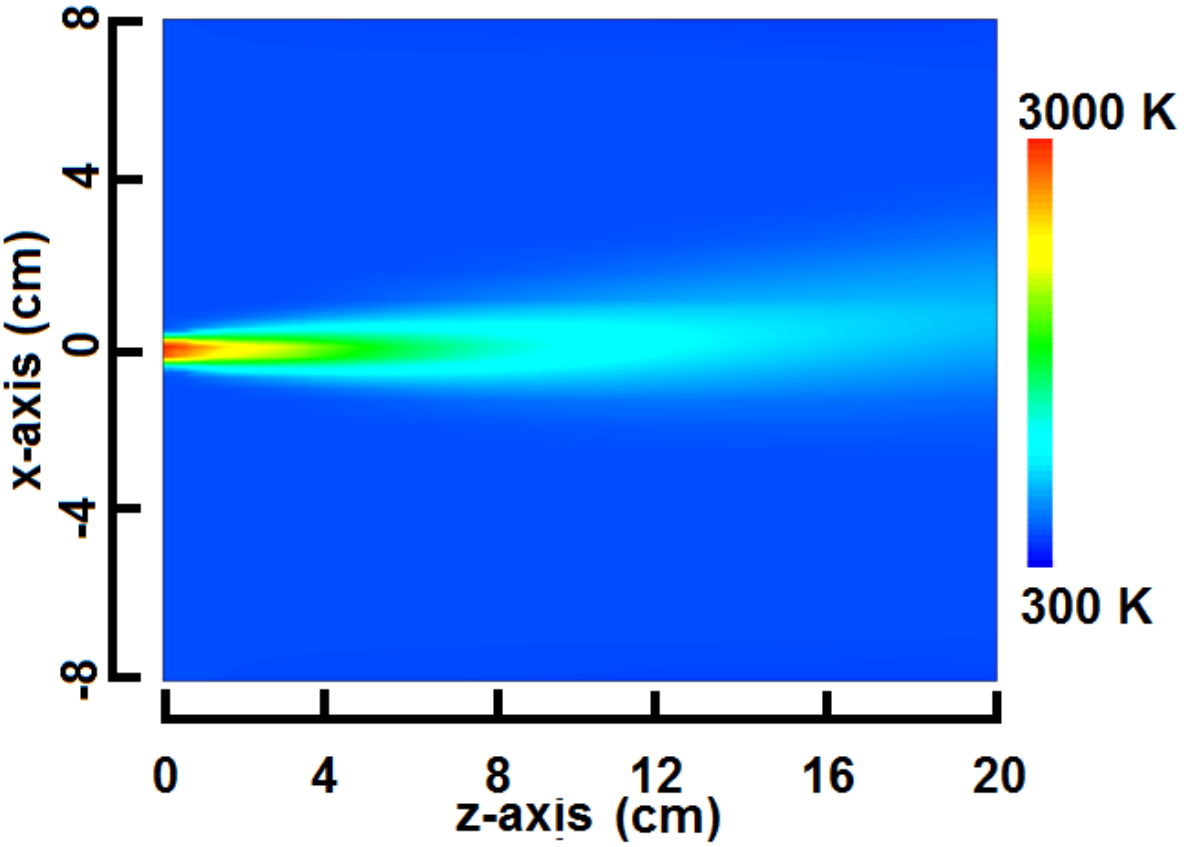

Figure 5.4.3 Control CFD simulation with no combustion computations.

The computational instances in Table 5.4-1 were determined to be sufficient to show the characteristics of the combustion dynamics for the percentages of VAM

pertinent to the design of the VamTurBurner©. The temperature range from 300 K to 500 K and VAM concentrations from 0.5% to 3% were chosen as representative.

These selected representative simulations are based on the expected VAM concentrations in the mine ventilation air (see Figure 3.2.4) and the temperatures determined from the analytical model developed in chapter 4.

Simulation 1 is a 1% VAM concentration at an initial temperature of 300 K, which is a typical temperature that would be expected from the exhaust fans from the ventilation system. The central axis cross sections are presented in Figure 5.4.4 (a, b, c and d) were obtained at 0.015s, 0.020s, 0.025s and 0.030s respectively from initiation of the co-flow; these times are the same for all LES scenarios. The results of simulation 1 show that there is no ignition of the incoming VAM except that which comes directly in contact with outer edge of the flame as the mixture traverses the first half of the computational domain. At that point the turbulence increases and the turbulent mixing of the incoming fuel stream with the contents of the chamber exhibits a similar turbulence profile to a rising plume, but with the expansion of the gasses due to burning of the higher concentration fuel in the igniter flame jet. At a ventilation flow of 100 m^3/s, a concentration of 1% VAM would provide a valuable addition to the energy profile of nearly 38 MW_{th}.

The next model, simulation 2, is also at a temperature of 300 K, but for a 2% VAM concentration. Observation of the lower portion of Figure 5.4.5 (a, b, c and d) shows that an emerging “V-shaped” profile protrudes radially from the ignition jet. This feature proceeds to expand radially while continuing to move in the direction of the initial momentum. The shape changes to a more “bell-shaped” profile as the combustion of the igniter jet fuel continues to burn; however, the contour does not proceed backward to engulf the incoming VAM. This is an indication that there is combustion of the VAM in this region, but it is insufficient because the combustion is merely an interaction between the fuel of the incoming jet and the 2% VAM in the ventilation flow rather than a self-sustaining ignition of the VAM. The forward motion of the ignition zone confirms this aspect because there is no diffusion of heat, back to the pre-heating zone; see Figure 4.4.2 and the discussion in chapter 4 subsection 4 for the details of a diffusion flame.

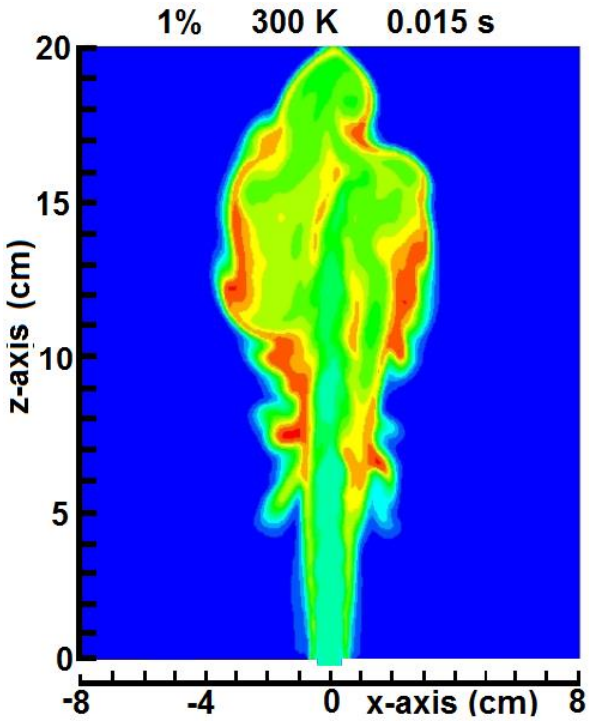

Figure 5.4.4 (a)

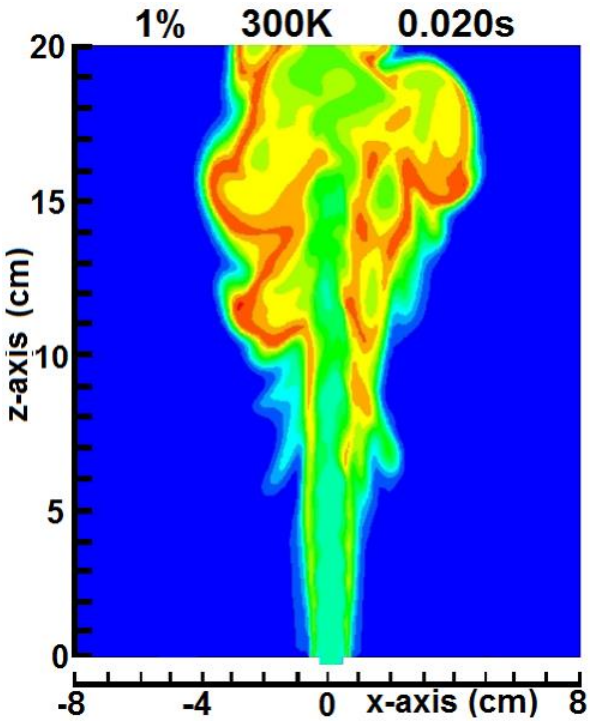

Figure 5.4.4 (b)

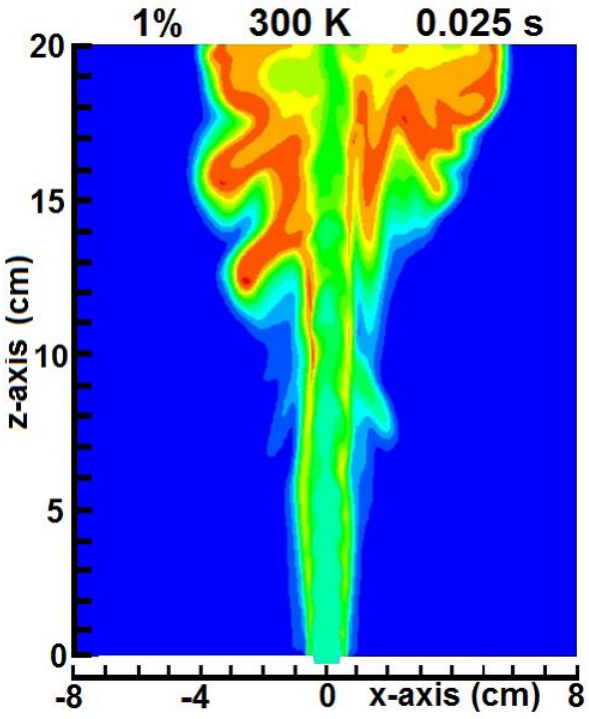

Figure 5.4.4 (c)

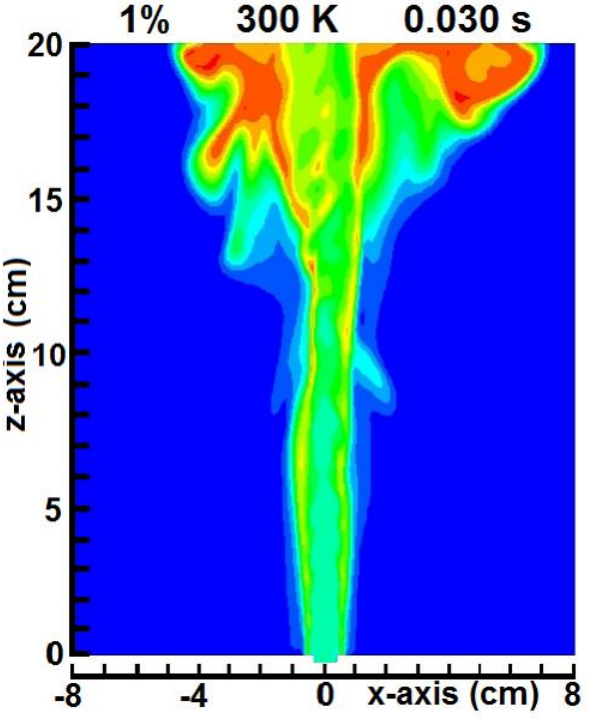

Figure 5.4.4 (d)

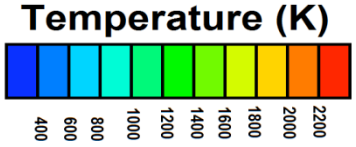

Figure 5.4.4 (a, b, c and d) are cross sections, for simulation 1 of the flame characteristics for 1% VAM at an initial temperature of 300K at 0.015s, 0.020s, 0.025s and 0.030s (Mira-Martinez, Cluff and Jiang, 2014).

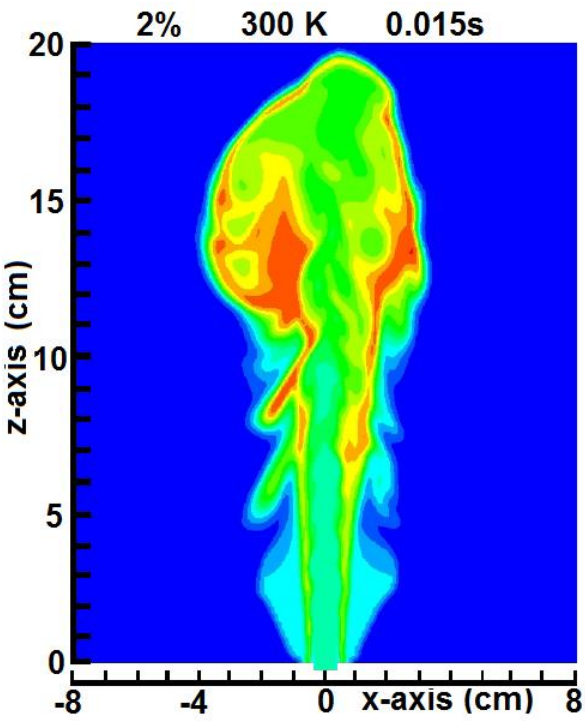

Figure 5.4.5 (a)

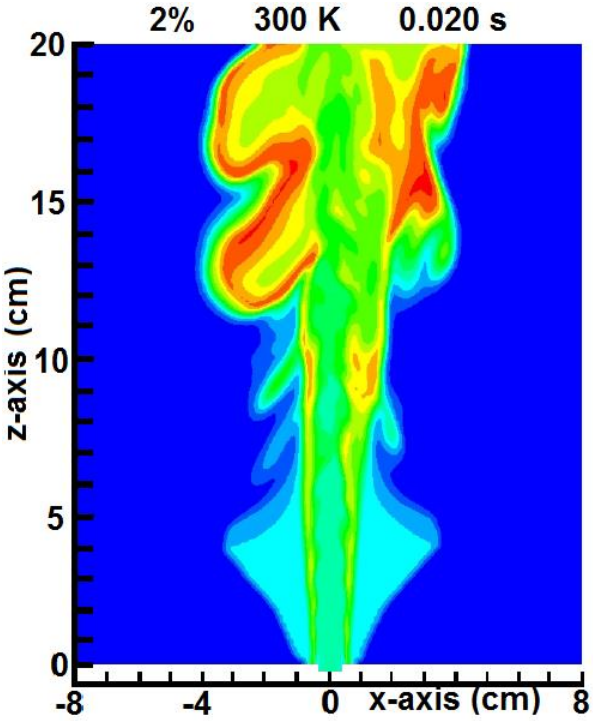

Figure 5.4.5 (b)

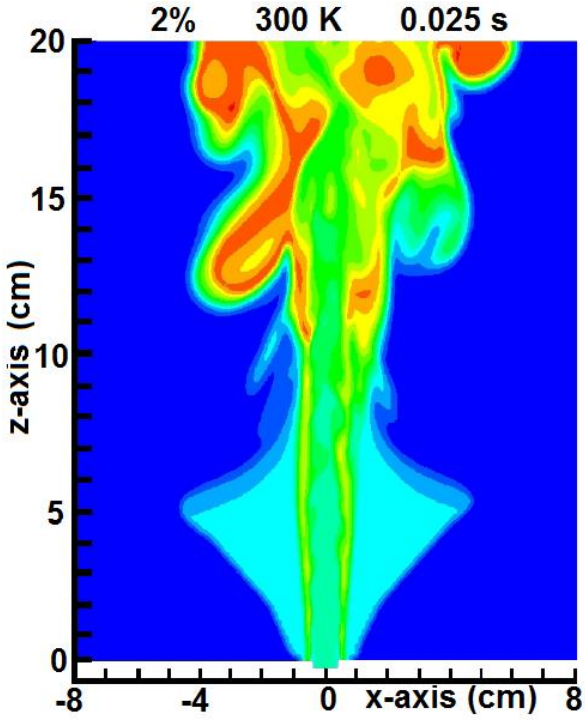

Figure 5.4.5 (c)

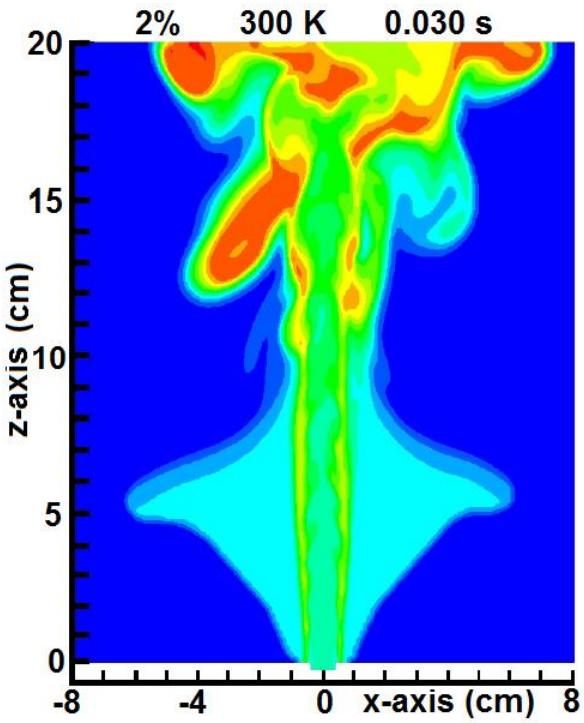

Figure 5.4.5 (d)

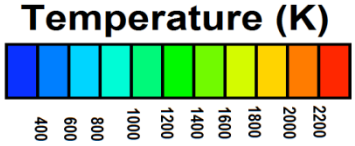

Figure 5.4.5 Figure 5.4.5 (a, b, c and d) are cross sections, for simulation 2, the flame characteristics for 1% VAM at an initial temperature of 300K at 0.015s, 0.020s, 0.025s and 0.030s (Mira-Martinez, Cluff and Jiang, 2014).

There are three instances studied at an initial temperature of 400 K, simulations 3, 4 and 5 having VAM concentrations of 1, 2 and 3% respectively. These simulations confirm combustion of VAM, similar to the other technologies such as RTO, TFRR, but at lower temperatures for the CFRR due to the addition of catalysts.

The 1% VAM concentration at an initial temperature of 400 K, Figure 5.4.6 (a, b, c and d), can be described as slightly more active than that at an initial temperature 300 K in terms of the initiation of some combustion radially to the igniter jet. The profile exhibits some similarity to that in the 2% VAM concentration at an initial temperature of 300 K in terms of the slight initiation of some combustion of the VAM radially, but not as dynamic as that seen in that at an initial temperature of 300 K. This demonstrates that the increase in temperature from 300 K to 400 K has a slight effect on the 1% VAM concentration, but that an increase from 1 to 2% VAM at the same temperature has a greater effect on the ignition of the VAM in the computational domain.

The effect of increasing the VAM concentrations is even more pronounced in the simulations for a 2% and 3% VAM concentration at 400 K. The 2% VAM concentration readily ignites when the initial temperature is 400 K, see the initial figure at 0.015 s from initiation of the flow shown in Figure 5.4.7 (a). All the simulations for 2% VAM, at an initial temperature of 400K, Figure 5.4.7 (a, b, c and d), show high levels of turbulent mixing and a temperature above the threshold temperature of 800 K to 1000 K over the computational domain from the bottom at z = 0 and across the entire x-axis. This is clear evidence that for a VAM concentration of 2% at an initial temperature of 400 K that ignition initiates self-supporting flameless combustion. Further increases in the VAM concentration will increase the temperature in the combustion zone, providing more heat diffusing back from the combustion zone to the preheating zone as outlined Figure 4.4.2. Observation of the temperature profiles for a 3% VAM concentration at an initial temperature of 400 K, Figures 5.4.8 (a, b, c and d), shows an increase in the temperature of the combustion zone to over 1000 K. This is consistent with the analytical model developed in Chapter 4; see Figures 4.3.1 and 4.3.2, and an indication of the potential for a sustained reaction due to the availability of heat diffusion back from the combustion zone to the preheating zone.

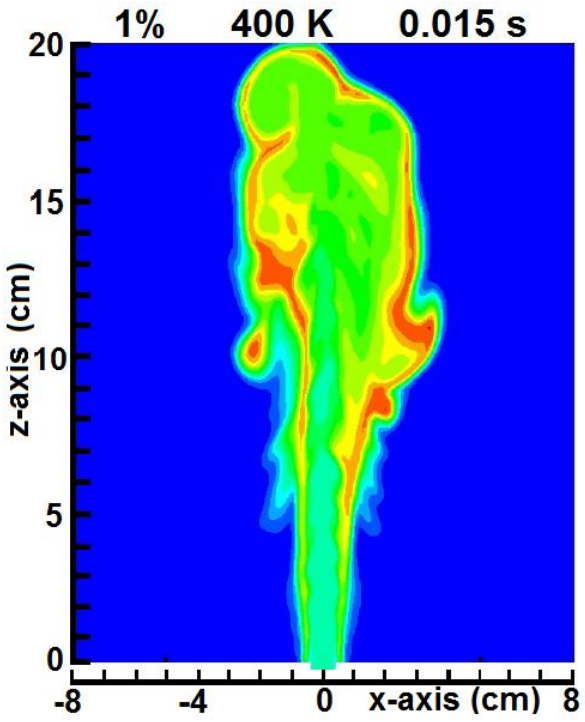

Figure 5.4.6 (a)

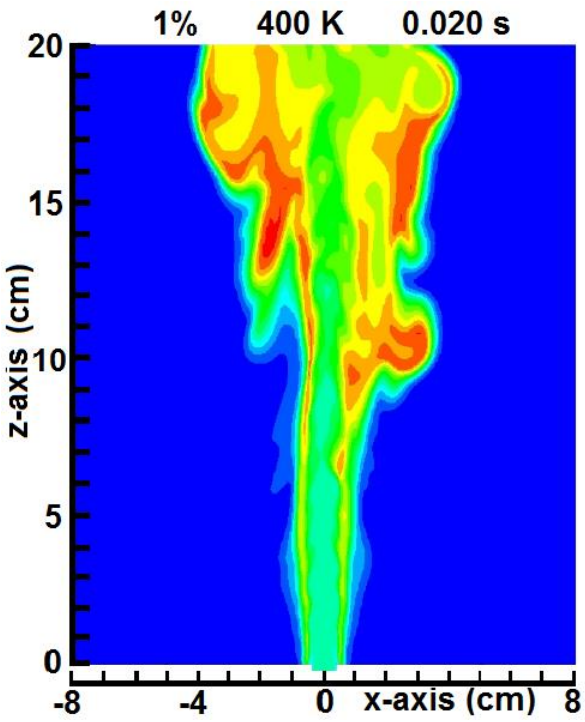

Figure 5.4.6 (b)

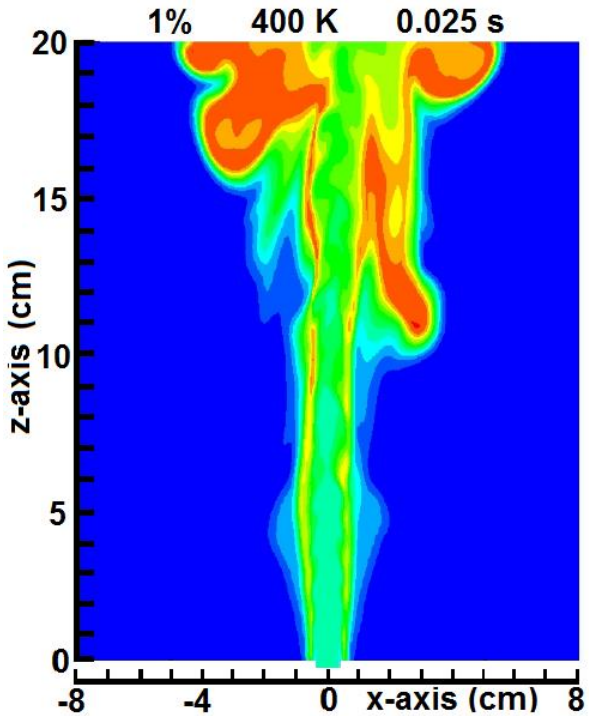

Figure 5.4.6 (c)

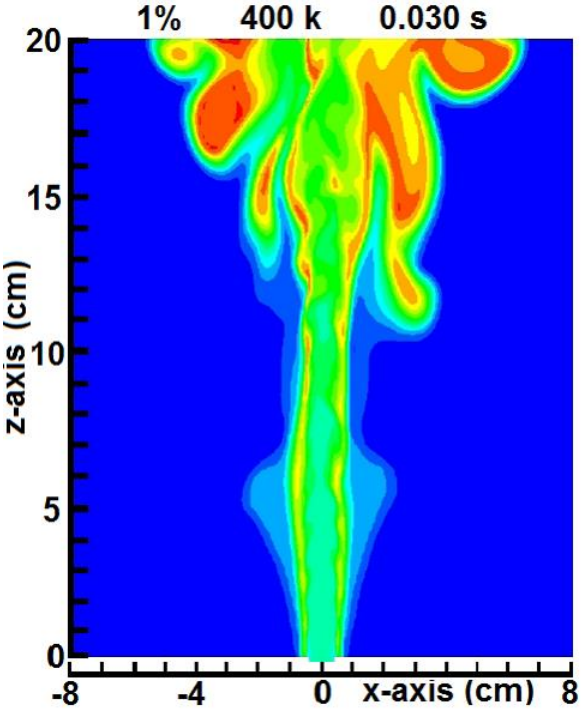

Figure 5.4.6 (d)

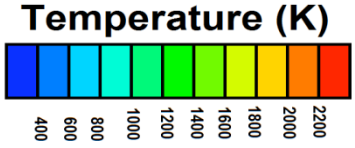

Figure 5.4.6 (a, b, c and d) are cross sections, for simulation 3, the flame characteristics for 1% VAM at an initial temperature of 400K at 0.015s, 0.020s, 0.025s and 0.030s (Mira-Martinez, Cluff and Jiang, 2014).

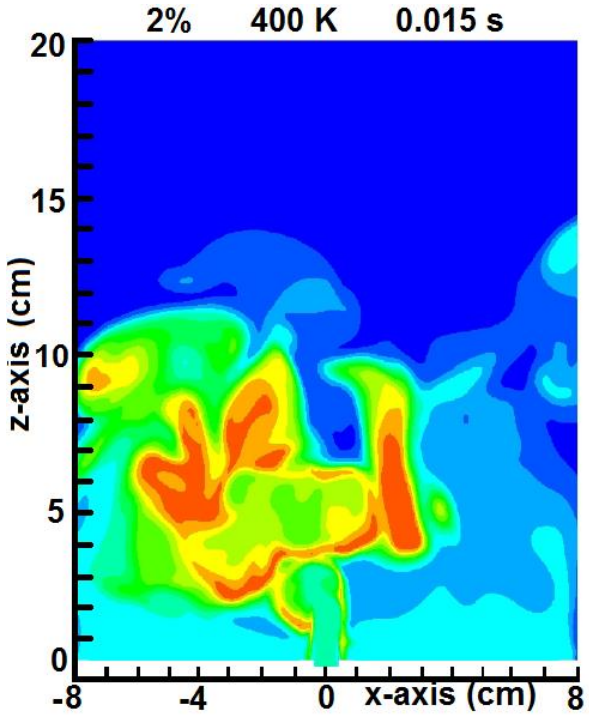

Figure 5.4.7 (a)

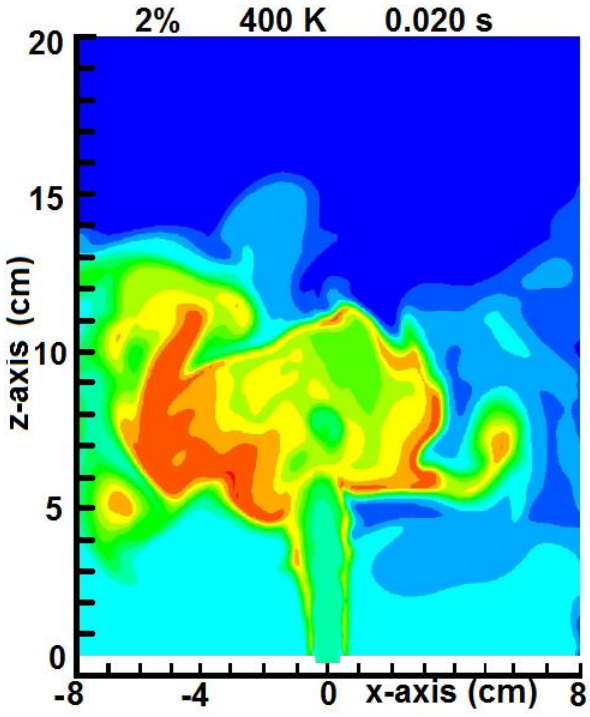

Figure 5.4.7 (b)

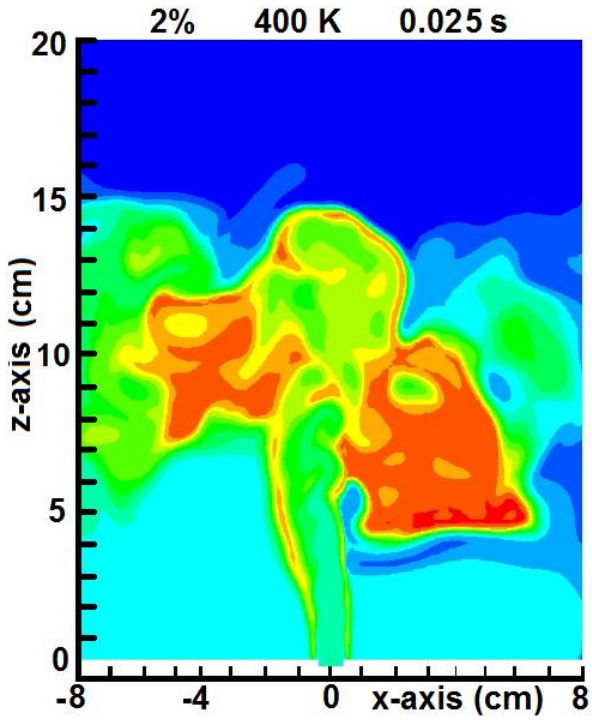

Figure 5.4.7 (c)

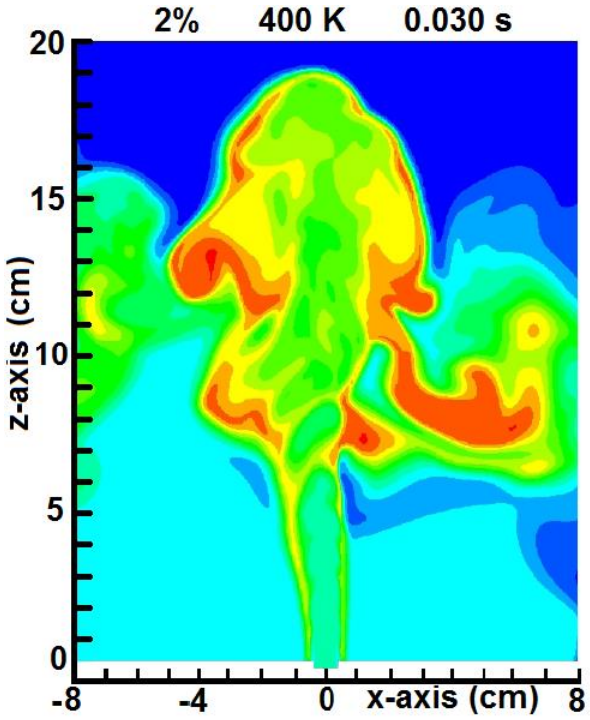

Figure 5.4.7 (d)

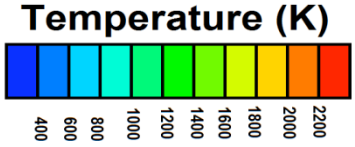

Figure 5.4.7 (a, b, c and d) are cross sections for simulation 4, the flame characteristics for 2% VAM at an initial temperature of 400K at 0.015s, 0.020s, 0.025s and 0.030s (Mira-Martinez, Cluff and Jiang, 2014).

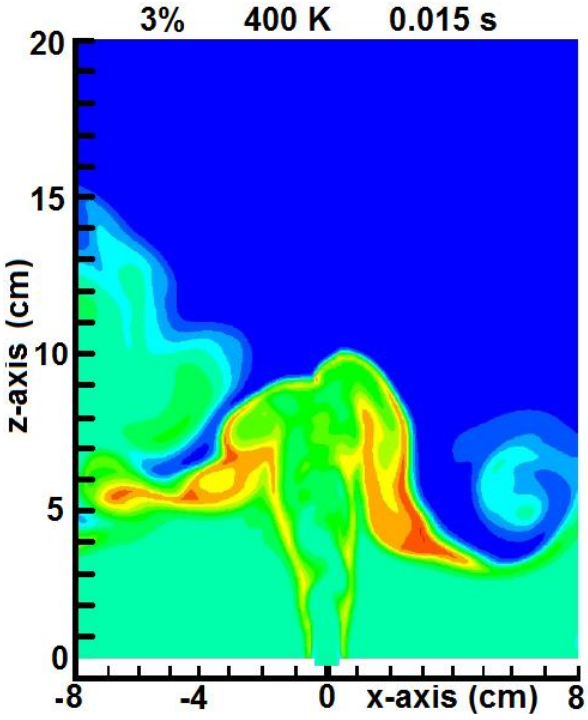

Figure 5.4.8. (a)

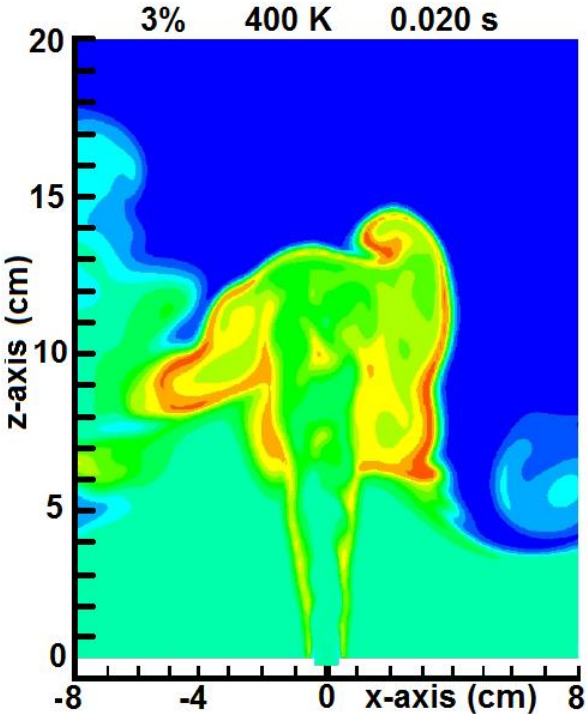

Figure 5.4.8 (b)

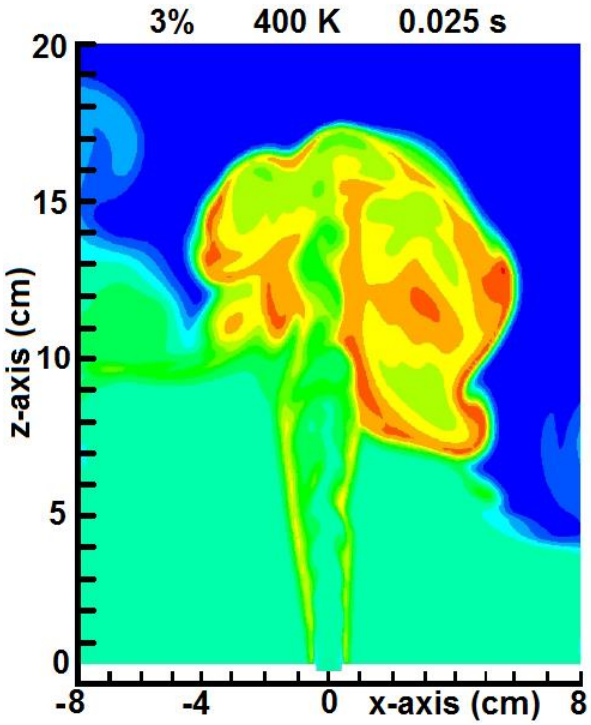

Figure 5.4.8 (c)

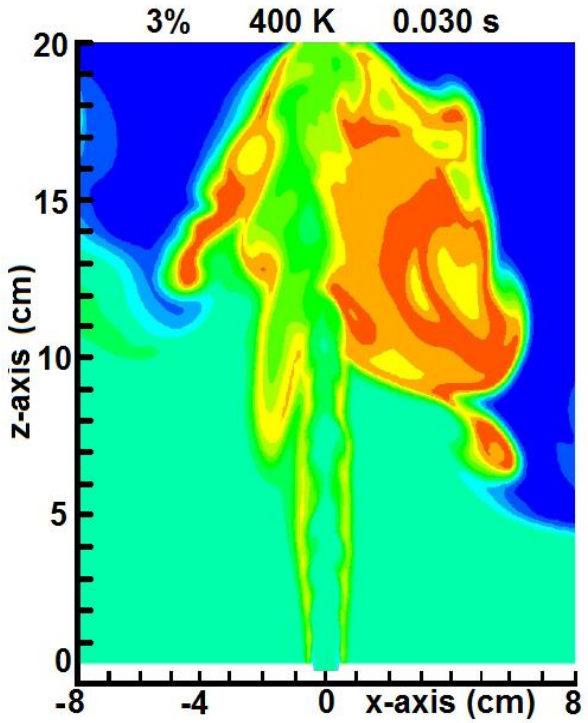

Figure 5.4.8 (d)

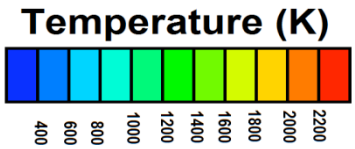

Figure 5.4.8 (a, b, c and d) are cross sections for simulation 5, of the flame characteristics for 3% VAM at an initial temperature of 400K at 0.015s, 0.020s, 0.025s and 0.030s (Mira-Martinez, Cluff and Jiang, 2014).

The remaining three simulations 5, 6, and 7 are at an initial fresh gas temperature of 500 K for VAM concentrations of 0.5, 1 and 2% respectively. The critical simulation at the 500 K preheating temperature is that at 0.5% VAM concentration, because further increases in temperature may carry further increases in risk, but the 0.5% VAM concentration is a design threshold. The increased risk as the temperature rises is due to the higher probability of inadvertent ignition. This is a familiar concept of any premixed fuel/oxidizer system and discussed in chapter 4.

There was no ignition proceeding to combustion from any simulations at an initial temperature of 300 K, although the 2% VAM simulation did begin to show signs of an initiation of combustion. At the initial temperature of 400 K, the 1% VAM concentration showed signs of initiation while the 2% VAM concentration fully ignited and exhibited sustained combustion and the 3% VAM concentration was the same as the 2 per cent simulation, but burned at a higher temperature. These results are significant for reasons that will be discussed in chapter 7. It is critical that a sustained combustion be demonstrated at a concentration of 0.5% VAM concentration because the mine ventilation systems are designed to dilute the methane to a safe level, but about 70% of the US underground mine shafts have methane concentrations above about 0.4%. For those less than 0.4% it is not a difficult matter, and a standard industry practice, to supplement the VAM concentration to achieve 0.5% and many of the existing methane mitigation projects are supplemented to a value of 0.9% methane.

Comparison of the 2% VAM simulations, at initial temperatures of 400 K and 500 K, Figures 5.4.7 (a, b, c and d) and 5.4.9 (a, b, c and d) respectively, shows that the effect of raising the temperature is not as effective as raising the VAM concentration. The 2% VAM concentration ignited readily establishing the characteristics of a sustained reaction, evidenced by the temperature being above 800 K from the z = 0 position and from the initiation of the co-flow. However, at the initial temperature of 500 K, the initiation of combustion is faster and more stable as can be seen by comparison of Figure 5.4.7 (d) to Figure 5.4.9 (d) in terms of the turbulence and vorticity of the flow. The potential for a more stable and sustained reaction is improved at the higher temperature, but the preheating temperature for a percentage VAM concentration will not be required to be increased to 500 K for operational purposes.

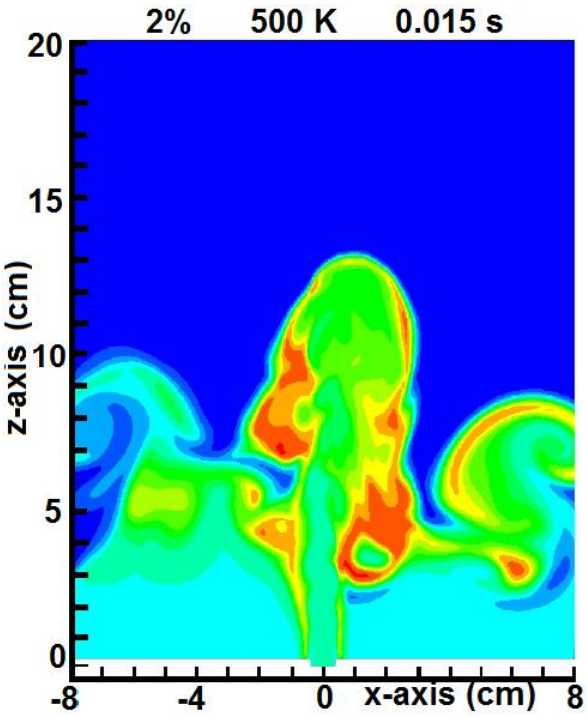

Figure 5.4.9 (a)

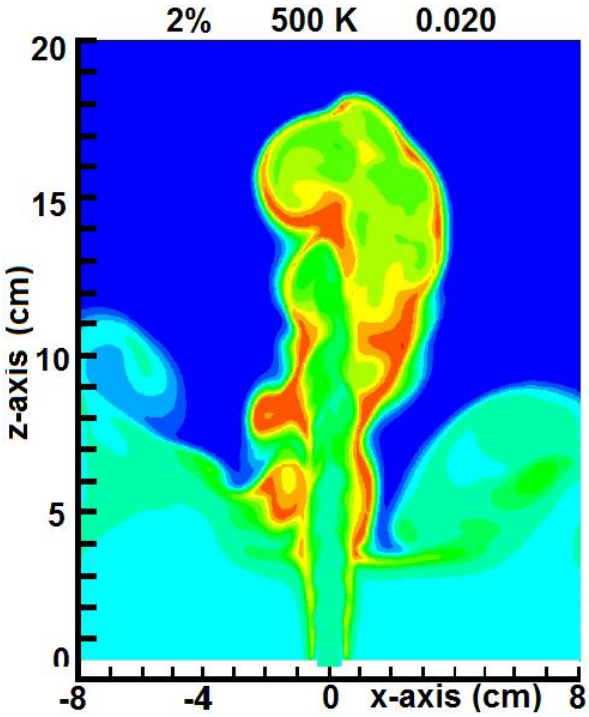

Figure 5.4.9 (b)

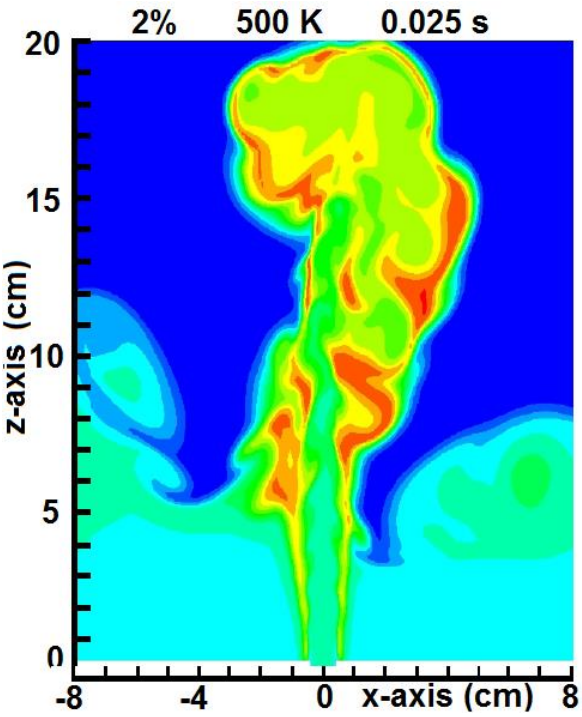

Figure 5.4.9 (c)

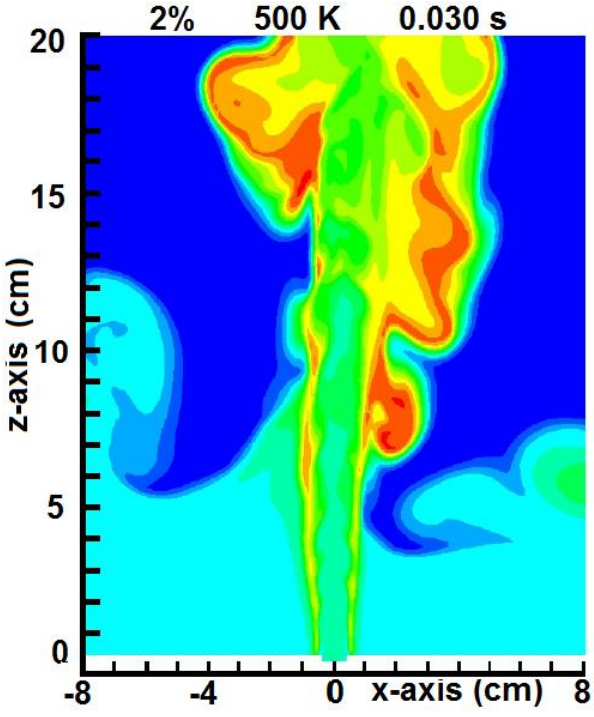

Figure 5.4.9 (d)

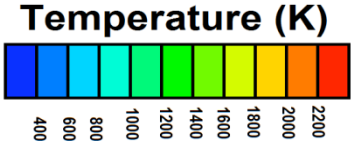

Figure 5.4.9 (a, b, c and d) are cross sections for simulation 6, of the flame characteristics for 2% VAM at an initial temperature of 500K at 0.015s, 0.020s, 0.025s and 0.030s (Mira-Martinez, Cluff and Jiang, 2014).

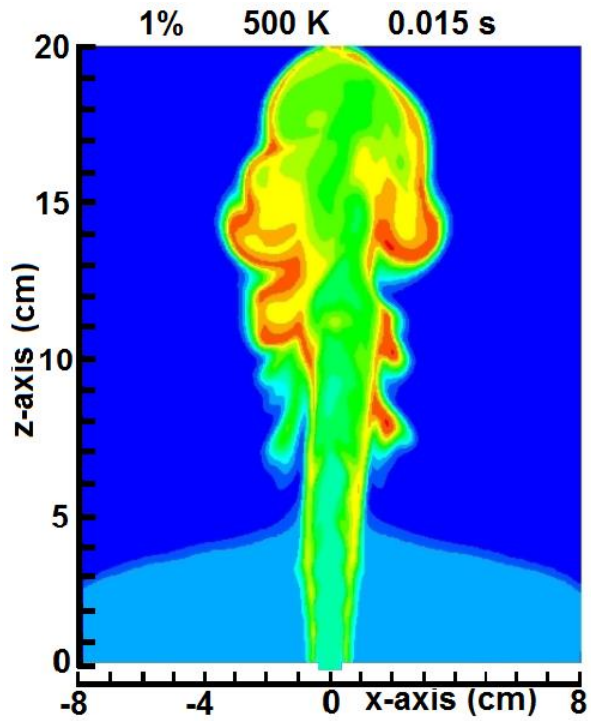

Figure 5.4.10 (a)

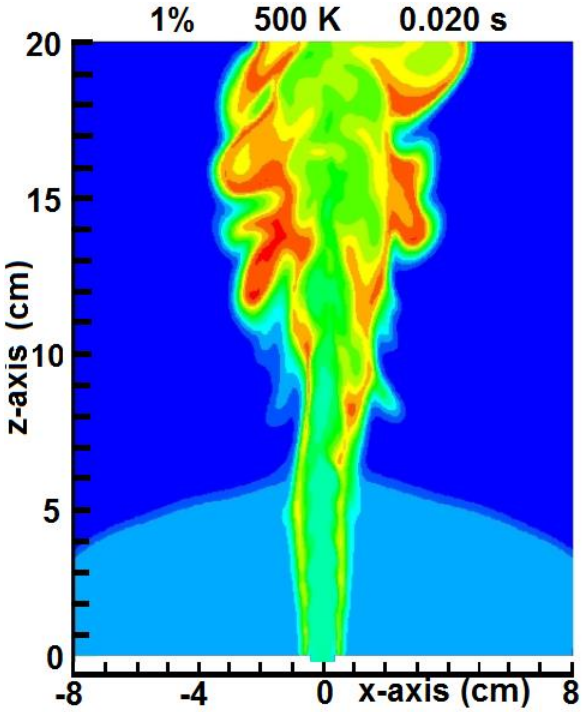

Figure 5.4.10 (b)

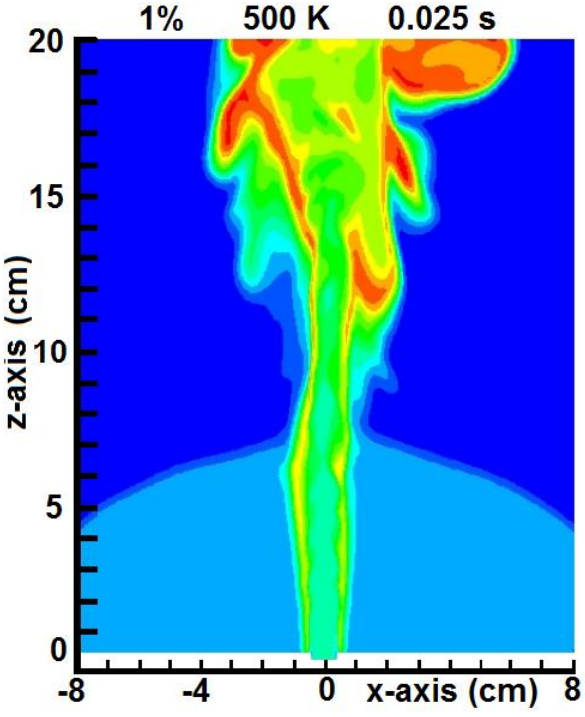

Figure 5.4.10 (c)

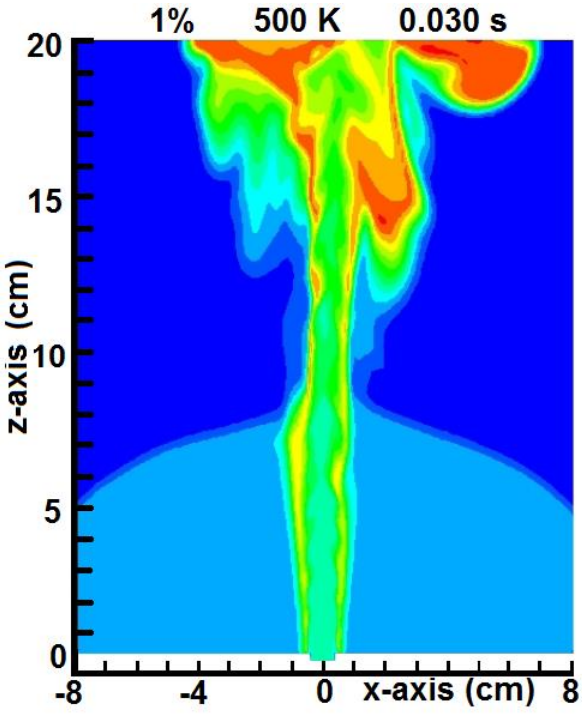

Figure 5.4.10 (d)

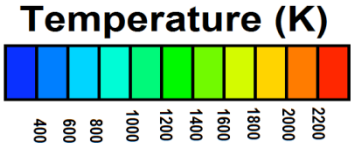

Figure 5.4.10 (a, b, c and d) are cross sections for simulation 7, of the flame characteristics for 1% VAM at an initial temperature of 500K at 0.015s, 0.020s, 0.025s and 0.030s (Mira-Martinez, Cluff and Jiang, 2014).

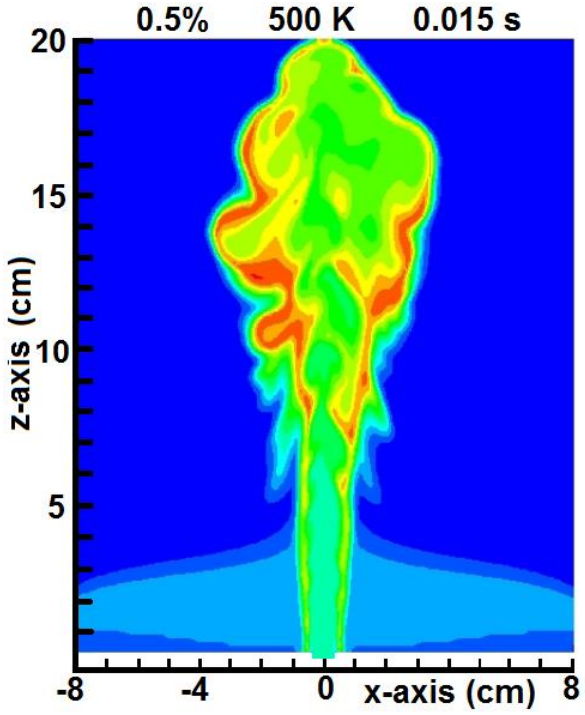

Figure 5.4.11 (a)

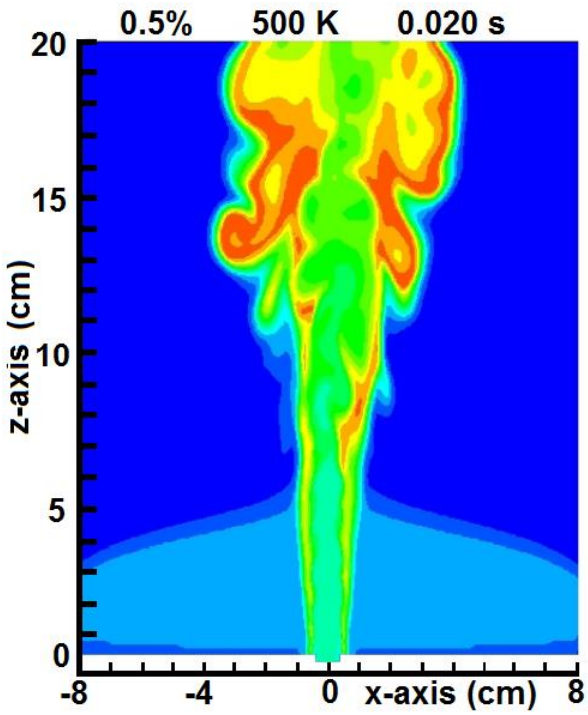

Figure 5.4.11 (b)

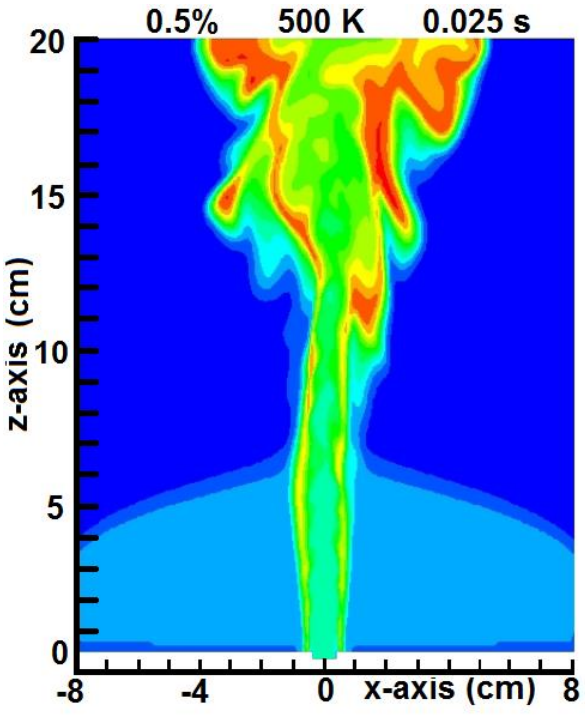

Figure 5.4.11 (c)

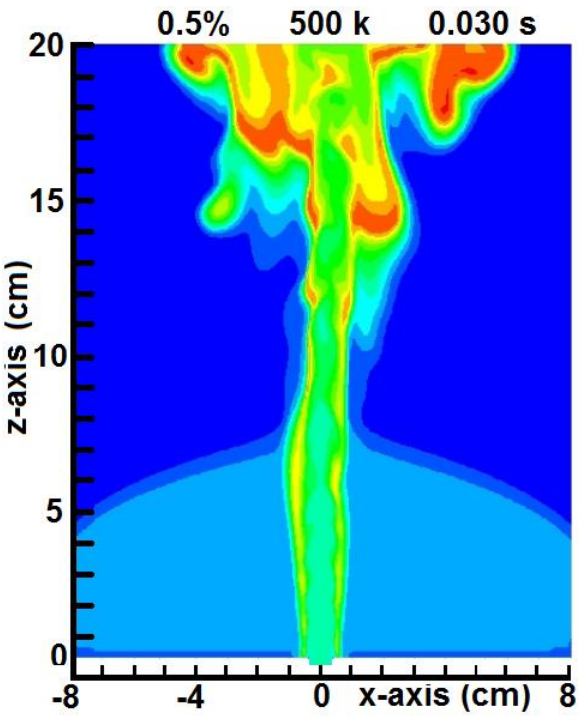

Figure 5.4.11 (d)

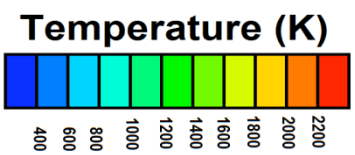

Figure 5.4.11 (a, b, c and d) are cross sections for simulation 8, of the flame characteristics for 0.5% VAM at an initial temperature of 500K at 0.015s, 0.020s, 0.025s and 0.030s (Mira-Martinez, Cluff and Jiang, 2014).

The 1% VAM concentration at an initial temperature of 500 K in Figure 5.4.10 (a, b, c and d) is the only simulation at 1% to demonstrate ignition and self-sustained combustion. The progression of at 1% and 500 K shows a smooth profile across the entire computational domain while progressing in the direction of the initial momentum of the flow. This is a key result (Cluff, Mira-Martinez and Jiang, 2014) that shows there is sufficient heat generated in the combustion zone to cause diffusion back to the preheating zone; thus, providing the heat needed for sustaining the reaction. The smooth nature of the combustion zone or conversely the lack of turbulence is an excellent indication that the combustion is flameless. The flameless combustion regime is a recent area of flame research and has been accomplished experimentally with modest air preheating (Ayoub et al, 2012). The observation of the flame front or the top part of the smooth combustion zone in the series of Figures for 1% VAM at 500 K in Figures 5.4.10 (a, b, c and d) shows a cooler zone in the 600 K to 800 K region moving forward and a hotter zone following behind in the 800 K to 1000 K region. This demonstrates the diffusion of heat is moving from the combustion zone to the flame front and is an indication of good potential for a sustainable reaction. Further evidence of the sustainability of the reaction is demonstrated by considering the temperature radial to the inlet at the bottom of the figures. There are no gaps, which validates that the methane in the mixture has ignited and continues burning smoothly.

The most critical simulation in this study is for the 0.5% VAM concentration because if it is viable this concentration then allows for a reasonable number of mines to be targeted as potential users of the technology. The similarities to the simulation for the 0.5 and 1% VAM concentrations are quite remarkable; the differences are subtle. It takes longer for the heat to diffuse from the combustion zone to the preheating zone at the lower VAM concentration. Comparing the 1% and 0.5% VAM concentrations at 0.015 s from the onset of the co-flow, Figure 5.4.10 (a) and Figure 5.4.11 (a) respectively, there is a slight delay of the combustion of the VAM in the 0.5% VAM concentration. The temperature of the incoming VAM, at the bottom of the cross section of the 0.5% VAM concentration at 0.015 s, is not at the same temperature as that in the combustion zone, but it is clear that it is being heated due to the elevated temperature. By the end of the simulation, at 0.030 s, the VAM is in a steady state of combustion as the gap at the inlet level seen at 0.015 s is

now closed. At this point in the simulation, for the 0.5 and 1% VAM concentrations in Figure 5.4.10 (d) and Figure 5.4.11 (d) respectively, the profiles are virtually indistinguishable except the combustion zone of the 0.5% VAM concentration lags that of the 1% VAM concentration by about 1 cm.

The key result for the 0.5% VAM concentration, which is sufficient to justify the argument that the VamTurBurner© design is viable. A means of preheating the incoming ventilation containing the VAM will be required. The use of heat exchangers or recirculation flows are explored in chapter 7.

6. The VamTurBurner© multi-generation system

6.1. Introduction:

Multi-generation systems combined with robust energy storage systems, are similar to combined heat and power systems or trigeneration systems. When combined with an energy storage system such as: compressed air, batteries, flywheels or liquid air the flexibility allows for arbitrage between higher and lower energy cost regimes, the system produces less GHG or pollution and would operate at higher efficiency than when producing each of the outputs separately. These aspects suggest that there are techno-economic and socio-economic benefits in connection with the improved efficiency of such systems. Many aspects of modern energy strategy, such as: mitigating climate change, reacting to the scarcity of certain energy resources like the concept of "peak oil" or responding to a change in the composition of the resource supply have prompted the establishment of energy conservation programs, renewable energy research efforts and energy efficiency programs. These programs are designed to protect and use energy resources or enhance the economic competitiveness of the energy products obtained. The concept of multi-generation in Distributed Multi-Generation Systems: Energy Models and Analyses is emphasised in the quote below. (Mancarella and Chicco, 2009).

> *"The recent development of distributed generation technologies is changing the focus of the production of electricity from large centralized power plants to local energy systems scattered over the territory. Under the distributed generation paradigm, the present research scenario emphasises more and more the role of solutions aimed at improving the energy generation efficiency and thus the sustainability of the overall energy sector. In particular, coupling local cogeneration systems to various typologies of chillers and heat pumps allows setting up distributed multi-generation systems for combined production of different energy vectors such as electricity, heat (at different enthalpy levels), cooling power, and so forth. The generation of the final demand energy outputs close to the users enables reducing the losses occurring in the energy chain conversion and distribution, as well as enhancing the overall generation efficiency."*

The amount of energy and the variation in intensity required by the mining industry suggests that the acquisition of energy at a lower price or reduction in the quantity of energy purchased from the grid for the basics such as electricity, hot water, heating and cooling or higher energy demand processes such as industrial drying, crushing, grinding and milling would be highly beneficial to mining companies. A multi-generation system coupled with energy storage is a notion that

forward thinking CEO's should embrace. The optimum configuration of a multi-generation system is a multifaceted problem because of the variety of technologies available, the time-series nature of the fluctuations in energy consumption that need to be matched to the fluctuating price structure of energy or the variations in the nature of the environmental assessments. However, the concepts of the design of a multi-generation system capable of mitigating VAM and the incorporation such a system into the distributed energy system is an endorsement of the concepts of distributed energy as a viable option for future supply.

Widespread acceptance of multi-generation systems in the mining industry is decidedly dependent on overcoming the inertia opposing the introduction of new technology in the industry. Mining companies are well known for requiring that any technologies implemented in the development of a project be mature and well tested. This work suggests that the mining industry introduce pilot multi-generation projects in the immediate term with the full intent to scale up the projects in the medium term in order to take advantage of the changes in the changing energy horizon. This is especially pressing given the current expectations for the availability of low priced natural gas because of changes in the supply horizon due to the technological changes in securing supply known as fracking.

The impact of transferring from centrally located power plants, such as large scale nuclear or coal installations, to on-site power production could tip the energy supply balance toward a more sustainable and reasonably priced energy supply system. Currently price is dictated by the oligopoly of a closely connected industry that provides inherently expensive and at times unreliable energy supply. There is an expectation that changing over to distributed power generation leads to a reasonably priced, robust power supply with a price set by market conditions. Power generation concepts are currently evolving to meet the projected future demand and microturbines are attractive because they offer compactness and simplicity of design (Hamilton, 2003). The proposed VamTurBurner© system depends on a microturbine based cogeneration system, which is considered to be a mature design proven in several different situations. The concept of distributed energy is discussed from the perspective that promoting the notion is advantageous and similar to cogeneration systems, which have proven to be advantageous. The additional benefit of including the windfall power derived from the VAM flow sets the VamTurBurner© apart.

Distributed power generation is central to the theme of this work; therefore, a brief discussion on the concepts of distributed energy generation is included. It is discussed, in *The Industrial Application Guide For Innovative Combined Heat and Power*, how the notion of distributed energy generation has…

> *"captured the interest of policymakers at the federal and state level, potential users and developers, and is entering into the business strategies of many utilities, unregulated energy service providers, and customers".*

The notion that a distributed energy generation system may be capable of a more dynamic response to sudden changes or surges, compared to centrally produced power, was made abundantly clear to this author during the North American power failure of 2003. A few days suddenly became available for uninterrupted thought on the matter of power supply. An excerpt from the Scientific American article, *Preventing Blackouts Building a Smarter Grid* (Amin and Schewe, 2007) illustrates the problem with our current grid structure.

> *"Without sufficient reactive power to support the suddenly shifting flows, overburdened lines in Ohio cut out by 4:05 P.M. In response, a power plant shut down, destabilizing the system's equilibrium. More lines and more plants dropped out. The cascade continued, faster than operators could track with the decades-old monitoring equipment that dots most of the North American power grid, and certainly much faster than they could control. Within eight minutes, 50 million people across eight states and two Canadian provinces had been blacked out. The event was the largest power loss in North American history.*
>
> *The 2003 disaster was a harbinger, too. Within two months, major blackouts occurred in the U.K., Denmark, Sweden and Italy. In September 2003 some 57 million Italians were left in the dark because of complications in transmitting power from France into Switzerland and then into Italy. In the U.S., the annual number of outages affecting 50,000 or more customers has risen for more than a decade."*

The problems associated with power disruption are often related to an outdated grid, with a somewhat negligible capacity to react to the impact of a large power plant failure. When a failure occurs, the difficulty of ramping up to re-establish the power supply to meet the demand is also related to the scale of the suppliers on the grid. It is a difficult problem to determine the ramp-up rate of a large power plant when the demand is indeterminate or essentially assumed. It seems to be quite practical to consider the potential for a distributed power production grid with upgraded sensors and a workable system for storage of excess power.

A distribution system is the part of the grid that is lower voltage transmission of electricity to the homes and businesses in a community seen in Figure 6.1.1. When the distributed power generation system is enhanced by an appropriate power storage system, such as the liquid air systems under development at Highview

Energy, the savings can be increased because of the opportunity for arbitrage of the power price at peak times.

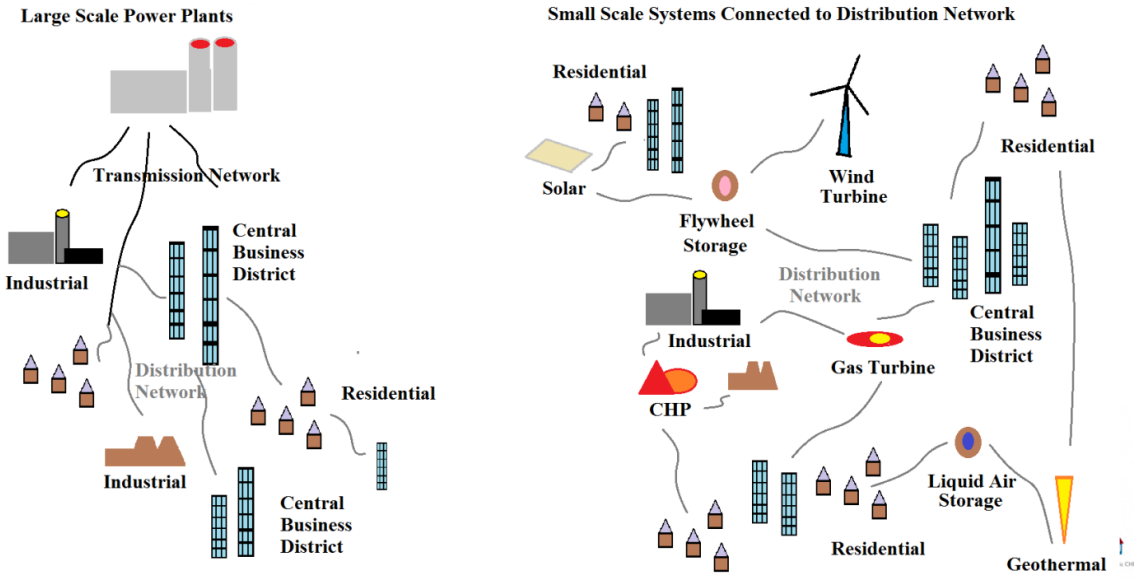

Figure 6.1.1 Comparison of the transmission based network to the locally produced distributed network for power production.

The gas turbines considered to be useful for the VamTurBurner© fall into the microturbine category. The microturbine has an expected efficiency of 18% to 27% for production of electricity and overall combined efficiency of 65% to 75%. In the application outlined for the VamTurBurner© the electrical efficiency is the main attribute carried over from the design of the cogeneration system because the exhaust heat is combined with other sources of heat in the system and so is only a part of a larger heat based system.

The capacity of microturbines, in the 30 kW_e to 250 kW_e neighborhood is expected to be the typical size chosen for the cluster of gas turbines. As mentioned the default position taken is to use the rotational energy of the microturbines for the production of electricity; however, it is interesting to note that by employing a cluster, not every microturbine is required to be directed to the same task. In fact, several tasks could be selected for the microturbines, such as dedicating units to: compressing air for underground use, providing pumping, turning the ventilation fans and the remainder can be directly connected to electrical generators. This is an indication of the flexibility available through the selection of a cluster of lower power

units and configuring the system to the needs of the site rather than using a single unit capable of providing the entire amount of power rated for the system.

The reliability and availability of the microturbines are both excellent and with a start-up time of only 60 seconds is certainly amenable to the responsiveness required of a system designed for this purpose. Although fuel options are available, natural gas is the fuel upon which this design would be based. Part of the attractiveness of such a system is the opportunity to take advantage of the newly available sources of natural gas. Increases in supply resulting from a technology shift has placed natural gas in an elevated position of being the fuel of choice due to expected continuation of lower prices and the clean burning of natural gas compared to other fossil based fuels is attractive. The other aspect of natural gas ultimately attractive to industry is the continuation of natural gas deliveries during power failures and the increasing number of Liquid Natural Gas (LNG) plants under construction at present. This aspect provides security of electrical power production at a site even during an extended power outage because LNG can be trucked in if the pumping stops due to grid failure. Although it may be that the total power requirements of the site may not be entirely met by the systems in place at the site, there is certainly a motivation to build in capacity capable of maintaining critical operations such as ventilation for an underground mine, refrigeration for a product sensitive to temperature or emergency hoisting. Using natural gas energy production on military installations will provide energy security because of its separate distribution pathway (Judson, 2013). Although the electrical power was not assured in many of the scenarios that disrupted the electric grid, natural gas has demonstrated energy security benefits during all historical electricity outages, as was the case when Hurricane Sandy hit New York (Revkin, 2012). Natural gas has a demonstrated security of supply, expected long-term price stability and is relatively clean burning when compared to many combustion fuels. The proposed system is designed to operate on natural gas because an investment in the opportunity to have a stable low cost energy production facility on site may provide an ongoing benefit to any industry and especially a mining company.

6.2. Contrasting the VamTurBurner© with existing systems.

The VamTurBurner© is comprised of several stages. The first step is the assessment of the ventilation air, containing the VAM from the mine, if it can be

accepted as is without any attempt at modifying the concentration of fuel then it simply continues as a flow from the mine to the system. If there is insufficient fuel contained in the VAM then supplementation may be required. The second stage is comprised of a cogeneration system based on a gas turbine cluster configured to produce electricity through geared electrical generators while the heat in the exhaust stream is used in the initial preheating stage of the VamTurBurner© system. It is understood the rotational energy of the microturbines can easily be used for other purposes normally encountered at a mine such as pumps or compressors; however, the default strategy for the purposes of this discussion, will be to couple the axel to a generator to produce electricity.

The preheating of the VAM is essential to the combustion process as outlined in the details of Chapter 4 and confirmed in Chapter 5 by the Large Eddy Simulation modeling. The initial preheating of the incoming ventilation air to raise the temperature to near 500 K is followed by a heat exchange section. In the pre-heater section the temperature of the ventilation flow containing the VAM is raised to a state where the methane readily oxidizes in the combustor stage when the flow encounters the igniters.

The current systems capable of VAM mitigation, while using the VAM as a primary fuel, such as the Thermal Flow Reverse Reactor (TFRR) and the Catalytic Flow Reverse Reactor (CFRR), generally do not use all the available VAM to produce an energy product (Marín, Ordóñez and Díez, 2009). This is due to the design feature that some of the energy obtained from oxidizing the VAM is required to sustain the internal heat needed to maintain the ongoing oxidation reaction. These systems use either an electrical heater or gas burner to bring the temperature up to the level where oxidation begins and are used to supplement the thermal balance if the amount of VAM in the flow is insufficient to maintain the oxidation reaction. The graphs shown in Figure 6.2.1 (Cluff, Kennedy and Bennett, 2013) are typical energy recovery horizons for a TFRR and CFRR requiring VAM concentrations of 0.12% and 0.45%, respectively, simply to provide enough heat to sustain the reaction. The amount of heat recovered as a percentage of the total heat available provides a simple description of the efficiency of the system based on the amount the input converted to a useable output. Since the system requires a so-called maintenance concentration level of methane simply to keep the ceramic beds

hot enough to oxidize the methane contained in the VAM, there is a base amount of energy that is not recoverable from the total energy available because when that heat is taken from the system the oxidization reaction will cease.

The values of 0.12% VAM for a TFRR and 0.45% VAM for the CFRR, used in Figure 6.2.1 to demonstrate the effect, are representative values; thus, a particular system may require slightly higher or lower amounts of sustaining methane in the flow depending on the design parameters. The cutoff value of 1.3% represents the VAM concentration at which heat would have to be discarded, because the high temperatures experienced at this level of VAM would start to cause the damage to the reactor materials. This is purely an engineering constraint due to the selection of materials, heat flow rates and reactor size. As is usually the case, the more

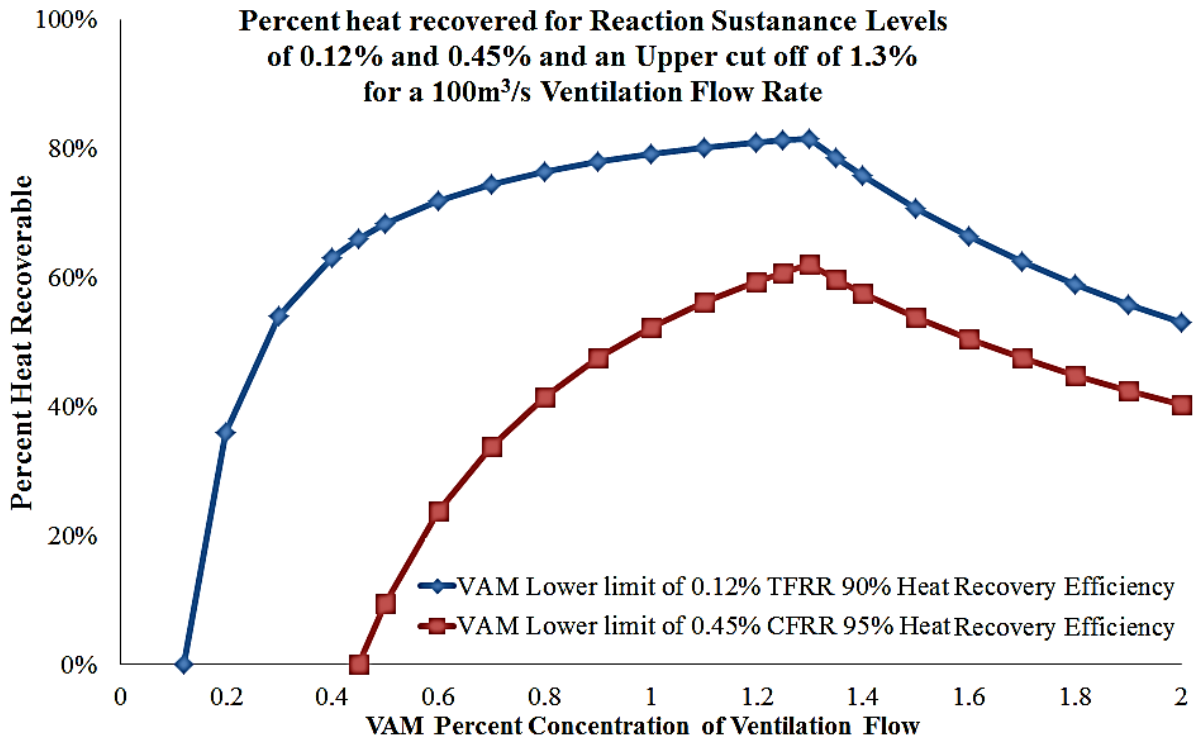

Figure 6.2.1 Recoverable energy after reaction sustenance (Cluff, Kennedy and Bennet, 2013)

expensive materials are able to withstand higher temperatures. Typically, the materials needed to extract energy are metals because of the high thermal conductivity or higher capacity to transfer heat through the material to the fluid flow capturing the heat. For example, if ceramic tubing is used, the temperatures attainable are much higher but the thermal conductivity or heat flow rate is reduced substantially. These trade-offs are not the subject matter of this work, but it is sensible to provide some indication as to why a non-differentiable curve would exist

in the description of heat flows and it is quite simply that this is a limiting amount of VAM that can be reasonably dealt with by the TFRR or CFRR systems.

In the TFRR and CFRR designs, the heat is contained internally in a ceramic bed with heat pipes collecting heat generated from combustion in an insulated containment system. In the VamTurBurner© the heat is confined to a flow through system; thus, readily accessible to heat exchange systems. Consequently, due to the flow of gasses through the large diameter system of the VamTurBurner©, the energy generated can be collected quickly because it is not required to reside in an insulated containment. As a result it is expected that the VamTurBurner© will be able to convert VAM concentrations, containing higher percent methane to a thermal product in a safe and effective manner. In Figure 6.2.1, the numerical values from the graphs show that energy retrieval at a VAM concentration of 0.7%, is only 34% and 75% for the CFRR and TFRR, respectively. These systems may also introduce a pressure drop across the ventilation system, due to the requirement for the flow to pass through a bed of ceramic beads or even in the case of the recent developments using foam, a lower flow resistance material, as the heat transfer agent in the reactor. This pressure drop may be of such a magnitude as to require supplemental booster fans to overcome the pressure drop or to force the VAM through the system.

There are two methods of heat extraction from TFRR or CFRR either the extraction of the entire gas stream through a heat exchanger outside the reactor, which is then returned as a colder stream to the reactor, or the extraction of part of the gas steam with no gas return. Depending upon the type of heat extraction, the reactor behaviour is affected differently. Modelling of these situations is accounted for by adjusting the model parameters (Marín, Ordóñez and Díez, 2009). Adjusting the gas extraction and return temperatures or simply the amount of heat extracted at the location in the ceramic bed where the gas extraction takes place or by changing the amount of gas flow through the heat exchanger, as a fraction of the total gas flowing through the reactor.

Many other systems have proven to be subject to intractable problems, such as the catalytic gas turbines, resulting in the cessation of further development. The use of VAM as a secondary or supplementary fuel for a Diesel or internal combustion engine is quite viable; however, the amount of VAM used as a secondary fuel depends on the normal air-intake flow rate of the particular power plant employed.

The drawback of taking this approach is that a volumetric constraint, based on the size of the combustion chambers of the individual fuel consumption units, may lead to the need to install a financially prohibitive number of units to capture all the VAM. Say in the case of internal combustion engines, the amount of airflow compared to the fuel mixture required is a limiting factor since the amount of methane in the supply air is at such a low concentration the amount of airflow is not substantially changed from what would typically be the amount of airflow needed without the low concentration methane. As a direct result, the number of Diesel engines or internal combustion units needed to accommodate the typical amount of VAM from coalmine operating at a flow rate of 100 m^3/s with a 0.5% VAM concentration is numerically prohibitive or costly to implement. To illustrate the point, calculations for two Diesel engines are provided. The Allis Chalmers 17000 MKII is a 300 HP (0.2238 MW) Diesel with an air flow rate of 0.368 m^3/s so about 270 units would be needed for a VAM flow of 100 m^3/s of VAM. The Caterpillar 3616 is a 6655 HP (4.96 MW) Diesel with an air flow rate of 6.82 m^3/s so about 15 units would be needed for a VAM flow of 100 m^3/s of VAM. The power output for these configurations is 60.79 MW and 72.69 MW for the Allis Chalmers and Caterpillar units respectively. Considering the capitol cost/MW and the ongoing maintenance, fuel costs and installation of separate ducting to each unit or a complicated ducting manifold to accommodate the row of units it is suggested that the current VamTurBurner© design is certainly competitive. These factors, would in all probability, prevent the full amount of the VAM available at the mine from being used in a given project. It is suggested that improved economics may be realized by the installation of a system capable of converting all of the VAM to a useable energy product. The rotary kiln systems outlined in Chapter 3, that CSIRO has worked on look promising, but require the existence of a coal burning facility in close proximity.

6.3. Gas turbine operational parameters

In order to provide as complete as possible a response to the project specification, a computer model has been developed to provide a rapid method to simulate operational parameters of a microturbine. This enables a basic understanding of the specific microturbine needed or a combination of several microturbines of differing power specifications, fuel consumption and turbulent air from the exhaust that may be required to satisfy a particular design.

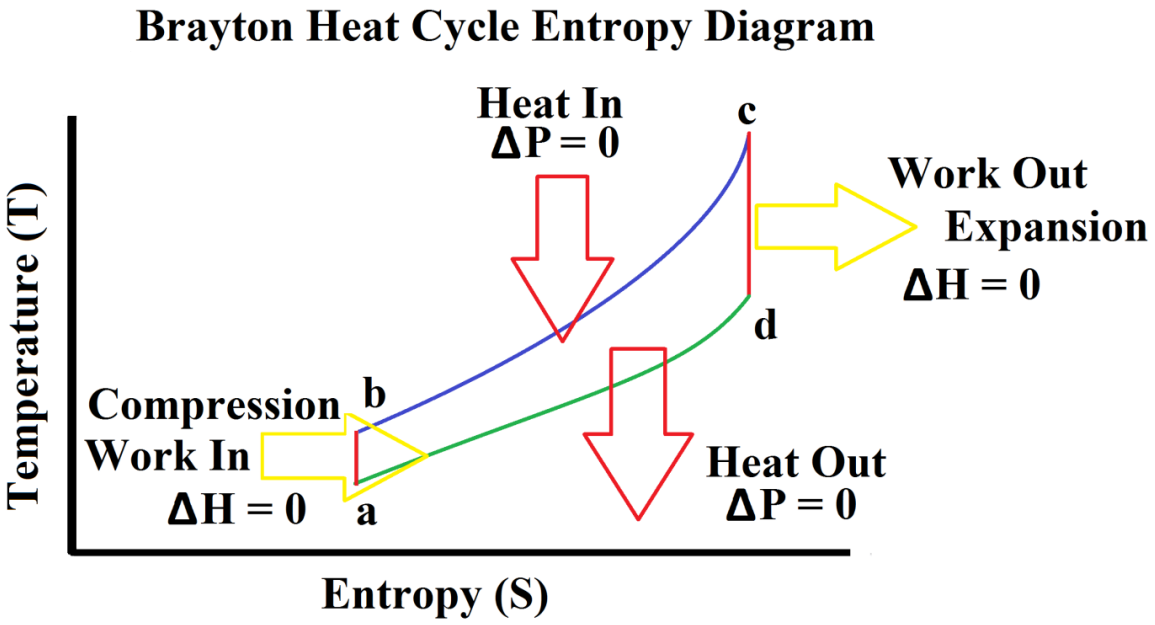

Figure 6.3.1 A stylized description of the Brayton Cycle or the gas turbine operating principle.

An interactive program to simulate a design for the matching of a compressor-combustor-turbine system has been written in MATLAB and provides the capacity to model gas turbine fuel consumption and other operational parameters such as the surge line on the compressor map, the turbine map and other fuel/air ratio related parameters. Given the geometrical parameters of diameter, axial rotational speed, gas flow dynamics and ambient conditions, the program matches the compressor to the turbine using an iterative technique. The application to mine site energy lies in the ability to gain information on the fuel flow effects and output temperatures for use as a component in a VAM combustor system.

In Figure 6.3.1 a basic description of the Brayton cycle is provided as a guide for the descriptions that follow. It should be noted that the Brayton cycle is very similar to the Diesel cycle, but operates in a continuous open flow rather than a discrete closed cycle.

The following is a description of for each sub process outlined in Figure 6.3.1.

i. a to b Adiabatic Compression - air is drawn into the turbine and compressed at each stage.
ii. b to c Isobaric Ignition - fuel is mixed with the high pressure air and burned at constant pressure.
iii. c to d Adiabatic Expansion - hot gases expand in the turbine stages and provide mechanical energy.

iv. d to a Isobaric Exhaust - constant pressure discharge of the hot gases to the environment.

The primary assumption taken is that the gas in the compressor – combustor – turbine system is ideal with the consequence that partial pressures of gasses in the flow are each an ideal gas. This assumption is reasonable for the temperatures and pressures associated with the flow through the system, as they are not expected to be greater than 5000° K or in the form of a plasma. When an ideal gas flows through the compressor – combustor - turbine system, it can be further approximated that it flows through a simple tube. Due to the high velocity of the flow in confinement, a pressure develops on the walls of the tube because the high velocity gas molecules exert momentum and kinetic energy in all directions. The Mach number, defined as the ratio of the speed of the flow to the speed of sound, depends on the temperature and pressure, but is also related to the level of compressibility of the gas. In cases where the velocity of the flow in the forward direction nears the speed of sound, usually referred to as the z-direction in gas turbine engineering, the compressibility of the gas becomes relevant as it can vary spatially, otherwise the gas density remains constant. If the velocity of the flow increases as the flow moves through a constriction in a tube and then gradually expands, such that the flow conditions are returned to the original state, the process is reversible (Saravanamuttoo, Rogers and Cohen, 2001). The second law of thermodynamics requires a reversible flow to preserve a constant value of entropy; thus, the processes involved in gas turbine flows are isentropic, which allows for gradual changes in flow. The equations describing an isentropic flow are best started with a definition of the Mach number since it is contained in many of the isentropic flow equations. The Mach number **M** is the ratio of the speed of the flow $\mathbf{v_f}$ to the speed of sound $\mathbf{v_s}$.

Eqn. 6.1. $$M = {}^{v_f}/_{v_s}$$

The speed of sound varies as a function of density $\boldsymbol{\rho}$, pressure **P**, temperature **T**, and the ratio of the specific heats $\boldsymbol{\gamma}$. For a diatomic gas, with five degrees of freedom f, three translational and two rotational at room temperature and with the vibrational degree of freedom becoming involved at high temperatures $\boldsymbol{\gamma = 1 + 2/f}$, with $\boldsymbol{f = 5}$ for a diatomic gas so $\boldsymbol{\gamma = 1.4}$ and can reduce to $\boldsymbol{\gamma = 1.33}$ at high temperatures.

Eqn. 6.2. $$v_s = \sqrt{\frac{\gamma P}{\rho}} = \sqrt{\gamma RT}$$

The entropy equations for the pressure and density of an isentropic flow:

Eqn. 6.3. $$Constant = \frac{P}{\rho^{\gamma}}$$

The value of the constant depends on the pressure and density when the flow is gradually slowed to rest isentropically and with the ideal gas law or equation of state, which was first stated by Émile Clapeyron in 1834 as a combination of Boyle's law and Charles's law.

Eqn. 6.4. $$PV = nRT$$

Using the equation of state Eqn. 6.4 and the relationship of Eqn. 6.3 to derive Eqn. 6.5.

Eqn. 6.5. $$\left(\frac{P}{P_t}\right) = \left(\frac{\rho}{\rho_t}\right)^{\gamma} = \left(\frac{T}{T_t}\right)^{\frac{\gamma}{\gamma-1}}$$

The dynamic pressure involves the movement of the gas, or is considered as a velocity pressure in the gas, so there is some similarity to the kinetic energy in that the dynamic pressure P_d is defined to be:

Eqn. 6.6. $$P_d = \frac{1}{2}\rho {v_f}^2 = \frac{1}{2}\gamma P M^2$$

The physical concepts of conservation play a significant role in developing the equations for isentropic flow in a gas turbine. The conservation of mass relates to the fluid flow, including additions of fuel as the flow passes through the combustion chamber, in some elementary calculations that small amount of fuel is often ignored (Hill and Peterson, 1992). The conservation of momentum is essentially a statement regarding the pressure and that due to the confinement of the walls the pressure will not decrease due to expansion until the gas leaves the turbine to provide thrust. The conservation of energy includes the addition of energy due to the burning of the fuel and that the confinement of the flow within the tube, which provides for all the energy to be contained until leaving the system as thrust and heat.

The total enthalpy in the flow is discussed first, which is needed to derive the equations below:

Eqn. 6.7. $$\Delta E = \Delta Q - \Delta W \quad where, \ \Delta W = (P\Delta V + V\Delta P) \ and \ \Delta E = E_2 - E_1$$

In the second law of thermodynamics above, the pressure is considered as a constant and the terms specific to the initial and final states are collected with the difference being the quantity of heat; thus.

Eqn. 6.8. $\Delta H_2 - \Delta H_1 = \Delta Q \quad where,\ H = E2 + PV_2 \quad and\ \Delta Q = mC_p\Delta T$

So the specific enthalpy or enthalpy/mass is written as:

Eqn. 6.9. $\Delta h = C_p\Delta T$

The following equations are the ratio of the variable to the total variable; for example, the total pressure is the stagnation pressure derived from Bernoulli's Equation such that the static and velocity pressures are calculated for an incompressible flow for a negligible height of fluid above the reference level.

Total pressure = Dynamic pressure + Static pressure = Stagnation pressure

At the stagnation point for an isentropic flow the fluid velocity has come to zero, so the dynamic pressure is zero because of the conversion of the kinetic energy into pressure energy as the fluid gradually comes to rest. The ratio of the static to stagnation pressure, temperature to stagnation temperature and density to stagnation density plays an important role in the design of gas turbine engines and is central to the MATLAB programme written to calculate the match between the compressor and the turbine of a compressor-combustor-turbine system (Kurz and Brun, 2000).

Eqn. 6.10. $P/P_S = \left(1 + M^2\left(\frac{\gamma-1}{2}\right)\right)^{\frac{\gamma}{\gamma-1}}$

Eqn. 6.11. $T/T_s = \left(1 + M^2\left(\frac{\gamma-1}{2}\right)\right)^{-1}$

Eqn. 6.12. $\rho/\rho_s = = \left(1 + M^2\left(\frac{\gamma-1}{2}\right)\right)^{-\frac{-1}{\gamma-1}}$

Then isentropic flow is a maximum when the flow velocity is at Mach-One, **M = 1**. This is the point when the compressibility of the flow becomes a factor. The calculations performed in the MATLAB program considers this through the continuity equation. In the discussion provided below, a guide to the consideration of the compressible mass flow equation is expressed as a consequence of the continuity equation. Generally, the mass remains constant for a given problem; thus, mass is neither created nor destroyed in the process. In fluid flow problems, and especially in problems of ideal gas flow, the density can change appreciably as a function of

temperature, due to volume changes of the confinement, as the shape of the containment varies or may increase due to compression in circumstances that arise if the flow speed is beyond **M = 1**. Gas turbine engineers commonly refer to the mass flow as m-dot, which is in reference to the $\dot{m}$ **= dm/dt** or rate of change of mass per unit time. Typically a flow through a tube, such as in the case of a mine ventilation system or heat exchanger is **Q = vA**, the product of the velocity and the cross sectional area, and is relatively constant. In this case, **Q** is the flow (m^3/s) so should not be confused with the same variable name but different context when **Q** is used to represent the amount of heat in the context of thermodynamic calculations.

Eqn. 6.13. $\dot{m} = Q\rho = Av\rho$

Upon consideration of the compression effects on the mass flow rate at higher velocities and the density variations due to temperature changes, the mass flow equation when combined with the ideal gas law and the isentropic flow relations to provide the compressible form of the mass flow rate equation.

Using Eqns. 6.1, 6.2, 6.13 and the ideal gas law to obtain.

Eqn. 6.14. $\dot{m} = MA\rho\sqrt{\gamma RT} = \frac{MAP\sqrt{\gamma RT}}{RT} = MAP\sqrt{\frac{\gamma}{RT}}$

Combining the equations for isentropic flow, using Eqns. 6.10, 6.11 and 6.12 the mass flow can be written as:

Eqn. 6.15. $\dot{m} = \frac{AP_s}{\sqrt{T_s}}\sqrt{\frac{\gamma}{R}}\,M\left(\frac{T}{T_s}\right)^{(\gamma+1)/(2(\gamma-1)}$ and with T/T_s obtaining from Eqn. 6.11;

Eqn. 6.16. $\dot{m} = \frac{AP_s}{\sqrt{T_s}}\sqrt{\frac{\gamma}{R}}\,M\left(1 + M^2\left(\frac{\gamma-1}{2}\right)\right)^{\frac{-(\gamma+1)}{2(\gamma-1)}}$

When the Mach number is unity the mass flow equation reduces to a function of the stagnation pressure and stagnation temperature, the cross sectional area and ideal gas constants, this should be indicative of the relatively central position that Mach number occupies in the internal flow parameters of a gas turbine engine. For all variables remaining fixed, the maximum flow occurs at **M = 1**, the choked flow condition (Markunas, 1972). When the Mach number is known all of the flow parameters can be determined through the isentropic flow equations specified. Correspondingly, when flow relations can be determined by measurements, such as the stagnation pressure measured by a Pitot tube to provide the pressure ratio, the Mach number becomes fully determined and can be used to select all the other flow

conditions. The **A*** designation is a gas turbine terminology commonly used to represent the area of the throat in the choked state, that is when the flow is at Mach-One, or at the maximum compressibility. The ratio of the two areas provides the basis for the following gas turbine design equation.

Eqn. 6.17. $$\frac{A}{A^*} = \frac{(\gamma+1)^{\frac{-(\gamma+1)}{2(\gamma-1)}}}{2} \frac{\left(1+ M^2\left(\frac{\gamma-1}{2}\right)\right)^{\frac{\gamma+1}{2(\gamma-1)}}}{M}$$

The isentropic flow can be passed through a nozzle to increase the flow velocity. Thrust is produced according to, **F = ma**. The amount of thrust available depends on the containment shape and flow velocity, the smallest cross-section in the flow is called the throat of the nozzle, **A*.** The maximum flow rate will occur at the minimum area where the flow is choked at the throat, so the flow value of **M = 1** in the throat and the mass flow rate $\dot{m}$ is determined by the throat area. The area ratio from the throat to the exit area A_e sets the exit velocity V_e and the exit pressure, P_e. The exit pressure is only equal to the free stream pressure at some design condition (Sheppard, 1978).

Eqn. 6.18. $$F = ma = \dot{m}v + A\Delta P = (mass\ flow)(escape\ velocity) + (Area)(P_e - P_o)$$

Matching a compressor to a turbine is essentially the main problem and determining factor of gas turbine design. The essentials used in this analysis can be applied to turboprop and turbofan engines, which may be the configuration of choice for a system involving ventilation systems; however, the program is written to match turbojet engines or straight through gas flow situations, which are the currently expected components for the VamTurBurner© VAM mitigation system considered in this thesis.

When the flow is assumed to be in a steady state the performance of the engine can be calculated by taking the continuity equations and power balance into account. In cases of higher complexity the continuity will account for a bleeder flow to leave the compressor, this calculation only takes the gas flow and adds the fuel flow to provide the total flow in the turbine. The matching of the power output of the turbine must balance the power demands of the compressor and any load placed on the system, which is usually accompanied by an increase in fuel flow (Kurz and Brun, 2000).

Once the ambient conditions are decided or assumed the Mach number of the intended flow is selected, which is a major and determining characteristic of the internal gas flow. The ambient conditions of pressures and temperatures are selected and the velocity triangles are set to reflect a sensible expectation for the rotation speed and the various efficiencies and flow areas or normalized flow ratios are set. The compressor and turbine maps are the defining characteristics of the gas turbine engine; thus, these maps can be used to determine the expected performance of the gas turbine .

The essentials of the calculation that the MATLAB program performs are as follows and outlined in (Hill & Peterson, 1992) and (Dhariya, 2008).

v. A number of physical constants, ambient conditions and system parameters are input such as the efficiencies, velocity triangles properties, temperatures, pressures and operating point of the gas turbine.
vi. The design based Mach number and an inlet temperature are decided or assumed.
vii. The compressor pressure ratio is set.
viii. The compressor work/mass and turbine pressure required to create this amount of work is calculated.
ix. The mass flows are matched by a loop calculation.
x. The pressure ratio across the outlet nozzle is calculated from the pressure ratios of the diffuser, compressor, combustor and turbine by assuming continuity of pressure through the flow.
xi. The normalized area ratio needed to allow the mass flow passing through the previous elements, which becomes that of the turbine outlet is calculated.
xii. The stagnation temperature is calculated.
xiii. If the calculated area of the outlet nozzle and the design specification area are not consistent then go back and assume a new value of T_{04}, which is expected to move the area in the proper direction, to reconcile the calculation with the design specification area and go through the calculation steps again until matching is achieved.

The compressor should be operating near the efficiency value set for the calculation, assumed to be the peak efficiency, this is observed from the compressor map operating line, (Walsh & Fletcher, 2004) the operating line follows the peak efficiency through the full range of RPM values. The operating line is formed by the intersection with the several lines at different RPM values. The compressor to turbine matching procedure depends on the condition that for the most part the main

outlet nozzle and turbine are operating in a choked condition. This means that the flow is in a state such that the flow speed is not moving at a fast enough speed to overcome the pressure wave so is not impeding the flow, over the operating range see Eqn. 6.17 (Hill & Peterson, 1992). This compressor-combustor-turbine matching program can determine the operating parameters, such as the fuel mass flow, fuel air ratios and thrust created at the exhaust of the microturbine. These are needed to calculate the amount of mixing and heat available from the particular configuration and the thrust provides a good description of the exhaust gas velocities. The point "b" in Figure 6.3.2 is the operating point of the microturbine, drawing on our mining engineering experience to simplify the explanation; this is actually quite similar to the concepts found in mine ventilation fan curves where the pressure-volume plots show the intersection of the fan curve and the mine resistance curve to establish the operating point. In the MATLAB program, the fan curves on the compressor map are assumed to be parabolic functions, shown in red on the compressor map plot, and the system resistance curve intersection forms the surge line, shown in blue on the same plot in Figure 6.3.3.

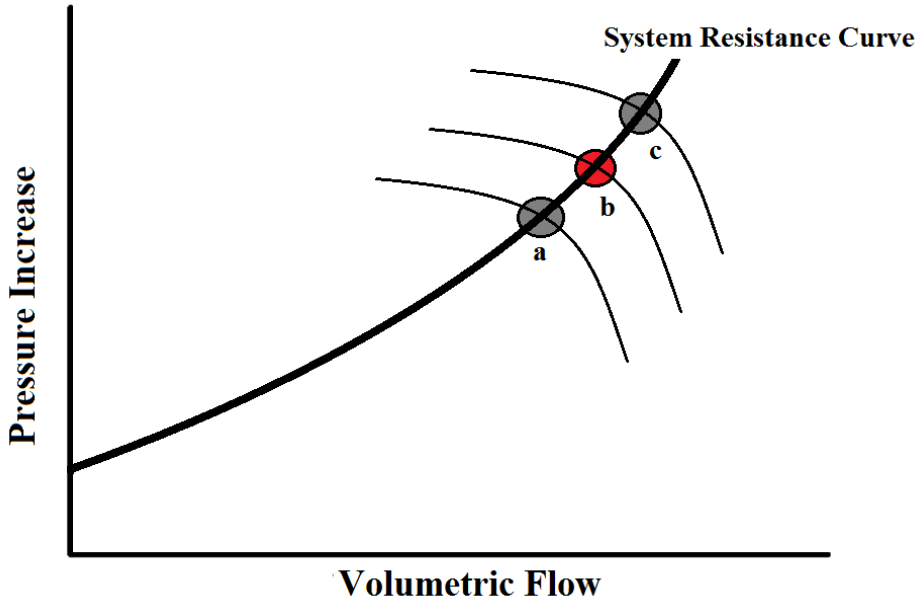

Figure 6.3.2 A schematic to assist with the concept of selecting an operating point for the purpose of using the gas turbine matching program written for use in this work.

The compressor map in Figure 6.3.3 is an output of the program for the following input parameters and design constraints. This compressor map shows that the system operates smoothly as long as the ambient conditions and fuel flow rates are maintained. The number of fan curve lines is determined by the number of

revolutions per minute (RPM) selected. As is often the case the descriptive terms used to write computer programs are not often easily translated into language that would normally be used in a proper English sentence. For the most part the terms used here are close to either self-explanatory or commonly used, but "*the number of compressor RPM scenes*" actually means the number of fan curve lines, which is determined by taking the highest RPM value and subtracting the "*delta rotation*" value in a calculation loop, which is performed "*the number of compressor RPM scenes*" times. All other graphs are related to this calculation; the points on all the other plots are determined by these RPM values and so corresponding data can be directly taken for a given RPM value from each of the plots.

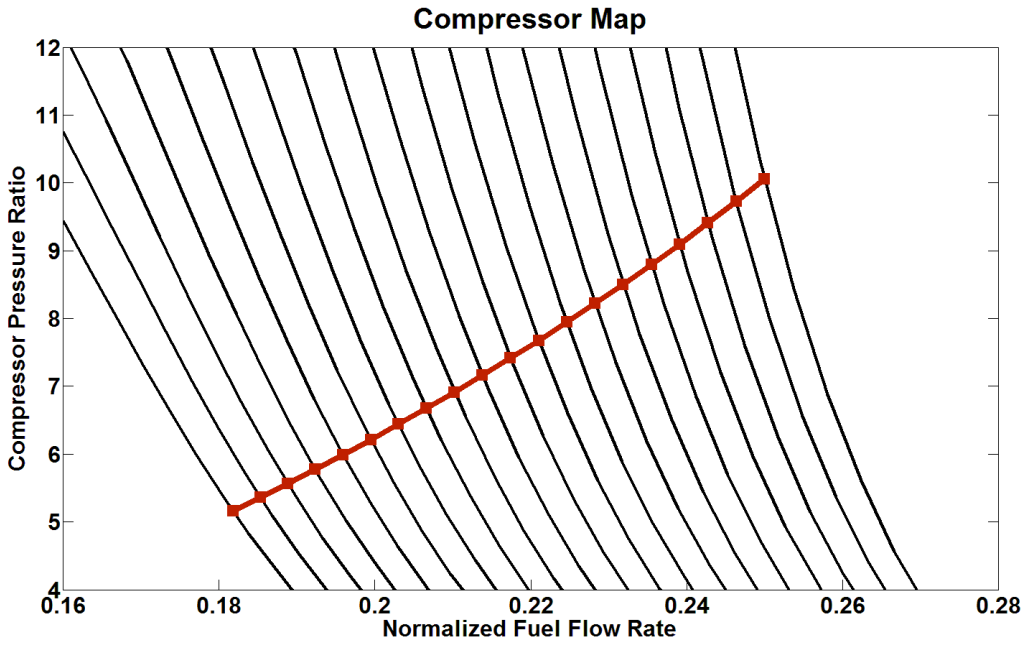

Figure 6.3.3 Compressor map derived from the data in Table 6.3-1, which is the main descriptive tool for the understanding of the operation of the microturbine.

The microturbine design arrived at for the data in Table 6.3-1, has a turbine diameter of 24 cm and uses a maximum of 0.05 kg/s of fuel with a calorific value of 38 MW/kg. These are the type of data needed to develop the design concept with the view that the design should be tailored to aim toward off-the-shelf components for large-scale and correspondingly expensive items such as the microturbines. The target gas turbine for this current design would be similar to the 250 kW Ingersol Rand microturbine, configured to have a higher exhaust gas temperature. The Compressor map derived from the data in Table 6.3-1 shows the operating line for the microturbine established by those parameters in Figure 6.3.3.

The key point to derive from the compressor map is that as the engine is throttled up, the normalized fuel flow rate increases. As more fuel is added the rotational speed increases, each red line on the plot represents a 1000 RPM increase in RPM with the maximum set to 80,000 RPM, and the compressor pressure ratio correspondingly increases as the rotational energy is more rapidly pushed between the compressor blades. The mass flow rate, corresponding the range of the pressures in the compressor map, is provided in Figure 6.3.5.

The ideal RPM rate was set to 70,000 and that the desired mass fuel flow for that RPM value is a numerical output of the program, but only the values from the graphs will be used in the text for the ease of visualization of the calculation. The fuel air ratio determined for 70,000 RPM is 0.077 as shown by the indicator lines on Figure 6.3.4. From that fuel air ratio, the indicator lines on the graph in Figure 6.3.5 show the desired mass fuel flow

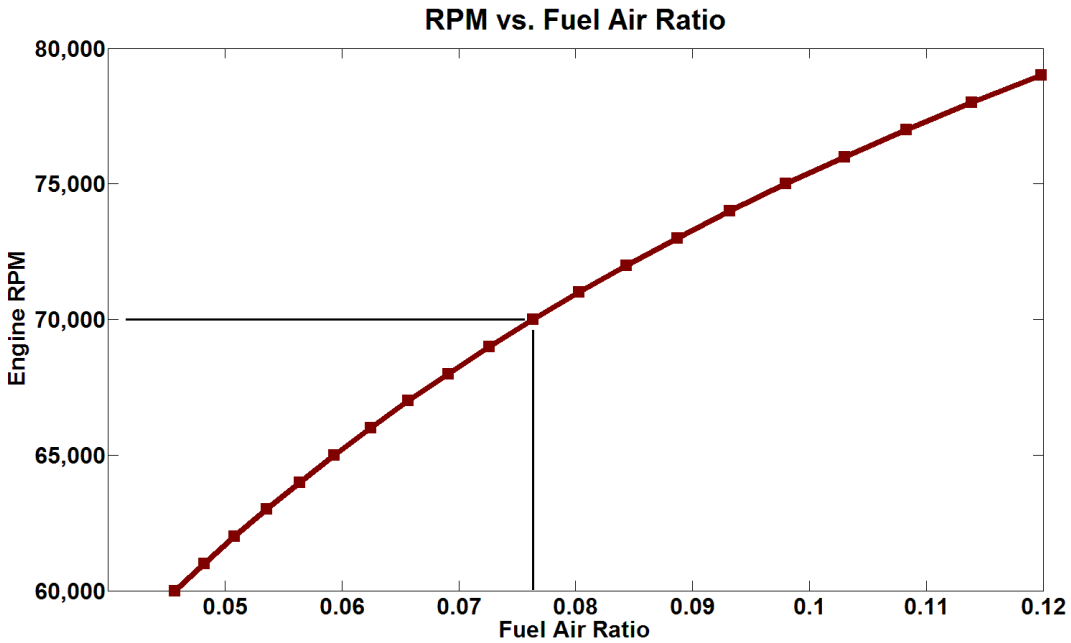

Figure 6.3.4 The RPM's vs. Fuel Air Ratio for the data in Table 6.3-1 with the fuel air ratio corresponding to an RPM value of 70,000 singled out for use in calculations

The corresponding mass flow rate obtained for 70,000 RPM is about 0.0345 kg/s at a fuel air ratio of about 0.077. This is the data needed to calculate the amount of heat expected from the microturbine depending on the electrical conversion efficiency. For the ease of calculation a typical value of 20% electrical conversion efficiency will be used throughout, unless a specific product is being discussed.

For a fuel such as natural gas with a calorific value of 38 MJ/kg and a mass flow rate of 0.0345 kg/s the total power input is 1.311 MW. When the electrical conversion of 20% is subtracted from the total power input, the remaining available thermal energy/s is 1.088 MW_{th}. Since the suggested design calls for six microturbines the amount of heat energy available would be 6.2928 MW_{th}. This power is the first stage of heating that is mixed with the incoming VAM in the initial pre-heating stage. Computational flow dynamics calculations to establish the mixing and temperature profiles resulting from this mixing has been performed and is discussed in chapter 7.

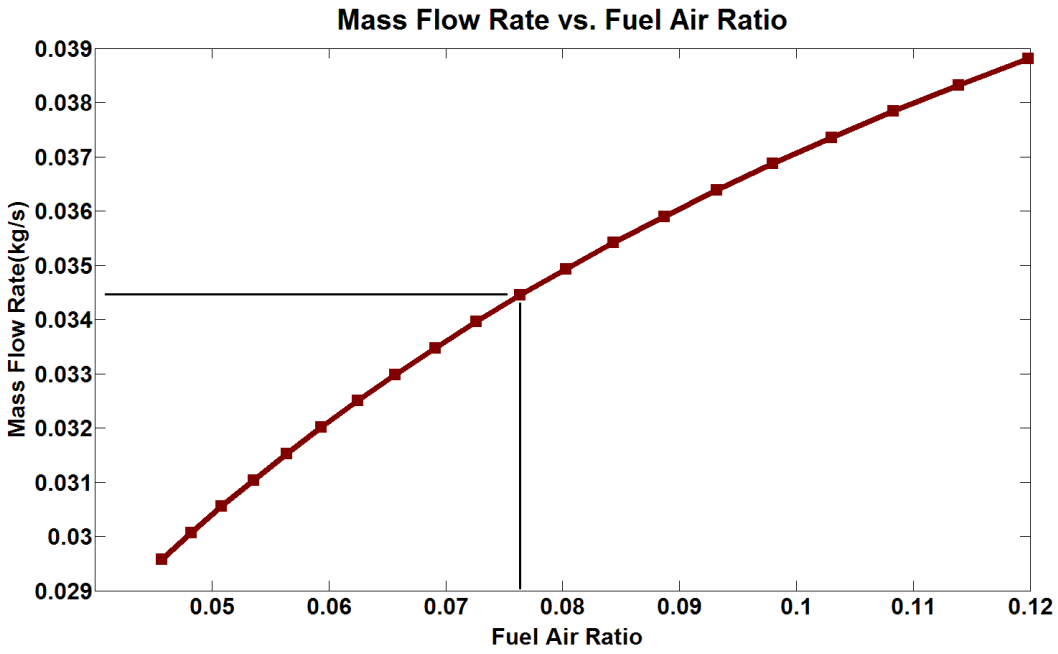

Figure 6.3.5 The mass flow rate corresponding to the RPM value of 70,000 is found by using the fuel air ratio from Figure 6.3.4.

The "mass flow", in the calculations obtained using the gas turbine MATLAB program, is specifically the amount of fuel flow (kg/s) in the airflow through the gas turbine. The results from this simulation have arrived at a fuel air ratio of 0.077 or 7.7% for the mass flow rate of 0.0345 kg/s. This is within normal limits for a "proper fuel mix", see chapter 4 for the discussion on stoichiometric mixtures where the value for methane was given as 5.5% at stoichiometry or an equivalence ratio of unity. Since natural gas is mostly methane, the values for methane can be used for comparison with little need for correction. The fuel air ratio of 7.7% is just above the exact stoichiometric mixture for methane and is an excellent air/fuel mixture ratio of about 13:1 for the combustion of the fuel. In fact, observation of Figure 4.4.7 and 4.4.8 shows that the flame speed is greatest or the combustion proceeds most

readily for an equivalence ratio of about 1.1. The amount of airflow through the gas turbine can now be calculated by taking the mass flow rate as 7.7% of the airflow rate, which gives 0.448 kg/s. For a temperature of 700 K, an assumed temperature for the exhaust gasses, the density is 0.504 kg/m^3, which gives a flow of 0.8889 m^3/s per microturbine for a total of 5.333 m^3/s for six microturbines.

Table 6.3-1 The values and corresponding names from the computer program used to determine the characteristics for a generic microturbine for the purposes of trial 1 calculations.

Mach Number, 0 to 1	**0.7**
Ideal gas constant, ratio of specific heat capacities	**1.4**
Rydbergs constant	**287**
Air heat capacity at constant pressure (kJ/kg K)	**1003.5**
Inlet diffusion efficiency (.9 to .95)	**0.9**
Ideal compressor adiabatic stage efficiency (0.85 to 0.9)	**0.85**
Total to total turbine efficiency (.85 to .95)	**0.85**
Mass flow for the fuel (kg/s)	**.05**
Pressure ratio, for the compressor	**5**
Ambient pressure (Pa)	**101300**
Ambient temperature (K)	**290**
Operating point'	**0.0005**
Fuel calorific value, (kJ/kg)	**38000**
Ideal RPM, ideal number of revolutions per minute	**70000**
Highest RPM value	**80000**
Number of Compressor RPM Scenes, number of loops	**20**
Delta Rotation, size of the change in RPM value per loop	**1000**
Outlet burner temperature (K)	**1600**
C1 velocity (m/s)	**60**
C2 velocity (m/s)	**100**
W1 velocity (m/s)	**100**
W2 velocity (m/s)	**60**
Mean radius of blade (cm)	**1.1**
Radius of Turbine (m)	**0.12**
Tip fraction	**1.25**
Hub fraction	**0.75**
Ratio of Hub to Tip Compressor	**0.4**
Normalization Constant	**3.5**
Arbitrary accuracy, stop calculation when difference <	**0.01**

6.4. The VamTurBurner© design features.

An alternative to the existing systems, based on a gas turbine cogeneration system, is proposed to fill the currently existing gap in the technology, but which is also adaptable with the potential to process higher VAM concentrations in the automated mines of the future. The VamTurBurner©, has been discussed peripherally in previous sections, the system depends on the design of a downstream combustion chamber to ignite and burn the VAM. The design specifies an internally constructed combustion system, which integrates the heat from both the exhaust gas of the cluster of electricity generating microturbines and a pre-heating stage to raise the temperature of the VAM to a pre-ignition state amenable to the concentrations of VAM as was outlined in the theory of Chapter 4. Elevating the temperatures of the premixed fresh gas, the term fresh gas and VAM are now used interchangeably as fresh gas is the commonly used term in combustion engineering, is normally a danger. The reason being that a premixed fresh gas is usually at or near stoichiometry; thus, in a state amenable to combustion upon encountering any ignition spark. Therefore, unless the ignition system is proximal and about to occur within a very short time frame, such that the premixed fresh gas is only in existence for the very brief time the flow takes to move from the pre-heating zone until the flow encounters an igniter, there exists a danger that it could be erroneously ignited. This VAM mitigation solution uses all of the VAM energy contained in the ventilation air and is scalable to the various sizes of mine ventilation systems, by changing the size and number of gas turbines in the system. The VamTurBurner© uses a staged heat exchange system of decreasing temperature for the production of electricity, hot water, ventilation air chilling/heating or industrial drying as needed to meet the future demand for coal mining activities in a carbon conscious atmosphere.

A diagram of the VamTurBurner© VAM mitigation system is presented in Figure 6.4.1, which also includes the multi-generation heat exchange system. The fan motors at the upcast ventilation shaft of the mine ventilation system are located at some reasonable distance from the inlet of the VamTurBurner©.

The fan motors, shown in proximity to the microturbine cluster, are obvious candidates targeted for the use of the electrical power produced through the gear driven generators connected directly to the gas turbines or eliminated by using the microturbine to drive the fans directly. To some extent the implications of the

potential for integrating the VamTurBurner© system into the ventilation system of a mine are quite a positive exploit. Since the system employs gas turbines, operating according to manufacturer's specifications, there is the potential to use the rotation of the central axel, as a driver for the fans of the ventilation system. This would avoid the conversion efficiency between the produced electrical power and the fan motor conversion of electrical energy to ventilation pressure energy. When operating in their typical cogeneration configuration the microturbines produce electricity with an efficiency of 18% to 27%, depending on the size of the microturbine system. This efficiency is a direct observation of the amount of power produced as a percentage of the input amount of natural gas. The electrical efficiency can be used as a benchmark to base the amount of natural gas needed to support the system. The total remaining energy is contained in the heat output at the exhaust of the microturbine with associated minimal losses. The heat generated by the microturbine is only a small percentage, to be calculated later, of the total heat in the VamTurBurner© system. The igniters also add heat to the system and finally the VAM contributes the windfall of free thermal energy to the system. The energy available from coal dust or other combustible gasses such as ethane are not considered in these calculations.

An important feature of the design is that a separate air intake system for the gas turbines protruding from the ventilation system ducting avoids any mine ventilation air from entering the microturbine combustion system. The decision to keep the ventilation air from entering the microturbines ensures the expected operating conditions are adhered to so as not to hinder the expected reliability and availability specifications of the chosen microturbine. If the mine ventilation air were allowed to flow through the microturbine combustion system, the changes in VAM concentration would cause the gas turbine to be in a continual state of compensating for the change in fuel level; thus, would be constantly adjusting the natural gas fuel flow. The mine air may contain noxious fumes, coal dust and abrasives that can potentially reduce the microturbine lifetime, as was experienced during the Solar Centaur 3000R trials. The microturbines can operate on a range of fuels, usually characterized by the Wobbe Index of the fuel, the fuel of choice for this design is natural gas, which guarantees the smooth operation of the microturbine due to fresh air intake and properly regulated fuel inputs. The exhaust gas from the

microturbines is hot, assumed to be in the neighborhood of 700-800 K and exits the gas turbine at a high velocity, typically more than 50 m/s. The hot, high velocity gas mixes with the incoming VAM in the pre-heating zone.

The mixture of VAM and exhaust gases then encounters a pre-heating stage where the gas temperatures are elevated to the pre-ignition temperatures required for oxidization in the combustion chamber. The required auto-ignition temperature depends on the VAM concentration; thus, the amount of pre-heating required is a critical variable. The pre-heated flow continues downstream where the flames introduced by the igniters are encountered. The igniters are also fueled by natural gas, but their fuel source can be comprised of any combination of other fuels available at the site, from CMM to any other volatile organic compounds. The heat transferred to the airflow at the pre-heater is derived from the heat created downstream in the combustion zone. Since the combustion zone heat is transferred to the airflow internally, losses are minimal because it is either recycled back to the higher temperature zones or proceeds on through to the multi-generation system. Steam generators, absorption chillers, or compression chillers are routinely coupled to a variety of energy sources for instance: geothermal, methane from waste disposal sites, solar heating, agriculturally produced methane, or VAM. Although the notion is not new, coupling to a VAM system has been a difficult problem, which has for the most part only resulted in the burning of the methane in the ventilation air with little or no retrieval of the heat of the reaction.

A mining company requires a spectrum of energy related systems to pump water, compress air, drive fans, hoist equipment, transport personnel or move Coal. The company could use the various energy products available from the VamTurBurner© system to alleviate to costs at their site or they may choose to sell electricity back to the grid, hot water to a community or provide services to other customers on an industrial site. It is clear that mining operations in different climates require different configurations of the multi-generation system. The adaptability of this system to provide heating or cooling to meet the needs during different seasons is an attractive feature.

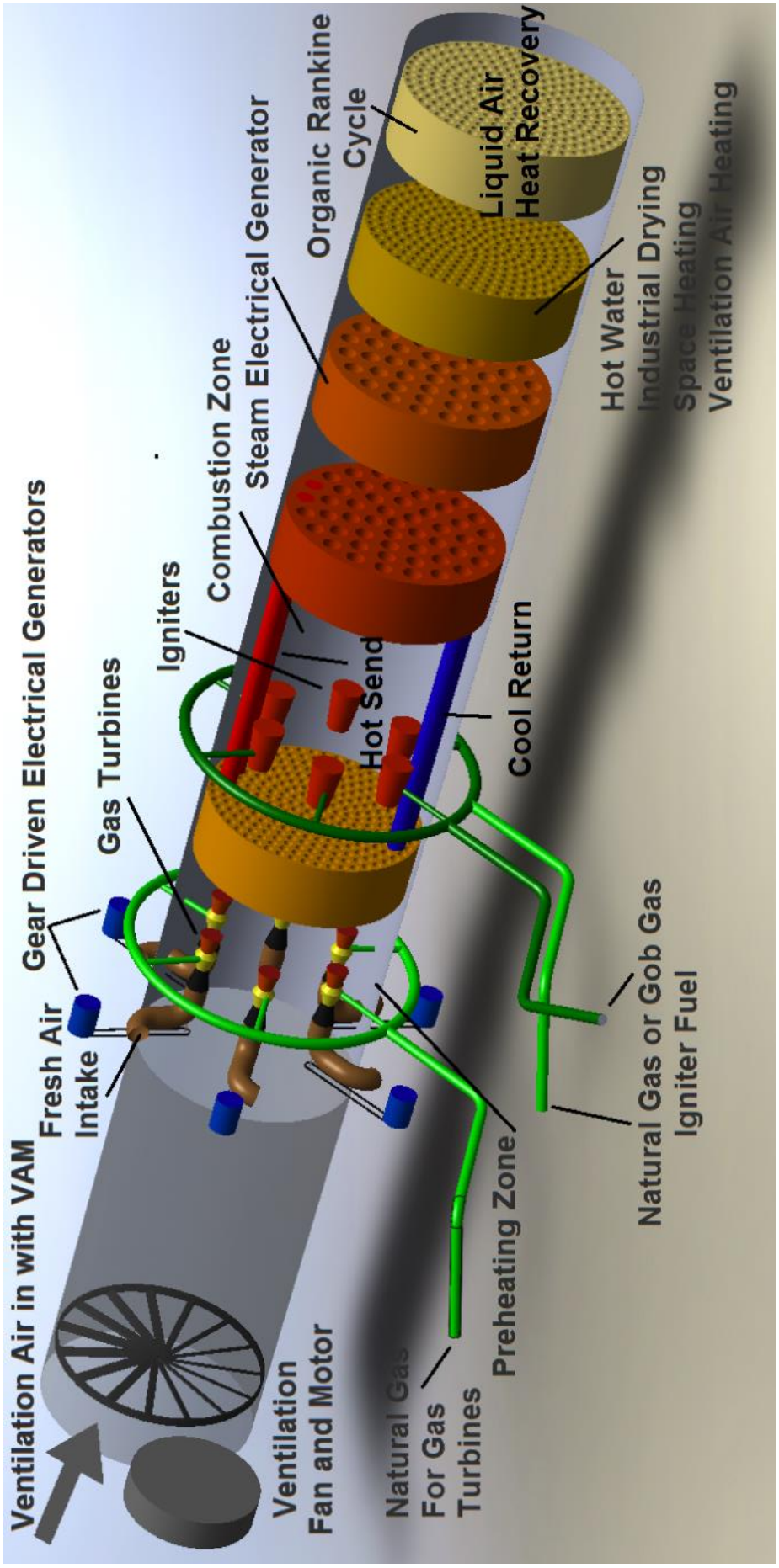

Figure 6.4.1 The VamTurBurner©, a multi-generation system for the mitigation of VAM (Cluff, 2013)

The benefits of this robust design are that it uses an external fuel source to balance the combustion chamber. This induces burning of the VAM while none of the energy is consumed to sustain the reaction. Since the energy contained in the VAM is considered as a free energy source the overall efficiency of the system is improved. The efficiency of any system is defined as the (work out)/(energy in). The "work out" is regarded as the useful work directed toward the intended purpose while the "energy in" is any energy consumed toward producing that intended work. The energy input to the VamTurBurner© arises from three separate fuel sources:

i. A co-generation system, which produces electricity plus exhaust heat,
ii. The igniters and
iii. The VAM.

Both the igniters and VAM only produce heat, while the exhaust heat from the microturbine is the remainder after the electrical conversion has been completed. The issue becomes what is designated as the intended purpose and what is defined as the energy consumed. The opinion of this author is to consider the input energy as only consisting of that which has been purchased for the purpose; thus, the additional VAM serves to increase the efficiency. The igniter fuel may contain CMM or any other fuel available from the mine to supplement the natural gas, which is a further reduction in overall cost to the company, but costs need to be assessed because drained methane is not free. Since the VAM energy is not considered as one of the input sources, but appears as part of the output, the overall system efficiency is substantially increased.

An essential element of the VamTurBurner© system is the design of the pre-heating section. The intractable problem associated with mitigating VAM to collect energy is that the high volume of the ventilation flow has too low a methane content to be ignited readily. Modeling the combustion dynamics of pre-heated VAM is described in chapter 5, using the concepts of Large Eddy Simulation numerical modeling it was shown that pre-heating the VAM to 500 K allows for flameless combustion of a 0.5% VAM concentration.

In the VamTurBurner© diagram of Figure 6.4.1 the principles of the system are outlined. As one follows the VAM flow through the system, several distinct sections are encountered. The descriptions provided in Table 6.4-1 are indicative of the design parameters, but subject to modification as the design progresses,

changes to suit different flow characteristics, equipment selection or technological advances. The outline in the table can be used as a guide to follow through the system as each stage is explained to clarify the brief explanation notes shown on Figure 6.4.1.

Table 6.4-1 A list of the sections with brief descriptions following the VAM flow through the VamTurBurner©.

Stage	Description or Configuration			
VAM	(100 m^3/s)	0.5% methane	300 K	101.13 kPa
T100 Microturbine (MT)	η = 30% electrical	105 kW_e	480 VAC	
MT Fuel supply	Natural gas 350 kJ/s	38 MJ/m^3	50 MJ/m^3	
MT Exhaust	0.8 kg/s	High temperature/velocity		167 kWth
Mixing volume	VAM	n (number of MT)	Increased temperature	
Pre-heater	Receives heat from combustion chamber, raises temperature of VAM			
Pre-heater rcve/ send	Steam from pre-heater heat exchanger deposits energy after mixing			
Igniter	Flame produced from external fuel with spark ignition			
Igniter fuel supply	Fuel can be a combination of natural gas with any other hydrocarbon			
Combustion chamber	High temperature zone where the VAM encounters flame from igniters			
Pre-heater exchanger	Collects heat from zone after VAM combustion returns to pre-heater			
Pre-heater snd/receive	Steam produced by heat in high temperature zone flows to pre-heater			
Heat exchanger 1	Heat exchanger produces steam for electrical generators (HE 1)			
Steam generator	High quality steam from HE1 through a turbine to produce electricity			
Heat exchanger 2	Adaptable to provide thermal product as desired			
Thermal product	Medium grade heat configuration			
Ventilation heating	In winter months some mines require heat added to the ventilation			
Hot water	Can be used at site for cleaning/staff hygiene or exported to community			
Industrial drying	Industrial drying this system has readily available hot flowing gasses			
Space heating	Distributing hot water for space heating or by forced air			
Heat exchanger 3	Low grade heat configuration			
Absorption chiller	Lithium bromide cycle or the ammonia-water cycle.			
Hot water	Direct supply of hot water to site or community			
Exhaust stack	Monitoring of exhaust gasses for contaminants and temperature			

The operational stages of the VamTurBurner© system are examined in more detail in the following sections. Calculations of heat flows, modelling of heat exchange parameters, pre-heating effect on the combustibility of VAM and discussions pertaining to the implementation of appropriate technologies to provide the thermal products at each stage are discussed in more detail.

These calculations are the type of design data needed to perform the computational flow dynamics simulations for the mixing of the exhaust gasses with the ventilation air. The values obtained for the operational parameters of the simulated microturbine are consistent with existing microturbines. The simulation provides a means of calculating the parameters of a VamTurBurner© system based

on and adaptable to the site-specific situations. Once a suitable scenario is determined, and a given set of parameters is available, a decision can be made on an appropriate microturbine or combination of various sizes of microturbines needed to produce an acceptable combination of electricity and heat output.

For a base case scenario, a ventilation flow of 100 m^3/s with a methane concentration of 0.5% at a temperature of 300 K is used for the incoming ventilation air. The initial mixing brings the stream from six microturbines together with the ventilation air. Calculating the expected influence of the mixing prior to the computational flow dynamics modelling provides a basis for establishing the boundary conditions of the computation.

Firstly, to calculate the energy contained in the ventilation air, the VAM is treated as a power source. Since the flow is 100 m^3/s at the temperature of 300 K, the ideal gas law yields a density of 1.1765 kg/m^3. For a specific heat capacity of 1.0357 kJ/kg-K, see Figure 4.1.1 for the molar specific heat capacities as a function of temperature, the VAM contains an energy/second of 36.555 MW. To be clear this is not the heat released from oxidation of the VAM. The same calculations for the total microturbine flow of 5.333 m^3/s at 700 K yields a density of 0.504 kg/m^3, a specific heat capacity of 1.1 kJ/kg-K and returns a power of 2.06963 MW. Combining these and calculating the temperature by $\boldsymbol{T = Q/mC}$ the temperature of the mixed gasses is determined to be 309.9 K. Since a value of 500 K is desirable for the pre-heated VAM a calculation of the amount of energy required to raise the temperature of the VAM flow from 309.9 K to 500 K is required to confirm the amount of fuel mass flow, which is needed from the igniters, provided the VAM is fully oxidized.

The amount of power available in the VAM upon full oxidization is calculated based on a fuel calorimetric value of 55.5 MJ/kg for methane. In the 100 m^3/s ventilation flow with a 0.5% methane concentration, which converts to a mass flow of 0.35 kg/s, using a methane density of 0.7 kg/m^3, if the methane is fully oxidized 19.425 MW_{th} of power is released to the ventilation flow. The calculated amount of power needed to raise the temperature of the ventilation flow to 500 K after mixing with the microturbine exhaust is 23.69 MW_{th}; thus, an additional 4.442 MW_{th} is needed from the igniters. The fuel colorimetric value used for the microturbine and for the fuel source of the igniters in these calculations is 38 MJ/kg so the mass flow

rate of fuel to the igniters is calculated as 0.117 kg/s. The combined fuel consumption of the six microturbines and igniters is 0.324 kg/s and that from the VAM is 0.35 kg/s almost miraculously equivalent, which gives approximately twice the power output for the purchased input.

The overall characteristics of the system are summarized as follows by assuming an 80% thermal conversion efficiency. A total of 1.5 MW_e is produced from a cluster of six 250 kW microturbines. The 1.5 MW_e is produced at a 20% efficiency from an input of 0.207 kg/s of fuel at a caloric value of 38 MJ/kg, a calculation of the electrical output for confirmation (20 %)x(38 MJ/kg)x(0.207 kg/s) = 1.573 MW_e. The amount of Power available from the VAM, 19.25 MW_{th}, additionally there is 6.29 MW_{th} available from the microturbines and 4.442 MW_{th} from the igniters so the total power available for use by the heat exchanger systems is 29.98 MW_{th}.

These systems are able to produce electrical power by producing steam at the high temperature end followed by various thermal products such as hot water or industrial drying and finally a third stage where an organic Rankin cycle absorption chiller can provide cooling. The total amount of power, by these calculations, is 29.98 MW_{th}, but when considered in terms of the purchased power and keeping in mind that this calculation is performed after the electric conversion has occurred; the purchased power only represents 35% of the total. Certainly, this is a strong incentive to consider when the installation of a pilot system is deliberated in a prefeasibility study.

7. A study of the thermal characteristics and flow dynamics of the various stages of the VamTurBurner©

7.1. Mixing of the gas turbine exhaust and the incoming VAM

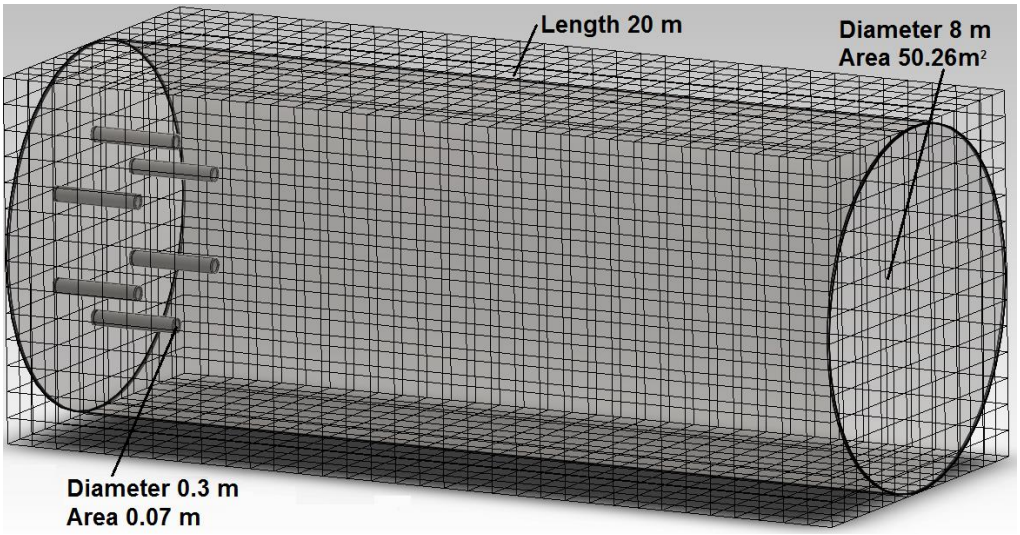

Figure 7.1.1 The mesh model used for analyzing of the mixing of the six gas turbines exhaust gasses with incoming VAM. The 6 tubes at the left represent the gas turbines.

The results of the LES modeling suggests that, for the benchmark case of 0.5% VAM, if the incoming ventilation air is preheated to about 500 K combustion occurs. The model displayed in Figure 7.1.1 is one of the several used for analysis of mixing of exhaust gasses from six gas turbines with the mine ventilation flow. In this instance, the gas turbines are simulated by introducing a flow rate of 50 m/s through the area of 0.07 m^2 at a temperature of 700 K and the ventilation air is simulated by a co-flow of 2 m/s through an area of 50.26 m^2 at a temperature of 300 K. The boundary conditions are varied to study different scenarios; nine simulations were run using various manifestations of this model with differing boundary conditions and dimensions, while only the most pertinent results are selected for viewing. These extra scenarios, calculated to obtain a wider view of the flow and dimensional interactions for final design purposes, are stored in the digital records. The simulations performed use variations of the boundary conditions in a similar model or modified design dimensions, such as the incoming ventilation flow set to 1.8 m/s or 2 m/s in different scenarios. This allows for some inter-model comparison and an increase in the validity of the overall system response.

Heat exchange systems at this scale are customarily designed specifically for the intended purpose, taking into account the unique nature of the system flows and temperatures for a given situation. There are two stages of heat addition for the preheating of the incoming ventilation air. The incoming ventilation air mixes with the gas turbine exhaust and then the mixture encounters the preheating section. In the first stage the VamTurBurner© collects all of the exhaust heat from the gas turbines internally; thus, losses are minimal. The second stage of preheating elevates the temperature of the mixture to an appropriate value for the VAM concentration in the ventilation flow, the value of 500 K is the target value for the benchmark VAM concentration of 0.5 %, for the methane to undergo ignition when it comes into contact with the igniter flame. The preheating can be accomplished either by heat transfer through conduction using a heat exchange system, or by recirculation of the upstream high temperature air from the combustion zone back to the incoming stream. These are the two options explored using CFD modeling.

The CFD modeling of the interaction between the incoming ventilation air and the exhaust of the six gas turbines was modeled independently to evaluate the resulting temperature and turbulent mixing of the two flows. Essentially, the final average temperature of the fluid and the distribution of the temperature over the area of the flow in the direction of the flow are the sought after results. These become the input to the physical preheating stage. A selected description of the CFD model data, boundary conditions and design are available in Appendix 7.1. Essential characteristics of the CFD simulation of this model are that the six gas turbines have a flow of about 3.53 m^3/s each at a temperature of 700 K with velocity of 50 m/s. The ventilation flow is initially at a velocity of 2 m/s through an area of 50.26 m^2 for a flow of 100.53 m^3/s.

Isotherms for the simulation are shown in Figure 7.1.2, Figure 7.1.3, Figure 7.1.4 and Figure 7.1.5 for 310 K, 320 K, 330 K and 340 K respectively. These Isotherms demonstrate the progression of temperature for singular temperatures and the extent of the interaction between the incoming ventilation air and the exhaust gas from the turbines. From observation of the Isotherms, the temperature increase is evident and the progression and extent of it is easily seen as the flow proceeds to the preheating stage of the VamTurBurner.©

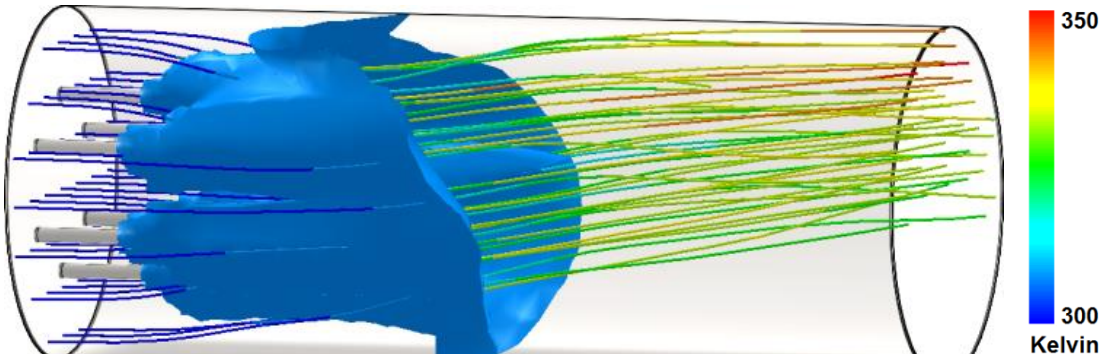

Figure 7.1.2 The 310 K isotherm for the model shown in Figure 7.1.1

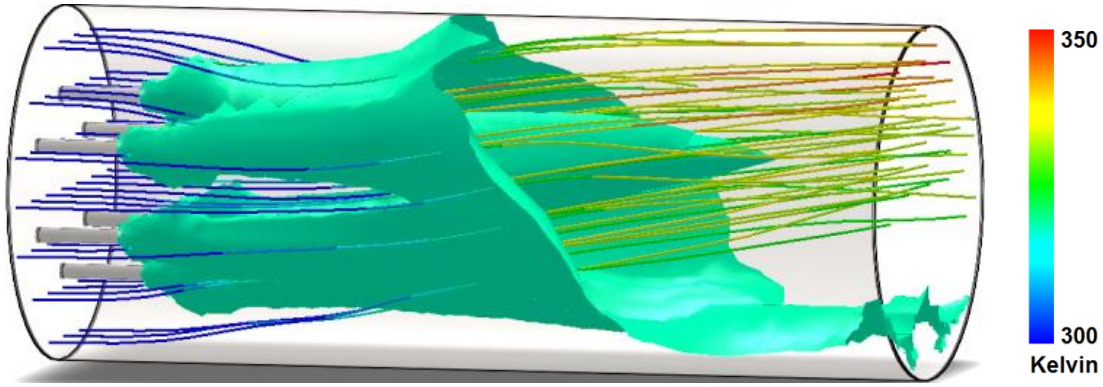

Figure 7.1.3 The 320 K Isotherm for the model shown in Figure 7.1.1

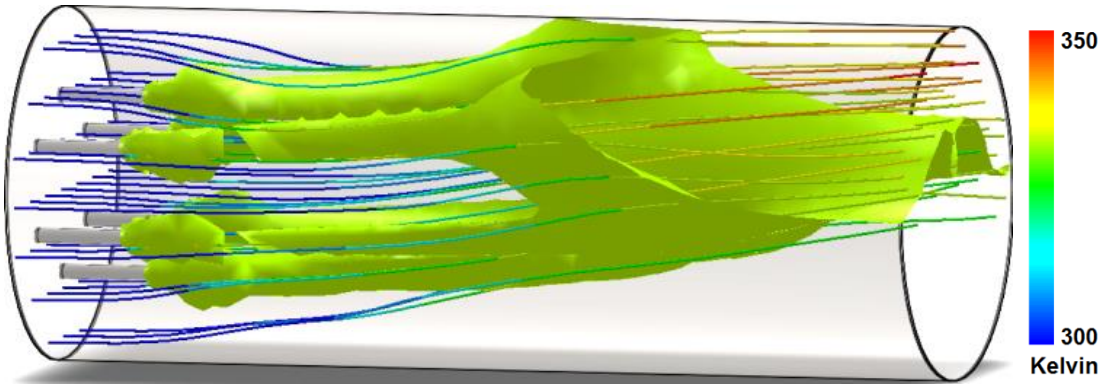

Figure 7.1.4 The 330 K Isotherm for the model shown Figure 7.1.1

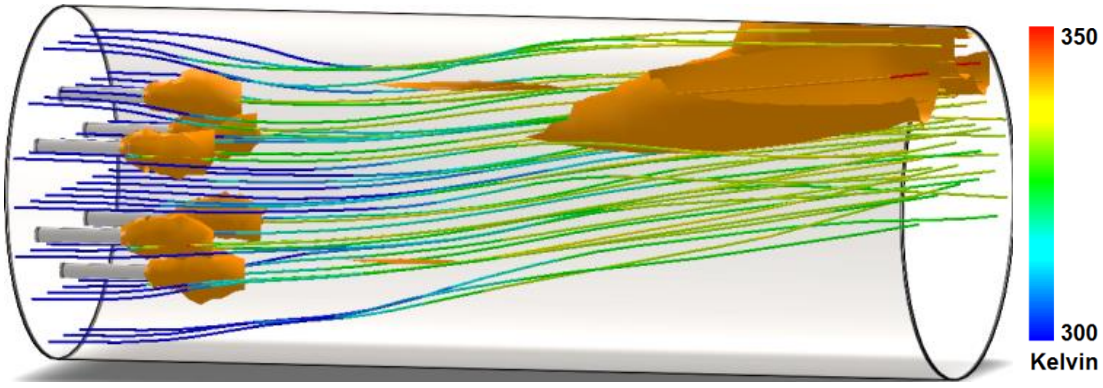

Figure 7.1.5 The 340 K Isotherm for the model shown in Figure 7.1.1

The isotherm at 310 K in Figure 7.1.2 engulfs the six gas turbine exhausts and extends to about half way down the 20 m length. In Figure 7.1.3 the isotherm for 320 K extends slightly further out from the gas turbine exhausts than the isotherm for 310 K with mixing of the co-flows occurring at about the 6 m mark of the simulation. The isotherm for 330 K extends out over the full region of the computational domain and the jet streams are seen to continue to approximately the same point as the extent of the 310 isotherm. The isotherm for 340 K only exists near the gas turbine exhaust outlets and at the top of the 20 m length at the end of the duct.

These data plots show that there is mixing of the two flows, which starts at about two meters and continues to about fifteen meters from the exhaust gas outlets of the gas turbines. An examination of the temperature profiles on horizontal and vertical cross sections through the central axis shows the extent of the mixing, which is a defining characteristic, the average temperature of the flow after mixing, which is needed for the design of the next stage. The average temperature of the ventilation flow after mixing with the gas turbine exhaust provides the initial conditions for the next preheating stage. The amount of additional heat needed to elevate the fresh gas temperature to an appropriate temperature, such that it will readily ignite in the presence of the flame encountered at the igniters, is added to that acquired from the gas turbines.

The temperature profile shown in Figure 7.1.6 and velocity profile shown in Figure 7.1.7, are a snapshot at 15 s from the initiation of flow mixing. By visual inspection of the profiles, the mixing deemed to be acceptable for input to the next preheater stage starts over the first few meters after introduction of the exhaust gas into the ventilation airflow. Apart from the obvious effect due to the rising of the higher temperature air, the temperature profiles through the center of the model show that the mixing of the gas turbine jets and the ventilation air occurs over a length of about fifteen meters. The slowing of the velocity and dispersion of the gas turbine jets or the onset of turbulent mixing between the co-flows also indicate mixing. Unfortunately, the mixing is incomplete over a reasonable distance using this configuration, as can be seen by the temperature differences in Figure 7.1.8 and the enlarged scale in Figure 7.1.8, which is also valid for Figure 7.1.2 to Figure 7.1.6 inclusive. In Figure 7.1.8 it is clear that the energy is not equitably distributed over

the flow area. Although this modeling is not necessarily intended to be exact enough to provide final designs, the intent of this work is to introduce the concept and determine the general viability of the overall design features. Therefore, an improvement in the mixing is required, in terms of reducing the distance from the gas turbines that it takes to mix the two flows, such that the degree of homogeneity of the temperature profile perpendicular to the flow direction occurs at some reasonable distance from the exhaust ports of the gas turbines.

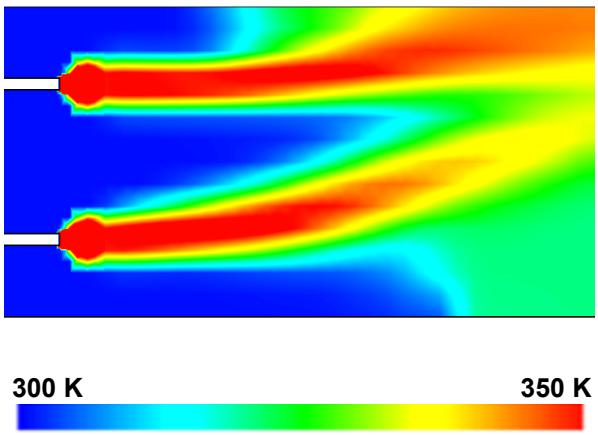

Figure 7.1.6 The temperature profile through the central axis of the flow.

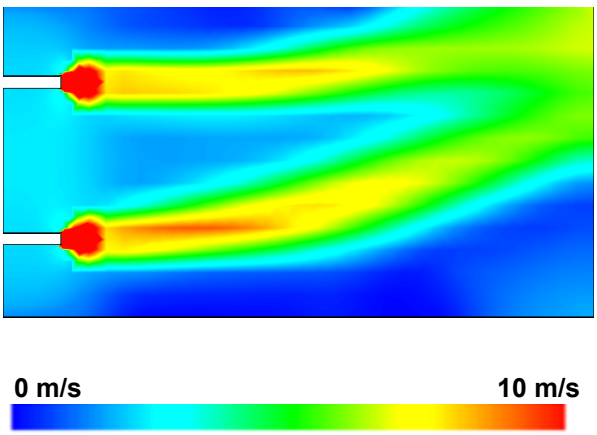

Figure 7.1.7 The velocity profile through the central axis of the flow.

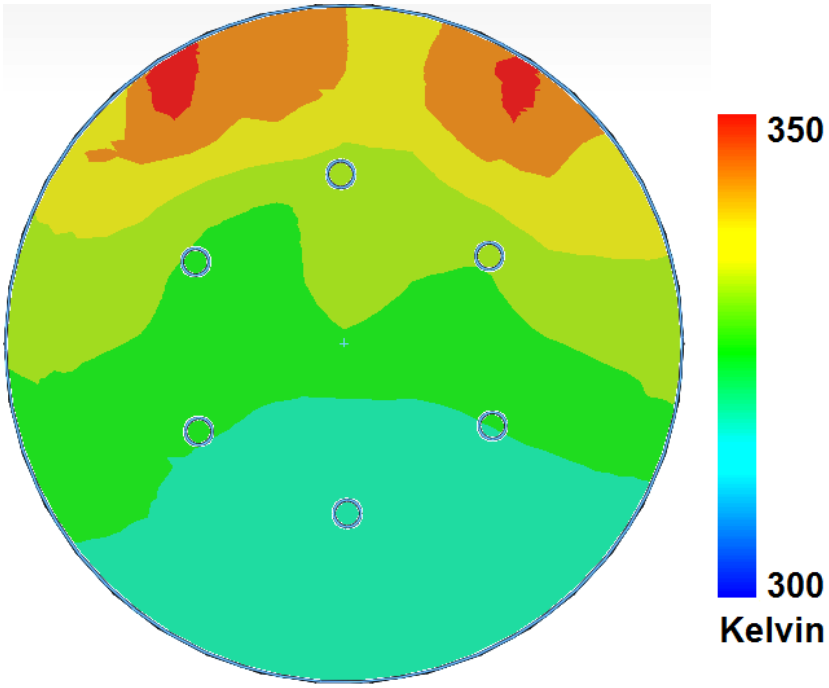

Figure 7.1.8 Temperature profile at the end of the ventilation duct, the distribution of temperature shows the gas turbine exhaust and ventilation flow are not mixed as required.

In a plot of the average temperature versus the time from the initiation of flow shows the that the average fluid temperature approaches about 320 K after 15 seconds, but more mixing is required. The desired mixing can be accomplished by

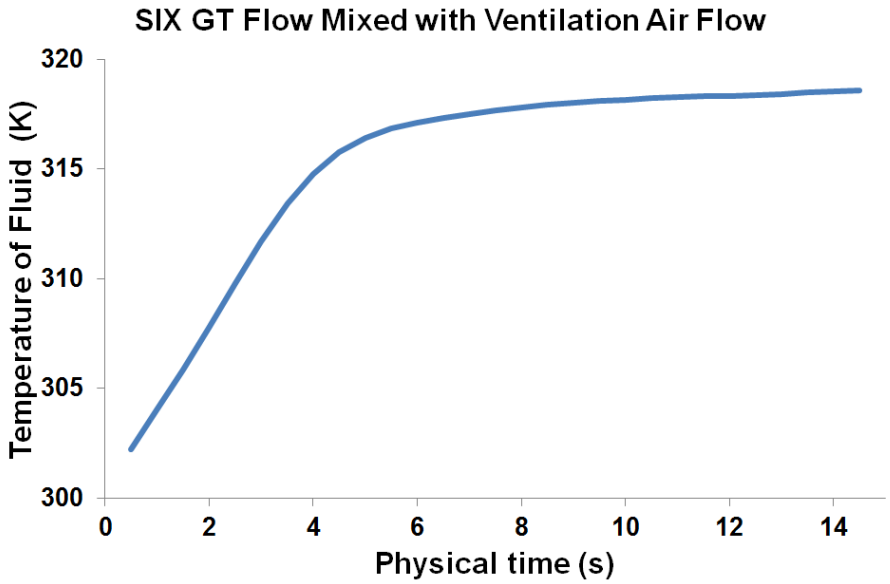

Figure 7.1.9 Average fluid temperature of mixed ventilation air and flow from six gas turbines.

additional gas turbines, a swirling annulus at the exhaust outlets or by the introduction of diffusers placed in the path of the flow.

The next simulation is included to provide a contrast between smaller and larger diameter ventilation systems. This simulation demonstrates the general concept that achieving mixing of the flows also depends on the initial temperatures of the exhaust gas flow, the size of the ventilation ducting, the flow rate of the VAM and the dimensions of the ventilation duct and also on the number and size of the gas turbines. To illustrate that point, a larger diameter ventilation duct at a slightly lower flow velocity of 1.8 m/s provides a flow rate of 361.91 m^3/s through an 8 m radius ventilation system. The six gas turbines have smaller diameter 0.15 m and a 50 m/s flow at 700 K. The composite Figure 7.1.10 is comprised of: a cross sectional cut plot at the end of the tube, flow trajectories originating at both the VAM inlet and the gas turbine exhaust and isotherms for 305 K, 308 K and 310 K.

The exhaust gasses from the gas turbines act more like plumes from an industrial stack in open air rather than a turbulent mixing system. The flow from the gas turbines follows a typical Gaussian dispersion pattern similar to a stack emission under laminar or low Reynolds number flow conditions. As such, it is shown that

either larger gas turbines or more gas turbines with diffusers are required at such large diameter ventilation outlets if mixing of the exhaust or incoming ventilation air is to be achieved. The flow trajectories show the obvious effect that heat rises, but the flows do not interact with each other consequently do not induce the desired mixing. The isotherms confirm the same and the cross sectional cut plot at the end of the ventilation simulation shows that the temperature distribution corresponds to the essentially intact flow of the gas turbine plumes in the ventilation flow.

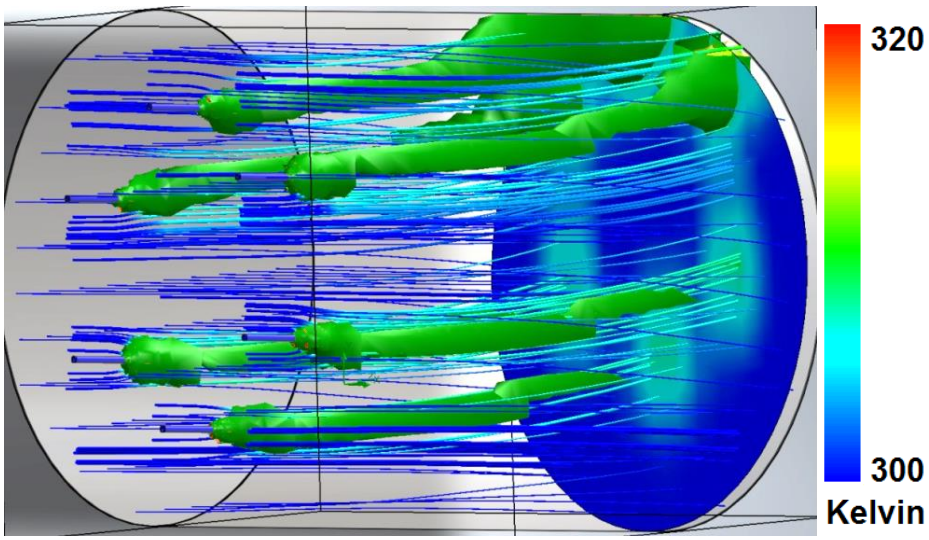

Figure 7.1.10 simulation for the same six gas turbines in the model shown in Figure 7.1.1, but with the radius of the ventilation system increased to 8 m with a flow rate of 361.94 m^3/s

7.2. Insertion of diffusers improves mixing of the gas turbine and ventilation air flows.

In order to promote mixing of the gas turbine flow with the ventilation flow over a shorter distance diffusers can be placed in the gas turbine exhaust flow to disrupt the forward momentum of the flow. A simulation of a ventilation system using a 100.53 m^3/s flow rate includes diffuser discs to promote the turbulent interaction of the exhaust gas flows with the ventilation air. For merely creating a simulation to provide an interruption of the flow and promote the mixing with the surrounding flow, the discs are simply placed in free space in the path of the exhaust gas flow; thus, engineering the design of brackets is not part of the simulation. The flow simulation shown in Figure 7.2.1 shows the diffusion discs placed in front of the gas turbine flow to improve the circulation of the hot exhaust within the cool ventilation airflow. In Figure 7.2.1 the flow trajectories originating at two of the gas turbine exhausts are sufficient to display the interaction between the exhaust gasses and the incoming

ventilation air; adding the flow trajectories for all the gas turbines obscures the view of the flows. Another flow trajectory, originating inside the flow system just after the diffusion discs, has its initial position shown by the blue dots in the figure. The flow trajectory in Figure 7.2.1 is connected to a vortex, which is a very good indicator of turbulent mixing of the co-flows.

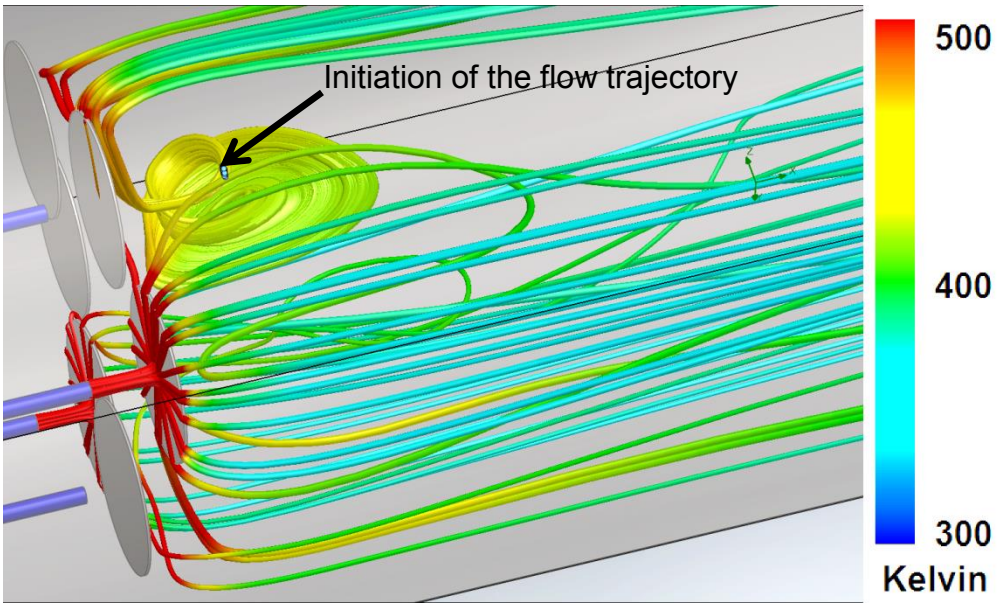

Figure 7.2.1 A 50 m/s flow interacting with an array of mixing diffusers included to promote the turbulent interaction of the exhaust gas flows.

As can be seen from Figure 7.2.1, the diffusion discs assist with the circulation and promote turbulent mixing of the hot exhaust gases from the gas turbine and the incoming cool ventilation air. Forcing the flow to travel around the discs improves the mixing. The flow continues toward the outlet and the temperature smoothing occurs as the flow mixes arriving at the end reasonably close to an even average temperature. In the following series of figures, Figure 7.2.3 to Figure 7.2.8, the same flow trajectories as in Figure 7.2.1 are shown, but from a different angle with the addition of a temperature profile cross sectional cut plot at the ventilation system outlet. The average temperature is about 316.2 K after mixing, which was determined by taking the average of the temperature values from 138 s to 198 s as shown on the plot in Figure 7.2.2. The modeling is in agreement with the calculations in Chapter 4 for the average temperature of the system flow after mixing of the gas turbine exhausts with the ventilation air.

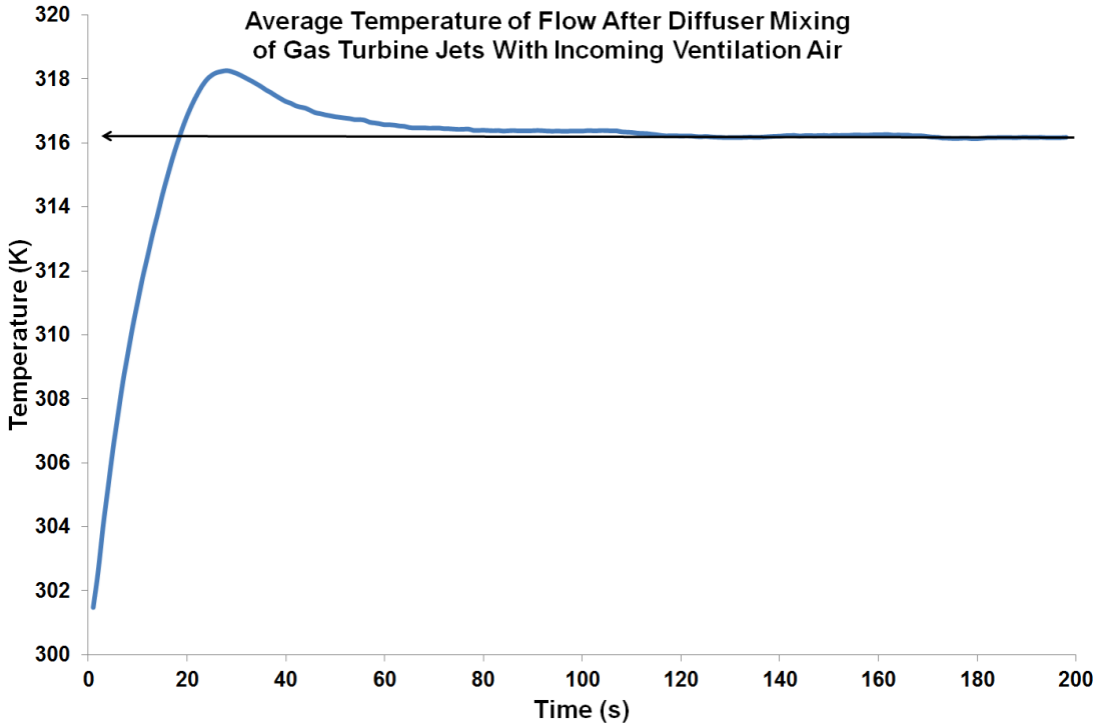

Figure 7.2.2 Average fluid temperature of diffusion mixed ventilation air and flow from six gas turbines

Isotherms at discreet temperatures are an exemplary characterization of the temperature evolution as the flow proceeds through the system. A sequence of isotherm temperatures for examination of the mixing regions is a means of developing the system design to answer the question how far from the exhaust of the gas turbines should the preheating heat exchanger or inlet for recirculation of hot air be placed? The sequence for temperatures of 300 K, 310 K, 320 K, 330 K, 340 K and 350 K are displayed for that reason. Observation of the isotherm progression shows that the average fluid temperature of 316.2 K is achieved within a few meters of the diffusion discs. This is confirmed by examination of the linear extent of penetration of the gas turbine jets, along the flow direction, of the 330 K isotherm into the 320 K isotherm. Although an outer envelope extends about half way down the ventilation duct, for the most part the 330 K isotherm only extends about a meter past the gas turbine exhaust ports. The 320 K isotherm extends the full linear extent of the ventilation duct, but tapers to impinge on the central portion at the exit of the duct where it is contained by about half the radius. For the purpose of design parameters involving the location of the preheater, there is sufficient mixing and the temperature distribution allows for placement of the preheater within a few meters from the gas turbine exhaust diffusers.

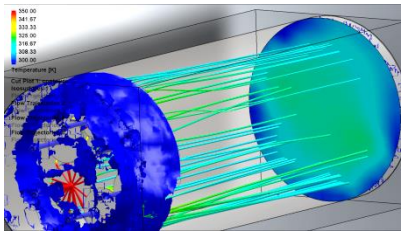

Figure 7.2.3 300 K Isotherm.

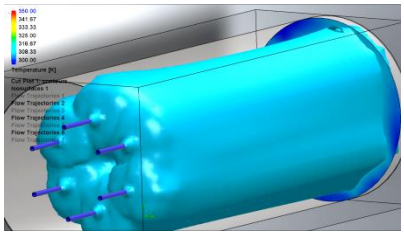

Figure 7.2.4 310 K Isotherm.

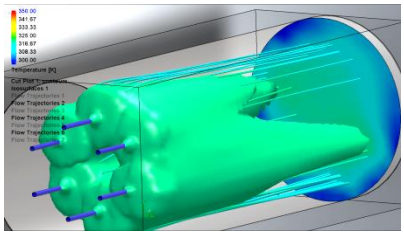

Figure 7.2.5 320 K Isotherm.

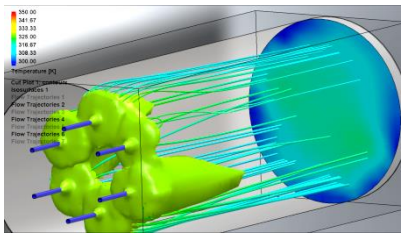

Figure 7.2.6 330 K Isotherm.

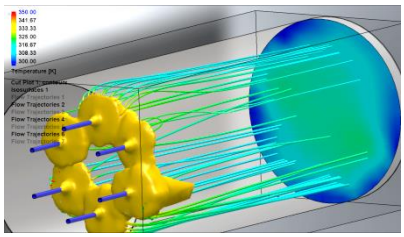

Figure 7.2.7 340 K Isotherm.

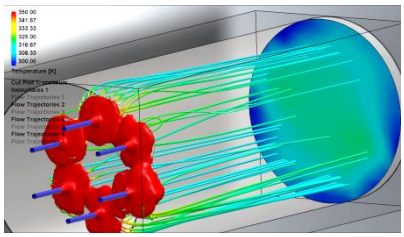

Figure 7.2.8 350 K Isotherm.

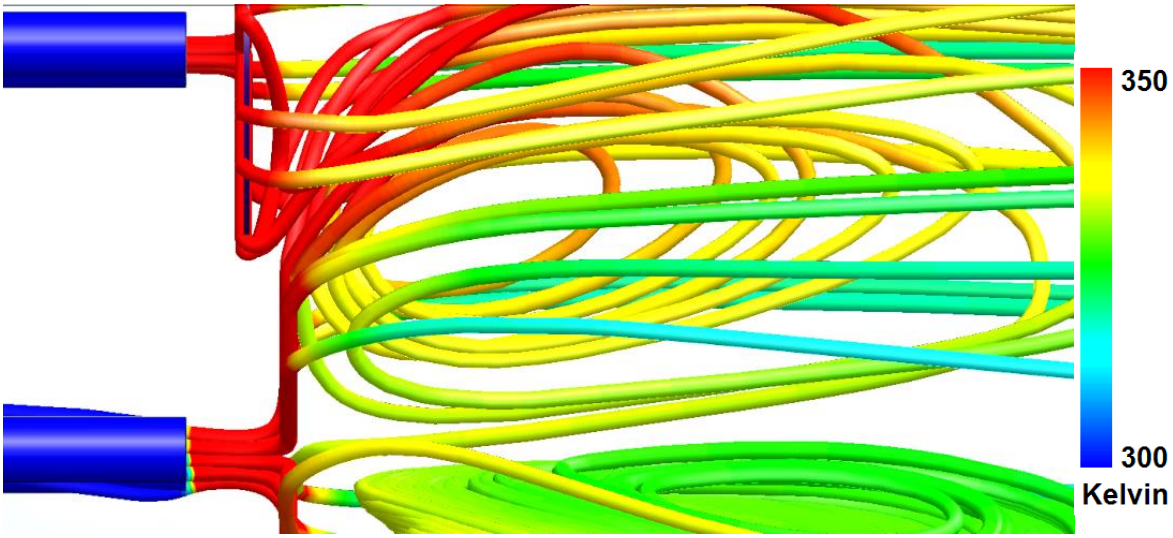

Figure 7.2.9 Close up of the offset diffusers positioning with flow trajectories. (Note the same scale applies to Figures 7.2.3 to Figure 7.3.8)

The position of the dispersion disc plays a significant role in the amount of local turbulence at the point where the high temperature exhaust gasses are mixing with the incoming ventilation air. The closer the dispersion disc is to the outlet of the turbine exhaust gas the more gas is redirected from the initial direction of flow, to the radial direction or perpendicular to the original flow direction. Positions ranging from 0.30 m to 1.5 m from the exhaust port of the gas turbines were studied. The best result, in terms of mixing the co-flows, was found to be a staggered arrangement with diffuser discs placed at 0.3 m to 0.4 m from the exhaust ports and offset. A close up of this arrangement is shown in Figure 7.2.9 and Figure 7.2.10.

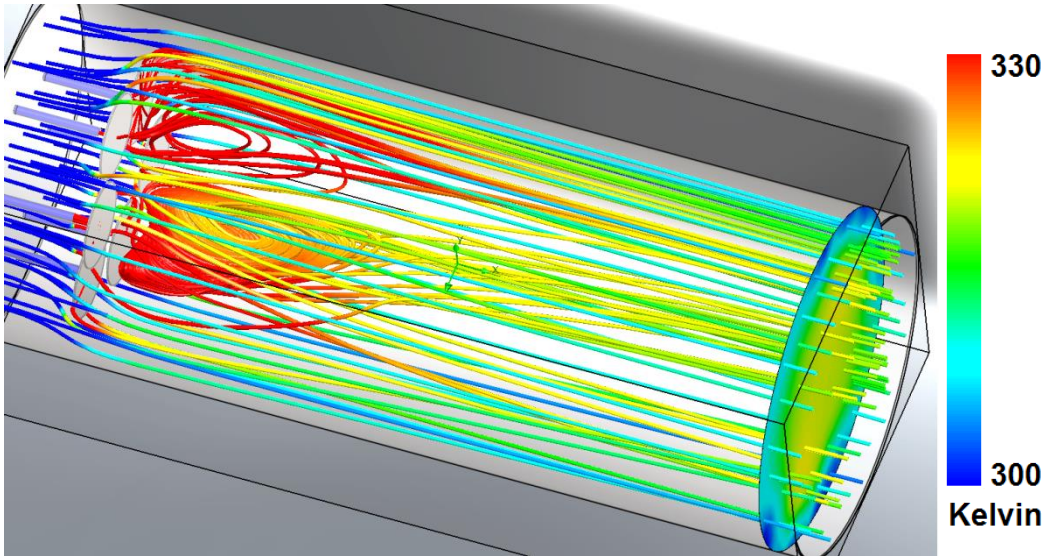

Figure 7.2.10 The same flow trajectories as in Figure 7.2.3 to Figure 7.2.9, but at a different angle and temperature scale from 300 K to 330 K, the temperature scale is narrowed in this model to show the variations with higher resolution.

Examination of the flow trajectories in Figure 7.2.10 indicates that the turbulence is increased in the mixing zone; this is confirmed by the increased activity of the vortices in the mixing volume also perceived in Figure 7.2.1 and Figures 7.2.3 to 7.2.9. The temperature profile at the exit of the ventilation duct has similar characteristics to the profile at the same location in Figures 7.2.3 to 7.2.9, but the scale is from 300 K to 330 K in Figure 7.2.10, which allows for increased definition of the temperature spread near the final average temperature. Although the result of the average temperature and the temperature profile at the exit of the ventilation duct is similar to nearly equal in both cases, the immediate effect of mixing as a result of placing the dispersion discs closer to the exhaust gas outlets is to cause the temperature distribution to smooth out over a lesser linear physical extent. This is a desired consequence from the viewpoint of the engineering economics of the design because if the preheater is closer to the gas turbine exhaust the cost of the system is reduced.

At the outer edges of the flow, close to the ventilation duct surface, there is reduced interaction consequently the VAM flow proceeds through the system at a lower temperature or is subject to less mixing. This is typical of any flow system, the velocity at a fixed surface is zero so the flow is substantially reduced. This effect is evident from the observation of the parabolic velocity profile in any standard text on flow dynamics or mine ventilation engineering (McPherson, 2013).

7.3. A study of the preheating zone design options

7.3.1. Concurrent heat exchanger concepts

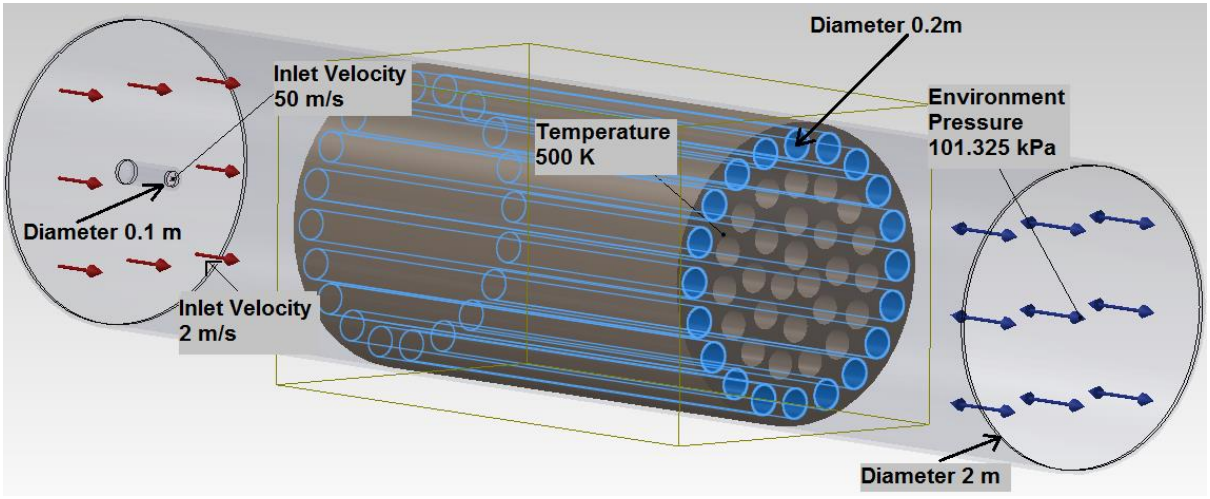

Figure 7.3.1 Model used for heat exchange study for preheater

The design of the preheating stage is an essential aspect for the successful operation of the VamTurBurner©. The preheater takes heat from the system flow further downstream and cycles it back to the incoming flow to raise the temperature of the flow to a level commensurate with the temperature determined by the LES modeling. Several possibilities were considered, but the shell and tube heat exchangers and plate heat exchangers are the emphasis. These systems are constructed with metals capable of operating at high temperatures such as stainless steel and having as high a thermal conductivity as feasible. Frequently used materials for the purpose of modeling were stainless steel 316 and copper. Several models and many iterations of the same model were studied with selected results presented.

The preheating stage may be accomplished using a heat exchanger operating to provide heat from a liquid or steam to the ventilation air by absorbing heat from the hot gas downstream after the combustion zone. The liquid used for this modeling is water (steam); thus, the heat will be transferred by steam from the downstream heat absorbing section to the upstream transfer section. This modeling is required essentially to determine the feasibility of using the downstream gas flows as to produce steam and the volumetric steam transfer required to determine if the method is feasible.

The first model presented in Figure 7.3.1 uses a single gas turbine, instead of the six used for the modeling in section 7.1 and 7.2, with a preheating stage comprised of flow through tubing. A single gas turbine followed by the heat exchange tubing is sufficient for the modeling of the heat balance at a given flow rate because the results can be algebraically scaled to the size of the VamTurBurner©. The design allows for efficiency of computation time; see Table 7.3-5 in appendix for a sample of the data input/output used in the heat exchanger spreadsheet. Figure 7.3.1 is a representation of one of the shell and tube designs. Each stage of the system is modeled separately; thus, the combustion chamber follows this section and the primary heat exchanger stage follows the combustion chamber. The initial conditions for each subsequent stage are derived from the output of the previous stage simulation. The boundary conditions for the simulation of the flow from a gas turbine interacting with typical ventilation airflow is shown on Figure 7.3.1, the ventilation air enters at a speed of 2 m/s at temperature of 300 K and the flow of the exhaust gas from the gas turbine is 50 m/s at 700 K. The diameter of the outer containment is 2 m and that of the exhaust port of the gas turbine is 0.1 m. The diameter of the heat exchange flow tubes are 0.2 m and they are constructed from copper tubing with a thermal conductivity of 390 W/m^2K and held at a constant temperature of 550 K. An isotherm of 500 K, displayed as a red grid pattern in Figure 7.3.2, exists at both the gas turbine exhaust and at the far right where the flow exits the heat exchange tubes. The ventilation airflow trajectories begin on the left side; the dark blue hue of the trajectories signifies the air is at 300K. The interaction between the ventilation air and the gas turbine exhaust yields a product gas with an increased temperature and turbulence length as seen by the increase in vorticity and temperature displayed on the flow trajectories. The exit temperature from the pre-heater is near 500 K, this is the target temperature for the 0.5 percent VAM concentration for the purposes of creating a mixture in a state ready to undergo auto-ignition upon encountering the igniters.

The design of heat exchangers is well represented in the literature (Mukherjee, 1998) and there are many off-the-shelf smaller units available, but at this scale, they would normally be designed specifically for the purpose, for a complete description of the design formulae and industry standards see (Edwards, 2008). Another standard design is the plate heat exchanger where a flow moves

across a series of parallel plates rather than tubes. Simulations of a plate heat exchanger were also undertaken for comparison. The temperature of the plates were held at 550 K to simulate a constant flow of steam near or just above that temperature. A calculation of the steam volume equivalent to the simulation elucidates the difficulties of such a steam flow.

The amount of steam required to maintain the temperature of the heat exchange surface at 550 K was calculated for the 100 m^3/s standard flow rate used for the benchmark of the VamTurBurner© design. The energy available from a 0.5% VAM concentration, calculated in Chapter 6 section 4 is 19.425 MW_{th}, but additional heat is added from the igniters. The heat available from the igniters is adjustable; thus, can add sufficient heat to the system to raise the hot gas flow at the exit up to an operational temperature or adjust to variations in the VAM concentration, but the value of 4.44 MW_{th} from Chapter 6 section 4 is taken as the steady state value.

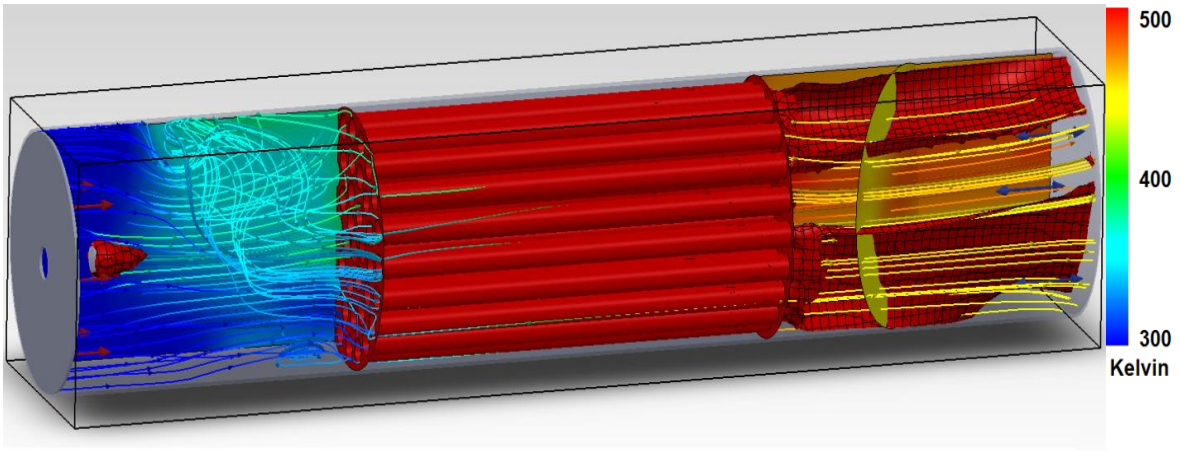

Figure 7.3.2 Simulation of a heat exchanger shell and tube concept.

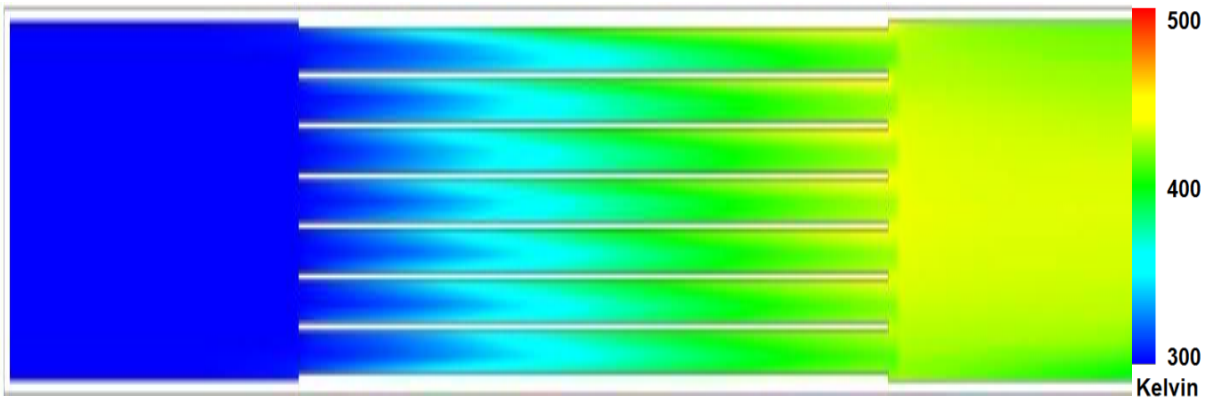

Figure 7.3.3 Cross section of plate heat exchanger.

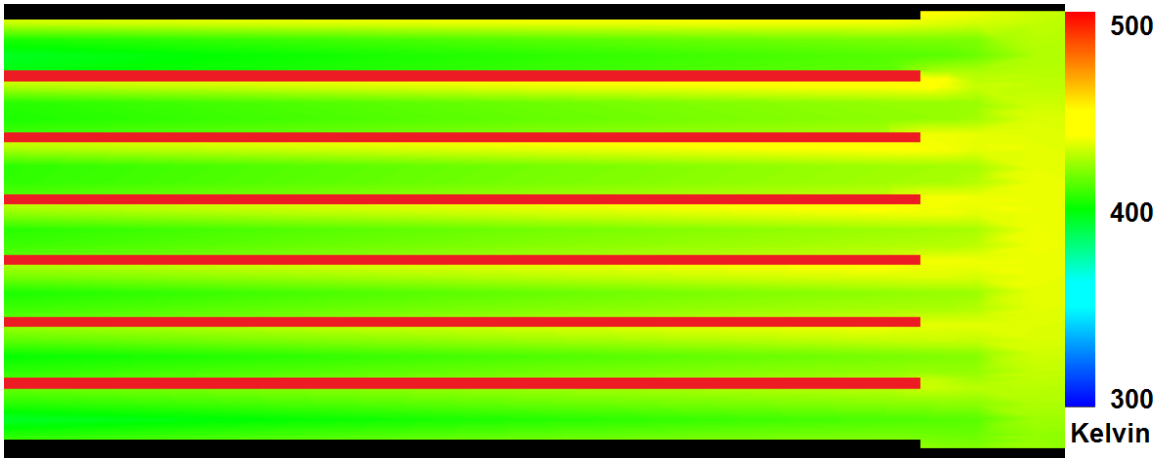

Figure 7.3.4 Expanded view of the plate heat exchanger outlet from Figure 7.3.3.

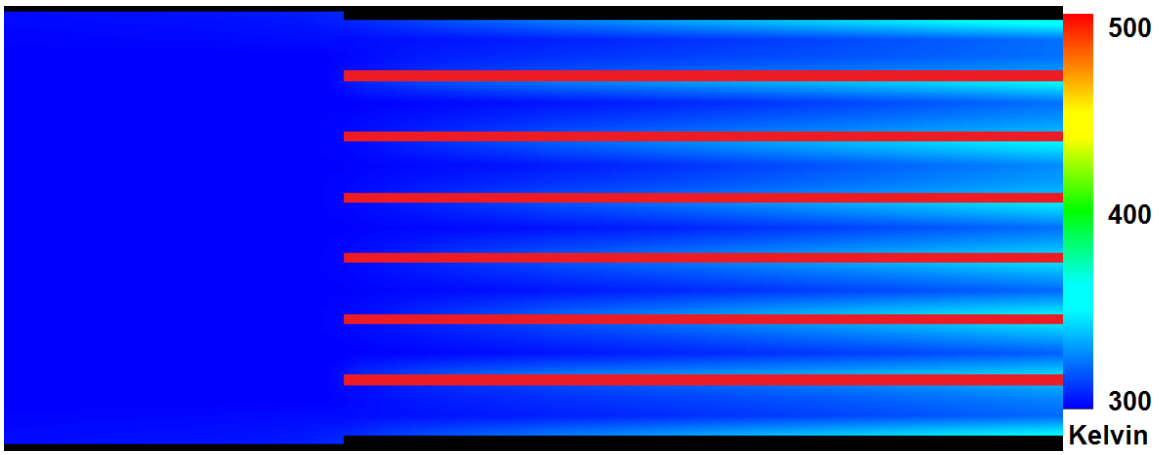

Figure 7.3.5 Expanded view of the plate heat exchanger outlet from Figure 7.3.3.

Using the amount of heat available for a 100 m^3/s flow at the benchmark VAM concentration of 0.5 percent plus the additional heat from the igniters a total of about 23.87 MW_{th} is available for the purpose of the following calculations. Firstly, a calculation of the temperature rise due to the addition of the gas turbine exhaust showed that the mixing of the flows raises the temperature of the incoming air to about 316 K. Taking 316 K as a starting temperature and 500 K as the final temperature, the amount of energy that must be added to the incoming ventilation air is calculated as 20.9 MW_{th}. If steam at 600 K is used to provide the heat to the incoming ventilation air and the exit temperature of the steam is 500 K, then the amount of steam required, using an average specific heat capacity for steam of 2 kJ/kg–K, would be about 104.5 kg/s. The assumption of inlet water at 288.15 K (15 C^o) is reasonable for a calculation of the amount of energy needed to produce the steam. The calculation considers raising the temperature of water from 288.15 K to 373.15 K, adding the latent heat of vaporization and then raising the temperature

of the steam from 373.15 K to 600 K represented by the heat quantities Q_1, Q_L and Q_2 respectively in Table 7.3-1. The energy available of 23.87 MW_{th} would be able to provide 7.75 kg/s of steam at 600 K.

Table 7.3-1 Calculation spreadsheet for the amount of steam able to be produced by the amount of energy available from a 0.5% VAM concentration

Mass water	7.75	kg		Kelvin	Celsius
S_w	4.19	kJ/kg K	T1	288.15	15.00
S_s	2.00	kJ/kg K	T2	373.15	100.00
L_v	2270.00	kJ/kg	T3	600.00	326.85
Q_1	2758.43	kJ			
Q_L	17598.27	kJ			
Q_2	3510.29	kJ			
Q_T	23867.00	kJ	=	23.87	MJ
Available heat	23.87	MJ			

Although the heat exchangers could provide the preheating based on the modeling, there is insufficient energy available from the minimum design criteria to provide the steam flow rate needed when the steam is produced from water at an initial temperature of 288.15 K, because the design is a flow through system. In a cycle between 500 K and 600 K, there are 23.7 MW available, which is sufficient energy to provide the 20.9 MW heating required, see Table 7.3-6 in appendix for a study of heat exchanger response. This essentially rules out the steam heat exchangers for this purpose in a flow through system, but not for energy conversion at later stages of the system. In a contained system operating between 500 K and 600 K, the required flow of 104.5 kg/s is possible, but expensive.

7.3.2. Co-flow turbulent mixing

An alternative to heat exchangers is direct mixing of the downstream airflow, after the combustion, with the incoming ventilation air. This would be a somewhat less expensive design due to the reduced complexity, design costs and the expense of high temperature materials. By redirecting the air from the hot end of the system, a straightforward temperature and flow feedback monitoring system would be sufficient to provide the necessary control. A calculation of the final temperature based on the incoming temperature of 316 K, which could be higher due to the

addition of more than six gas turbines or using larger gas turbines. The temperature of 1100 K for the combustion gas temperature is provided in Table 7.3-2.

Table 7.3-2 Calculation spreadsheet for the final temperature when mixing the incoming ventilation air with the combustion gas.

Ventilation	**Pressure**	**101325**	**Pa**			
	Mass	**0.02896**	**kg/mole**	**ρ =**	**1.11701**	**kg/m^3**
	Rydberg's	**8.31447**		**V =**	**1333.46704**	**Pa/kg mole K**
	T_i	**316**	**K**	**34.85**	**°C**	
Specific heat capacity		**1.00554**	**kJ/kg - K**	**mass**	**111.70162**	**kg/s**
Combustion	**Pressure**	**101325**	**Pa**			
	Mass	**0.02896**	**kg/mole**	**ρ =**	**0.32088**	**kg/m^3**
	Rydberg's	**8.31447**		**V =**	**382.49417**	**Pa/kg mole K**
	T_f	**1100**	**K**	**826.85**	**°C**	
Specific heat capacity		**1.149193**	**kJ/kg - K**	**mass**	**32.08883**	**kg/s**
	Q	**62.57133**	**MJ**	**S_{avg}**	**1.07748**	**kJ/kg - K**
	Flow cold	**100**	**m^3/s**	**m_{avg}**	**71.89522**	
	Flow hot	**100**	**m^3/s**			

Q_h	**40563.90**	**kJ**
Q_c	**35493.31**	**kJ**
Q_t	**76057.21**	**kJ**
m_t	**143.790**	**kg**
S_{avg}	**1.031587**	**kJ/kg K**
T_F	**512.74**	**K**

Based on the calculations in Table 7.3-2 this approach is feasible provided losses are minimized. The initial temperature of 316 K is based on using an exhaust temperature of 700 K and a flow rate of 3.5 m^3/s for the gas turbines. Slight changes in the configuration of these units can have a marginal yet significant effect on the final temperature of the co-flow. This is due to the effect of a higher density at the lower initial temperature of the gas entering the preheating zone on the amount of energy needed to raise the temperature to near 500 K. For example, in a calculation using 0.7 m^3/s at a temperature of 700 K for the gas turbine exhaust, the average temperature of the mixed co-flows was 308 K and the temperature of the recirculation mix was 503.4 K.

Computational flow dynamics models were created to establish the feasibility for a preliminary design. The initial design is the same as Figure 7.2.1, but including an outer section that is an insulated tube not shown except for the inlet area with the boundary conditions. The hot gas inlet area is 28.27 m^2 and the flow velocity is 3.5

m/s, which provides a flow quantity of 98.96 m^3/s. This appears as though the entire flow of the system is being recirculated back to mix with the incoming ventilation flow, but since the flow is being recirculated the total flow at the exit is the sum of the recirculated flow and the incoming flow so only a fraction of the exit flow is recirculated.

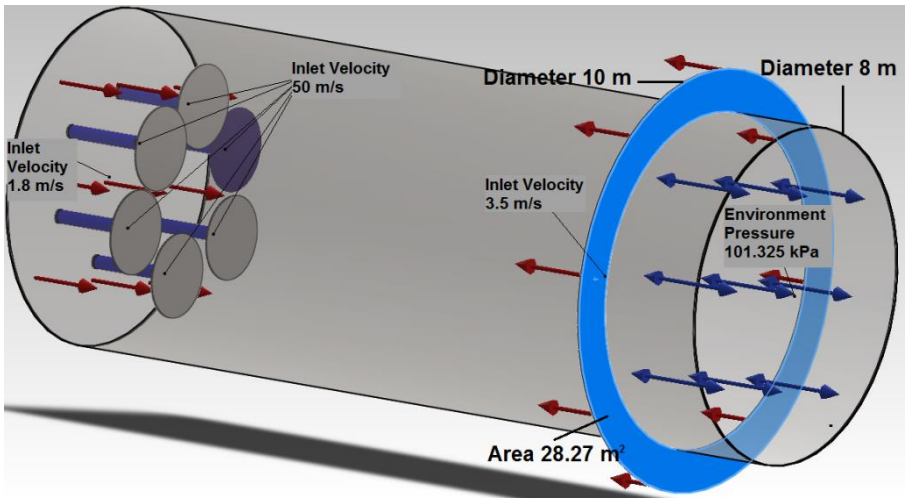

Figure 7.3.6 Model and boundary conditions used to determine the recirculation modality.

The incoming air of the ventilation air is 300 K and the recirculation air is set to 1100 K, which enters through the blue annulus. The gas turbine flow is the same as before, but the incoming ventilation air is 1.8 m/s rather than 2 m/s; thus, the incoming flow is 90.47 m^3/s, as mentioned earlier the parameters used for the models will vary to reflect operating conditions and to provide a spectrum of data for the design.

Observation of results from the initial model revealed that the temperature profile of the exiting gas was not smooth at the outlet as seen in Figure 7.3.8. If the profile across the area normal to the flow is not smooth, some gas volumes at the lesser temperatures may not ignite. Observation of the cut plot at the end of the ventilation duct clearly shows a gradation of temperature from hot at the top to cool at the bottom. Modification of the model to include a plate to redirect the flow seen at the top half of the duct, clearly separated by the isotherms, would assist in the mixing of the flows since most of the hot air enters the top half of the inlet redirecting it to the lower section would improve the turbulent mixing. In Figure 7.3.8, the incoming hot recirculation flow is interrupted by a half pipe inserted at the intersection of the co-flows. The flow rate was also adjusted to 84.82 m^3/s by

reducing the flow velocity to 3.0 m/s. This provides a realistic mixing profile while increasing the data available.

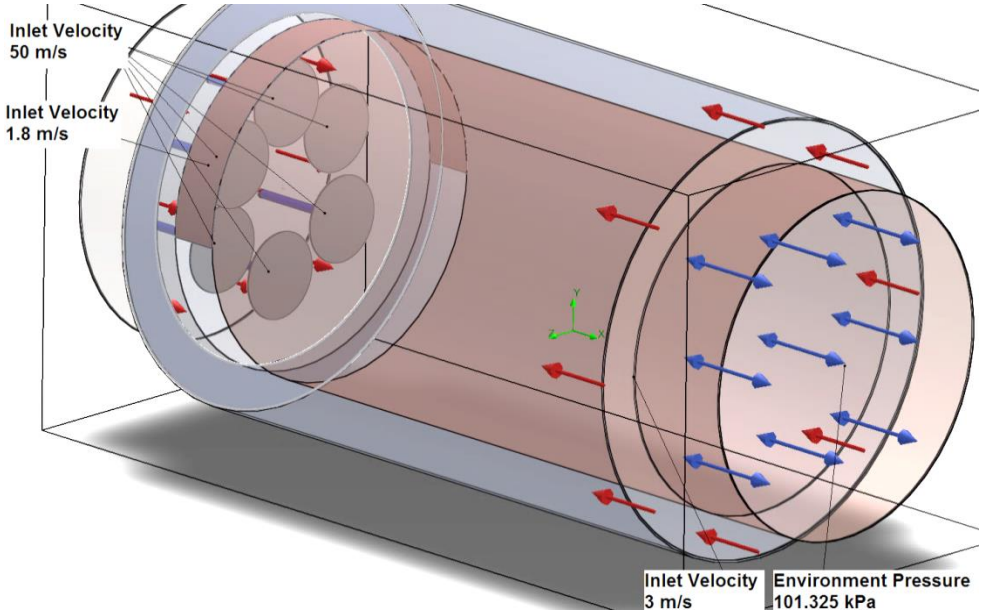

Figure 7.3.7 Initial recirculation model flow trajectories, isotherms and cut plot.

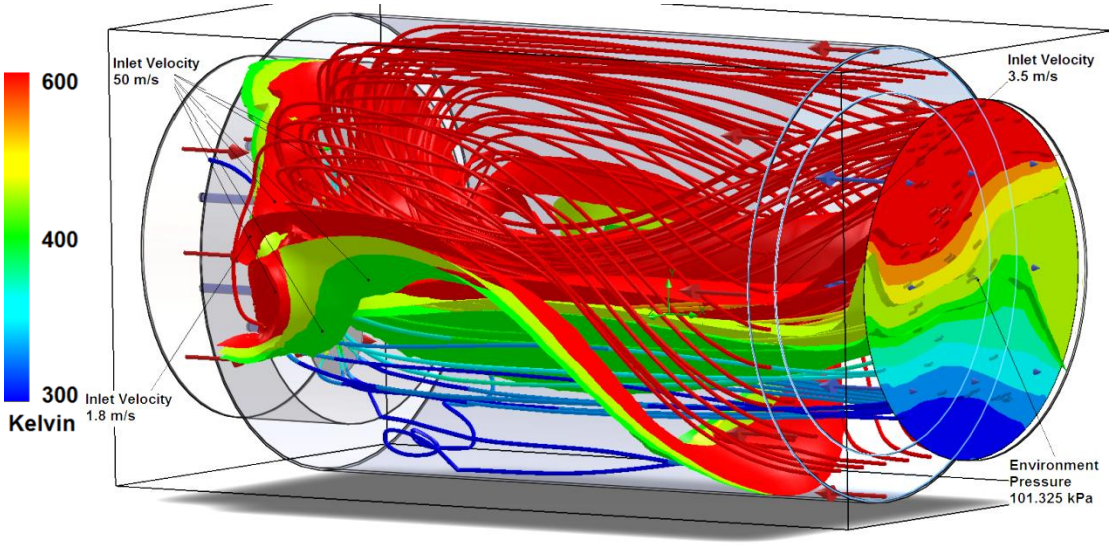

Figure 7.3.8 Revised model used to determine the recirculation characteristics. The inlet for the hot combustion air is blocked at the top to allow only hot air to enter from the bottom.

The half pipe introduced into the top half of the inlet vent is shown outlined in orange on the diagram in Figure 7.3.9. This interruption stops the flow from entering the top of the vent promoting extra mixing from the bottom by taking advantage of the natural tendency for heat to rise and providing an increase in velocity due to the reduction of inlet area.

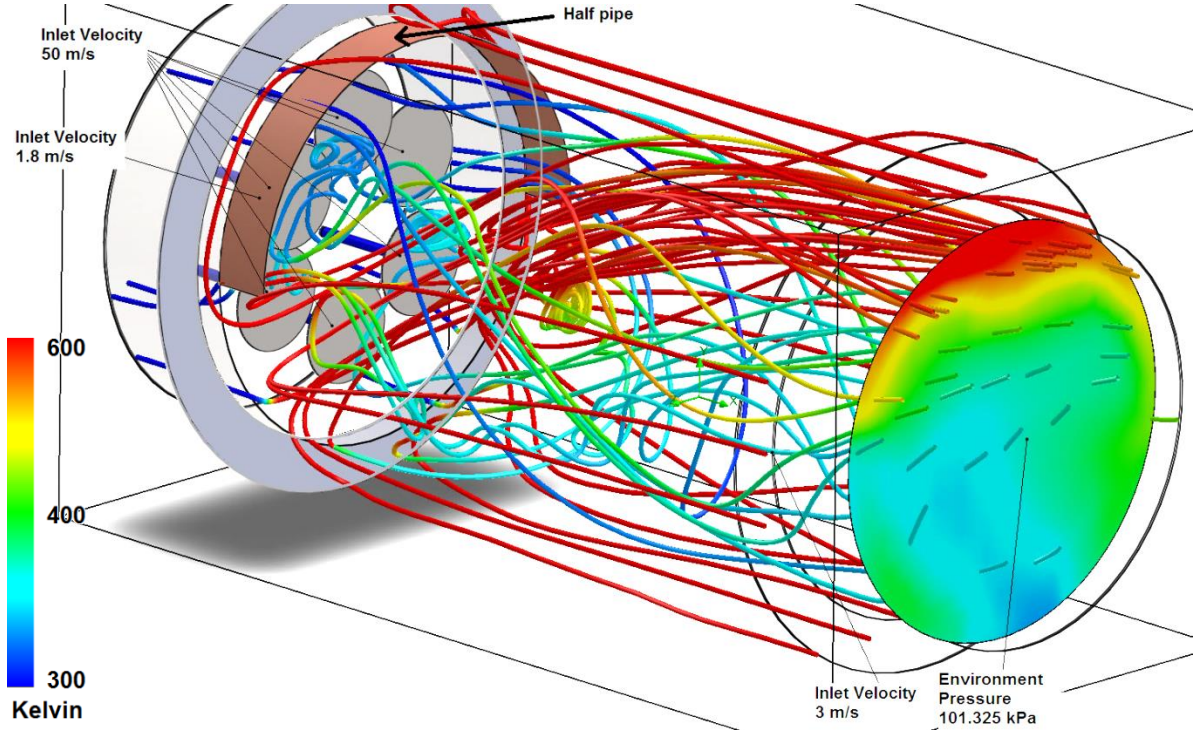

Figure 7.3.9 The second iteration recirculation model with flow trajectories, a cross sectional cut plot at end of duct.

Although there is an improved temperature profile at the exit of the ventilation duct, see the cross section cut plot on Figure 7.3.9, there is still a gradation of temperature with the cooler temperatures at the bottom. Observation of the flow patterns suggest that the introduction of baffles may provide the mixing required to smooth out the temperature profile at the exit of the ventilation duct.

A simulation with two baffles, including six 200 kW_e gas turbines configured as stand-alone CHP systems; thus, energy has been removed from the exhaust gas to provide heat to the independent CHP system. The total exhaust gas flow from the six gas turbines is 7.4 m^3/s and the exhaust gas temperature is 600 K. The incoming ventilation air was set to a velocity of 1.98 m/s to provide a flow of 99.52 m^3/s and the recirculation flow was reduced to 2.5 m/s to provide a flow of 70.67 m^3/s.

Cross sections at the central axis simulation results after the insertion of two baffles and with the inlet hot gas set to 71% of the incoming ventilation gas volumetrically are shown corresponding to 10s, 150s, 350s and 500s from the initiation of the flow. The dimensional configuration is the same as that shown in Figure 7.3.9 except for the inclusion of the two baffles visible in the temperature profiles below.

As can be seen from the series of hi-resolution results, the temperature of the mixed flow is about 450 K. Although not quite 500 K, the benchmark for a 0.5% VAM concentration 450 K is sufficient for a 1% VAM concentration.

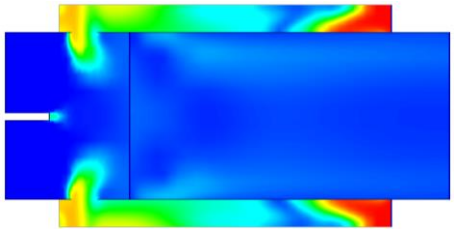

Figure 7.3.10 Top view at 10 s

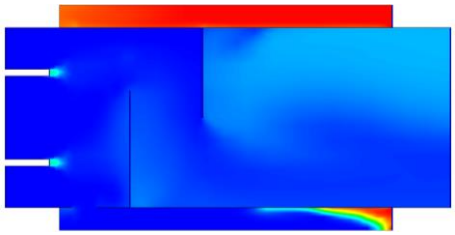

Figure 7.3.11 Side view at 10 s

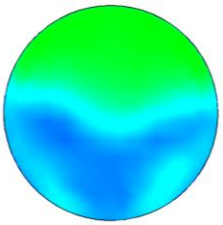

Figure 7.3.12 Outlet at 10 s

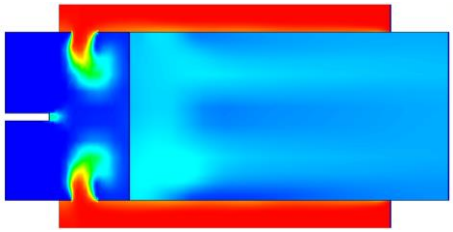

Figure 7.3.13 Top view at 150 s

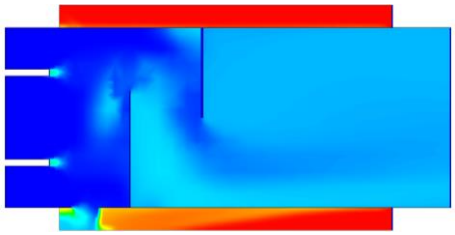

Figure 7.3.14 Side view at 150 s

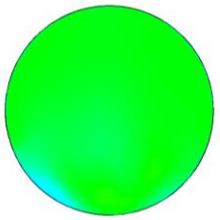

Figure 7.3.15 Outlet at 150 s

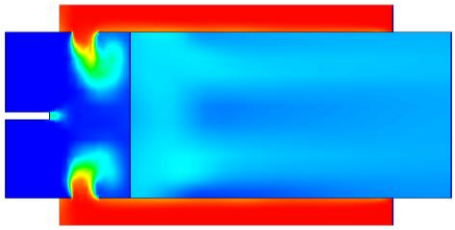

Figure 7.3.16 Top view at 350 s

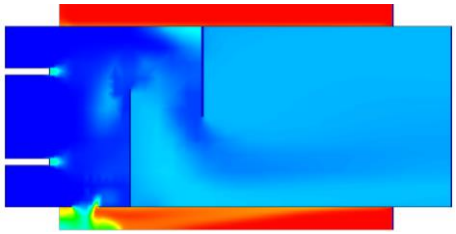

Figure 7.3.17 Side view at 350s

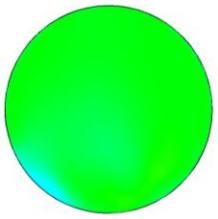

Figure 7.3.18 Outlet at 350 s

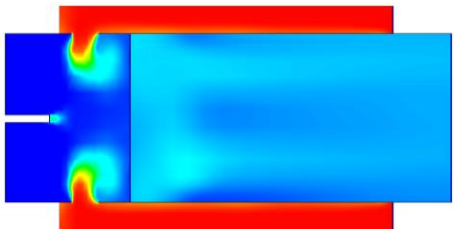

Figure 7.3.19 Top view at 500 s

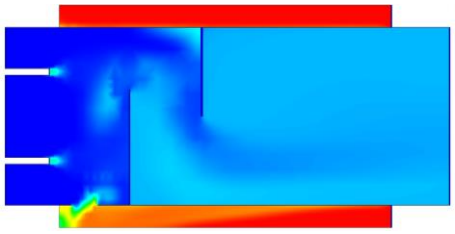

Figure 7.3.20 Side view at 500 s

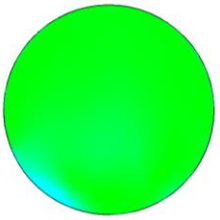

Figure 7.3.21 Outlet at 500 s

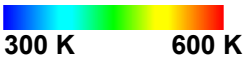

A similar simulation with the same geometry, but the exhaust gas temperature is elevated to 800 K with 3.53 m^3/s per gas turbine for a total exhaust gas flow of 21.2 m^3/s at 50 m/s. This represents a case where more of the flow and energy is directed from the gas turbine exhaust to the VamTurBurner©, rather than to the

independent cogeneration system. The flow rate of the incoming ventilation air and the hot gas inlet flow rates were set to 1.8 m/s and 2.5 m/s respectively.

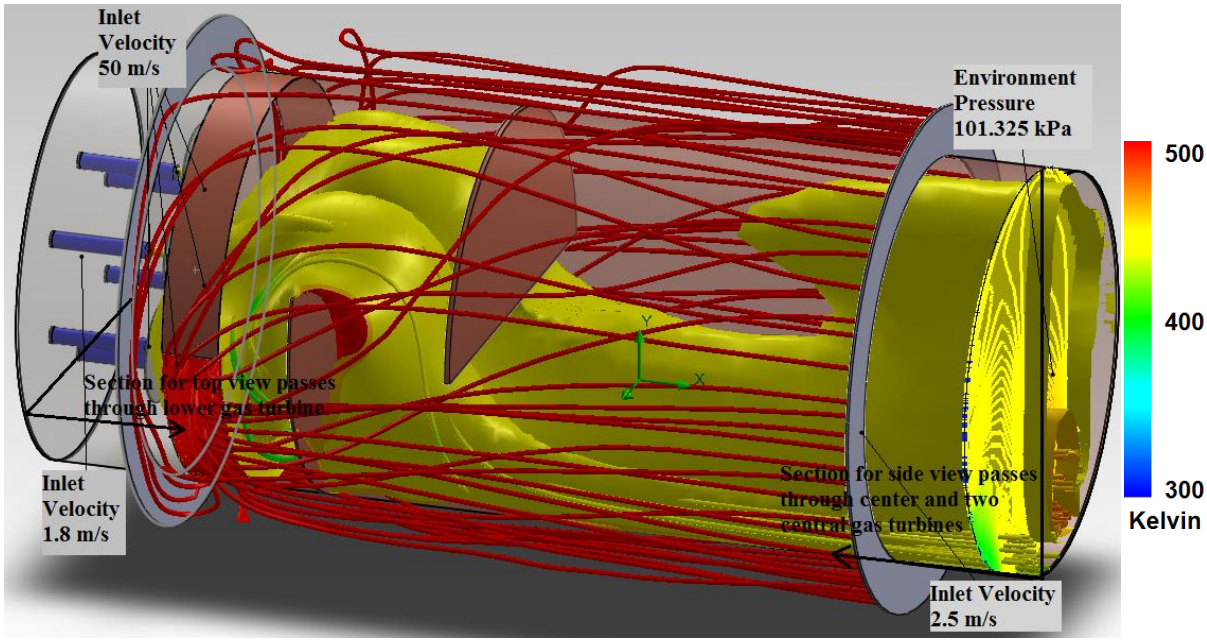

Figure 7.3.22 Model used to obtain the results shown in Figure 7.3.10 to Figure 7.3.21

In Figure 7.3.22, the flow trajectories originate at the inlet of the hot gasses and the isotherms shown are 450 K, 460 K and 500 K (note the scales differ: for Figures 7.3.12, 7.3.15, 7.3.18 and 7.3.21 it is 300 K to 600 K while 7.3.22 is 300 K to 500 K, which accounts for the differing colours representing the temperature). By observation of the diagram, it is clear that the baffles do provide improved mixing of the co-flows and the boundary conditions have resulted a temperature of 460 K at the end of the ventilation duct. The simulation was run to a real time of 120 s and the hi-resolution flow diagrams are shown for 20 s, 50 s, 80 s and 120 s from the initiation of the flow.

The 300 K to 600 K scale in the second series of high-resolution cross sections, Figures 7.3.23 to 7.3.34, is more revealing than the 300 K to 1100 K scale, needed to see the high temperature mixing, used for the side and top views in the previous series high-resolution figures, but the cut plots at the end are both on a 300 K to 600 K scale. Comparison of the cross sectional cut plots between the two series shows a slight temperature increase in the exit gasses. This temperature increase is mainly due to the increased flow of exhaust gas from the gas turbines at a higher temperature and the slight decrease in the ventilation airflow. A simulation

with baffle inserts, using the specifications of a Capstone 200 kW model C200 HZLC gas turbine, see Table 7.3-3, designed for operation in hazardous environments, was performed based on the integrated CHP system exhaust gas output profile. The Capstone systems are low-emission and scalable from 30 kW to 10 MW so the options for a design using different models either in the same system of for different systems using the identical model for all gas turbines are quite plentiful. The systems are capable of operating on: natural gas, propane, landfill gas, digester gas, aviation, diesel or kerosene fuels. This flexibility is desirable for this design as there are certainly many options for the use of various fuels, see Table 7.3-4.

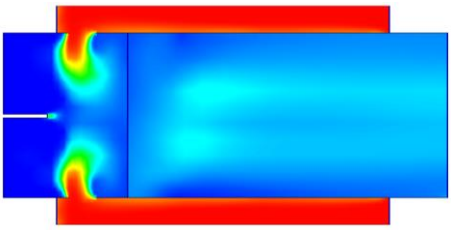

Figure 7.3.23 Top view at 20 s

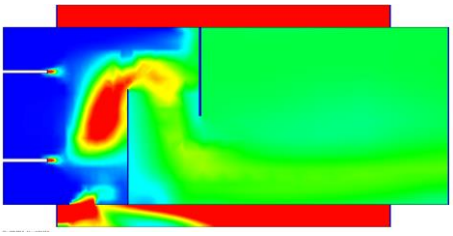

Figure 7.3.24 Side view at 20 s

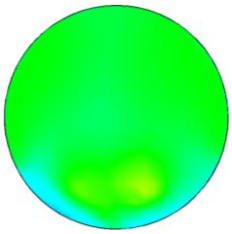

Figure 7.3.25 Outlet at 20 s

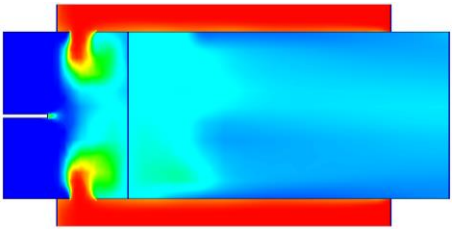

Figure 7.3.26 Top view at 50 s

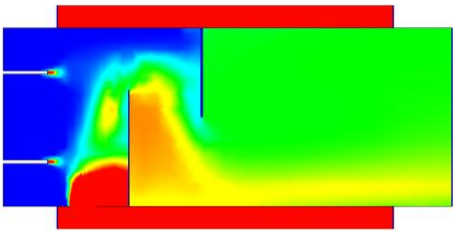

Figure 7.3.27 Side view at 50 s

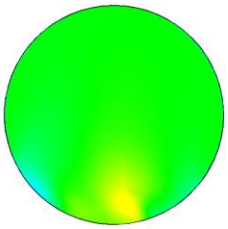

Figure 7.3.28 Outlet 50 s

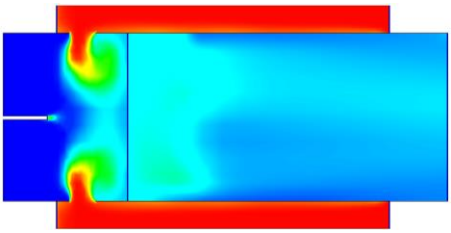

Figure 7.3.29 Top view at 80 s

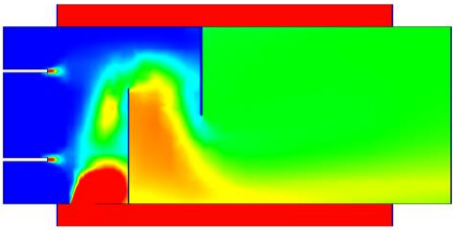

Figure 7.3.30 Side view at 80 s

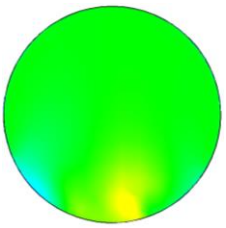

Figure 7.3.31 Outlet at 80 s

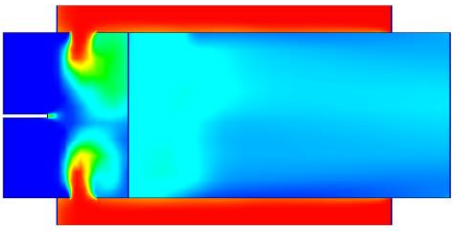

Figure 7.3.32 Top view at 120 s

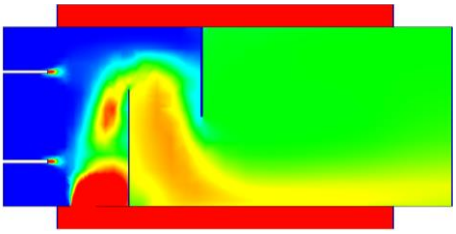

Figure 7.3.33 Side view at 120 s

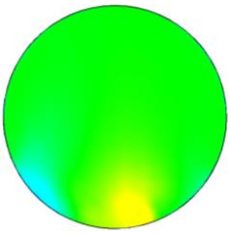

Figure 7.3.34 Outlet 120 s

Table 7.3-3 Capstone microturbine specifications for liquid fuels (Capstone Turbine Corporation).

	Power output	Electrical efficiency	Exhaust gas flow		Exhaust gas temperature		Net heat rate	
LIQUID	kW	%	kg/s	lbm/s	C°	F°	MJ/kWh	btu/kWh
C30 D, A, K	29	25%	0.31	0.69	275	530	14.4	13,700
C65 D, A, K	65	29%	0.49	1.08	309	588	12.4	11,800
C65 ICHP D, A, K	65	29%	0.49	1.08	309	588	12.4	11,800
C200 D	190	30%	1.3	2.9	280	535	10.9	10,300

Table 7.3-4 Capstone microturbine specifications for gas fuels (Capstone Turbine Corporation).

	Power	Electrical	Exhaust gas		Exhaust gas		Net heat rate	
Model and Fuels	kW	%	kg	lbm	C°	F°	MJ	btu
C30 LP NG	28	25%	0.31	0.68	275	530	13.8	13,100
C30 HP NG, P, LG, DG	30	26%	0.31	0.68	275	530	13.8	13,100
C30 HZLC NG	30	26%	0.32	0.7	275	530	13.8	13,100
C65 NG, P	65	29%	0.49	1.08	309	588	12.4	11,800
C65 ICHP NG, P, LG, DG	65	29%	0.49	1.08	309	588	12.4	11,800
C65 CARB NG	65	28%	0.51	1.13	311	592	12.9	12,200
C65 CARB LG, DG	65	29%	0.49	1.08	309	588	12.4	11,800
C65 HZLC NG	65	29%	0.5	1.09	325	617	12.9	12,200
C200 LP NG	190	31%	1.3	2.9	280	535	12	11,000
C200 HP NG, P, LG, DG	200	33%	1.3	2.9	280	535	10.9	10,300
C200 HZLC NG	200	33%	1.3	2.9	280	535	10.9	10,300
C600 LP NG	570	31%	4	8.8	280	535	11.6	11,000
C600 HP NG, P, LG, DG	600	33%	4	8.8	280	535	10.9	10,300
C800 LP NG	760	31%	5.3	11.7	280	535	11.6	11,000
C800 HP NG, P, LG, DG	800	33%	5.3	11.7	280	535	10.9	10,300
C1000 LP NG	950	31%	6.7	14.7	280	535	11.6	11,000
C1000 HP NG, P, LG, DG	1000	33%	6.7	14.7	280	535	10.9	10,300

A design similar in all respects to Figure 7.3.22 with the addition of two more baffles to provide more mixing to the flow of the combustion products and the incoming ventilation air is seen in Figure 7.3.35. The flow trajectories originate at the combustion air inlet, a cut plot taken at the central axis and at the end of the flow duct show the temperature on a scale from 300 K to 500 K. The temperature of the gas turbine exhaust gas is 900 K at a total flow rate of 4.9 m^3/s, which the total flow distributed over the six gas turbines. The flow velocity of the hot air inlet is 3.5 m/s providing a flow of 98.96 m^3/s and the incoming ventilation air is at a velocity of 1.8 m/s, giving a flow of 90.47 m^3/s

The average bulk temperature of the fluid at the end of the ventilation duct is just over 471 K; the final temperatures at 30 s from the initiation of the flow are shown as data labels on Figure 7.3.36, which correspond to the cross sectional cut

plot in Figure 7.3.35. This data is definitive in terms of the viability of the system because the average temperature is near enough to 500 K and not all of the combustion flow has been redirected to the incoming ventilation flow. The target value of 500 K at the VAM concentration of 0.5% is clearly an achievable goal that can be attained by either increasing the amount of mass flow or by using larger or more gas turbines. In addition, the exhaust flow characteristics of the gas turbines used for the modeling were modest because the full amount of the heat available has not been included in the model, due to the possible inclusion of the standalone systems, which operate as independent CHP systems.

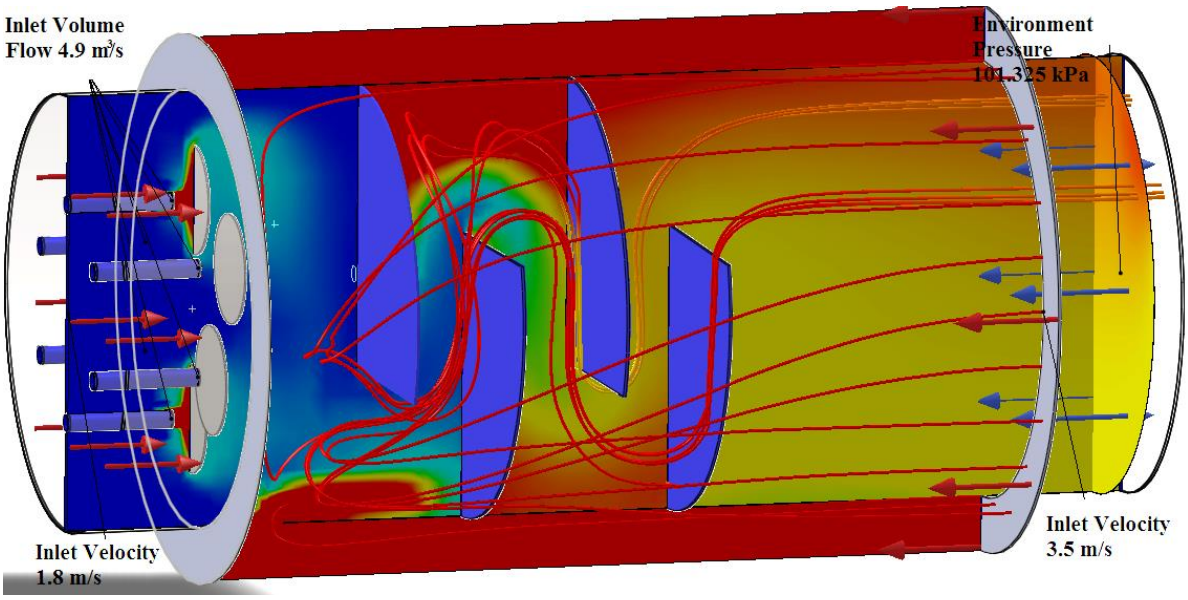

Figure 7.3.35 The same design as Figure 7.3.22 but with the addition of two more baffles. The cross sectional views (side view and outlet cross section) are at the same positions as those in Figures 7.3.10 to 7.3.21

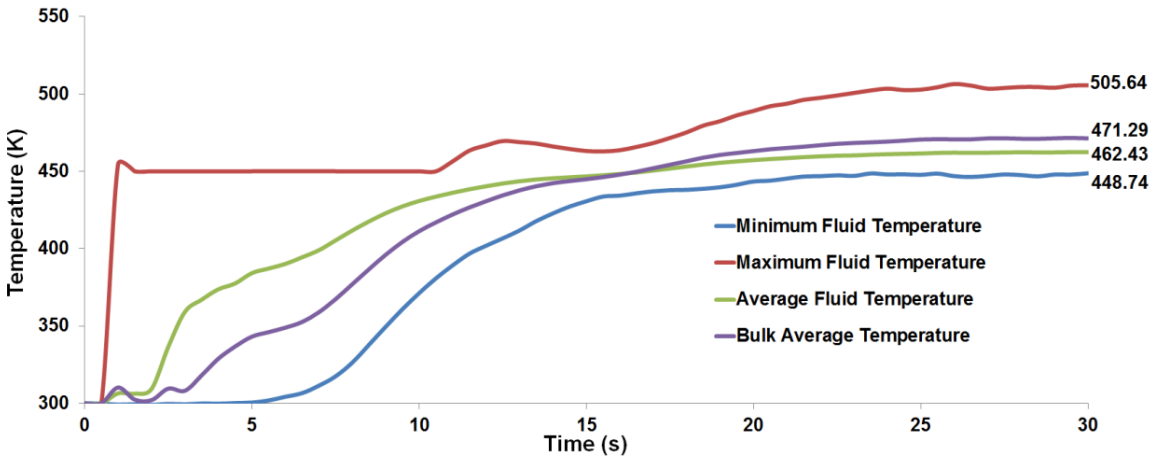

Figure 7.3.36 Temperatures at the end of the ventilation duct, corresponding to the temperatures shown on the cross cut plot at the right hand side of Figure 7.3.35

Although the flows in these modeling scenarios have been based predominantly of volumetric flows or velocities, which define the flow through an area, the density depends temperature of the gas. It is a common practice in psychrometric analysis to change the analysis from a volume flow to a mass flow, when the temperatures changes or under conditions such as auto-compression of the airflow as it reaches depth. However, this modeling has been performed on a volumetric basis, as it is easier to visualize the concept of a number of cubic meters mixing when setting up the boundary conditions. As an example of the effect of switching to a mass flow, using the boundary condition values from the simulation shown in Figure 7.3.35, the mass flow of the incoming 90.47 m^3/s ventilation air at 300 K is 106.45 kg/s and the 98.96 m^3/s of hot air inlet flow at 1100 K is 31.75 kg/s. When airflows are taken as a mass ratio, the m_{hot}/m_{cool} = 0.27, so the amount of hot flow mass is only 27% of the cool flow.

The modeling performed here has been deliberately kept at the lowest values as feasibly possible to reflect the feasibility of the system design at the benchmark value of 0.5 percent VAM at a 100 m^3/s ventilation flow. The mass flow calculation shows that that there is more than sufficient hot air remaining for the addition to the flow should the need arise to increase the temperature of the flow. The modeling is needed to establish feasibility of designs; however, the amount of air needed to provide a mixed air flow of exactly 500 K is performed using the method in Table 7.3-2, which occurs at a m_{hot}/m_{cool} = 0.284. When the entire combustion product airflow is used the final temperature of the mixed air can be as high as 725 K, which may be advantageous for VAM concentrations less than 0.5 percent, but as the VAM concentration decreases the available heat to increase the temperature of the mixed co-flows decreases. The main reason the modeling is targeted to the minimum case of 500 K is to provide the dimensions and flow characteristics for the basic design. If all the hot air is used to mix with the incoming ventilation air then the flow volumes are high, which leads to high flow velocities and potentially larger diameter systems. This is the realm of future work.

7.3.3. Cross flow plate heat exchanger

Further modeling of a heat transfer system that keeps the two flows separate by transferring heat across an array of copper tubing is also included and provides

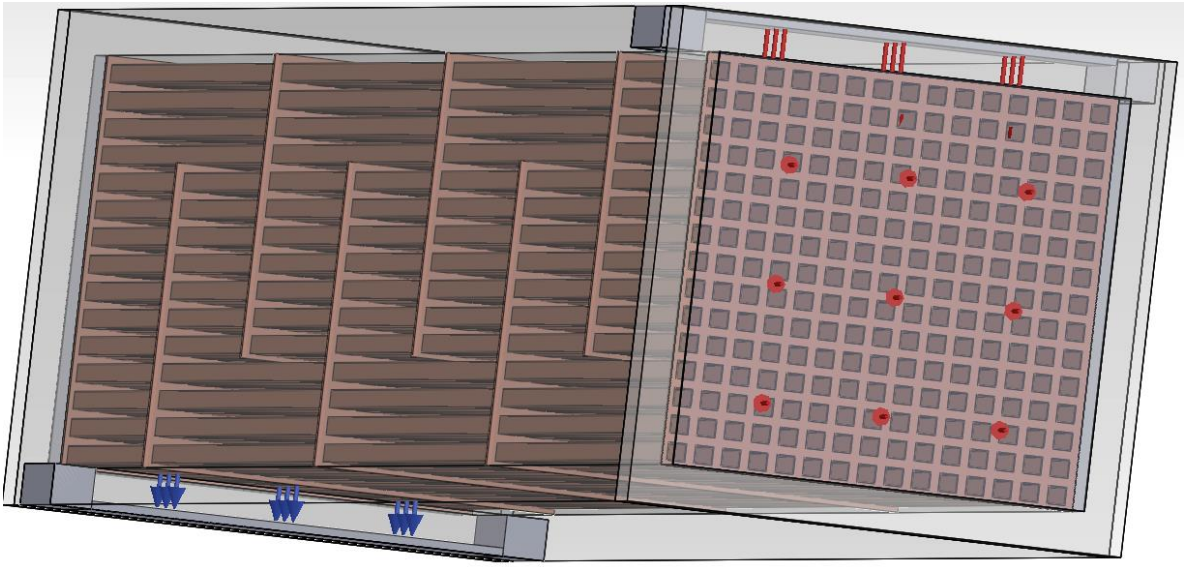

Figure 7.3.37 Model for gas flow heat exchanger comprised of 225 copper tubes with a 0.25 m^2 inlet area (0.5 m x 0.5 m) and 10 m long. The ventilation inlet flow is at front and the hot air inlet is at the top. The ventilation air flows straight through and the hot air is outlet at bottom.

similar results to the mixed flow modeling. Although the results are commensurate with the mixed airflow models the cost of introducing a 10 m long copper tubing system 8 m in diameter may be avoided by choosing the gas mixing option. Nonetheless, it may be advantageous to maintain separate flows, which provided by the heat exchange system. Two models that were the same in all respects except the temperature of the inlet air in the first was 300 K and 325 K in the second. This is to represent the effect of the incoming exhaust gas from the turbines; because these models push computational limits the gas turbines are not included in the model. The model is shown offset to reveal the inlets (red) and outlets (blue). This model is scaled down to save computer resources, it takes over 33 hrs. real time to model 4320 s physical time and at larger sizes, the system is not capable of creating a mesh. There are 225 copper tubes 10 mm long and 20 mm x 20 mm inner length by height with a 1 mm wall thickness. The total inlet area is 0.25 m^2 with an inlet velocity of 2 m/s giving an inlet flow of 0.5 m^3/s for both the incoming ventilation and the hot combustion products. The open flow area of the tubes is 0.09 m^2 resulting in a flow velocity in the tubes of 5.55 m/s. The scaled up version would need 50 m^2 inlet area, so about 7.07 m x 7.07 m square inlet tube with 45000 heat transfer tubes.

The results of the two simulations are shown Figure 7.3.38 and Figure 7.3.39 for the inlet ventilation temperatures of 325 K and 300 K respectively.

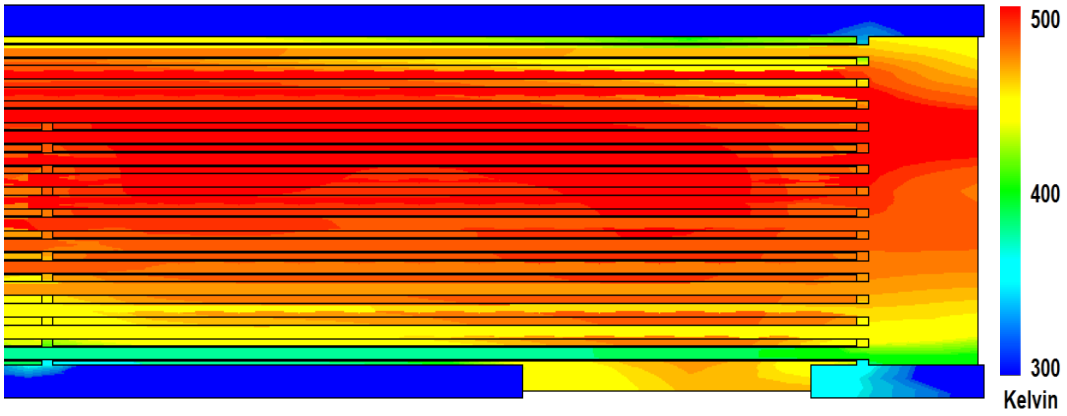

Figure 7.3.38 Cross section of simulation at initial temperature 325 K.

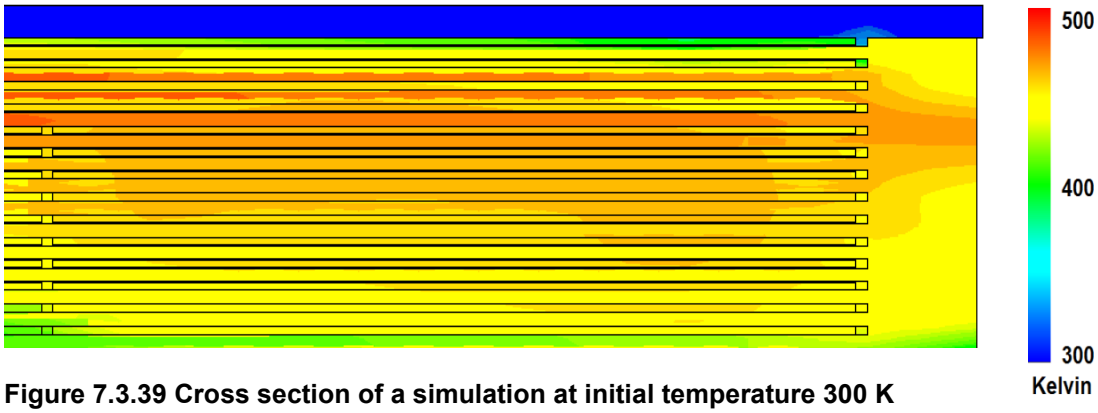

Figure 7.3.39 Cross section of a simulation at initial temperature 300 K

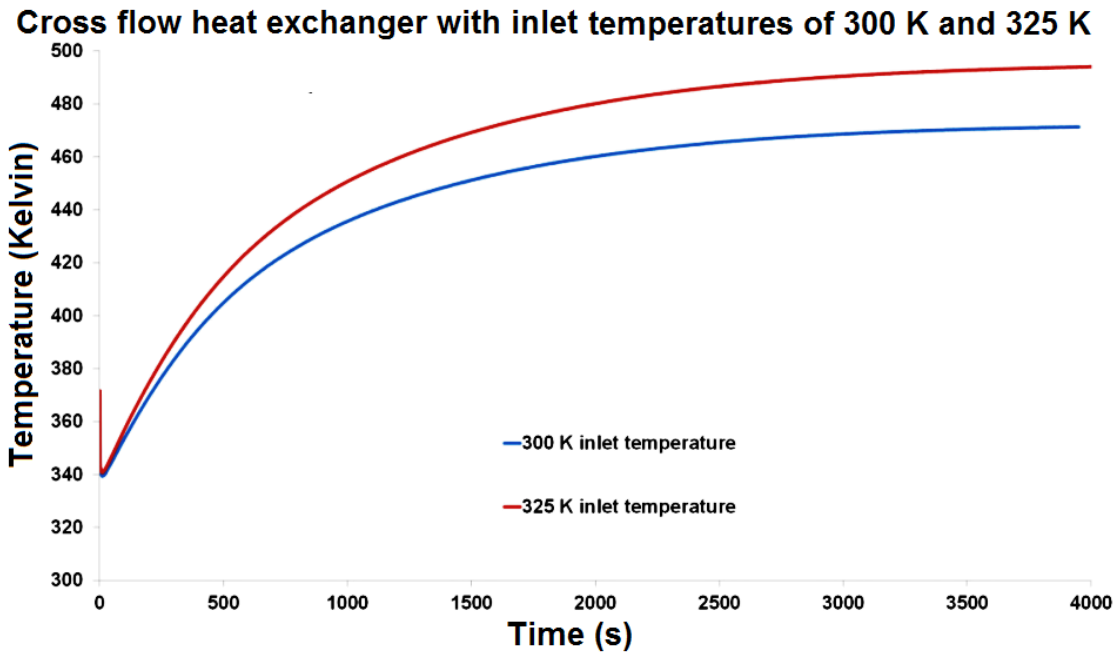

Figure 7.3.40 Temperature profile for the simulated cross flow heat exchanger for initial temperatures of 300 K and 325 K, demonstrates the effect of including the heat from the gas.

In Figure 7.3.40, the average fluid temperature of both simulations shows that after about an hour the average temperature of the mixed flow approaches a steady state. The asymptotic temperatures are 471.3 K and 494.6 K for the 300 K and 325 K inlet temperatures respectively. The difference of 23.25 K between the two simulations appears to be entirely due to the difference in the initial temperature due to the gas turbines hot exhaust mixing with the ventilation air, which validates the simulation and provides sensitivity data.

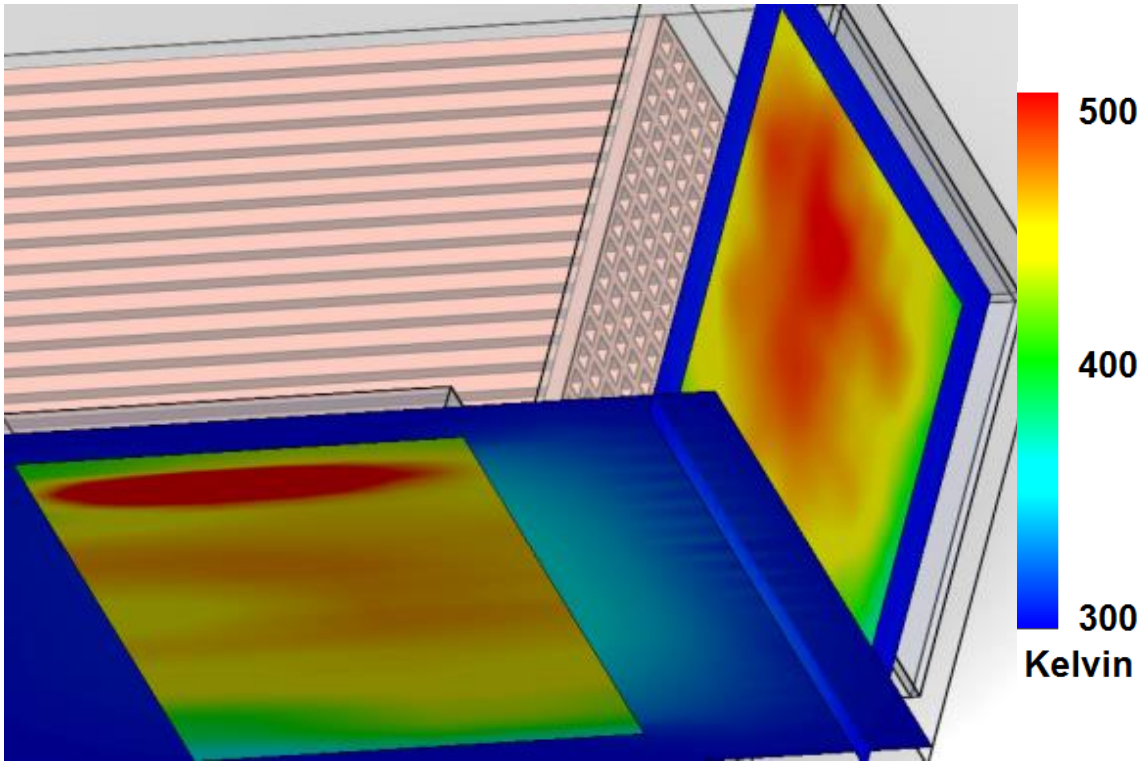

Figure 7.3.41 Visualization of the outlets of the simulation for the initial temperature of 325 K.

Cross section plots crossing the outlet of both the incoming ventilation air and recirculated combustion gasses are shown in The ventilation air flows straight through and appears as the vertical cross section at the right side of the figure and the hot combustion gas, which has taken the tortuous flow through the several baffles in the system appears at the horizontal cross section plot at the bottom of the figure. The similarity of the temperature distribution suggests that the two flows have come close to an equilibrium temperature.

It has been shown through computational fluid dynamics simulations that if the temperature of the temperature of the supply water coming into the system is

288.15 K, there is insufficient energy to produce steam in a flow through system to support the preheating requirements.

Table 7.3-5 Spreadsheet data used to calculate heat exchanger parameters.

Conditions for Shell Side Fluid		**Shell Side Fluid Flow**		
Fluid	Water	Mass Flow Rate	10	kg/s
Mass flow rate kg/s	10		0.01	m^3/s
Inlet temperature (K)	294		36.06	scm/h
Inlet Pressure (Pa)	101325			
Density (kg/m^3)	998.2	Inlet temperature	294	K
Viscosity (kg/m-s)	0.001	Outlet temperature	529	K
Specific heat (J/kg K)	4182	velocity Inlet/Outlet	0.08	m/sec
Conditions for tube side fluid				
Fluid	Dry Air	**Shell Side Fluid Properties**		
Mass flow rate kg/s	50	Fluid	Water	
Inlet temperature (K)	1000	Density	998.2	(kg/m^3)
Inlet Pressure (Pa)	101325	Viscosity	0.001003	(kg/m-s)
Density (kg/m^3)	1.225	Specific heat	4182	(J/kg K)
Viscosity (kg/m-s)	0			
Specific heat (J/kg K)	1006.4	**Tube Side Fluid Flow**		
Heat exchanger construction		Mass flow rate	50	kg/s
Shell side nozzle (mm)	400		141.36	m^3/s
Shell diameter (mm)	4000		146938.78	scm/h
Shell length (mm)	10000	Velocity in tube	126.97	m/s
Shell outer surface (m^2)	151	Reynolds number	427864	
Tube side nozzle (mm)	3800	Inlet temperature	1000	K
Tube inner dia (mm)	180	Outlet temperature	801.44	K
Tube outer dia (mm)	182	Friction factor	0.0181	
Tube length/pass (mm)	6800	Inlet pressure	101325	Pa
Number of passes	8	Pressure drop	17189.84	Pa
Number of tubes	350	Inlet/Outlet velocity	12.46	m/s
Tube outer surface m^2	1361	**Tube Side Fluid Properties**		
Pipe roughness (mm)	0.1	Fluid	Dry Air	
Heat transfer (W/km^2)	15	Density	1.23	(kg/m^3)
Shell Insulation		Viscosity	1.7894E-	(kg/m-s)
Thermal conductivity	0.93	Specific heat	1006.4	(J/kg K)
Thickness (mm)	10	**Heat exchanged between two fluids**		
Heat transfer (W/km^2)	10	Heat exchanged	9991649	J/s
Ambient temperature	294		9.991649	MW
Shell Side Heater		**Thermal Efficiency of Heat Exchanger**		
Heater Power (W)	0	Efficiency	0.333	

In a contained system, operating between 500 K and 600 K the steam flow required is 104.5 kg/s, which is possible but would be expensive compared to the recirculation concept. In a cross flow heat exchange system operating on an air to air heat exchange basis, the system needed is about 10 m long and would cost over

£3 million just to purchase the copper tubing, which is not competitive with the costs of a recirculation system. The most efficient, easily controlled and least expensive mode of operation appears to be a recirculation based system where the hot combustion gas is recirculated back to be combined with the incoming ventilation air. The modeling shows that there is sufficient energy and flow to raise the temperature to 500 K. A design using baffles is capable of mixing the co-flows sufficiently to create a flow of even temperature, consequently capable of being ignited and inclined to sustained combustion.

Table 7.3-6 Study of variations in heat exchanger response and parameters for inlet water at 294 K and inlet air at 1000 K.

Air inlet temperature 1000 K
Water inlet temperature 294 K

Scenario	1	2	3	4	5	6	7	8
Mass Flow Water kg/s	10	10	10	10	15	1	1	1
Mass Flow Air kg/s	50	50	50	50	40	1	1	1
Fluid nozzel diameter (mm)	400	400	400	400	500	50	50	50
Shell diameter (mm)	4000	4000	4000	4000	8000	700	700	1000
Shell length (mm)	10000	10000	22000	22000	22000	4000	6000	8000
Inlet feed tube dia. (mm)	3800	3800	3800	3800	7500	680	680	980
Tube inner diameter (mm)	180	180	180	180	180	40	40	40
Tube outer diameter (mm)	182	182	182	182	182	41	41	41
Tube length (mm)	6800	6800	2000	20000	20000	3800	5800	7800
Number of tubes	350	350	350	350	1200	200	220	450
Water outlet temperature K	529.00	529.00	381.00	721.0	664.7	522.9	569.3	548.5
Air outlet temperature K	801.44	801.44	925.33	632.7	395.0	514.0	410.5	440.5
Pressure drop in air flow Pa	17189.8	41.63	9771.4	122.4	8.92	56.36	72.52	110.4
Heat transferred MW	9.99	9.99	3.76	18.48	24.35	0.49	0.59	0.56
Efficiency	0.33	0.33	0.12	0.61	0.53	0.32	0.39	0.36

8. VamTurBurner© system utilisation

8.1. Energy availability base case

Multigeneration: the generation of several, specifically more than three, energy based outputs simultaneously or having the capacity to adjust outputs to meet the needs of changes in demand; thus, an ability to provide said outputs at different times or seasons although not simultaneously. The root word for generation is the Latin 'generare'/'generatum' (from 'genus', meaning 'a kind') and it means 'to produce' or 'to bring into being'. The root word for multi comes from the Latin “mulus” which means many or much. Although recently there has been a loosening of the convention by mixing Latin prefixes or suffixes with Greek roots, as in the case with the term polygeneration used in some published work, this author prefers to follow the convention of using a Latin prefix to modify a Latin root.

The intention of the VamTurBurner© system design is to use a flow through energy system to provide various outputs as the energy is converted. The first stage is amenable to producing electrical energy through a steam driven turbine. The amount of energy available is variable, but base case analysis for 0.5 to 3% VAM, used as examples of the capabilities of the system under differing conditions, provide the energy range for calculations. At this point, it is instructive to briefly discuss the elevated methane concentration of 3% under consideration because most countries legislate lesser amounts. As noted in Chapter 4, the limits for maximum methane concentration vary according to country, Germany, UK, France, Spain and the USA use 1, 1.25, 2, 2.5 and 3% respectively (Noack, 1998). Although a 3% value may be encountered in the USA, it is not an operational value, but rather a maximum value at which action will be taken to reduce the concentration. In this work, the value of 3% is included for the completeness of theoretical modeling because these values can occur in rare cases. For example a seismic event or in deep mines that would be operating under conditions where the methane per tonne of coal is higher and in the event of encountering and release of a high concentration pocket. Safety systems are expected to be installed to mitigate the higher methane concentrations if encountered, but it is instructive to assess the system response to higher concentrations.

Table 8.1-1 Calculation of the Ideal steam potential for VAM concentrations from 0.5% to 3% at the base case flow rate of 100 m^3/s using a methane density of 0.68 kg/m^3.

	Methane		Steam Metric Tonnes/hr.		
VAM%	kg/s	MJ/s	600 K	700 K	800 K
0.50	0.34	18.87	22.10	20.74	19.53
1.00	0.68	37.74	44.21	41.47	39.05
1.50	1.02	56.61	66.31	62.21	58.58
2.00	1.36	75.48	88.41	82.94	78.11
2.50	1.70	94.35	110.51	103.68	97.64
3.00	2.04	113.22	132.62	124.41	117.16

In Table 8.1-1, the calculations of the ideal energy, mass flow rate and conversion to metric tonnes/hr. were performed for 600 K, 700 K and 800 K steam temperatures at the flow rate of the ventilation air of 100 m^3/s. The availability of steam quoted in tonnes/hr. is an industry standard quantification typically used to characterize the steam generated by a boiler. These idealized calculations, neglecting any losses, give the maximum amount of steam possibly produced at the energies corresponding to the VAM concentration needed to calculate efficiencies. The calculation is based on raising the temperature of water initially at 288.15 K to steam at 600 K, 700 K or 800 K.

The calculations of the temperatures and mass flows are accomplished by either solving for the mass of steam capable of being produced at a target temperature or by solving for the temperature given a mass of steam produced. For a given amount of energy available to produce steam, a loss factor is applied it is assumed that usually about 93% of the energy is captured. The specific heat capacity for water of $C_w = 4.186$ J/g-K, specific heat capacity of steam as $C_s = 2.0$ J/g-K and the latent heat of vaporization of $L_v = 2257$ J/g are the constants used to calculate the energy. The initial temperature is assumed to be T_i =288.15 K, the temperature is raised to boiling T_b, upon absorption of the latent heat of vaporization the temperature rises to T_f.

Eqn. 8.1 $$\boldsymbol{Q_{available} = m_w C_w (T_b - T_i) + m_w L_v + m_w C_s (T_f - T_b)}$$

Table 8.1-2 Sample calculation solving for the mass flow at a target temperature of 600 K and (b) Sample calculation solving for the temperature at a mass flow of 6000 g/s for 18 MW available.

(a) fixed quantities in blue.					(b) fixed quantities in blue.				
18.00	MW	Mass	5459	g/s	18.00	MW	Mass	6000	g/s
0.93		Q_{init}	6.58	MJ	0.93		Q_{init}	7.24	MJ
16.74	MW				16.74	MW			
4.19	J/g K	Q_1	1.94	MJ	4.19	J/g K	Q_1	2.13	MJ
2257.00	J/g	Q_L	12.32	MJ	2257.00	J/g	Q_L	13.54	MJ
2.00	J/g K	Q_3	2.48	MJ	2.00	J/g K	Q_3	1.06	MJ
288.15	K	ΣQ	16.74	MJ	288.15	K	ΣQ	16.74	MJ
373.15	K				373.15	K			
600.00	K				461.75	K			

Table 8.1-3 Sample calculation of the average specific heat capacity and average density of the combustion products for the inlet and outlet temperatures.

Hot Air	Inlet	Outlet	
pressure	101325	101325	Pa
mass	0.028964	0.028964	kg/mole
Rydberg's gas constant	8.31447	8.31447	
Temperature	1100	700.00	K
Volume	382.4942	601.062	Pa/kg mole K
Density ρ	0.320888	0.504253	kg/m^3
Specific heat capacity C	1149.19	1074.64	J/kg K

ρ_{avg} = 0.412571 kg/m^3
C_{avg} = 1111.918 J/g K

Eqn. 8.2 $$Q_{available} = m_a C_a (T_i - T_f)$$

The energy transferred from the hot gas is calculated based on an average density and average specific heat capacity over the temperature range. The calculation is a straightforward application of Eqn. 8.2 using the values in Table 8.1-3 for T_i = 1100 K and solving for the final temperature of the water; the energy absorbed by the water is lost from the air. The actual temperature of the air depends on amount of heat added to the air from the combustion of the VAM, the heat from the igniters and the heat from the gas turbine exhaust as is done in Table 8.2-3.

8.2. Heat exchanger design for the multigeneration aspect

The energy will be transferred from the air to the water through a heat exchanger. As previously mentioned, this is not a treatise on heat exchanger design; however, the basics of the required design must be addressed in order to proceed with sensible calculations for VamTurBurner© electrical and process applications. Although there are off-the-shelf heat exchangers available, in case such as this it would normally be designed specifically for the purpose due to the scale and the unique application.

A defining characteristic of a heat exchanger is the overall heat transfer coefficient (Incropera and DeWitt, 1990). It characterizes the combined effect of a transfer of heat from the hot gas through a metal to water. The thermodynamic characteristics of each fluid and the metal all have an effect on the overall heat transfer coefficient. To establish the overall heat transfer coefficient, consider a straightforward application of the Fourier heat conduction equation (Fourier, 1822). The quantities involved in the calculations in this dissertation are usually performed using the amount available for a one-second time interval. The conversion from J to W is then numerically identical and calculations are simplified.

$$\boldsymbol{C_p \rho \frac{\partial T}{\partial t} = K \frac{\partial^2 T}{\partial x^2}}$$

C_p is the specific heat capacity,

ρ is the density,

T is the temperature,

K is the thermal conductivity and

x the thickness of the material.

For a simple heat flow across an area **A** and thickness **x** and defining the thermal diffusivity as $\boldsymbol{\alpha = K/C_p \rho}$ then:

Eqn. 8.3 $$\boldsymbol{\Delta Q = \frac{\alpha A \Delta T}{\Delta x} \Rightarrow \frac{\Delta T}{\Delta Q} = \frac{\Delta x}{\alpha A}}$$

For copper with $\boldsymbol{K} = 390 \frac{W}{m^2 K}$, $$\boldsymbol{\alpha} = \frac{\left(390 \frac{W}{m^2 K}\right)}{1117.4 \frac{\mathrm{J}}{\mathrm{gK}} 0.399 \frac{\mathrm{kg}}{\mathrm{m}^3}} = 0.873$$

The next variable of interest uses Newton's Law of Cooling to determine the convective heat transfer.

Eqn. 8.4 $$dQ = h_c A\, dT$$

Where h_c is the convective heat transfer coefficient. The overall heat transfer coefficient is defined by the construction of the system, the materials selected, the losses and operational variances. It is often not actually known until a system is in operation and confirmatory measurements are reviewed. The easiest means of relating the conduction and convection equations is to define the quantity of thermal resistance as $\boldsymbol{R} = \frac{\boldsymbol{\Delta T}}{\boldsymbol{Q}}$ K/W, sum the thermal resistances over the system, Eqn. 8.5, and define the overall heat transfer as $\mathbf{Q} = \mathbf{UA\Delta T}$, Eqn. 8.6, where **U** is the overall heat transfer coefficient and A is the area. The contact area can be defined as the average of the inner and outer flow tube areas, $\mathbf{A_i = A_o}$ for very thin tube wall thickness, unless there are fins attached to one or both sides of the flow tubes. In these calculations case, the wall thickness is negligible, but the average area is used.

Eqn. 8.5 $$R_a = \frac{1}{h_a A_a};\ R_w = \frac{1}{h_w A_w};\ R_x = \frac{\Delta x}{\alpha A_x};\ R_T = \frac{1}{UA_T}, and\ R_T = R_a + R_w + R_x$$

Eqn. 8.6 $$\frac{1}{UA} = \frac{1}{h_a A_a} + \frac{1}{h_w A_w} + \frac{\Delta x}{\alpha A_x}$$

The contact areas in Eqn. 8.6 are the inner tube area and outer tube area for the water and air respectively and the area used for the overall heat transfer coefficient is an average of the two. These values are determining characteristics of the heat exchanger design and a sample calculation is shown below.

Table 8.2-1 Sample calculation of the inner and outer tube areas in the heat exchanger, a key variable in the calculation of the overall heat transfer coefficient.

A = 1461 m^2	Outer (air)	Inner (water)	
Diameter	32	30	mm
Area flow	0.000804	0.000707	m^2
Circumference	0.100531	0.094248	m
Length	5	5	m
Number of tubes	3000	3000	
Area contact	1508	1414	m^2

The convective heat transfer coefficient is affected by the flow rate of the fluid. In heat exchangers the ranges for air and water are quoted in several sources and for several ranges, the values of overall heat transfer coefficient are also quoted in a similar manner. The variance in these values is due to the wide variety of materials, system designs, fluids and flow rates used to build and operate heat exchangers. The range of convective heat transfer coefficients used for these calculations for Water are 500 to 10,000 W/m^2-K and Air 10 to 100 W/m^2-K, taken from the Engineering Tool Box. Using these as the range of values for the convective heat transfer coefficients and the dimensions calculated in Table 8.2-1 the overall heat transfer coefficient can be calculated for the maximum and minimum values expected. Comparing the values in Table 8.2-1 to the reported overall heat transfer coefficient range from the literature for air to water 15 to 70 W/m^2-K, water-to-water 800 to 1500 W/m^2-K and air-to-air 5 to 35 W/m^2-K, the actual overall heat transfer coefficient would be expected to lie somewhere in between the maximum and minimum. The minimum values are associated with difficulties such as fouling or improper material selections and the higher values arise when geometrical variations such as fins are added to increase the heat transfer area. Some intermediate values were also calculated for these particular dimensions appearing in lines 5, 6 and 7 of Table 8.2-2. The values obtained are consistent with basic heat exchanger theory and practise (Schlünder, 1993).

Table 8.2-2 Calculation of the overall heat transfer coefficient for the tube dimensions from Table 8.2-1 using Eqn. 8.6.

	K_{copper} =	390	W/mK
	dx =	0.001	m
	hw (W/m^2-K)	ha (W/m^2-K)	U (W/m^2-K)
1	500	10	10.11
2	10000	10	10.31
3	500	100	85.06
4	10000	100	102.1
5	1000	20	20.21
6	1500	35	35.24
7	800	25	24.97

An overall heat transfer coefficient of 20 W/m^2-K to 50 W/m^2-K is consistent with the data in Table 8.2-2 and that from the literature so a midrange value of 35 W/m^2-K will be assumed for the purpose of the design.

The characterization of a heat exchanger by the Log Mean Temperature Difference (LMTD) is a standard method of heat exchanger design (Lienhard IV and Lienhard V, 2000). When the overall heat transfer coefficient and absorbed energy are known, the contact area of the flow tubes can be determined from Eqn. 8.6. The LMTD is defined by the temperature differences between the hot and cold inlets and outlets and the LMTD formula is derived in (Lienhard IV and Lienhard V, 2000).

Eqn. 8.7 $$LMTD = \frac{[(T_{hi}-T_{ci})-(T_{ho}-T_{co})]}{ln\left[\frac{(T_{hi}-T_{ci})}{(T_{ho}-T_{co})}\right]}$$

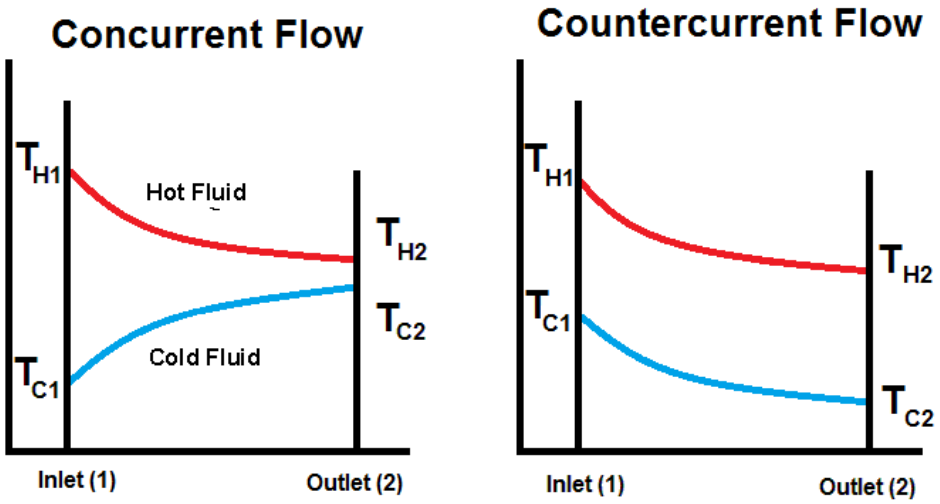

Figure 8.2.1 A description of the temperature profiles for concurrent and cross-flow heat exchangers showing the temperatures used for the calculation of LMTD.

The LMTD is calculated for the benchmark flow of 100 m^3/s and cold the outlet temperature T_{co} = 616.7 K, remains fixed for calculations over the range of energy availability, this establishes an operational range for the LMTD.

The method of calculation used to obtain the LMTD for two average values of 271.33 K and 319.61 K follows: (i) fix a cold outlet temperature (ii) solve for the mass flow of water entering at T_{ci} = 288.15 K (iii) define the energy absorbed and follow Eqn. 8.1 and the method outlined in Table 8.1-1. The energy absorbed ranged from 18.87 MW$_{th}$ to 113.22 MW$_{th}$ with a 93% absorption efficiency. The energy gained by

the water is contributed by the air; so the final temperature of the airflow following Eqn. 8.2 and Table 8.1-3 is determined by that energy loss. The specific heat capacity in Eqn. 8.8 is determined from the trend line function of Excel, based on Janaf table data. The average density is determined from the high temperature and low temperature values of the inlet gas by the ideal gas law following Table 8.1-3.

Eqn. 8.8 $$C_p = -6.3\times10^{-19}T^6 + 3.1303\times10^{-15}T^5 - 5.93370826\times10^{-12}T^4 + 5.13732196424\times10^{-9}T^3 - 1.84342602921706\times10^{-6}T^2 + 2.89242721080375\times10^{-4}T + 0.986042608746025$$

The initial energy state of the air is based on an air temperature of 325 K, which is one of the temperatures previously modeled for the combined flow of the gas turbine exhaust and incoming ventilation air at 300 K. The energy added to the ventilation airflow, as outlined in Table 8.1-1, accounts for both the VAM and igniters.

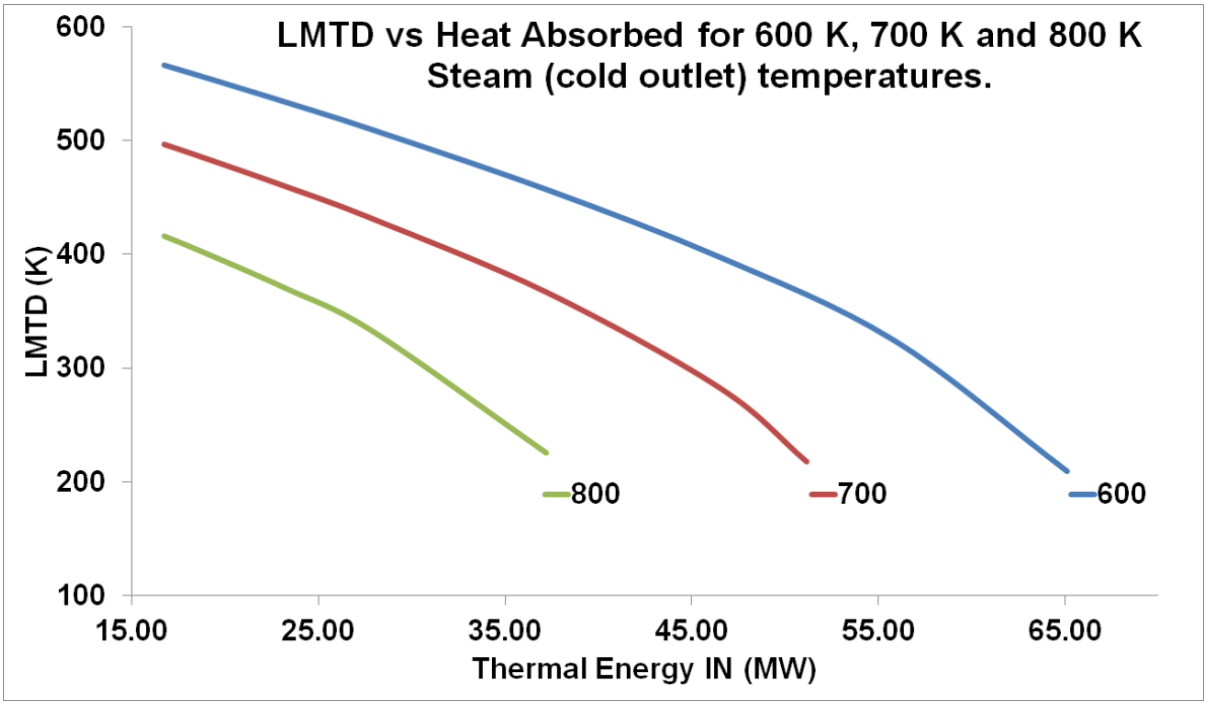

Figure 8.2.2 LMTD as a function of the heat absorbed.

The igniter flow is set to 1 kg/s, at a calorific value of 55 MJ/kg, for the 0.5% VAM case and is reduced by 0.1 kg/s for each 0.5% increment of the VAM up to 3%. The hot air inlet gas temperature is a key variable because as the temperature of the air increases not only is there more heat, but the heat transfer efficiency increases.

Table 8.2-3 Calculation of the inlet temperature of the hot gas entering the heat exchanger T_{H1} in Figure 8.2.1

Initial Energy MJ	VAM Energy MJ	Igniter Fuel Rate kg/s	Igniter Energy MJ	Total Energy MJ	Inlet Gas Temperature K
38.45	18.87	1.0	55.0	112.32	859.7875
38.45	38.87	0.9	49.5	126.82	955.4745
38.45	58.87	0.8	44.0	141.32	1051.321
38.45	78.87	0.7	38.5	155.82	1147.658
38.45	98.87	0.6	33.0	170.32	1244.587
38.45	113.22	0.5	27.5	179.17	1304.354

Table 8.2-4 Calculations leading to the LMTD for two cases (1) $LMTD_{avg}$ = 271.33 K and (2) $LMTD_{avg}$ = 319.62 K T_{ci} = 616.7 K.

		$LMTD_{avg}$ 271.33 K ± 2.47				$LMTD_{avg}$ 319.62 K ± 1.96			
Heat VAM MJ	T_{hi} K	Heat Trans. MJ	T_{ho} K	Mass Flow kg/s	Area m^2	Heat Trans. MJ	T_{ho} K	Mass Flow kg/s	Area m^2
18.87	859.788	16.74	722.0	5.40	1735.3	11.16	767.9	3.60	1009
38.87	955.475	32.55	691.8	10.50	3431.1	26.97	737.0	8.70	2414
58.87	1051.321	47.43	671.9	15.30	5028.1	42.59	710.6	13.74	3811
78.87	1147.658	61.85	657.9	19.95	6562.8	57.66	691.0	18.60	5137
98.87	1244.587	75.79	649.1	24.45	7939.1	72.54	674.6	23.40	6470
113.22	1304.354	84.54	642.6	27.27	8952.2	81.38	667.4	26.20	7223

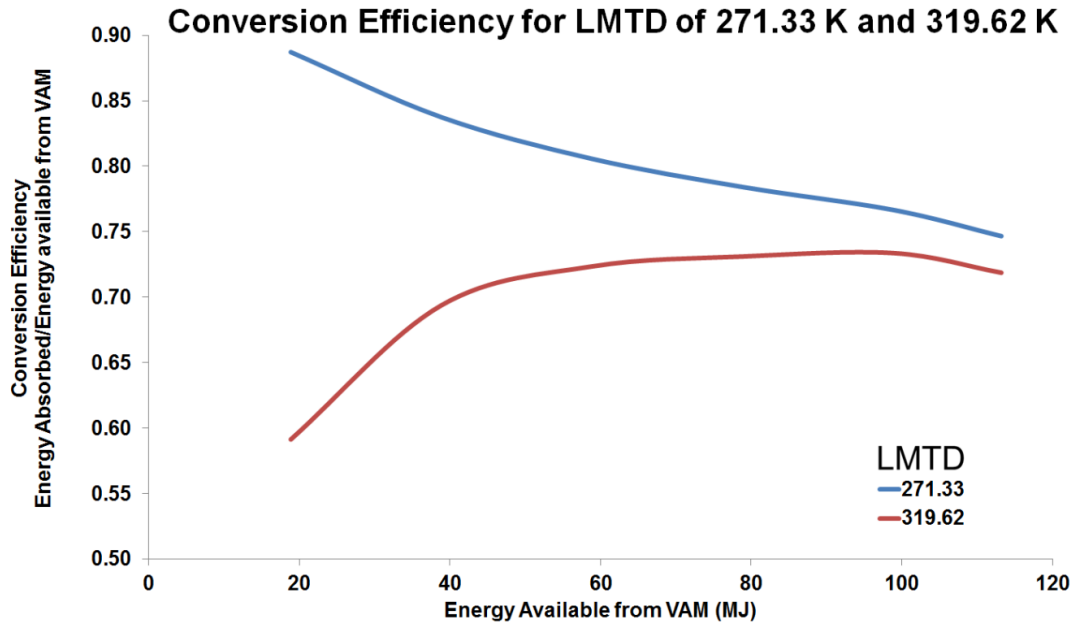

Figure 8.2.3 Efficiency = (the energy absorbed)/(energy available from VAM).

At this point decisions must be made with regard to the dimensions and operating conditions of a heat exchanger for the purpose of converting energy from the air to the steam. Calculations have shown that an overall heat transfer coefficient of 35 W/m^2-K and the LMTD = 300 K are acceptable values for the heat exchanger design. In Figure 8.2.3, the LMTD of 271.33 overestimates the heat transfer at lower energies while the LMTD of 319.62 underestimates for the same range; thus, an LMTD of 300 is justifiable. The efficiency converges to about 75% at the VAM energy of about 50 MJ and the amount of energy transferred is directly related to the LMTD calculation. By keeping the T_{co} constant at 616.7 K and with the inlet temperature T_{ci} = 288.15 K the solution is iterated by adjusting the mass flow until the desired LMTD is obtained for the range of temperatures of the hot inlet gas T_{hi} from 859.8 K to 1304.4 K. In all calculations the $T_{ho} > T_{co}$ or the LMTD becomes undefined. The values in Table 8.2-4 were found by keeping the LMTD as close to constant given the iterative approach for each block of calculations and the standard deviations are included to show the small variance in the LMTD over the range of heat available. These values are required to permit the calculation of the contact area needed to produce the desired energy transfer. The areas in Table 8.2-4 were calculated from the relation below in Eqn. 8.9.

Eqn. 8.9 $$A = \frac{Q}{U(LMTD)}$$

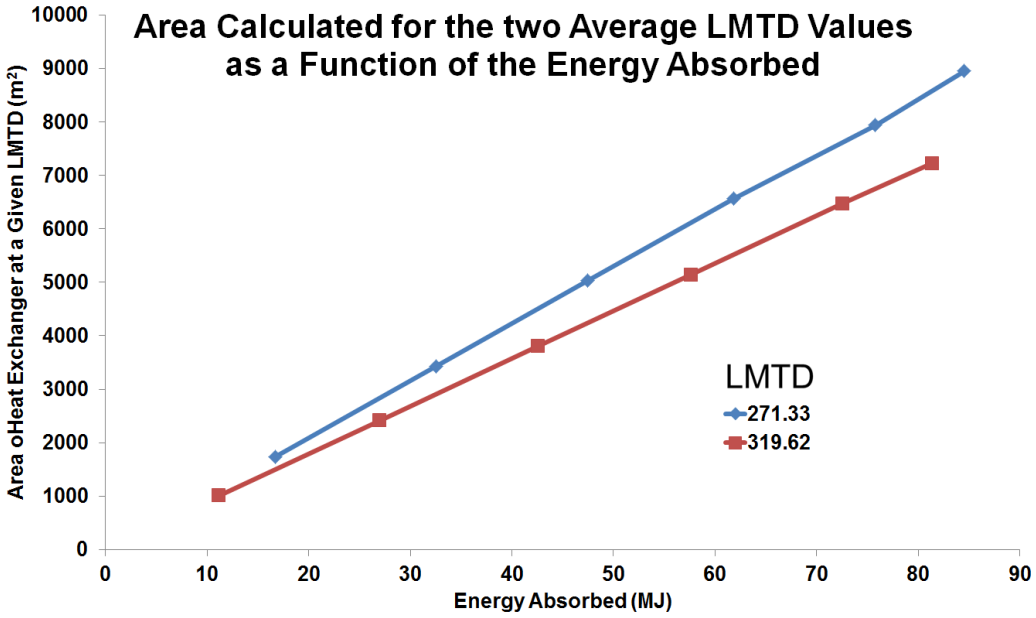

Figure 8.2.4 Heat exchanger area for two LMTD values.

From the data in Table 8.2-4, Figure 8.2.3 and Eqn. 9, heat exchanger designs with areas of 2000 m^2 and 5000 m^2 would be acceptable to cover the lower and upper energy ranges. At the lower range, 0.5% to 1% VAM a 2000 m^2 area is almost ideal and 4000 m^2 is obtained by two units operating in parallel for a concentration of 1.5% VAM. The 5000 m^2 area would be used for the 2% VAM and may be sufficient to capture the energy at the 2.5% VAM concentration with some loss of energy, but a 2000 m^2 and 5000 m^2 in parallel is recommended for the 2.5% and two 5000 m^2 for the 3% VAM. The 2000 m^2 and 5000 m^2 option is a direction that may be taken especially for situations where a single heat exchanger will be used. Given the area of 2000 m^2 and 5000 m^2, an LMTD of 300 K and an overall heat transfer coefficient of 35 W/ m^2 K the typical heat capture for a heat exchanger design is calculated using Eqn. 8.9.

An alternative is to consider a single 1500 m^2 unit that can be applied incrementally to cover the energy range available. The 1500 m^2 option almost perfectly matches the data progression of energy increments in Table 8.2-4; however, it is merely a data illusion that would not be the operationally expected result as the VAM concentration can easily vary between upper and lower limits. The control of the inlet water flow, to provide the target temperature of the steam, becomes a determining factor to compensate for the variations in energy availability. This is a situation that can be forced, but is not calculated here. For example, a single 5000 m^2 could be used to cover the entire range, these are engineering decisions that the proponents decide based on other financial variables as well.

Table 8.2-5 Configurations of various heat exchangers given the calculated contact areas.

U = 35 W/m^2-K
LMTD = 300 K

Option 1	Energy	Parallel	Ref. #	Option 2	Energy	Parallel	Ref. #
2 k	21.0	2k	1	1.5 k	15.8	1	1
4 k	42.0	2x2k	2	3.0 k	31.5	2	2
5 k	52.5	5k	3	4.5 k	47.3	3	3
6 k	63.0	3x2k	4	6.0 k	63.0	4	4
7 k	73.5	5k+2k	5	7.5 k	78.8	5	5
8 k	84.0	4x2 k	6	9.0 k	94.5	6	6
9 k	94.5	5 k+2x2k	7				

At the lower energy availability, the mass flow of the water can be reduced using control system to monitor the outlet temperatures. For the higher energy availability the water flow would be forced to higher Reynolds numbers and may be at a higher temperature than the target temperature of T_{co} = 616.7 K, which may actually be a requirement of an alternative design. In short, there is no exact solution due to the nature of the engineering involved.

As the amount of energy available from the VAM increases the amount of energy required from the igniters may be reduced. The temperatures of the inlet gas T_{hi} is also dependant on the amount of energy input to the flow. This becomes a key variable in the costing of the system because the VAM is considered as a free source of thermal energy. In Figure 8.2.5 a plot of the energy contribution from the VAM versus the VAM concentration is provided as an aid in the determination of breakeven points for design calculations.

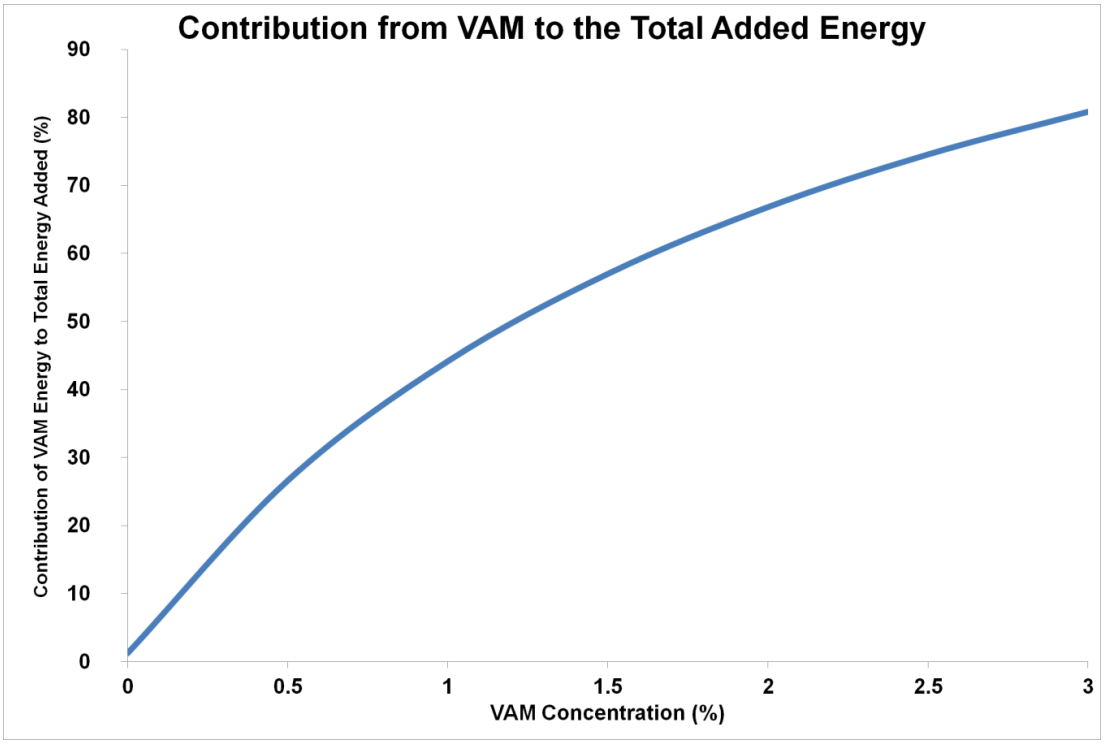

Figure 8.2.5 The energy contribution to the system as a function of the VAM concentration. Based on Table 8.2-3.

A spreadsheet was developed to design a heat exchanger incorporating all the variables discussed above, including packing efficiency controls for the dimensions of the tubes within the shell diameter and a labeled diagram is generated for the dimensions supplied. A sample diagram from the spreadsheet appears below in

Figure 8.2.7 and Figure 8.2.8. The dimensions are intended to reflect that at the 1500 m^2 contact area the flows are at the lowest energy rating resulting in with a water flow of 5.7 kg/s. The second heat exchanger design corresponds to the 5000 m^2 contact area and the energy input of 58.87 MJ from the VAM, a midrange value in Table 8.2-4.

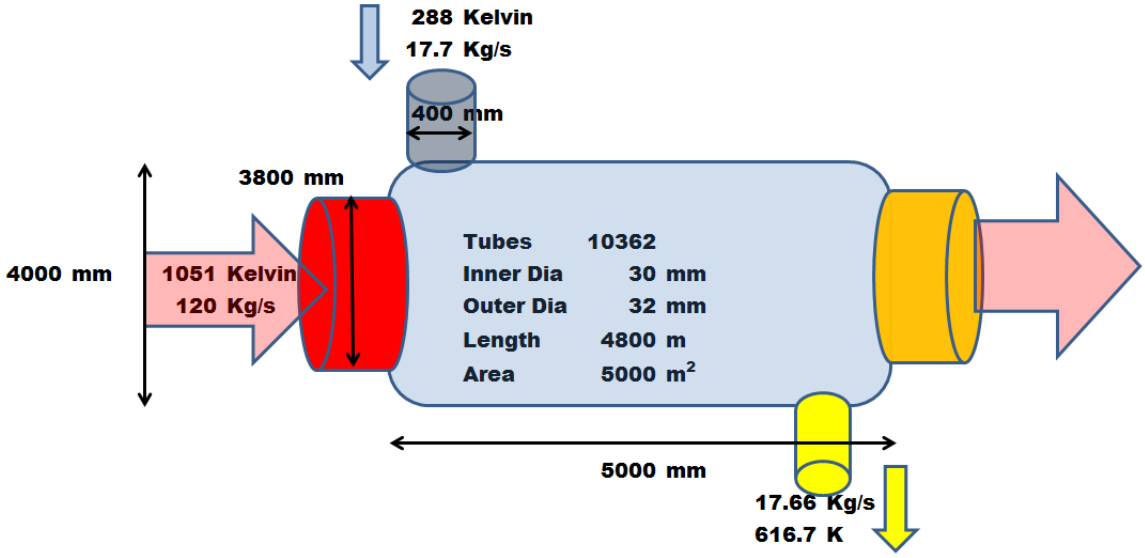

Figure 8.2.6 Heat exchanger design for a contact area of 5000 m^2 output design generated by the spreadsheet

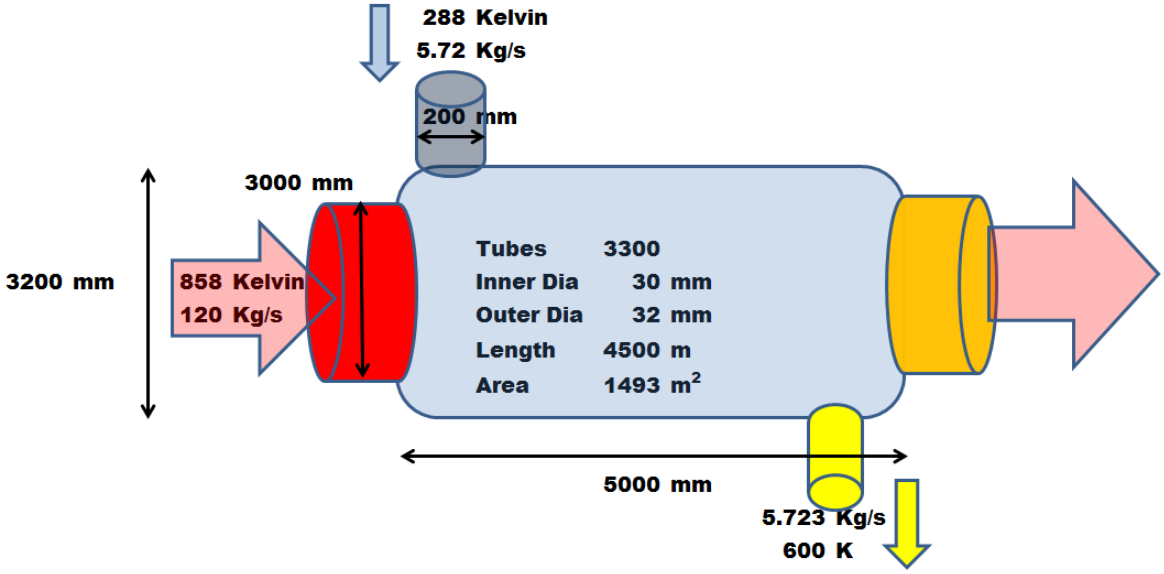

Figure 8.2.7 Heat exchanger design for a contact area of 1500 m^2 output design generated by the spreadsheet.

TUBE		Density	Viscosit	Specific heat c	density	viscosity	Specific
Fluid	Water	selection		100	958.4	2.7E-04	4082.2
Mass flow rate	17.662	Kg/s		90	964.5	3.1E-04	4074.7
Inlet temperature	15	Celsius	288.2 Kelvin	80	971.8	3.5E-04	4069.6
Inlet pressure	101325	Pascals		70	977.4	3.9E-04	4066.8
Density	999.1	Kg/m^3		60	983.2	4.5E-04	4065.8
Volume flow	0.0177	m^3/s					
Velocity at inlet	0.1407						
Viscosity	0.0011	Kg/(m-s)		50	987.7	5.3E-04	4066.0
Specific heat capacity	4081.8	J/(Kg-K)		40	992.2	6.4E-04	4067.3
SHELL				35	993.6	7.0E-04	4068.5
Fluid	Dry Air	Selection		30	995.7	7.8E-04	4070.2
Mass flow rate	120	Kg/s		25	997.0	8.7E-04	4072.7
Inlet temperature	777.85	Celsius	1051 Kelvin	22	997.8	9.3E-04	4074.8
Inlet pressure	101325	Pascals	Custom density	20	998.2	9.8E-04	4076.4
Density (standard)	1.225	Kg/m^3	0.336 Kg/m^3	15	999.1	1.1E-03	4081.9
Volume flow	357.3						
Velocity at inlet	48.784						
Viscosity	0	Kg/(m-s)		10	999.7	1.3E-03	4089.7
Specific heat capacity	1.143	J/(Kg-K)		4	1000	1.5E-03	4103.6
Physical Attributes				0	999.8		
Fluid nozzle diameter (SHELL	400	mm	0.4 m				
Nozzle area	0.1257	m^2					
Shell diameter	4000	mm	4 m				
Shell length	5000	mm	5 m				
Shell surface area (outer)	87.965	m^2					
Tube inlet diameter	3800	mm	3.8 m	Fraction of shell di	0.95		
Tube inner diameter	30	mm	0.03 m	Inner diameter/ou	0.9375		
Tube outer diameter	32	mm	0.032 m	Wall thickness par	Tube wall thickne		
Tube total area for flow	7.3242			Tube area/inlet ar	0.6458		
Tube length (per pass throug	4800	mm	4.8 m	Fraction of tube le	0.96		
Number of returns	1	dimensionless		Packing efficiency	Tube area is acce		
Number of tubes	10362	dimensionless		Tube area is less than ideal packing			
Tubes total surface area (out	5000	m^2					
Tube roughness coeficient	0.1	mm		Inner tubes calculations		Shell	
Shell outer Insulation				0.03	Tube inner diameter		
Thermal Conductivity	0.93	W/(m-K)		0.03	Tube outer diameter		
Thickness	20	mm	0.02 m	1	Number of returns		
Surface heat transfer coefici	37.318	$W/(m^2-K)$		10361.6	Number of tubes		
Ambient external temperatu	288	Kelvin	6.25%	Use 1% or greater as a good first approximation of th			

Figure 8.2.8 Sample section of the heat exchanger design spreadsheet inputs are yellow and outputs are blue.

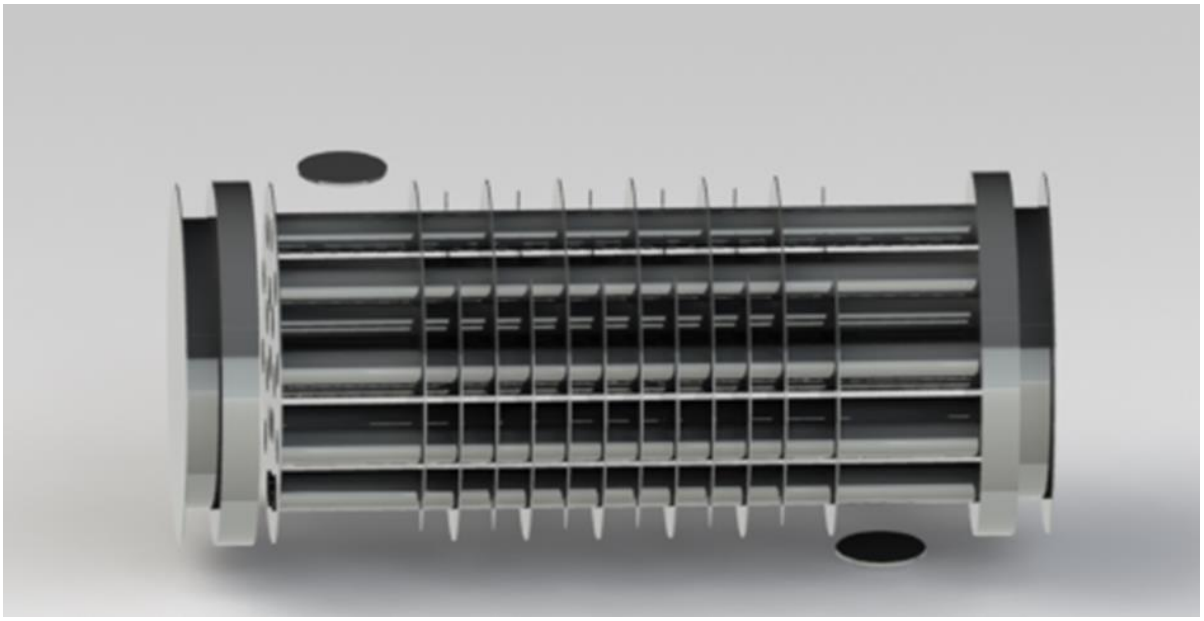

Figure 8.2.9 Heat exchanger 1 designed with Solidworks© 20 m long internally, 10 m diameter, baffle separation 1 m with 4 m entry and exit ports.

These two designs were used in a Solidworks CFD simulation the dimensions and boundary conditions pushed the limits of the computing capacity causing computer systems failures. Modeling of final designs like these is usually performed after calculations such as those shown here; however, calculations alone are often sufficient.

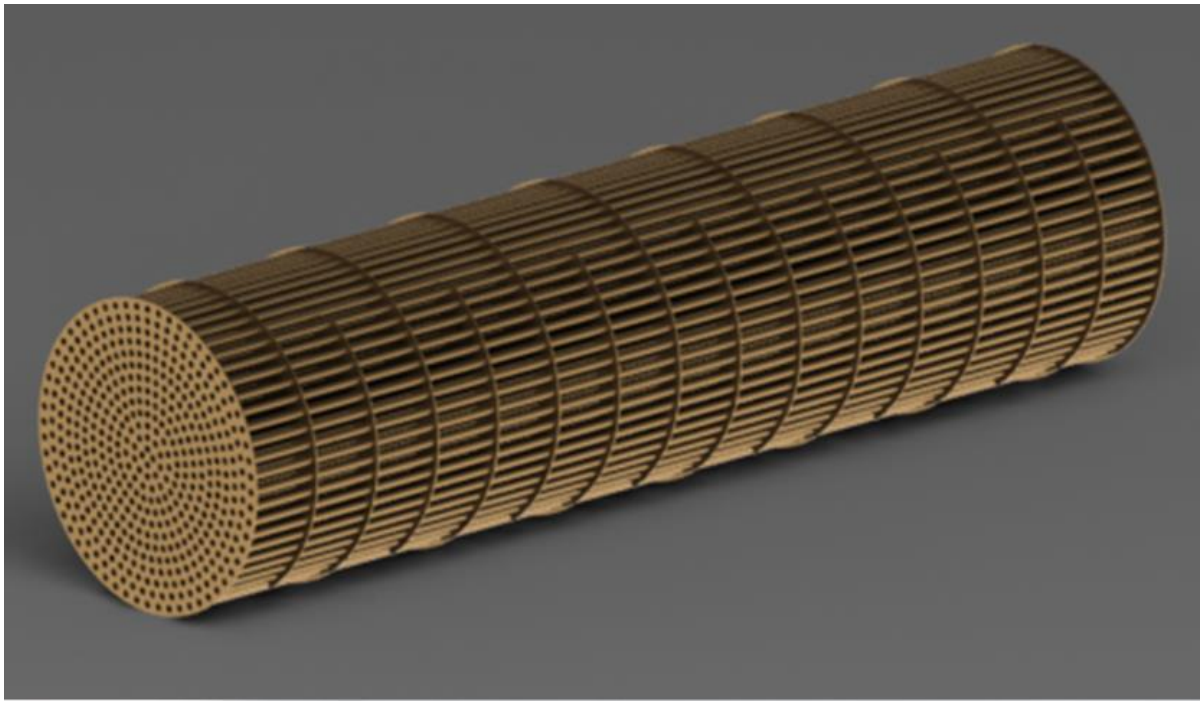

Figure 8.2.10 Heat exchanger 2 designed with Solidworks©. Revisions of smaller internal tube diameters 30 m long, baffle separation 2 m, 8 m diameter.

8.3. Driving a steam turbine with the energy from the VAM

Steam turbine calculations, required to establish the electrical power output in MW_e follow the sample calculation below.

1) The specific enthalpy for the inlet pressure and temperature is obtained from standard steam tables or available steam calculator programs. The product of specific enthalpy and mass flow determines the inlet energy flow available to produce the steam, for this sample analysis the pressure and temperature are:
    a. Pressure = 5.00 bar (g)
    b. Temperature = 616.74 K
2) Obtain either the specific enthalpy for the inlet parameters from the standard steam tables or by calculation; a sample calculation follows the outline below.
    a. The reference point for the energy transfer is 273.15 K. The energy to raise the temperature from 273.15 K to the boiling point at the pressure of the inlet of 431.99 K is 664.90 kJ/kg.
    b. The latent heat of vaporization is 2085 kJ/kg.
    c. The energy to raise the steam to 616.74 K, using a specific heat capacity of 2.19 kJ/kg-K, is 403.69 kJ/kg.
3) The sum of the three is the Specific Enthalpy of 3153 kJ/kg.
4) Inlet Energy Flow = 3153 kJ/kg x 5.40 kg/s = 17.029 MW
5) The ideal outlet properties, found by assuming an isentropic process, require that the inlet entropy equal the outlet entropy. A decrease in the specific entropy occurs because the outlet pressure is less than the inlet pressure; thus, the volume is greater. An assumed isentropic efficiency of 70% is used for these calculations. The ideal outlet specific enthalpy is determined by using the outlet properties, inlet specific enthalpy and isentropic efficiency.
6) Given the inlet specific entropy of 7.527 kJ/kg-K at 5 Bar(g), the ideal enthalpy is 2,881kJ/kg for the outlet pressure of 1 Bar(g).
7) The outlet Specific Enthalpy is 3153 kJ/kg -0.7(3153 -2881.1) kJ/kg = 2963 kJ/kg
8) The same method as step 2 is followed to find the outlet temperature, but the latent heat of vaporization is 2257 kJ/kg and the specific heat capacity of the steam is 2.02 kJ/kg-K, resulting in an outlet temperature of 515.8 K.

9) The energy output is determined by the difference between the inlet specific enthalpy and the outlet specific enthalpy, 3153 kJ.kg – 2963 kJ/kg = 189 kJ/kg and the mass flow remains constant so 190 kJ/kg x 5.5 kg/s = 1.026 MW
10) For a typical conversion efficiency of 95% the electrical output is 0.9747 MW_e.

Therefore, the input of 5.4 kg/s of steam at 616.74 K will provide 0.9747 MW_e. The following table gives the potential output electrical output for the mass flows in Table 8.2-4 for the LMTD of 271.33.

Table 8.3-1 Energy constants for the inlet and outlet of the steam turbine.

Isentropic efficiency 70% Conversion efficiency 95%		
	Inlet	Outlet
Pressure Bar (g)	5	1
Temperature K	616.74	515.8
Specific enthalpy kJ/kg	3153	2963
Specific entropy kJ/kg-K	7.527	7.527

Table 8.3-2 Electrical power output and remaining energy flow produced from the mass flow of steam at 616.74 K for the range of energies from the VamTurBurner steam conversion.

VamTurBurner©		Steam Turbine		Water flow 245.8°C
Mass Flow kg/s	Energy MW_{th}	Energy Out MW_{th}	Power Out MW_e	Remaining Energy MW_{th}
5.40	17.02	1.03	0.98	15.99
10.50	33.12	2.00	1.90	31.11
15.30	48.25	2.92	2.8	45.33
19.95	62.91	3.80	3.60	59.12
24.45	77.10	4.66	4.43	72.44
27.27	85.99	5.20	4.94	80.79

Depending on the amount of energy available from the VAM, an electrical generation capacity of between 1 MW to 5 MW exists with a remaining energy flow contained in hot water or steam. The goal of this design is to follow the energy through a Multigeneration system, which produces electrical output from a steam generator and then several more processes. The data in Table 8.3-2 shows that there is energy remaining in the system flow after producing an electrical output using the steam generated.

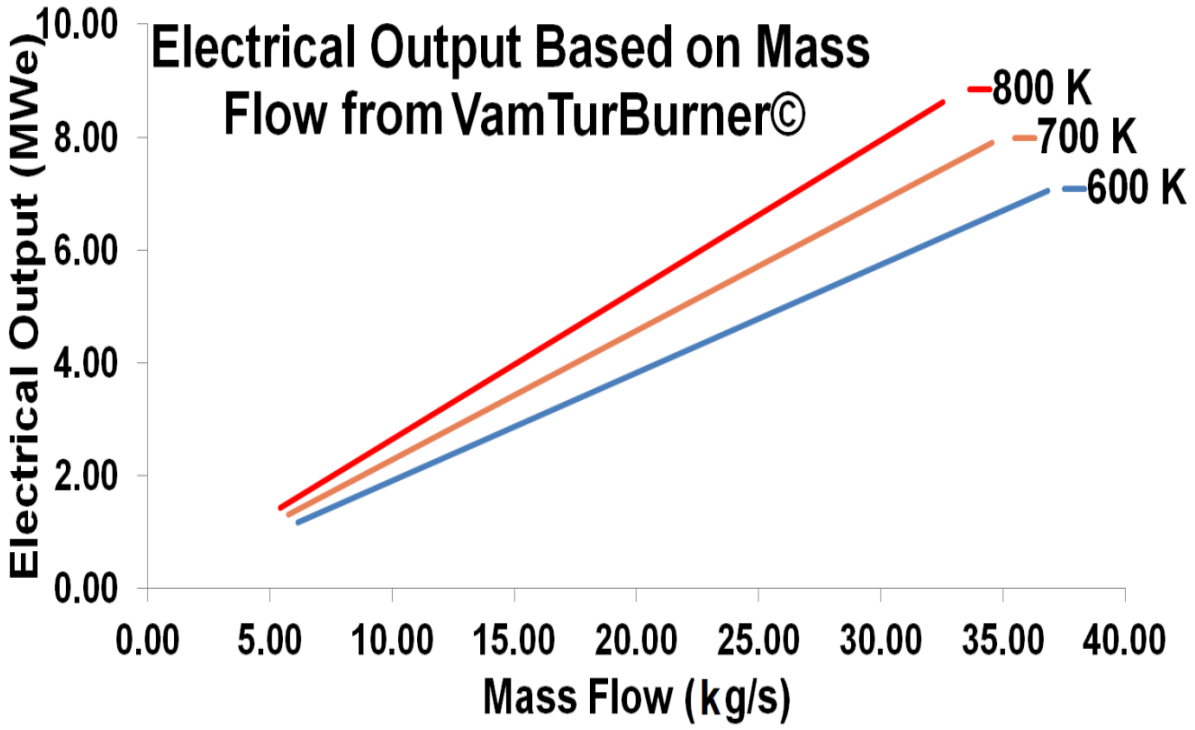

Figure 8.3.1 Electrical output for mass flow of steam at 600 K, 700 K and 800 K.

Since all the energy is obtained from the hot gasses exiting the VamTurBurner, rather than a boiler, the cost of commissioning and operating a boiler are not incurred, but a heat exchanger configuration is required. Typical boiler efficiencies are 75% to 85%, but the efficiency of the heat exchanger can vary from 60% to 90% depending on the operational parameters in use at the time, see Figure 8.2.3 Although there appears to be more than sufficient energy to produce more electrical power with the large amount of energy remaining, the difficulty is that the steam is now at a lower temperature. The temperature of the outgoing steam after a second electrical power production stage would be lowered and less useful to the process' following on after the electricity was produced. In Table 8.3-2 the calculated electrical output is nearly at 1 MW increments for the given mass flows and initial temperature of the steam, so for the process modeling following the electricity production approximate incremental values of 0.5 MW will be used. The electrical power capacity of the steam increases as the temperature is increased; Figure 8.3.1 displays the results of calculations for three temperatures as a function of mass flow.

8.4. Multigeneration illustrated by a steam turbine coupled with processes using steam headers at high, medium and low pressures.

A brief discussion on the energy requirements of the VamTurBurner© system suggests contemplation of the price of electrical energy and natural gas. Both are subject to market forces, but no attempt will be made to contemplate the future prices of these commodities. The onset of fracking and the change in the natural gas price horizon is considered to be a positive event and an incentive for the implementation of a VamTurBurner© system or CHP natural gas systems. It is this author's expectation that natural gas prices will remain low for many decades to come. The recent decoupling of natural gas prices from oil prices is a significant market indicator of the lower natural gas prices. The prices used for all calculations in the following scenarios are: US$ 0.05/KWH for electricity purchased from the grid, US$ 0.10/m^3 for natural gas based on Figure 8.4.1 and an inlet water cost of 0.66/m^3.

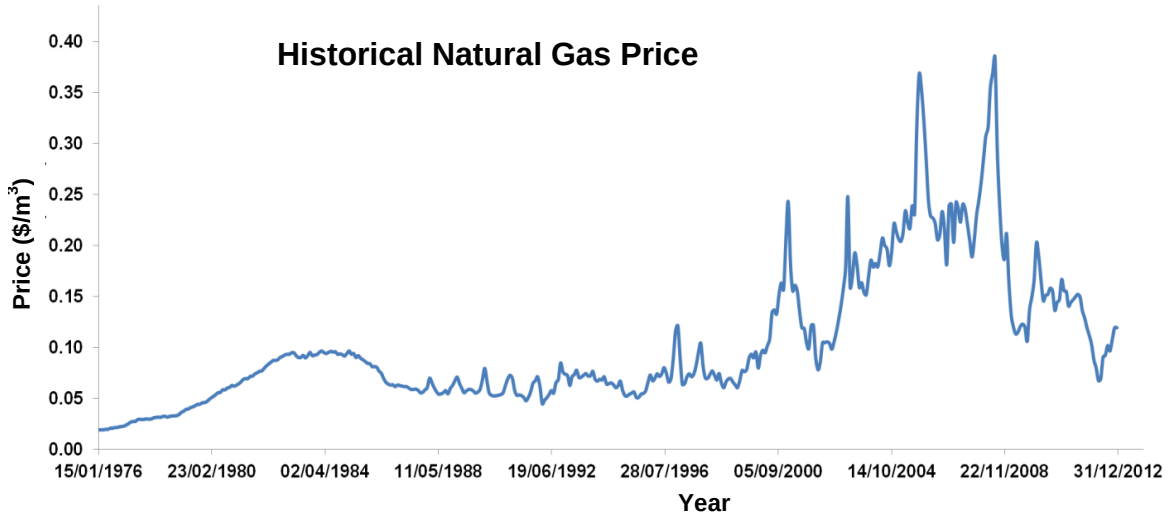

Figure 8.4.1 Historical price of natural gas.

Mining companies have historically used diesel engines to provide energy in remote areas. The growth of Liquid Natural Gas (LNG) facilities, on an international scale, due to transportation of LNG by truck, train and ocean tanker is opening up the market for LNG. The similarities of operation and the convenience of liquid fuels supports a move to the use of gas turbines, which are finding their way into feasibility studies. The historical natural gas price chart in Figure 8.4.1 shows the effect of

shale gas on the price, a 73% decrease from US$ 0.3689/m^3 in June 2008 to US$ 0.09650/m^3 in September 2012.

In Figure 8.2.5, a relationship between the amounts of energy contributed to the total energy available due to the oxidation of the VAM also effects the calculation of the costs because the purchased energy decreases as the total amount of energy increases. There are two factors involved (i) the increasing VAM concentration and (ii) the decreasing amount of energy applied through the igniters. This scheme is outlined in Table 8.2-3 and would vary in actual operation, but will also remain fixed for calculating the costs. The energy costs are calculated as though a boiler had provided the energy and then the costs will be reduced by an amount based on the relationship in Figure 8.2.5. The following steam system designs are facilitated by the steam system modeller available from the US Department of Energy and revised accordingly.

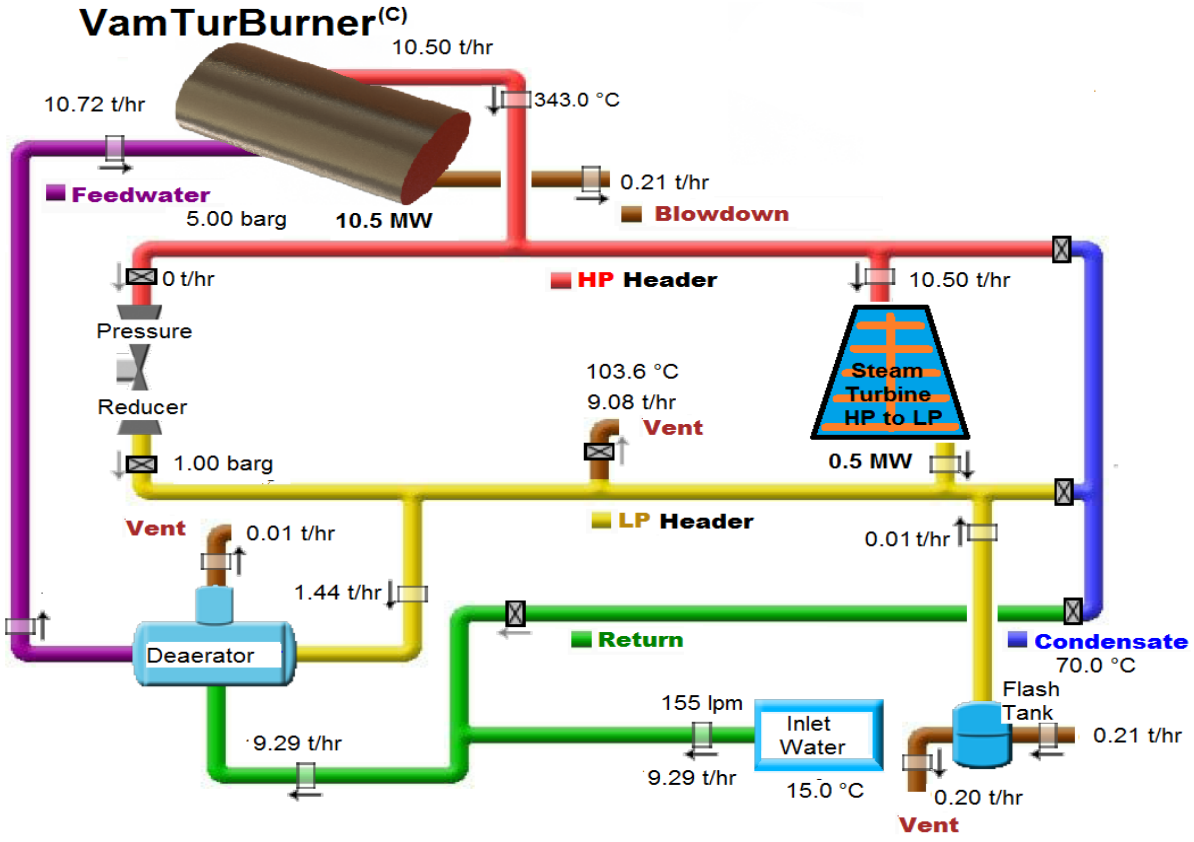

Figure 8.4.2 System 1(a) 0.5 MW electrical production steam generator operating between a high pressure 5 Bar(g) and low pressure header 1 Bar(g).

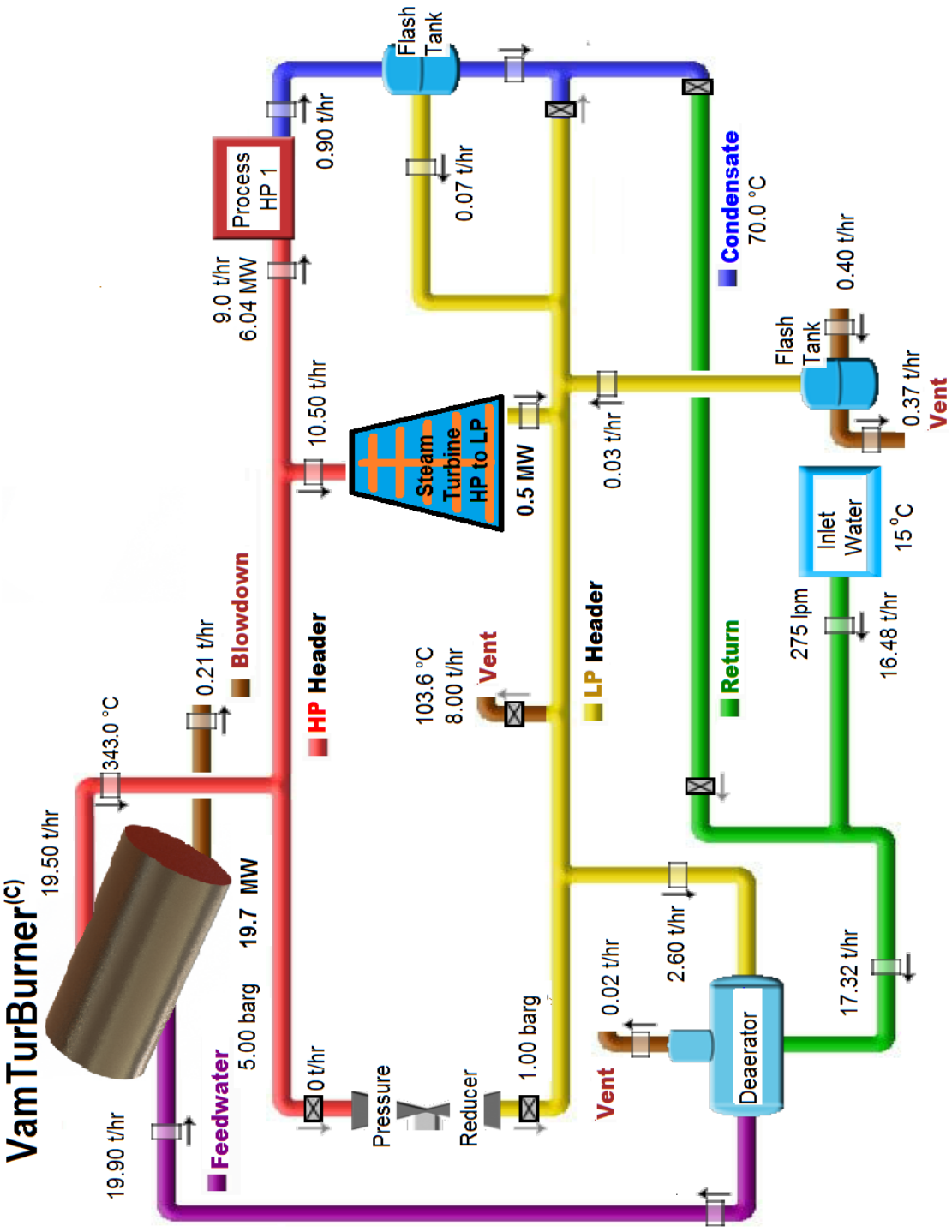

Figure 8.4.3 System 1(b) revised configuration based on Figure 8.4.2 corresponding to option 1, reference # 1 in Table 8.2-5.

A process diagram with a steam turbine placed between a high pressure, mid or low pressure headers to produce electrical output is the first design step to simulate generic process' representative of the Multigeneration concept. The energy range will follow the energy available from the heat exchanger displayed in Table 8.2-5 from 15.8 MW_{th} to 94.5 MW_{th}. The inlet flow rates and energy flows correspond to the steam output from the VamTurBurner©; thus, it replaces the boiler. The costs associated with the operation of the system are based on a typical electrical energy cost of US$0.05/KWH and a natural gas cost of US$0.10/$m^3$.

The 0.5 MW_e system in Figure 8.4.2 operates between a high pressure header at 5 Bar (g) and a low pressure of 1 Bar (g). System 1(a) only requires 10.5 MW_{th} to produce the 0.5 MW_e of electrical power; thus, at the low end of the energy availability or about 0.5% VAM, thermal energy is still available. The remaining vent output of steam is 9.08 Tonnes/hr. at 103.6 ^oC and 1 Bar, which is an appropriate output for space heating or a hot water system. By adding a generic process system 1(a) was altered to system 1(b) in Figure 8.4.3 to consume 9.0 t/hr. of the remaining steam with a 10% recuperation factor; thus, 8.1 tonnes/hr. of steam is available for the process. All of the flows adjust accordingly and the amount of vented hot water out is reduced to 8.0 tonnes/hr.

The possibilities are numerous; as such, the system would be designed to correspond with the needs of a given site. The hot water could be used for space heating during colder months, directed to the hot water needs of a locality or for other nearby industry. Continuing with this example, in system 1(c) Figure 8.4.4 a 0.50 MW condensing steam turbine could replace a 670 HP motor to provide the rotational power needed to operate a water pump. The steam turbine for this application is of a different design than the type needed to produce electricity. The isentropic efficiency is 55% and the conversion efficiency is 80% rather than the 70% and 95% respectively used in previous calculations. Given that such an application would be normally operating for 8000 hr./yr. (the figure of 8000 hours of operation per year is a 91.32% reliability factor used as the standard number of operation hours for all calculations). Such a pump operating at an 80% pumping efficiency would be able to raise 203.8 kg/s of water up to a head of 200 m, say between levels of an operating mine. At an energy cost of $0.05/KWH the normal electricity cost of operating the pump is $200,000/yr.

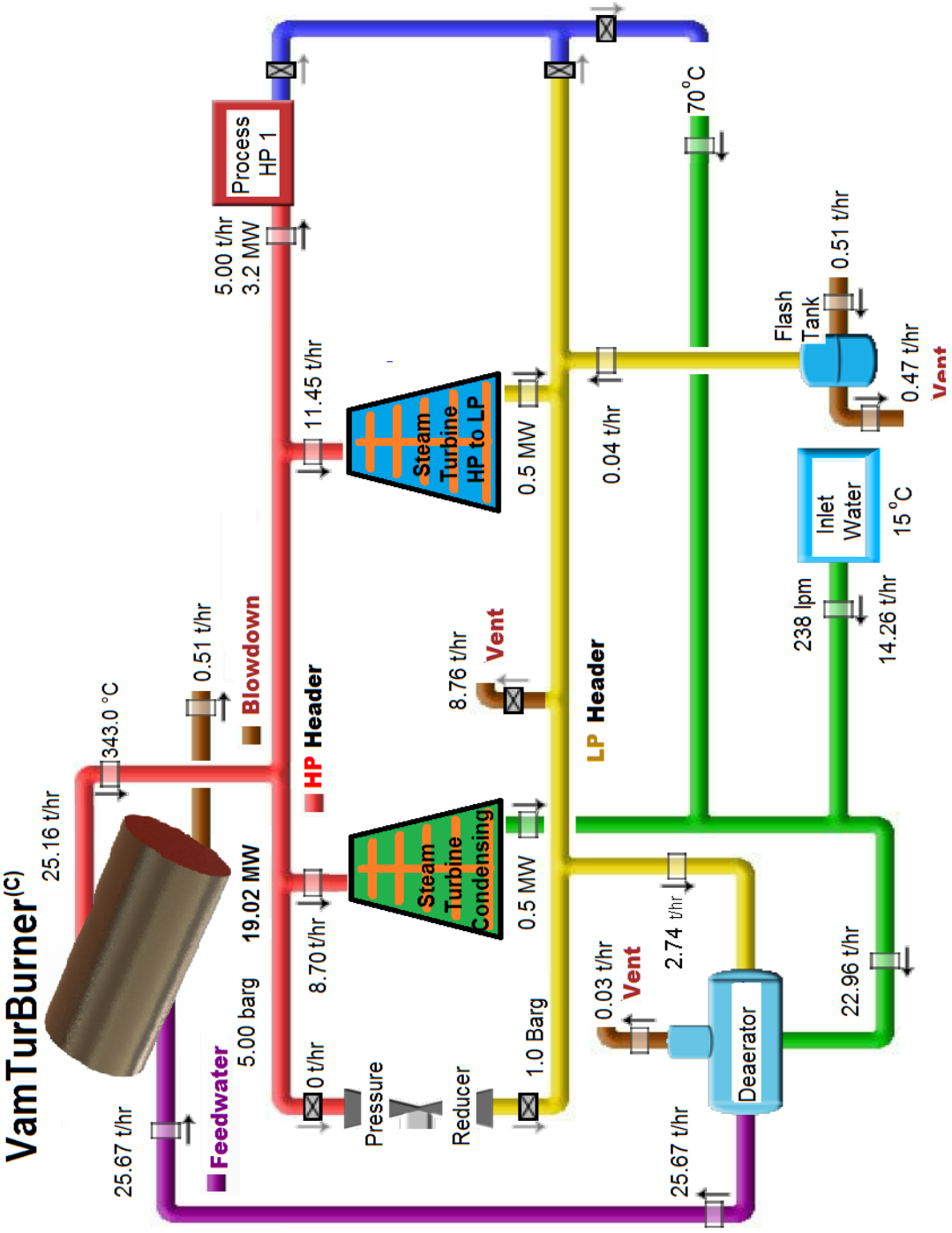

Figure 8.4.4 System 1(c) using a steam turbine to provide rotational power to operate a pump.

The 0.5 MW_e of electricity produced by the high pressure to low pressure steam turbine would have cost $200,000/yr to purchase. The vented hot water is deliberately released at a temperature of 103.6 ^oC to include the latent heat and has a flow of 8.76 tonnes/hr. The electrical energy equivalent required to produce that amount of hot water with an initial temperature of 15 ^oC would be 6.35 MW_e at a cost of $2.54 Million/yr. The total energy cost is $2.943 Million/yr. and for the total energy equal to 19.02 MW the contribution from the VAM is 25.6% or a saving of $753,530/yr.

The configurations in Figure 8.4.3 and Figure 8.4.4 are representative of an energy that lies between option 1 and option 2 reference 1, the lowest energy level in Table 8.2-5. The remaining models are slightly more complex, but the above example was shown in more detail to allow the reader the opportunity to follow the evolution of the model in terms of the selected modes and the variations in the flow parameters and energies that occur when the configuration is altered. Similar calculations are performed for the remaining models, but using the cost of natural gas to produce the thermal energy as though a boiler was used and with the addition of the electrical output of the gas turbines, results are tabulated in Table 8.4-1, Table 8.4-2 and Table 8.4-3.

The output of system 2 includes 1.5 MW_e, 13 t/hr at 5 Bar(g), 12 t/hr. at 3 Bar(g) 8 t/hr. at 1 Bar(g) with a 20% recovery of the process steam and a final venting of 15.44 t/hr of hot water at 103.6 ^oC.

The output of system 3 includes 2.5 MW_e, 12 t/hr. at 5 Bar(g), 8 t/hr. at 3 Bar(g) 8 t/hr. at 1 Bar(g) with a 25% recovery of the process steam for the high and medium pressure process' and 20% for the low pressure process with the final venting of 33.33 t/hr. of hot water at 103.6 ^oC.

The output of system 4 includes 3.5 MW_e, 10 t/hr. at 5 Bar(g), 10 t/hr. at 1 Bar(g) with a 20% recovery and the final venting of 61.99 t/hr. of hot water at 103.6 ^oC.

The output of system 5 includes 4 MW_e, 10 t/hr. at 5 Bar(g), 10 t/hr. at 3 Bar(g), 10 t/hr. at 1 Bar(g) with 20%, 15% and 10% recoveries respectively and a final venting of 76.27 t/hr. of hot water at 103.6 ^oC.

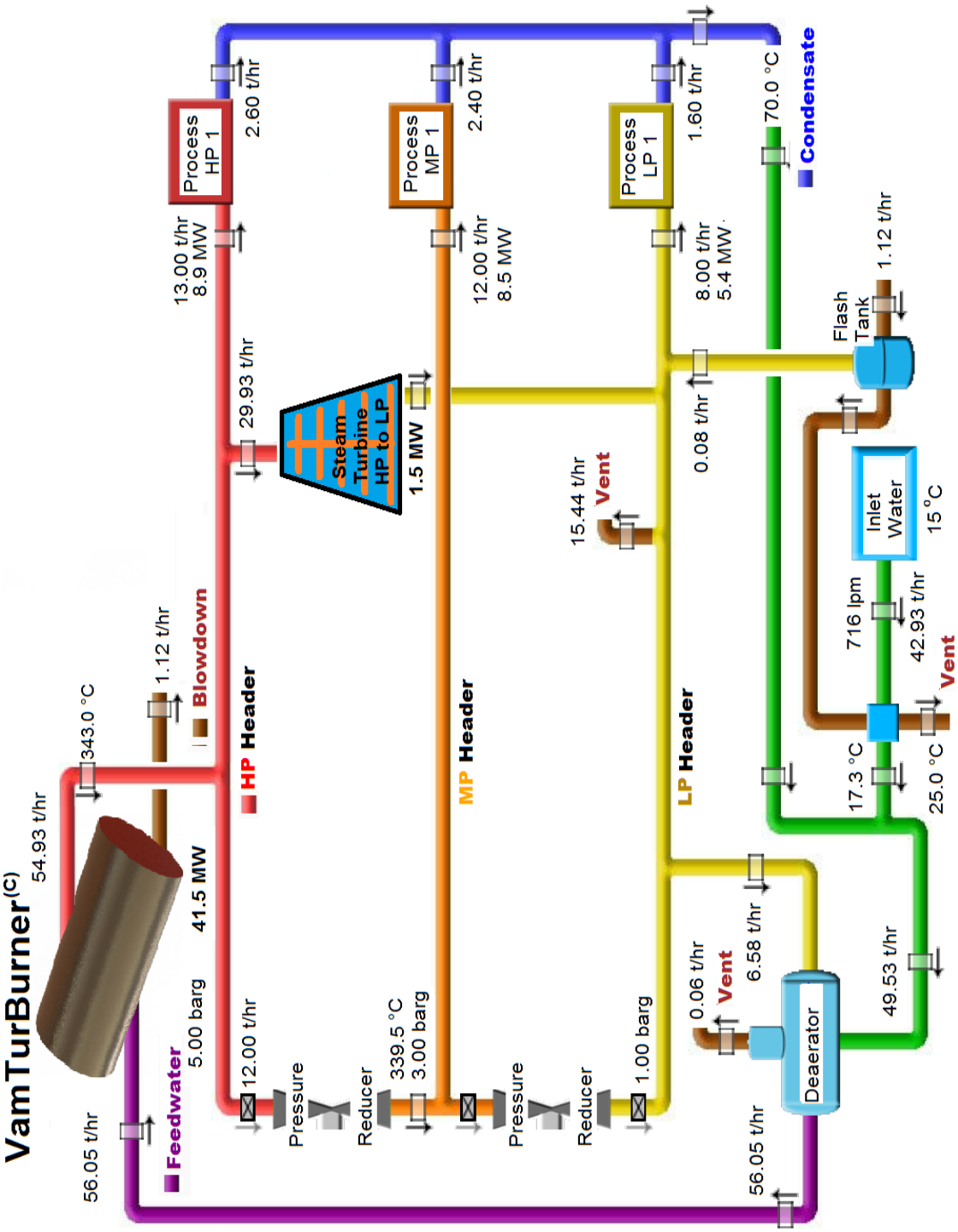

Figure 8.4.5 System 2 corresponding to option 1, reference 2 in Table 8.2-5.

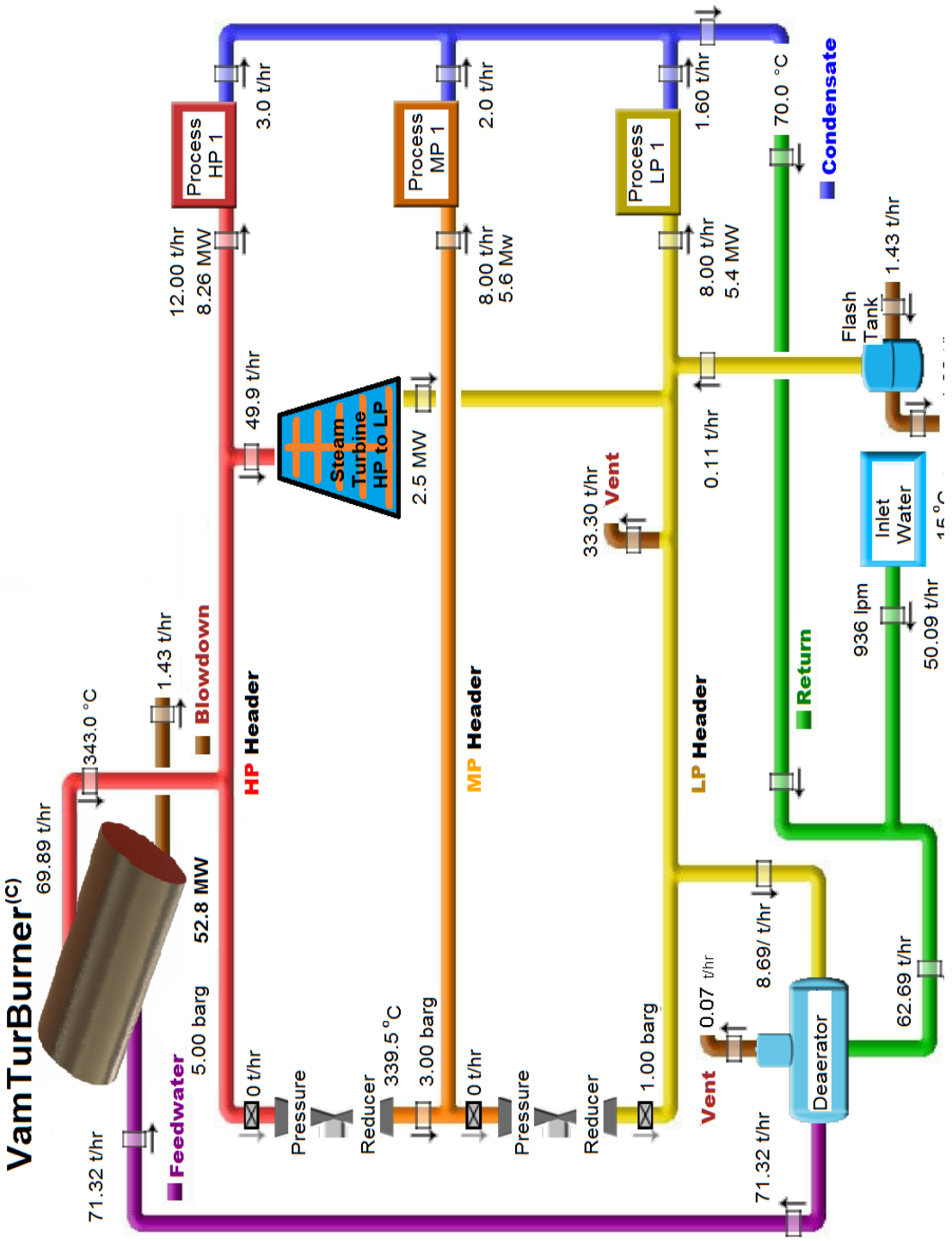

Figure 8.4.6 System 3, corresponding to option 1, reference 3 in Table 8.2-5.

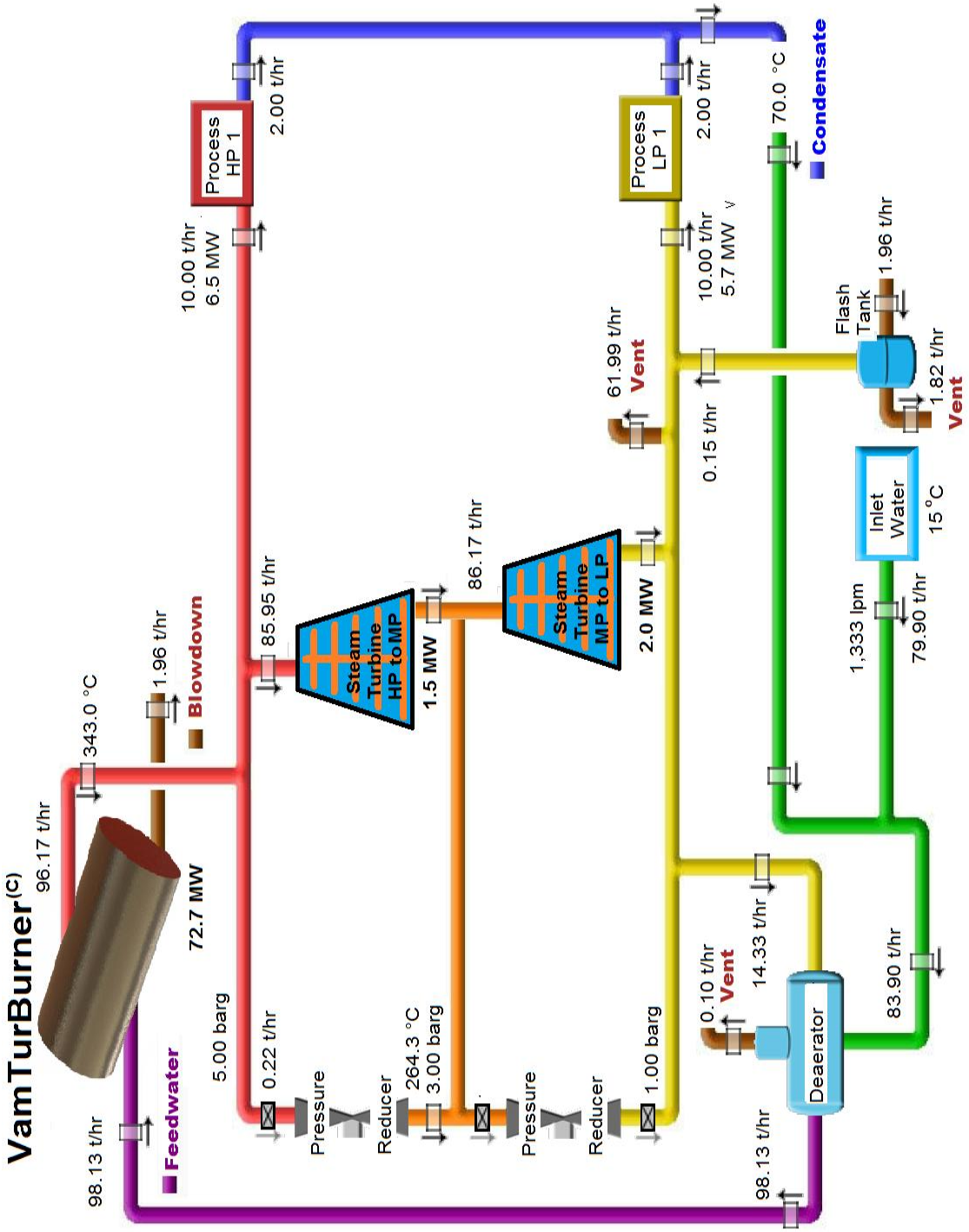

Figure 8.4.7 System 4, corresponding to option 1, reference 5 in Table 8.2

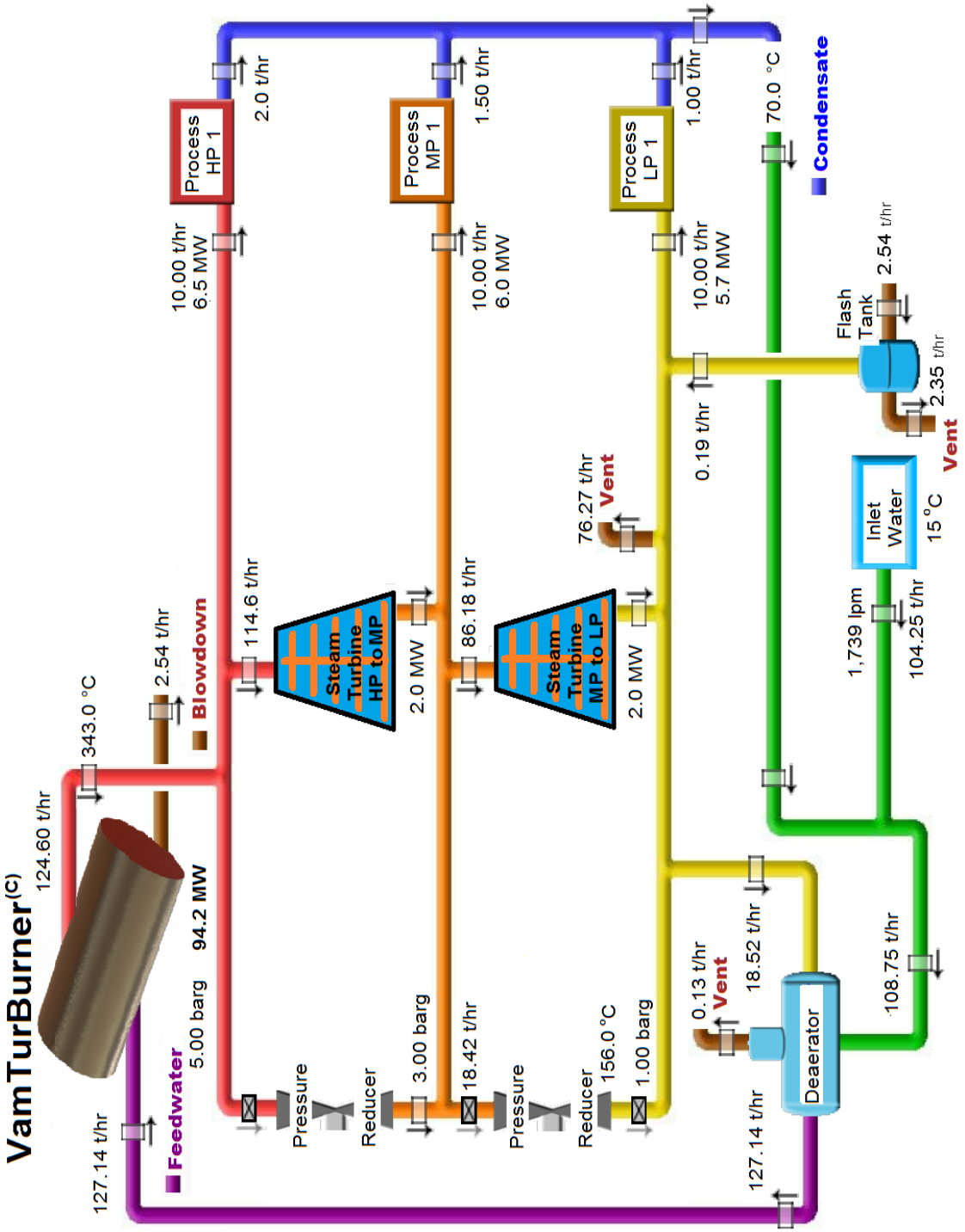

Figure 8.4.8 System 5, corresponding to option 1, reference 7 in Table 8.2 5.

Electrical energy cost US$/KWH	**$0.05**
Natural gas cost US$/$m^3$	**$0.10**
Inlet water cost US$/$m^3$	**$0.60**

Table 8.4-1 Energy transfer and operating costs of VamTurBurner© system

System Configuration	Initial Energy Available	VamTurBurner© 75% Energy Transferred	Boiler Fuel Costs 85% Efficient	Total Operating Cost
	MW	MW	US$	US$
system 1	25.4	19.0	$ 2,232,034	$5,034,528
system 2	55.3	41.5	$ 4,869,672	$4,760,991
system 3	77.6	58.2	$ 6,829,274	$4,384,000
system 4	96.3	72.2	$ 8,472,055	$4,115,946
system 5	125.6	94.2	$11,053,568	$3,410,203

Table 8.4-2 details of electrical and thermal outputs of VamTurBurner© system

System Configuratio	Total Electricity Generate	Cost to Purchase Electricit	Process Energy Pressure headers			Hot Water 103.6	System Therma Output
			HP 1	MP 1	LP 1		
	MWe	1000 US$	MW_t	MW_t	MW_t	MW_{th}	MW_{th}
system 1	2.5	$ 1,000	3.2	0.0	0.0	5.5	8.7
system 2	3.0	$ 1,200	8.9	8.5	5.4	9.7	32.5
system 3	4.0	$ 1,600	8.3	5.6	5.4	20.9	40.1
system 4	5.0	$ 2,000	6.5	0.0	5.7	38.9	51.1
system 5	5.5	$ 2,200	6.5	6.0	5.7	47.8	66.0

Table 8.4-3 Details of energy costs compared to costs recovered by combustion of VAM.

System Configuration	Actual Cost for Natural Gas	Recovered Cost if NG Purchased	System Thermal Energy Transfer	Percent Cost Recovered	%Energy In Flow from VAM	Percent VAM In Flow
	1000 US$	1000 US$	Percent			
system 1	$ 650.2	$1,650.2	45.70	32.78	32.21	0.642
system 2	$2,429.6	$3,629.6	78.27	76.24	55.20	1.421
system 3	$3,002.4	$4,602.4	68.96	104.98	66.85	2.001
system 4	$3,819.9	$5,819.9	70.73	141.40	74.40	2.489
system 5	$4,938.5	$7,138.5	70.08	209.33	83.53	3.252

In Table 8.4-1 the energy available is that due to the combustion airflow, 75% is taken as the transfer efficiency through the heat exchanger. The boiler fuel costs are based on the cost of an 85% fuel-efficient boiler and a 75% energy transfer. The

operating costs are determined from the cost of the natural gas needed to operate the gas turbines, supply the igniters and the cost of the water flowing in through the inlet. The boiler costs can be used as a benchmark pertaining to the energy cost of the system with no VAM involvement. The boiler costs increase as the amount of energy required increases, but the operating cost of the VamTurBurner© decreases due to the increasing fraction of energy available from the increasing VAM concentration and the reduction in the amount of igniter energy required. As such, the plot of the costs of a boiler versus the costs for the VamturBurner© shows that at a VAM concentration of about 1.4% the system cost is equal to that of the boiler, which can be considered as the breakeven point.

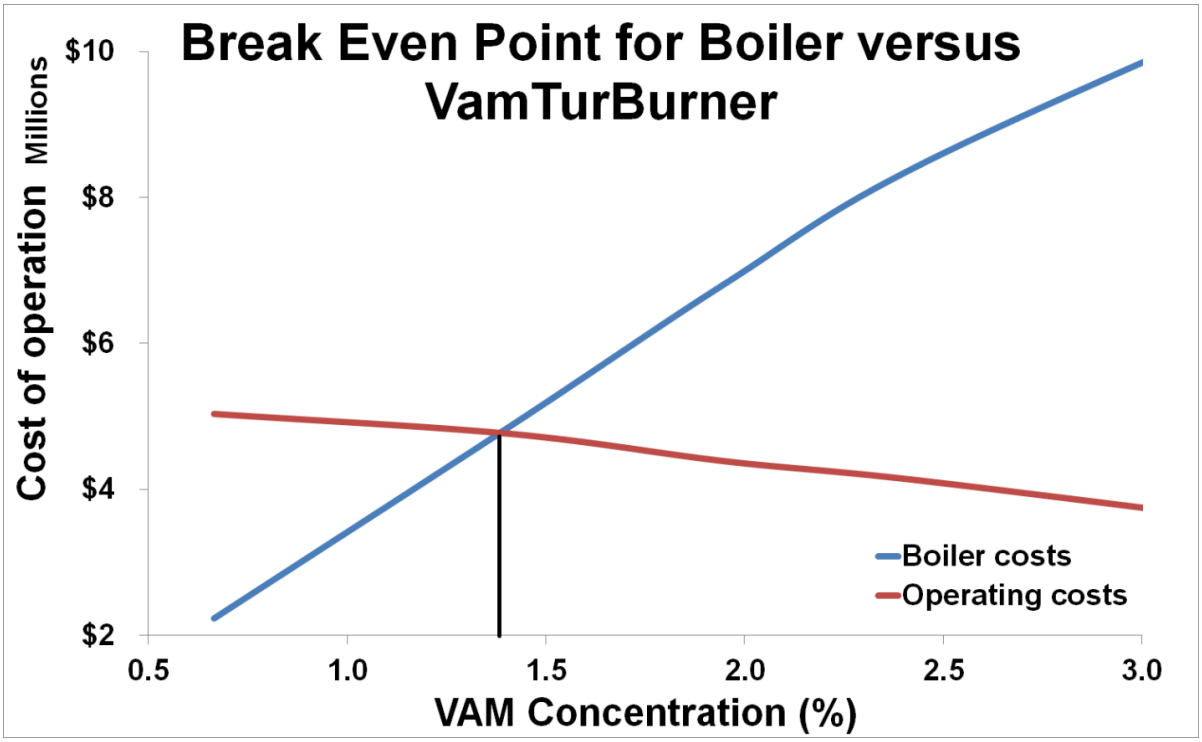

Figure 8.4.9 VamTurBurner© costs and boiler costs as a function of VAM concentration.

The comparison to a boiler is relevant from the point of view that the energy is similar to that which would be obtained from a boiler. The cost recovery is performed based on the outputs of the system. In Table 8.4-2 the details of the electrical and thermal output of the system are given. The electrical output uses steam turbines operating between a high-pressure header and medium or low-pressure header. The cost recovery for the electrical output is calculated for the costs that would be incurred if the electricity had to be purchased. The thermal outputs are isolated to high, medium and low-pressure process, which can be

dedicated toward various tasks. The energy used in these process are summed along with the energy for the remaining hot water vented at the outlet and the cost is calculated as though natural gas had been purchased to provide the energy to drive them. When the costs are compared in this manner, the system cost neutral point occurs at a VAM concentration of about 1.38%. This means that any VAM percentage above 1.38% would actually provide revenue.

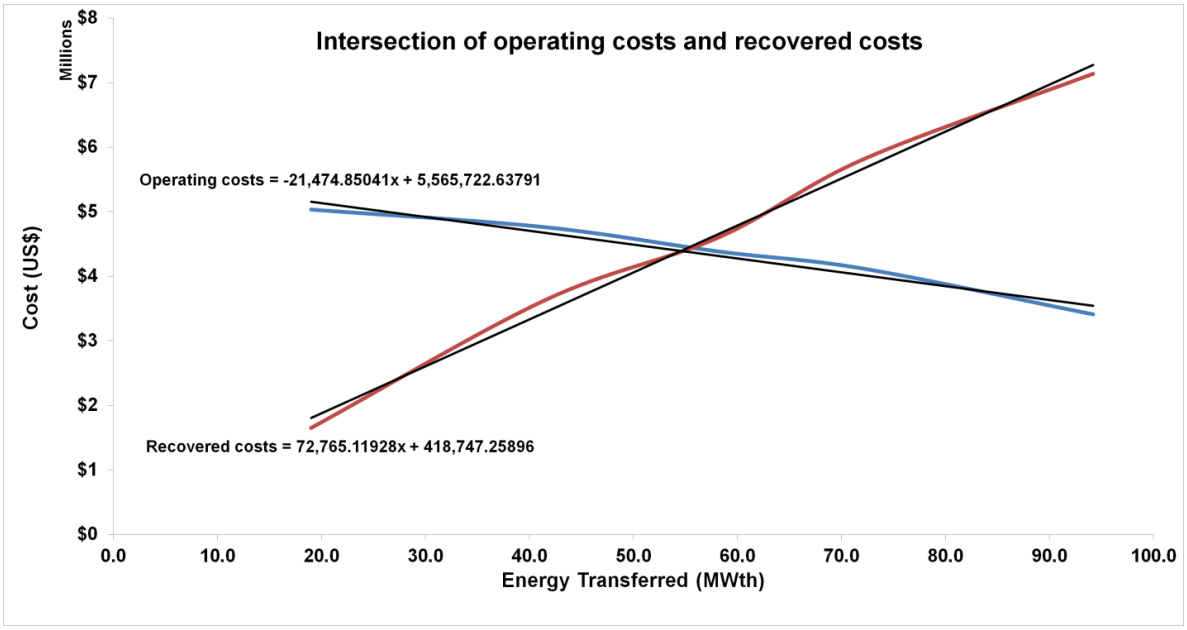

Figure 8.4.10 Intersection of operating costs and recovered costs.

Regression equations were used to solve for the cost neutral point and it corresponds almost exactly with the breakeven point for the boiler versus the VamTurBurner© in Figure 8.4.9.The details of the calculations are shown below. Using the data in Table 8.2-3 regression equations for the VAM energy and total energy added.

Eqn. 8.10 $$\boldsymbol{VAM\ Energy = 38.386\ (VAM\%) + 0.7533 \quad R^2 = 0.9976}$$

Eqn. 8.11 $$\boldsymbol{Total\ Energy\ Added = 27.386\ (VAM\%) + 61.253 \quad R^2 = .9954}$$

The regression equation obtained from Figure 8.2.5 provides the contribution of the VAM to the energy as a function of the VAM concentration. Essentially the plot is derived from Eqn. 8.10, Eqn. 8.11 and results in Eqn. 8.12.

Eqn. 8.12 $$\boldsymbol{E(VAM) = 0.02(VAM)^3 - 0.1616(VAM)^2 + 0.5703(VAM) + 0.0142}$$

Eqn. 8.13 $$\boldsymbol{Operating\ costs = -21,474(E_{transfer}) + 5,565,722 \quad R^2 = .9652}$$

Eqn. 8.14 $$\boldsymbol{Recovered\ costs = 72,765(E_{transfer}) + 418,747 \quad R^2 = .9942}$$

Solving for Eqn. 8.13 = Eqn. 8.14 gives a value of 54.61 MW_{th} for the energy transferred and Eqn. 8.10 provides a value of 1.4% for the VAM concentration, which is also shown as a vertical line on the intersection of boiler operating costs and VanTurBurner© operating costs in Figure 8.4.9. The cost of purchase and installation of the systems have not been included in this analysis, nor have the fluctuations in energy cost due to incentive timing or the incentives provided by governments for small scale energy producers. The intent is only to develop the concept and operational principles associated with the viability of a system. The preceding design scenarios are sufficient to argue the system is a viable option for the mitigation of VAM.

9. Conclusions

Methane is a significant greenhouse gas; thus, any opportunity to mitigate methane leading to a reduction in atmospheric emissions should be capitalised upon whenever and wherever possible.

Emerging economies will increase their dependency on coal for power; thus, coalmining needs to become more environmentally practical and the proponents have to be motivated to mitigate methane emissions. The VamTurBurner© may be a solution that can improve the mitigation of methane while producing power.

The analytical model below is based on combustion dynamics theory and was found to provide appropriate tools to determine the adiabatic flame temperature for the concentrations of methane found in ventilation air from coalmines. The adiabatic flame temperature was used to calculate the temperature for the expected methane equivalence ratios $\boldsymbol{\phi}$ = 0.15 to $\boldsymbol{\phi}$ =0.6 and the results were consistent with advanced numerical modeling, which provided the confidence to proceed to numerical modeling.

$$\boldsymbol{T_2 = T_0 + \frac{\left(\phi C_p^m(CH_4) + 2C_p^m(O_2) + 2aC_p^m(N_2)\right)(T_1 - T_0) + \phi Q^m}{\left(2\phi C_p^m(H_2O) + \phi C_p^m(CO_2) + 2aC_p^m(N_2) + 2(1-\phi)C_p^m(O_2)\right)}}$$

The critical temperature $\boldsymbol{\theta_c}$, the initial fresh gas $\boldsymbol{T_1}$ and adiabatic flame temperatures $\boldsymbol{T_2}$; were modeled in terms of the normalized reaction rate by the source term method in order to determine ignition times. The increase in reaction rate, due to increased temperature of the incoming fresh gas, is taken up entirely by the increase in ignition time because the fuel concentration is considered as a constant over the time of the reaction.

The safety of the workers and mine are paramount, as such the probability of the conditions leading to a flashback were explored. Using the ignition time and the flame thickness to determine the flame speed it was determined that flame speed is not sufficient and the characteristics of the flow are not conducive to a flashback to the mine workings.

Numerical modeling using Large Eddy Simulation was used to study the combustion dynamics of the ventilation air methane. The chemical kinetics were modeled by the four step model, derived specifically for the for the oxidation of

methane and has been shown by comparison to experimental data to be sufficiently accurate for the purpose of the current numerical simulation. The numerical modeling confirmed that given appropriate preheating of the low concentration high flow rate fresh gas mixture, the methane will ignite to a sustainable flame for temperatures in the neighbourhood of 500 K for VAM concentrations as low as 0.5%, but for a 3% concentration, the preheating temperature can be as low as 400 K.

The computational fluid dynamics of the system were studied to ascertain the best method of preheating. A detailed study of heat exchange systems was compared to a recirculation scheme. The recirculation scheme was determined to be the most efficient means of providing the heat to the preheating zone with as little a loss of energy and as low a cost as possible. A design of the system was developed based on the use of baffles and diffusers, which can be placed in the gas turbine exhaust, to improve the turbulent mixing of the incoming ventilation air and the hot gasses from the combustion zone.

Given the energy availability, based on inlet gas temperature and mass flow, a study of heat exchange systems for the production of steam for electricity production and various other thermal processes was undertaken. It was determined that an LMTD of 300 K and an overall heat transfer coefficient of 35 W/ m^2 K are the appropriate values for the designs required at these energy levels and material flow rates.

Calculations based on various multigeneration schemes were performed to show the benefit of a system that incorporates the amount of energy available from the VAM . A sample system is summarized as follows: by assuming 80% thermal conversion efficiency, 1.5 MW_e is produced from a cluster of six 250 KW microturbines. The 1.5 MW_e is produced at a 20% efficiency from an input of 0.207 kg/s of fuel at a caloric value of 38 MJ/kg. The amount of power available from the VAM is 19.25 MW_{th} with 6.29 MW_{th} available from the microturbines and 4.44 MW_{th} from the igniters providing a total power available for conversion by the heat exchanger systems of 29.98 MW_{th}. Depending on the amount of energy available from the VAM, an electrical generation capacity of between 1 MW to 5 MW exists with a remaining energy contained in hot water or steam. A set of scenarios, modeled using increasing amounts of energy, corresponding to increasing methane

concentration in the incoming ventilation air, showed that if the energy remaining after electricity production was allocated to processes divided into high, medium and low-pressure categories numerous thermal products become available. From this analysis a cost recovery model was developed based on the operating costs, determined from the cost of the water flowing from the inlet, the cost of the natural gas needed to operate the gas turbines and to supply the igniters. The cost of a boiler acted as a benchmark in the determination of a breakeven methane concentration of 1.4%, that is, for methane concentrations above 1.4% the system thermal outputs are free.

9.1 Future work

An argument to use an energy storage vector wherein the VamTurBurner© becomes part of a distributed energy supply system is suggested. Liquid Air as an energy storage vector (Strahan D. (Ed), Radcliffe J. and Williams R.A. 2013) has advantages over other approaches; however, when including the potential for using Liquid Air as a ventilation supply and as a fuel for mine equipment, using the Deerman engine, there are synergistic effects. The Liquid Air ventilation also provides cooling to underground workings, which is more advantageous as the mines descend to greater depths and offsets auto-compression. An integrated mine using: a VamTurBurner© multigeneration system, Liquid Air energy for storage, ventilation and fuel, is proposed as a potential future mine design.

At present, the VamTurBurner© is well supported by the calculations, numerical modeling and engineering design. Using this design concept, a project to determine feasibility of operating principles was undertaken at the masters' project level by a Camborne School of Mines student (Griffin, 2013) with this author as the principle supervisor. At the small scale undertaken in this study the results support the concept of developing a VamTurBurner© to the next stage of prototype development.

Further numerical modeling to confirm the technical feasibility of the system is required. A proposal involving the development of ultra-low methane combustion is currently underway with partners from Spain, Greece, Canada and the United Kingdom. Field trials involving prototypes built to a higher degree of sophistication than the previous trials is an essential part of the work undertaken in this work.

The incorporation of a Liquid Air Energy storage system (Fox, 2012), as has been demonstrated by Highview Power Storage Corporation in Slough UK, would improve the efficiencies of waste heat recovery and avail the mine of the benefits of having a Liquid Air source at their site. The development of techno-economic models to support the further integration of the technology into mines would benefit the notion of becoming part of the distributed energy grid.

10. References

Amin, M, and Schewe P.F., (2007). Preventing Blackouts: Building a Smarter Power Grid. A smarter power grid that automatically responds to problems could reduce the rising number of debilitating blackouts. *Scientific American*. May (2007), 60 - 67.

Arfken, G., (1985). *Mathematical Methods for Physicists*, Orlando, FL: Academic Press. 303-313.

Ayoub M., Rottier C., Carpentier S., Villermaux C., Boukhalfa A.M. and Honore D., (2012). An experimental study of mild flameless combustion of methane/hydrogen mixtures. *The International Journal of Hydrogen Energy*. 37 (8), 6912 to 6921.

Batchelor G. K., (1967). *An Introduction to Fluid Dynamics*. The Edinbourough Building CB2 2RU: Cambridge University Press. 645.

BBC News., (2006). *Methane bubbles climate trouble (2006/09/07)*. Available at: http://news.bbc.co.uk/2/hi/science/nature/5321046.stm. [Accessed September 19, 2013]

Bibler C. and Carothers P., (2003). *PE Overview of coalmine gas use technologies*., Raven Ridge Resources, Incorporated, Grand Junction, Colorado USA, Alternative Energy Development, Inc. Silver Spring, Maryland USA

Bibrzycki J. and Poinsot T., (2010). Reduced chemical kinetic mechanisms for methane combustion in O_2/N_2 and O_2/CO_2 atmosphere, *ECCOMET WN/CFD/10/17 CERFACS*, (February 24)

Biothermica brochure., (2010), *Create Value From VAM*, 25 May

Bradley, B., (2005). *More storms, high gas prices predicted*. Northern Life News, Laurentian Publishing, 19 August. 2005. (Interview article with Daniel L. Cluff, Available at: http://www.northernlife.ca/news/localNews/2005/9434808-31-05-gas.aspx [Accessed May 16, 2012]

Chase Jr, M.W., Davies, C.A., Downey Jr., J.R., Frurip, D.J McDonald, R.A., and. Syverud A.N.,(1985). NIST Standard Reference Database 13, *Nist Janaf Thermochemical Tables Version 1.0.*, Gaithersburg, MD 20899,: Standard Reference Data Program National Institute of Standards and Technology

Cluff D. L. Kennedy G. A and Bennett J. G., (2013). Capturing Energy from Ventilation Air Methane at Operating Coal Mines. In *23rd World Mining Congress 2013 Proceedings*. Montreal, Canada; ISBN 978-1-926872-15-5. 1 (Track 8 - Energy & Mines, Lowering Cost and Energy with Improved Mine Ventilation and Refrigeration), paper 582.

Cluff, D.L. and Kazakidis V.N., (2013). Opportunities and Constraints of Engineering Frozen Backfill for Underground Mining Applications in Permafrost. *In ISCORD 2013: Planning for Sustainable Cold Regions*. Anchorage, Alaska, June 2013. Proceedings of the 10th International Symposium on Cold Regions Development (Frozen ground and permafrost: American Soceity of Civil Engineers. 175 - 191.

Cluff, D.L., Mira-Martinez, D., and Jiang X., (2014). A numerical investigation using Large scale eddy simulation of the burning characteristics of ultralow methane concentration flows. *In Canadian Association of Physicists Congress June 2014*. Sudbury, Ontario, June 18, 2013. Ottawa, Canada: Canadian Association of Physicists. 1 - 60.

Cummings R., (2004). *Use and Elimination of Methane in Coalmine Ventilation Air*. DUT Pty Ltd., 1 – 8

Cummings R., (2006). *Submission to the Senate Alternative Fuels Enquiry*, Australia, DUT Pty Ltd., 1 - 28.

Deardorff, J., (1970). A numerical study of three-dimensional turbulent channel flow at large Reynolds numbers. *Journal of Fluid Mechanics*, 41 (2), 453 - 480.

Delworth, T. Stouffer, R and Winton, M., (2007). Patterns Of Greenhouse Warming. The Geophysical Fluid Dynamic Laboratory's (*GFDL) Climate Modeling Research Highlights*. 1 (6), 1 - 3.

Dhariya, A., (2008), Compressor Turbine Matching for gas turbine engine, *Gas Turbine Propulsion,* 1 - 2

Dlugokencky, Ed., (2012). NOAA CMDL , http://www.esrl.noaa.gov/gmd/Photo_Gallery/GMD_Figures/ccgg_figures/ch4_surface_color.png [Accessed September 14 2013]

EDGAR., (2013), *Nasa, Emission Database for Global Atmospheric Research*, Available at: http://gcmd.gsfc.nasa.gov/index.html [Accessed November 15, 2012].

Edwards, J.E., (2008). *Design and Rating of Shell and Tube Heat Exchangers*. 1st ed. Teesside, UK: P & I Design Ltd.

Energy Developments., (2011). *Appin Tower & Westcliff Power Stations,* Available at: www.energydevelopments.com. [Accessed January 12, 2012]

Engineering Tool Box., (2013). *Fuels and Chemicals Auto-ignition Temperatures*. Available at: http://www.engineeringtoolbox.com/fuels-ignition-temperatures-d_171.html. [Accessed June 13 2013]

Favre, A., (1983). Turbulence: space-time statistical properties and behavior in supersonic flows. *Physics of Fluids A,* 23 (10), 2851–2863.

Foias C., Manley, O., Rosa R., and Teman, R., (2008). *Navier-Stokes Equations and Turbulence (Encyclopedia of Mathematics and its Applications)*. Cambridge, United Kingdom,: Cambridge University Press, ISBN 13: 9780521064606

Forster, P., V. Ramaswamy, P. Artaxo, T. Berntsen, R. Betts, D.W. Fahey, J. Haywood, J. Lean, D.C. Lowe, G. Myhre, J. Nganga, R. Prinn, G. Raga, M. Schulz and Van Dorland, R., (2007). *Changes in Atmospheric Constituents and in Radiative Forcing: Climate Change 2007: The Physical Science Basis. Contribution of Working Group I to the Fourth Assessment Report of the Intergovernmental Panel on Climate Change* [Solomon, S., D. Qin, M. Manning, Z. Chen, M. Marquis, K.B. Averyt, M.Tignor and H.L. Miller (eds.)]. Cambridge University Press, Cambridge, United Kingdom and New York, NY, USA

Fourier, Jean Baptiste, Baron., (1822). Theorie Analytique de la Chaleur, A Paris: Chez Firmin Didot, Pere et Fils.

Fox T., (2012), *Storing Electricity Using Cryogenic Technology in a UK Policy Context*, Energy Storage Symposium, Columbia University

Frenklach M., Wang H., Goldenberg M., Smith G. P., Golden D. M., Bowman C. T., Hanson R. K., Gardiner W. C., and Lissianki V., (1995), *Gri-mech: An optimized detailed chemical reaction mechanism for methane combustion*, Technical Report GRI-Report GRI-95/0058, Gas Research Institute

Global Methane Initiative., (2011). *Coal Mine Methane Mitigation and Utilization Technologies and Project Profiles*. November 16, 2011.

Griffin, R., 2013. *The VamTurBurner(C) Multigeneration System*. M.Sc., Penryn Campus: University of Exeter, Camborne School of Mines.

Gunning, P. M., (2008). *Methane - mitigation technologies, options, and policies. Presentation to arctic council task force on short-lived climate forcers, climate change division*. Office of Atmospheric Programs.

Hamilton, S. L., (2003). *The Handbook of Microturbine Generators*. Penwell Corporation, ISBN 0-87814-897-3

Heravi, H.M. Azarinfar, A. Kwon, S.I. Bowen, P.J. and Syred N., (2007) Determination of Laminar Flame Thickness and Burning Velocity of Methane-Air . *In Third European Combustion Meeting ECM 2007*. Crete, Greece, April 11 - 13, 2007. Greece: Mediterranean Agronomic Institute Of Chania. 1 - 6.

Hill P. and Peterson C., (1992). *Mechanics and Thermodynamics of Propulsion.* 2nd ed. Workingham, United Kingdom: Addison Wesley Publishing Company. 705 - 713., ISBN0-201-14659-2

Holman, J. P., (2010). *Heat Transfer*. 10th ed. The McGraw-Hill Companies, Inc., 1221 Avenue of the Americas, New York, NY 10020: McGraw-Hill. 567 570., ISBN 978–0–07–352936–3

IEA CCC 2005, M2M 2006., (2013). *What is Coal Seam Gas?.* Available at: http://www.worldcoal.org/coal/coal-seam-methane/. [Accessed January 18 2013].

Incropera, F. P. and DeWitt, D. P., (1990). *Introduction to Heat Transfer.* 2nd ed. New York, USA: John Wiley & Sons.

IPCC., (1996). *Second assessment - climate change. Inter-Governmental Panel on Climate Change.* Available at: www.ipcc.ch/pdf/climate-changes-1995/ipcc-2nd-assessment at 08.11.12, [Accessed November 08, 2012]

IPCC., (2001). *Third Assessment Report, Climate Change 2001*. Available at: http://www.grida.no/publications/other/ipcc_tar/. [Accessed January 23, 2012]

IPCC., (2007), Solomon, S., D. Qin, M. Manning (Eds). *Summary for Policymakers. In: Climate Change 2007: The Physical Science Basis*. Contribution of Working Group I to the Fourth Assessment Report of the Intergovernmental Panel on Climate Change

Johnson P. W., Thomas N., Senior Member, IEEE, White D.J., Stevenson J. W., Mills R. A., Lasseter, Jr. E. L., and Boyer C. M., (1998). Use of mine ventilation exhaust as combustion air in gas-fired turbo-electric generators. *Transactions on industry applications*. 34 (2)

Jones, W. P. Lindstedt, R. P., (1988). Global Reaction Schemes for Hydrocarbon Combustion. *Combustion and Flame*. 73 (3), 233-249.

Judson N., (2013). *Interdependence of the Electricity Generation System and the Natural Gas System and Implications for Energy Security*. ESC-EN-HA-TR-2012-121, Technical Report 1173 (May 13)

Karakurt I., Aydin G. and Aydiner K., (2011). Mine ventilation air methane as a sustainable energy source. *Renewable and Sustainable Energy Reviews.* 15 (1), 1042-1049.

Kasting, J., (2004). When Methane Made Climate. *Scientific American*. July (1), 78 - 87.

Kawasaki (2011)., *Catalytic Combustion Gas Turbine to Contribute to the Future Global Environment*. Japan: Kawasaki. 1 - 2.

Khanna, V.K., (2001). *A Study of the Dynamics of Laminar and Turbulent Fully and Partially Premixed Flames*. PhD. Faculty of Mechanical Engineering: Virginia Polytechnic Institute and State University.

Kissell, F. N., (2006). *Handbook for methane control in mining*. National Institute for Occupational Safety and Health. Information Circular 9486

Kosmack, D.A. Winschel R. A. and Zak K.P., (2007). First US field trial of oxidation technology for ventilation air methane. In *1st Annual US Coal Mine Methane Conference.* St. Louis, Missouri USA, Tuesday, September 25th . St. Louis, Missouri USA: Coalbed Methane Outreach Program . 1 - 67.

Kurz, R, and Brun, K., (2007). Gas Turbine Performance, What makes the Map. In *29th Turbomachinery Symposium.* Texas, USA, 2000. Texas, USA: Texas A&M University System Turbomachinery Laboratory. 247 - 262.

Lemke, P., J. Ren, R.B. Alley, I. Allison, J. Carrasco, G. Flato, Y. Fujii, G. Kaser, P. Mote, R.H. Thomas and Zhang T., (2007). *Observations: Changes in Snow, Ice and Frozen Ground: Climate Change 2007: The Physical Science Basis. Contribution of Working Group I to the Fourth Assessment Report of the Intergovernmental Panel on Climate Change*. Cambridge, United Kingdom: Cambridge University Press, Solomon, S., D. Qin, M. Manning, Z. Chen, M. Marquis, K.B. Averyt, M. Tignor and H.L. Miller Eds.

Lienhard J.H. IV and Lienhard V J.H., (2000). *A Heat Transfer Textbook*. 3rd ed. Cambridge Massachusetts USA: Phlogiston Press. 755.

Lorenz, E.N., (1963). Deterministic non-periodic flow. *Journal of the Atmospheric Sciences*. 20 (3), 130 - 141.

Mallett C. W. and Su S., (2004). *Progress in developing ventilation air methane mitigation and utilization technologies*. Technology Court, Pullenvale, QLD 4069,

Australia: CSIRO Exploration and Mining. 18.

Mancarella, P. and Chicco, G., (2009). *Distributed multi-generation systems*. Hauppauge, New York: Nova Science Publishers. 1 - 264.

Marín, P., Ordóñez, S. and Díez, F.V., (2009). Procedures for heat recovery in the catalytic combustion of lean methane-air mixtures in a reverse flow reactor. *Journal of Chemical Engineering*. 147 (1), 356 - 365.

Markunas, A.L., (1972). *Modeling, Simulation and Control of Gas Turbines.* M.Sc. Massachusetts: Massachusetts Institute of Technology.

Martinez, I., (2013). *Heat Exchangers.* Available at: http://webserver.dmt.upm.es/~isidoro/. [Accessed February 15 2012]

McPherson, M.J. (2013). *Subsurface Ventilation Engineering*. 1625 Shaw Ave #103: Mine Ventilation Services, Inc. 1 - 555.

Menon, S. W., (1996). Subgrid mixing and molecular transport modeling for large-eddy simulation of turbulent reacting flows,. *Proc. Combust. Inst.*. 26 (1), 59 - 66.

Mira-Martinez, D, Jiang X, Moulinec, C and Emerson, D.R., (2013). Numerical simulations of turbulent jet flames with non-premixed combustion of hydrogen-enriched fuels . *Computational Fluids*. 88 (1), 688 - 701.

Mira-Martinez, D., Cluff D. L., Jiang X., (2014). Numerical Investigation of the Burning Characteristics of Ventilation Air Methane in a Combustion Based Mitigation System. *Fuel*. 133 (1), 182 - 193.

Mukherjee R. (1998). Effectively Design Shell and Tube Heat Exchangers. *Chemical Engineering Progress*. 1, 12.

NOAA - National Oceanic and Atmospheric Administration., (2011). *Monitoring & Understanding Our Changing Planet.* Available at: http://www.noaa.gov/features/02_monitoring/methane.html. [Accessed Feb. 22, 2012]

Noack, K., (1998). Control of gas emissions in underground coal mines. *International Journal of Coal Geology*. 35 (1), 57 – 82

Oakley G. L. and Thomas G. O., (2004). *Investigations into Concerns about Flame Arresters,* United Kingdom: UK Health and Safety Executive Research Report RR281

Oliveira, T. F. Miserda, R. B. and Cunha. F. R., (2007). Dynamical Simulation and Statistical Analysis of Velocity Fluctuations of a Turbulent Flow behind a Cube. *Mathematical Problems in Engineering*. Hindawi Publishing Corporation, Article ID 24627, (1), 1 - 28.

Panckhurst, G. Hon Justice, Bell S. and Henry D., (2012). *Royal Commission on the Pike River Coal Mine Tragedy*. 146 Mackay Street, Greymouth. New Zealand: Department of Internal Affairs . 1 - 42.

Pitsch, H., (2006). Large-Eddy Simulation of Turbulent Combustion. *Annu. Rev. Fluid Mech.*. 38 (1), 453 - 482.

Poinsot, T, Veynante, D. and Edwards R. T., (2005). *Theoretical and numerical combustion.* 3rd ed. 31400 Toulouse Cedex: Institut de Mécanique des Fluides de Toulouse. 1 - 223.

Poinsot, T. and Veynante, D., (2011). *Theoretical and numerical combustion*. 3rd ed. 31400 Toulouse Cedex: Institut de Mécanique des Fluides de Toulouse. 1 - 456.

Pope, S.B., (2000). *Turbulent Flows*. Cambridge, United Kingdom: Cambridge University Press. 1 - 770. ISBN-10: 0-521-59886-9

Pyper, W., 2003. Hybrid Turbine Powers Mine from Waste. *Ecos*, January - March, 9. Available at: http://www.ecosmagazine.com/?act=view_file&file_id=EC114p9.pdf [Accessed May 16 2013]

Revkin, A, 2012. How Natural Gas Kept Some Spots Bright and Warm as Sandy Blasted New, York City. *The New York Times*, November 05 2012. Available at: http://dotearth.blogs.nytimes.com/2012/11/05/how-natural-gas-kept-some-spots-bright-andwarm-as-sandy-blasted-new-york/ [Accessed September 19, 2013]

Reynolds, O., (1883). An experimental investigation of the circumstances which determine whether the motion of water shall be direct or sinuous, and of the law of resistance in parallel channels. *Philosophical Transactions of the Royal Society* . 174, 935 - 982.

Robinson C., and Smith D.B., (1984). The Auto-ignition Temperature of Methane, Journal of Hazardous Materials. *Journal of Hazardous Materials*. 8 (1), 199 - 203.

Saravanamuttoo, H. I. H. Rogers, G. F. C. and Cohen H., (2001). *Gas Turbine Theory*. Upper Saddle River, New Jersey 07458: Prentice Hall. 1 - 491.

Schlünder E.U., (1993). *Heat Exchanger Design Handbook*. 1025 Vermont Ave., N.W., Washington, D.C.-20005, 19 W. 44th St., New York: Hemisphere Pub. Corp. 1 - 33.

Schultz H. Mattus Lee R. and Carothers F.P., (2005). Mitigation of methane emissions from coal mine ventilation air. *In Western states coal mine methane recovery and use workshop*. Grand Junction, Colorado, April 19-20, 2005. MEGTEC Systems, De Pere, WI: Environmental Programs, BCS Inc. 1 - 10.

Schultz K., (2003). Coal Mine Ventilation Air Mitigation: Technologies to Harness and Energy and Environmental Resource. *Energeia, UK Center for Applied Energy Research*. 14 (5), 1 - 5.

Schweiger A., Lindsay R., Zhang J., Steele M., Stern H. ,and Kwok R. (2011). Uncertainty in Modeled Arctic Sea Ice Volume. *JGR Oceans, America Geophysical Union*. Accepted for publication

Scribbler, R., (2012). *Arctic Methane Concentration for August 2012 Shows Jump From August 2011, Part of Larger Arctic Trend.* Available at: http://robertscribbler.wordpress.com/2012/09/13/arctic-methane-concentration-for-august-2012-much-higher-than-august-2011/. [Accessed June 25 2013].

Sheppard, W.M., 1978. *The Simulation of Gas Turbines by a State of the Art Analogue Device*. M.Sc. Thesis Ocean Engineering. Massachusetts: MIT.

Simpson, I.J., Sherwood R.F. Meinardi, S. and Blake, D.R. (2006). Influence of biomass burning during recent fluctuations in the slow growth of global tropospheric methane. *Geophysical Research Letters*. 33 (22), 1 - 5.

Sindicatum Sustainable Resources. (2012). *Duerping Phase 1& 2*. Available at: http://www.sindicatum.com/portfolio/duerping/. [Accessed November 15, 2012]

Smagorinsky J., (1963). General Circulation Experiments with the Primitive Equations. *Monthly Weather Review* . 91 (3), 99 - 164.

Smith C.L. et. al., (2004). *Final Report on the August 14, 2003 Blackout in the United States and Canada: Causes and Recommendations*. Canada, USA: U.S.-Canada Power System Outage Task Force. 1 - 223.

Solomon S., D., Qin, M., Manning Z. Chen, M. Marquis, K.B. Averyt, M. Tignor and H.L. Miller (Eds.)., (2007). *Contribution of working group I to the fourth assessment report of the intergovernmental panel on climate change*. United Kingdom and New York, NY, USA: Cambridge University Press. 1 - 996.

Somers J.M. and Schultz H.L., (2009). *Coal mine methane ventilation air emissions: new mitigation technologies*. Climate Change Division: U.S. Environmental Protection Agency. 1 - 12.

Somers, J.M. and Burklin, C., (2012). A 2012 update on the world VAM oxidizer technology market. *In 14th United States/North American Mine Ventilation Symposium, 2012 – Calizaya & Nelson (Eds)*. University of Utah, 2012. Utah, USA: University of Utah, Dept. of Mining Engineering. 259 - 263.

Somers, J.M. and Schultz H.L., (2008). Thermal oxidation of coal mine ventilation air methane. *In 12th US/North American Mine Ventilation Symposium, Wallace (Ed)*. Reno, Nevada, June 9 - 11, 2008. Reno, Nevada: University of Nevada, Reno. 301 - 306.

Somers, J.M. and Schultz H.L., (2010). Coal mine ventilation air emissions: project development planning and mitigation technologies. *In 13th United States/North American Mine Ventilation Symposium, 2010 – Hardcastle & McKinnon (Eds.)*. Sudbury, Ontario, 2010. Sudbury, Ontario: MIRARCO. 115 - 121.

Stokes, G.. (1851). On the Effect of the Internal Friction of Fluids on the Motion of Pendulums. *Transactions of the Cambridge Philosophical Society*. 9, 8 - 106.

Strahan D. (Ed), Radcliffe J. and Williams R.A. et al (May 9, 2013). *Liquid Air in the energy and transport systems, Opportunities for industry and innovation in the UK*. United Kingdom: The Centre for Low Carbon Futures. 1 - 67.

Su, S. Beath, A. Guo, H. Mallett, C., (2005). An assessment of mine methane mitigation and utilisation technologies. *Progress in Energy and Combustion Science*. 31 (1), 123 - 170.

Taylor, B. (1715). *Methodus Incrementorum Directa et Inversa [Direct and Reverse Methods of Incrementation], (Proposition VII, Theorem 3, Corollary 2)*.

London, United Kingdom: Royal Society. 21 - 23.

The Enginering Toolbox. (2013). *The Saturated Steam Table with properties as boiling point, specific volume, density, specific enthalpy, specific heat and latent heat of vaporization.* Available at: http://www.engineeringtoolbox.com/saturated-steam-properties-d_457.html. [Accessed July 10 2013]

The U.S. Department of Energy. (2012). *Steam Turbine Calculator.* Available: http://www4.eere.energy.gov/manufacturing/tech_deployment/amo_steam_tool/equipTurbine. [Accessed January 20 2013]

Turns, S.R. (2000). *An Introduction to Combustion: Concepts and Applications*. 2nd ed. New York, NY: McGraw-Hill. 1 - 732.

U.S. Energy Information Services, US Department of Energy. (2010). *China dominates global coal production.* Available at: http://www.eia.gov/todayinenergy/detail.cfm?id=3350#. [Accessed December 27 2013].

U.S. Environmental Protection Agency (2012). *Inventory Of U.S. Greenhouse Gas Emissions And Sinks: 1990 - 2010*. 1200 Pennsylvania Ave., N.W.Washington, DC 20460 USA: Environmental Protection Agency. EPA 430-R-12-001.

USEPA., (2012). *Methane Emissions, Climate Change.* Available at: http://epa.gov/climatechange/ghgemissions/gases/ch4.html. [Accessed March 01 2012]

USEPA., OAR, Climate Change Division, (2010). *US Underground Coalmine Ventilation Air Methane Exhaust Characterisation*. USA: Coalbed Methane Outreach Program. 1 - 17.

USEPA., United States Environmental Protection Agency (2004). *Using ventilation air methane (VAM) as combustion air in reciprocating engines and turbines*. USA: EPA Coalbed Methane Outreach Program Technical Options Series. 1 - 4.

USEPA., United States Environmental Protection Agency, (2013). *Evaluating Climate Policy Options, Costs and Benefits, Economics, Climate Change*. Available at: http://www.epa.gov/climatechange/EPAactivities/economics.html. [Accessed September 19, 2013]

Vagelopoulos, C.N., and and Egolfopoulos,F.N., (1997). Direct Experimental Determination of Laminar Flame Speeds. *In Western States Section/Combustion Institute Meeting*. Livermore, CA, 1997. Livermore, CA: Paper WSS/CI 97S-022.

Walsh, P. and Fletcher P., (2004). *Gas Turbine Performance*. 2nd ed. Blackwell: Rolls-Royce plc. 1 - 22.

Warmuziński, K., (2008). Harnessing methane emissions from coal mining. *Proc. Safety Env. Prot.,* 86.

Wendt, J. (Ed.)., (2009). *Computational Fluid Dynamics an Introduction*. 3rd ed. New York, USA: Springer. 1 - 215.

Whiteman, G. Hope, C. and Wadhams, P., (2013). Vast costs of Arctic change. *Nature*. 499 (July), 401 - 403.

Yurganov, L.N., Xiaozhen X., and Wofsy S.C., (2012). Atmospheric Methane over the Arctic Ocean: Satellite Data. *In AGU Autumn Meeting A31* D-0062. San Francisco, California, USA, December 03 - 07, 2012. ?: American Geophysical Union. 1.

Zeldovich, Y.B., (1940). On the Theory of Propagation of Detonation in Gaseous Systems. *Zhur. Eksp. Teor. Fiz.*. 10 (1), 147 - 154.

Zhang, J. and Rotherock D.A., (2003). Modeling Global Sea Ice with a Thickness and Enthalpy Distribution Model in Generalized Curvilinear Coordinates. *American Meteorological Society*. 131 (1), 845 - 861.

Zhengzhou Coal Industry (Group) Co., Ltd. (2009). *Coalmine Methane Utilization Project, Abatement of VAM emissions and generating hot water from the energy released in VAM oxidation*. Zhengzhou: SET at Work Consortium Members. Project 1603.

Fuel 133 (2014) 182–193

Contents lists available at ScienceDirect

Fuel

journal homepage: www.elsevier.com/locate/fuel

Numerical investigation of the burning characteristics of ventilation air methane in a combustion based mitigation system

D. Mira Martinez [a,*], D.L. Cluff [b], X. Jiang [c]

[a] CASE Department, Barcelona Supercomputing Center (BSC-CNS), Barcelona 08034, Spain
[b] College of Engineering, Mathematics and Physical Sciences, University of Exeter, Exeter EX4 4QF, UK
[c] Engineering Department, Lancaster University, Lancaster LA1 4YR, UK

HIGHLIGHTS

- A new combustion mitigation system of ventilation air methane is numerically studied.
- The effects of preheating and methane concentration are revealed.
- Preheating has a significant influence on the oxidation of ventilation air methane.
- Combustion of mixtures with high methane concentration is more unsteady and vortical.

ARTICLE INFO

Article history:
Received 13 September 2013
Received in revised form 1 May 2014
Accepted 8 May 2014
Available online 23 May 2014

Keywords:
Ventilation air methane (VAM)
Greenhouse gas (GHG)
Mitigation system
Flameless oxidation
Large-eddy simulation

ABSTRACT

Large-eddy simulation of the reacting flow field in a combustion-based mitigation system to reduce the emissions of methane contained in ventilation air methane is presented. The application is based on the preheating and combustion of ventilation air methane. Effects of preheating and methane concentration are examined in five computational cases. The results indicate that the oxidation of the ventilation air methane can take place in a co-annular jet configuration provided that the preheating temperature is as high as 500 K for mixtures containing a low methane concentration of 0.5%. It is found that the oxidation process that eventually leads to reaction and combustion is controlled by the methane concentration and the level of preheating.

1. Introduction

Methane is a greenhouse gas (GHG) with a global warming potential (GWP) that varies over the atmospheric residency time [1]. Upon release to the atmosphere and using a reference value of unity for carbon dioxide, the GWP is initially 56 over the first 20 years, 21 over 100 years and 6.5 over 500 years. The radiative forcing factor of methane is second only to that of carbon dioxide. These two attributes are central to the argument that methane released to the atmosphere has an immediate effect far more intense than that of the carbon dioxide release and could be responsible for creating a short-term high temperature perturbation or positive feedback loop [2–4]. Therefore, reduction of methane releases to the atmosphere is essential to minimize these global hazards. Besides, the absence of mitigation actions not only increases the global warming effect, but also has economical implications [5].

The atmospheric concentration of methane associated with coal mining is estimated to be about 15% of the total anthropogenic methane produced, while coal handling, abandoned underground mines and surface mines represent about 26% of the total emissions [6]. The largest fraction of atmospheric methane from coal mining activities is due to the release of ventilation air methane (VAM) [7]. Methods to mitigate VAM are desirable from a global climate perspective and could be economical if the energy contained in the ventilation flow is captured. Since methane is a high impact GHG, VAM from coal mining operations or abandoned mines should be targeted for mitigation and for the development of cost effective technologies for mitigation [8].

VAM has been difficult to exploit because it is a low methane concentration high volumetric flow case. A number of technologies have been developed to mitigate VAM and there are essentially two basic methods for the mitigation and utilization of VAM: ancillary and principal uses [9]. Ancillary use is referred to as the use of

* Corresponding author. Tel.: +34 93 4054286.
E-mail address: daniel.mira@bsc.es (D. Mira Martinez).

http://dx.doi.org/10.1016/j.fuel.2014.05.022
0016-2361/

VAM as an oxidizer instead of ambient air in combustion engines, gas turbines or rotary kilns to improve combustion performance [10,11]. When the VAM replaces air in a combustion process, it is employed as a secondary fuel residing in the intake air. Higher concentration sources of methane, such as drained sources are either flared or sold to the market [9]. The principal uses for VAM as a primary fuel can be found in thermal flow reverse reactors, catalytic flow reverse reactors, lean burn gas turbines (GTs), recuperative GT or regenerative thermal oxidation [12,13]. In these instances, the VAM is oxidized when it comes in contact with ceramic beads or rock particles at a sufficiently high temperature. These systems usually require an external energy source to raise the temperature to the operating point and then it becomes sustainable as the VAM is consumed [14]. The addition of catalysts serves to reduce the oxidation temperature, but catalysts are expensive and may require replacement.

Mitigation systems based on the oxidation of the low concentration methane contained in VAM mixtures have some potential for power generation [7]. A technology based on VAM oxidation, the VamTurBurner (C) currently being developed [7], uses waste heat from gas turbine exhaust to preheat the VAM and requires a second preheating stage, where energy is drawn from downstream by a heat exchanger or recirculation system to preheat the VAM further. This configuration allows a rise in temperature to a state such that the methane may be oxidized by an igniter flame. This new multi-generation system [7] uses the total heat from a cogeneration cluster, igniters and VAM as a heat source for the production of more electricity, industrial drying, hot water, heating or cooling. These thermal outputs of the multi-generation system might be available to other industries or to a community depending on proximity and demand. The preheating of the VAM is essential to the combustion process, since it contributes to flame stability and allows the ignition to take place under restrictive operating conditions and for ultra-lean mixtures.

The study of the combustion characteristics of ultra-lean mixtures is still at an early stage. Some groups have studied the combustion of ultra-lean hydrocarbon mixtures reporting the oxidation of the mixtures under certain conditions. A comprehensive analysis of the chemical kinetics involved in the ignition of ultra-lean methane for catalytic combustion was undertaken in the work by Wang et al. [15] for the mixtures of interest here. Ignition in ultra-lean mixtures by extending the flammability limit has also been reported using subcritical microwaves [16] and preheating [17,18]. The work by Cheng et al. [19] showed that preheating extended the flammability limit for ultra-lean methane mixtures. The fuel oxidation takes place after the interaction with hot combustion products. Analysis of the flame structure for different mixtures and levels of flame stretch are found in the literature [20,21]. It was reported that ignition was very sensitive to the amount of preheating, concentration and flame stretch. Simple flame configurations have been investigated using detailed chemistry in the literature [20,21], but to the authors knowledge, the interaction of ultra-lean mixtures with a well-established turbulent flame has not been addressed.

This study aims to investigate the oxidation process and the dynamics of VAM mixtures interacting with the heat release at different preheating temperatures and methane concentrations for a simplified combustor configuration. The concept of large-eddy simulation (LES) is employed in the present work and similar reacting conditions as those found in mild combustion [22,23] are investigated here. The difference in this case is that there is no recirculation zone to mix reactants and products to achieve lean premixed conditions, since the lean homogeneous fuel mixture or VAM is directly supplied. The challenges of this configuration are associated with finding adequate operating conditions (preheating temperature and fuel concentration) for low concentration methane streams, so that VAM mixtures can be burnt in practical combustors.

This paper starts with an introduction of the background and motivation of the study. It is followed by the description of the governing equations and the theoretical aspects of the numerical strategy, while results for instantaneous and time-averaged flow fields are described and analyzed subsequently. Finally, some conclusions and directions for future work are also given.

2. Mathematical modelling

The analysis of the combustion dynamics of mixtures containing different methane concentrations is addressed here using large-eddy simulation. In LES, the large-scale structures of the flow are resolved by governing equations, while the small-scales are modelled using closure rules [24]. The flow field is filtered in space using a box filter given by $\Delta = V^{1/3}$, where V represents the cell volume.

In order to reduce the complexity of filtering variables with density variations, a Favre-averaged filtering is employed [25]. The filtering process is given by $\widetilde{f} = \overline{\rho f}/\overline{\rho}$, where '$\overline{\ }$' is used for space-filtered quantities and '$\widetilde{\ }$' for Favre-averaged variables. The LES governing equations for multi-species reacting compressible flows are presented in the next section, which include the conservation of mass, momentum, energy and species mass fractions respectively.

2.1. LES governing equations

The filtered governing equations for LES are given by:

$$\frac{\partial \overline{\rho}}{\partial t} + \frac{\partial (\overline{\rho}\widetilde{u}_j)}{\partial x_j} = 0 \tag{1}$$

$$\frac{\partial (\overline{\rho}\widetilde{u}_i)}{\partial t} + \frac{\partial (\overline{\rho}\widetilde{u}_j\widetilde{u}_i)}{\partial x_j} = -\frac{\partial \overline{p}}{\partial x_i} + \frac{\partial \overline{\tau}_{ij}}{\partial x_j} - \frac{\partial \tau_{ij}^{sgs}}{\partial x_j} \tag{2}$$

$$\frac{\partial (\overline{\rho}\widetilde{e})}{\partial t} + \frac{\partial (\overline{\rho}\widetilde{u}_j\widetilde{e})}{\partial x_j} = -\overline{p}\frac{\partial \widetilde{u}_j}{\partial x_j} - \frac{\partial \overline{q}_j}{\partial x_j} + \overline{\tau}_{ij}\frac{\partial \widetilde{u}_i}{\partial x_j} - \frac{\partial h_j^{sgs}}{\partial x_j} + \Theta^{sgs} + \overline{\dot{Q}^c} \tag{3}$$

$$\frac{\partial (\overline{\rho}\widetilde{Y}_m)}{\partial t} + \frac{\partial (\overline{\rho}\widetilde{u}_j\widetilde{Y}_m)}{\partial x_j} = \frac{\partial}{\partial x_j}\left(\overline{\rho}\overline{D}_m\frac{\partial \widetilde{Y}_m}{\partial x_j}\right) - \frac{\partial \Phi_{j,m}^{sgs}}{\partial x_j} + \overline{\dot{\rho}_m^c} \quad m = 1,\ldots,N \tag{4}$$

where $\overline{\rho}$, t, $\widetilde{u}_i$, x_i, $\overline{p}$, $\overline{\tau}_{ij}$, $\widetilde{e}$, $\overline{q}_i$, $\dot{Q}^c$, $\widetilde{Y}_m$ and $\overline{\dot{\rho}}_m^c$ are the density, time, ith velocity component with $i = 1, 2, 3$ in Cartesian coordinates, pressure, stress tensor, internal energy, heat flux, combustion heat release, species mass fraction and the source term due to chemical reactions respectively. The index $m = (1$ to $N)$ denotes the individual species, while the superscript *sgs* refers to the subgrid scale terms coming from the filtering process.

The filtered stress tensor $\overline{\tau}_{ij}$ is obtained neglecting the effect of the unresolved field [26] and is given by:

$$\overline{\tau}_{ij} = \overline{\mu}\left[\left(\frac{\partial \widetilde{u}_i}{\partial x_j} + \frac{\partial \widetilde{u}_j}{\partial x_i}\right) - \frac{2}{3}\frac{\partial \widetilde{u}_k}{\partial x_k}\delta_{ij}\right] \tag{5}$$

where μ represents the dynamic viscosity and δ_{ij} is the Kronecker delta. The temperature-dependent viscosity $\mu(T)$ is obtained from the Sutherland's law [27], while the filtered heat flux $\overline{q}_j$ is given by:

$$\overline{q}_j = -\overline{K}\frac{\partial \widetilde{T}}{\partial x_j} + \overline{\rho}\sum_{m=1}^{N}\widetilde{h}_m\overline{D}_m\frac{\partial \widetilde{Y}_m}{\partial x_j} \tag{6}$$

where $\overline{K}$, $\widetilde{T}$, $\overline{D}_m$, and $\widetilde{h}_m$ are the filtered thermal conductivity, temperature, diffusion coefficient and enthalpy of species m respectively. The heat conductivity is obtained by providing a constant

Prandtl number for each species contained in the flow field $K = \mu c_p/Pr$, while the equivalent diffusion coefficient of the mth species into the mixture D_m used in the calculations is obtained as [25]:

$$D_m = \frac{1 - Y_m}{\sum_{k \neq m}^{N} X_k / D_{km}} \tag{7}$$

where c_p is the heat capacity at constant pressure obtained from JANAF tables for a multi-component mixture and X_k is the species mole fraction of the kth species.

The subgrid scale terms τ_{ij}^{sgs}, h_j^{sgs}, Θ^{sgs} and $\Phi_{j,m}^{sgs}$ represent the unresolved momentum transport, the unresolved heat flux, the subgrid scale dissipation term and the subgrid scale species mass flux respectively. Note that the velocity–pressure gradient correlation term is neglected from the energy equations because of its negligible contribution to the energy equation. The subgrid scale diffusive mass flux was also neglected from the species conservation equations for the same reason [28].

The filtered reaction rates given in Arrhenius form are modelled without distinguishing between the resolved and unresolved scales. The reaction rates have been expressed in terms of the filtered variables and the effects of the subgrid scale motions are not considered in the reaction rates. The results are expected to provide estimations of the scalar fields that can be further improved by using a more precise reaction rate filtering approach.

The subgrid scale momentum transport is modelled using a one-equation model proposed by Menon et al. [29] including the subgrid scale turbulent kinetic energy k^{sgs}. This model is known to account for the local non-equilibrium between energy production and dissipation. The subgrid scale stress τ_{ij}^{sgs} in the momentum equation is modelled using the turbulent viscosity $v_t = C_v\sqrt{k^{sgs}}\Delta$, while the unresolved stress is obtained as:

$$\tau_{ij}^{sgs} = -2v_t\left(\widetilde{S}_{ij} - \frac{1}{3}\widetilde{S}_{kk}\delta_{ij}\right) + \frac{2}{3}\overline{\rho}k^{sgs}\delta_{ij} \tag{8}$$

where C_v is a constant set to be 0.067 [26], $\widetilde{S}_{ij}$ is the filtered strain rate and the subgrid turbulent kinetic energy k^{sgs} is obtained after solving the following transport equation:

$$\frac{\partial \overline{\rho}k^{sgs}}{\partial t} + \frac{\partial \overline{\rho}\tilde{u}_j k^{sgs}}{\partial x_j} = -\tau_{ij}^{sgs}\frac{\partial \tilde{u}_i}{\partial x_j} + \frac{C_\varepsilon \overline{\rho}(k^{sgs})^{3/2}}{\Delta} + \frac{\partial}{\partial x_j}\left(\frac{\overline{\rho}v_t}{Pr_t}\frac{\partial k^{sgs}}{\partial x_j}\right) \tag{9}$$

where Pr_t is the turbulent Prandtl number set as 1.0 and C_ε is a model constant set as 0.916 [26].

The heat flux in the subgrid scale h_j^{sgs} as well as the subgrid scale species mass flux $\Phi_{j,m}^{sgs}$ are both modelled using a gradient diffusion approach [25]:

$$h_j^{sgs} = -\overline{\rho}\frac{v_t c_p}{Pr_t}\frac{\partial \widetilde{T}}{\partial x_j} \tag{10}$$

$$\Phi_{j,m}^{sgs} = -\overline{\rho}\frac{v_t}{Sc_t}\frac{\partial \widetilde{Y}_m}{\partial x_j} \tag{11}$$

where Sc_t is the turbulent Schmidt number. The subgrid scale viscous work Θ^{sgs} in the energy equation is given by:

$$\Theta^{sgs} = \frac{C_\varepsilon \overline{\rho}(k^{sgs})^{3/2}}{\Delta} \tag{12}$$

2.2. Chemical kinetics

The four-step reduced mechanism proposed by Jones and Lindsted [30] is employed here to account for the chemical kinetics involved in the oxidation of methane. The reduced chemical scheme was derived based on the analysis of the flame structure showing good agreement with experimental data when compared for flame speed, flame thickness and species profiles within the flammability regime [30–32]. The assessment of the chemical scheme employed in the numerical simulations is undertaken by comparing the predictions of flame temperature for methane in the ultra-lean regime with the detailed mechanism GRI-mech 3.0 [33], which contains 53 species undergoing 325 reactions. The results were compared using the code PREMIX [34] and the predictions in the ultra-lean regime with a preheating temperature of 500 K are acceptable as shown in Fig. 1.

The chemical kinetic mechanism involves four reversible chemical reactions comprising seven species (CH_4, CO_2, O_2, CO, H_2O, H_2 and N_2) and is summarised in Table 1.

2.3. Numerical methods

The Favre-averaged governing equations for a compressible multi-species flow are solved using a parallel code based on the finite-volume approach. The equations are solved in two stages allowing an implicit solver for the diffusion, and an explicit quasi-second order upwind scheme for the advection [35]. The code has been validated and compared to experimental data in a previous study [28], where details of the parallel efficiency and the numerical schemes were also provided.

3. Application setup

This study aims to examine the feasibility of burning a stream of VAM by an existing flame in order to reduce the emissions of global warming gases. The VAM is usually released to the atmosphere because existing technologies still have difficulty making use of the methane contained in the VAM flow [7]. As a result, about 70% of the methane emissions of the mine occurs as VAM and are released to the atmosphere without any treatment or processing. A mitigation system capable of burning the low methane

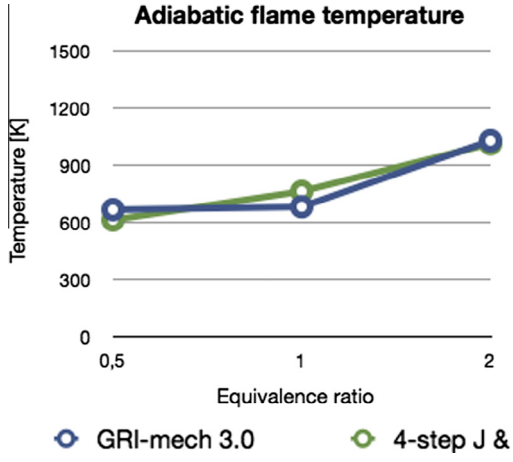

Fig. 1. Comparison of the four-step reduced mechanism with the GRI-mechanism 3.0.

Table 1
4-step reduced kinetic mechanism for CH_4/O_2 oxidation.

Reaction	
I	$CH_4 + 1/2O_2 \rightleftharpoons CO + 2H_2$
II	$CH_4 + H_2O \rightleftharpoons CO + 3H_2$
III	$H_2 + 1/2O_2 \rightleftharpoons H_2O$
IV	$CO + H_2O \rightleftharpoons CO_2 + H_2$

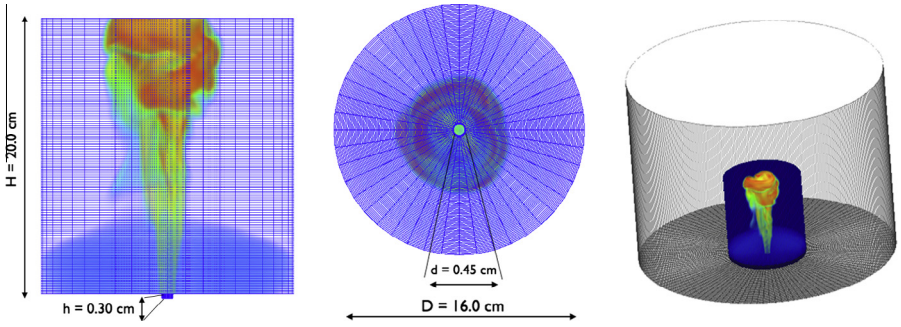

Fig. 2. Description of the computational domain (left and middle plots) and embedded domain in a realistic configuration (right plot).

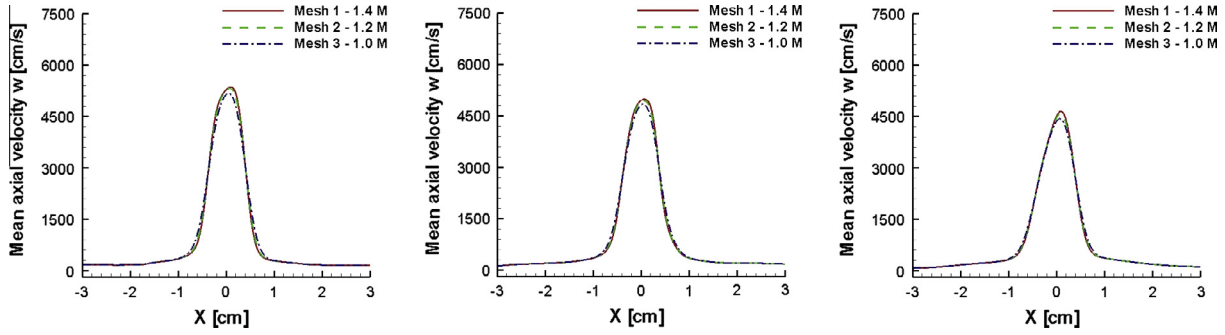

Fig. 3. Mean axial velocity component profile for the three meshes at three axial locations $Z = 2.0$ cm (left), $Z = 4.0$ cm (middle) and $Z = 6.0$ cm (right).

concentration stream not only produces benefits from the reduction of the global warming potential of the VAM, but also provides an alternative local energy source. The objective of this work is to provide some insights into the conditions required for the oxidation of these mixtures as well as the flame dynamics under conditions of interest for practical applications. The following sections describe the computational domain and the computational cases selected to address this application.

3.1. Computational domain

The computational domain chosen to study the oxidation process of a VAM mixture corresponds to a simple jet flame configuration in which the low concentration fuel is injected as a reacting co-flow. Provided a jet flame is already established in the combustor, the VAM stream is oriented toward the combustor surrounding the flame in a duct configuration. The configuration is shown in Fig. 2, where three main regions can be identified. The grey region in the right-hand side plot of Fig. 2[1] corresponds to a real-sized combustion chamber and the blue zone embedded in it is the computational domain used for the simulations. The primary fuel injection pipe used to burn the VAM mixture can be distinguished in the left-hand side plot of Fig. 2. The domain represents only a small portion of the required mitigation systems allowing an accurate study of the unsteady reacting flow by large-eddy simulation. This configuration permits the investigation of the ignition of the VAM at the boundary of the established jet flame and the subsequent oxidation of the VAM stream. This is considered a preliminary test for more sophisticated and appropriate configurations such as annular burners with swirling effects that improve the mixing and combustion [36,37].

A non-polar mesh system is used to represent the cylindrical computational domain. The radial direction is of a diameter $D = 16.0$ cm, which was proved to be sufficient to allow the flame spreading for all the computational cases, while the domain length was set as $H = 20.0$ cm to study the near field of the flow. The computational domain also includes a 0.3 cm section of the inlet channel of the primary fuel (see Fig. 2).

The nozzle of the primary fuel supply to develop a diffusion flame (also referred here as primary flame) has a diameter of $d = 0.45$ cm with a bulk velocity of 5000.0 cm/s. The secondary fuel supply (VAM mixture) has a bulk velocity of 135 cm/s (0.5–2.0% CH_4 + 99.5–98% air) and comes in from an annular duct with an external diameter of $D = 16.0$ cm.

The boundary conditions considered in this problem are non-slip for the inner wall of the primary fuel nozzle with a diameter $d = 0.45$ cm (see Fig. 2), while continuative outflow conditions are specified at the downstream and azimuthal boundaries of the domain. A top-hat velocity profile is specified at the inlet of the primary fuel and the VAM co-flowing mixture.

A convergence analysis was addressed to evaluate and select a suitable mesh for this problem. Three different meshes with 1.4, 1.2 and 1.0 million cells were tested for this purpose simulating the methane flame used to ignite the VAM mixture with a co-flowing air. The results for the time-averaged streamwise velocity at three axial locations are presented in Fig. 3. The results show some minor differences between the meshes investigated at capturing the peak values; however, the trends are well predicted in all three cases. Considering the efficiency and accuracy in the

Table 2
Computational cases.

Name	CH_4 concentration	Preheating temperature
Case A	1.0%	300 K
Case B	1.0%	400 K
Case C	1.0%	500 K
Case D	0.5%	500 K
Case E	2.0%	500 K

[1] For interpretation of colour in Figs. 2 and 5, the reader is referred to the web version of this article.

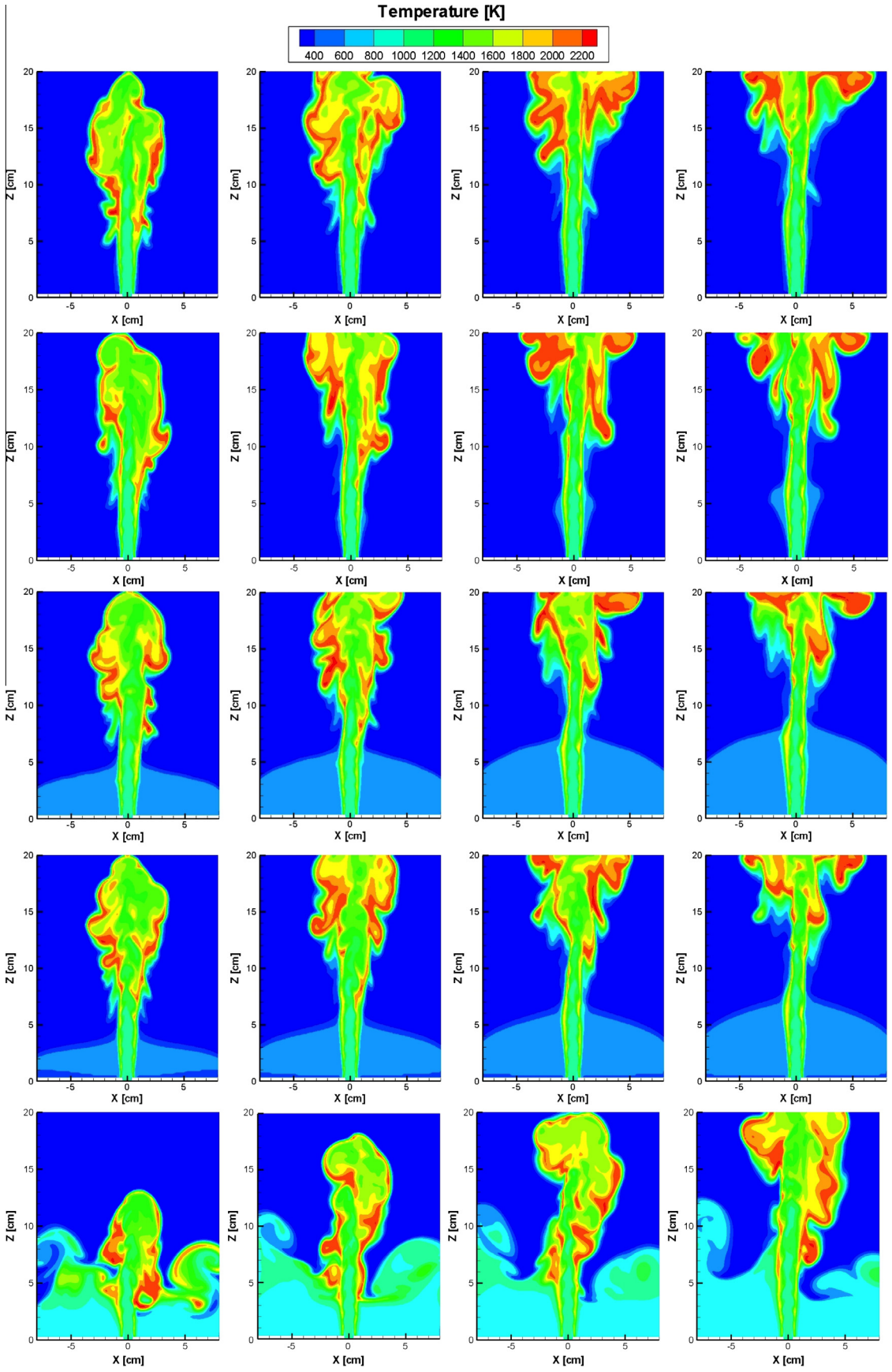

Fig. 4. Cross-sectional temperature contour plots at different time instants from left to right $t = 0.015$ s, 0.020 s, 0.025 s and 0.030 s for Case A (top) to Case E (bottom).

numerical simulations, the mesh with 1.2 million elements is used throughout the study.

3.2. Computational cases

Five computational cases are considered in this study to evaluate some suitable conditions for which VAM mixtures can be burnt in practical applications. For a simple jet flame configuration and the VAM mixture issued as a reacting co-flow, the five computational cases presented in Table 2 are investigated. These cases are selected to evaluate the effects of methane concentration and the VAM preheating temperature on the combustion dynamics of this simple mitigation system. Cases A, B and C are 1.0% methane with the preheating temperature of 300 K, 400 K and 500 K respectively. Maintaining a constant methane concentration with increasing preheating temperature serves to benchmark the effect of increasing preheating. Cases D and E are the lowest and highest methane concentrations of 0.5% and 2.0% respectively and are subject to the highest preheating temperature, as that in Case C, of 500 K. Cases C–E serve to benchmark the effect of high preheating as the methane concentration increases.

4. Results

The results of the large-eddy simulations of the computational cases described above are presented in this section. The results are divided into two separate subsections: Instantaneous results in which flame dynamics and vortical structures can be observed and time-averaged results for which mean variables and general trends are examined.

4.1. Instantaneous results

Instantaneous temperature contour plots at the middle plane $Y = 0$ of the domain for the five computational cases are presented in Fig. 4. It is observed that for a VAM mixture of 1.0% CH_4, the oxidation of VAM only takes place after the gas is preheated up to 500 K. In this case, the existence of a primary flame is observed, which acts as a source of ignition for the VAM mixture and the formation of a flameless oxidation zone in the co-flowing VAM.

No substantial differences can be discerned between the flow dynamics in Cases A and B and the flow field is rather similar in both cases. However, the last snapshot in Case B displays some evidence of the initiation of local oxidation of the VAM mixture in the region surrounding the core of the primary flame. Combustion in this region is initiated at the reacting shear layer between the two streams and is largely affected by advective effects. The temperature of the VAM mixture is increased by the heat released by the jet flame inducing the VAM oxidation. It is seen that after some time, partial ignition with combustion at low temperature might occur.

After further increasing the preheating temperature (Case C), the VAM mixture oxidizes as soon as the mixture enters the domain establishing a stable and uniform low temperature reaction zone upstream near the nozzle exit. The primary flame seems to be unaffected and the oxidation of the VAM mixture develops homogeneously downstream without showing significant interactions.

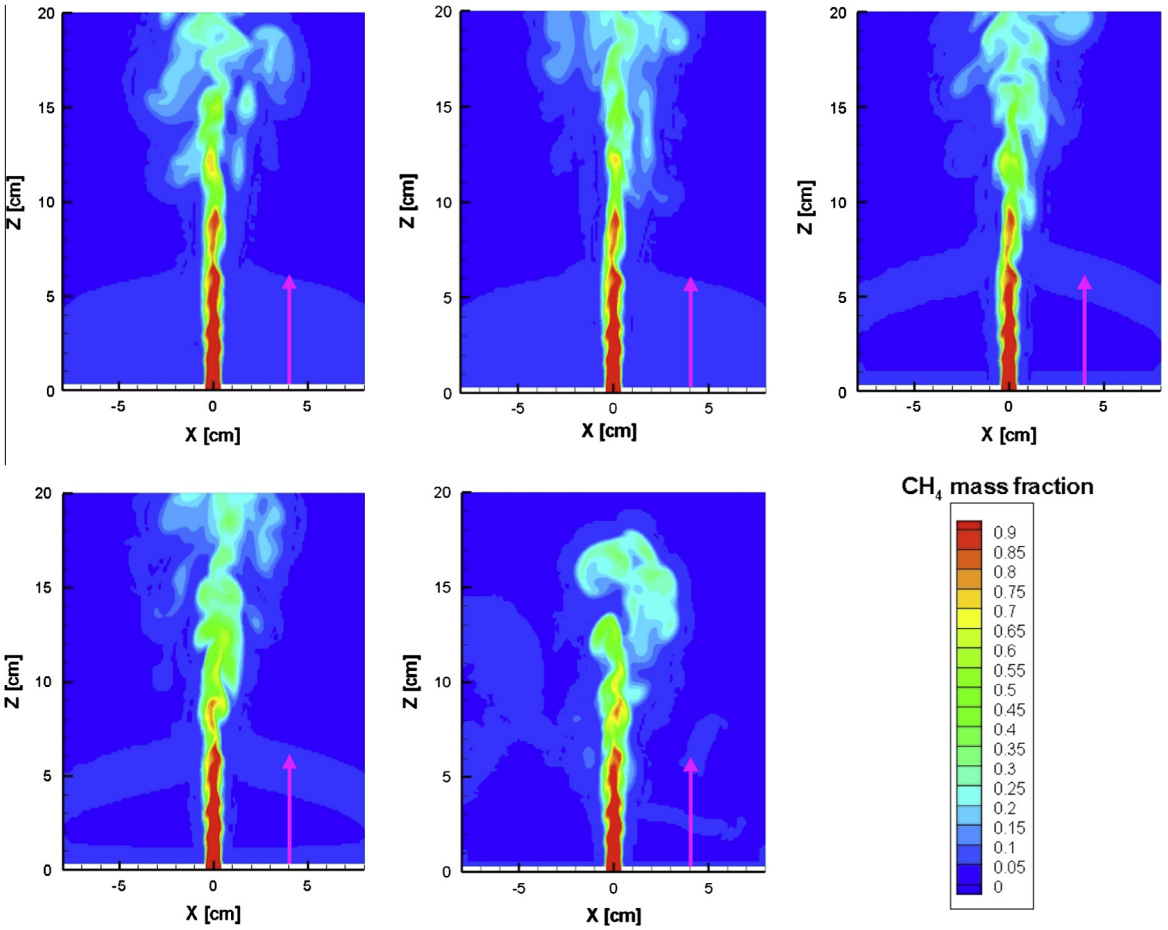

Fig. 5. Cross-sectional fuel mass fraction Y_{CH4} contour plots at time instant $t = 0.020$ s for Cases A to E from left to right.

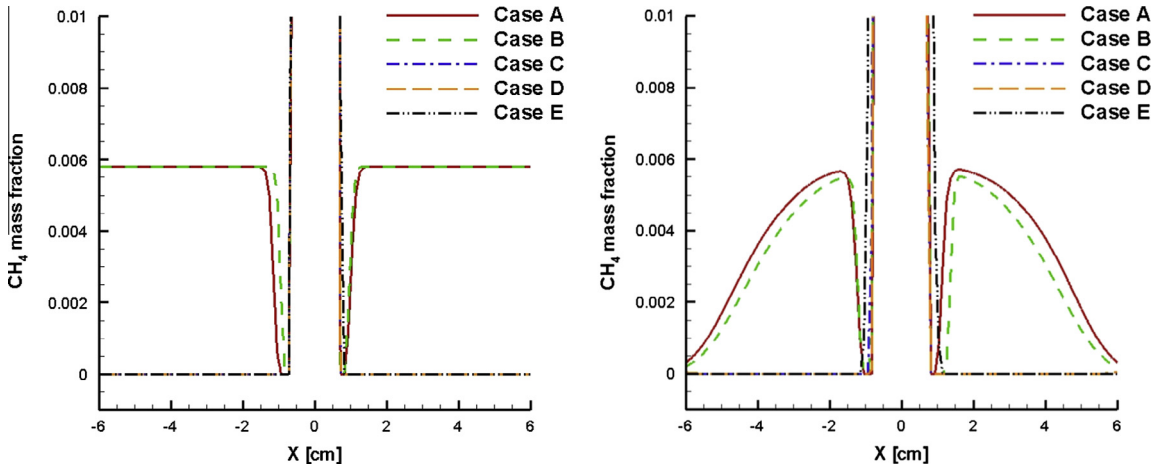

Fig. 6. Zoomed profile of the methane mass fraction Y_{CH4} at two axial locations $Z = 2.0$ cm (left) and $Z = 4.0$ cm (right).

Table 3
Location of the monitoring points.

Monitoring points	Location (x,y,z) (cm)
*P*1	(3.0, 0.0, 0.5)
*P*2	(5.0, 0.0, 0.5)

The analysis of Cases A–C, demonstrates the effect of increasing preheating temperature on a VAM flow of constant methane concentration. It is shown that increasing the preheating temperature of the incoming VAM flow has a strong impact on the ignition mechanism of the VAM mixture causing the oxidation despite the relatively low concentration of the VAM.

The effects of increasing the methane concentration can be observed by comparing Cases C and D with E. It is observed that for ultra-lean methane mixtures, the preheating temperature has a strong impact on the oxidation mechanism of the mixtures, while the fuel concentration largely affects the flow field. For the conditions under investigation, the flammability limit of the VAM has been extended substantially by preheating the mixture leading to the oxidation of the three mixtures. Nevertheless, the fuel concentration at high temperature could lead to unstable flames as shown in Case E. In Cases C and D, the flame front has a smooth profile, which is evidence of flameless oxidation, while Case E shows a vortical flame front in the VAM stream at higher temperature. This reacting layer diffuses more heat to the preheating zone creating hot spots and inducing vortical structures (see the 0.03 s Case E cross section in Fig. 4). The heat released induces large density variations and strong pressure gradients leading to a more vortical and unstable flame. The dynamics of Case E are more complex than any of the lower methane concentration cases. As the methane concentration increases, an enhanced flame spreading is observed due to the influence of thermal conduction, oxidation of fuel in a CH_4-rich environment and the formation of dynamic vortical structures. Case D shows that the low methane concentration of the VAM can be oxidized provided that a sufficiently preheated flow exists. Because a smaller amount of methane is consumed in Case D, the reacting zone progresses slower than that of Case C. However, higher preheating conditions at high methane concentration may lead to unsteady flames (see Case E in Fig. 4) and potential blow off.

The distribution of the methane concentration over the domain can also be used to further understand the combustion dynamics of the VAM mixtures. Fig. 5 shows the CH_4 mass fraction for the five computational cases at given time instant with a purple arrow added to represent the distance travelled by the VAM stream at that time instant. From Figs. 4 and 5, it can be deduced that there is no methane oxidation in Cases A and B, while for Case C, the methane at upstream location is mostly consumed. The absence of methane at upstream locations provides clear evidence of the flameless oxidation surrounding the primary reacting zone. This

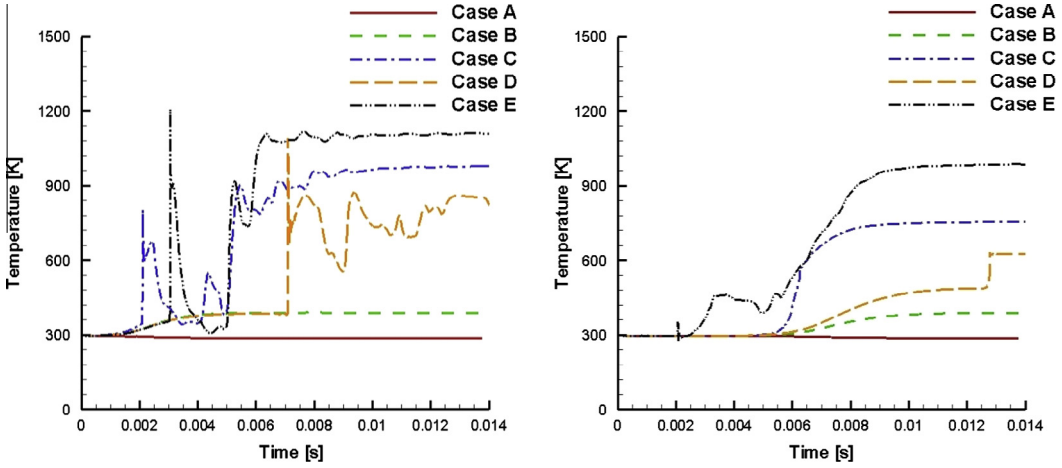

Fig. 7. Time traces of temperature of two points located in the VAM mixture *P*1(3.0, 0.0, 0.5) (left) and *P*2(5.0, 0.0, 0.5) (right).

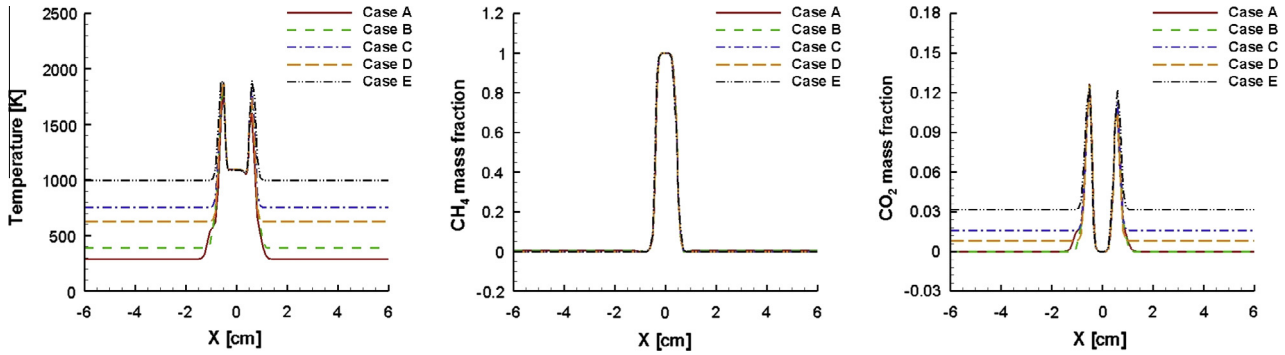

Fig. 8. Radial profiles of scalars (T, CH_4 and CO_2) at the axial location $Z = 2.0$ cm at the time instant $t = 0.020$ s.

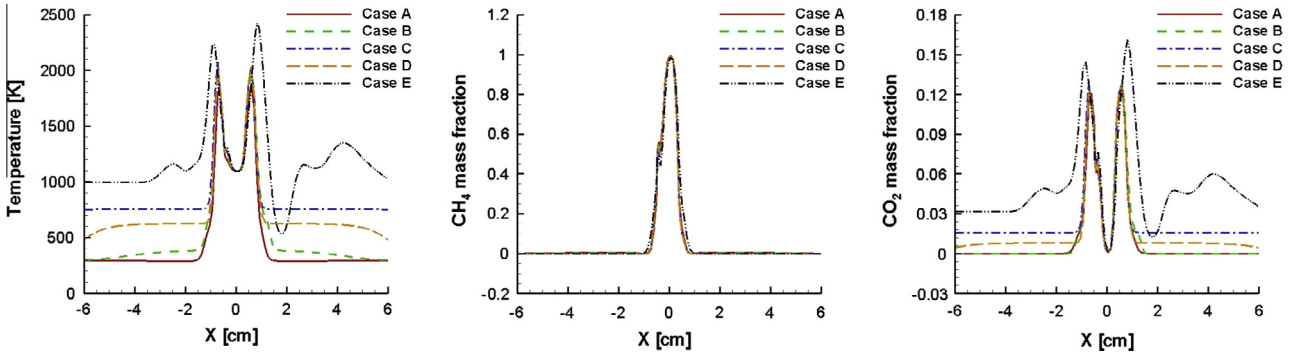

Fig. 9. Radial profiles of scalars (T, CH_4 and CO_2) at the axial location $Z = 4.0$ cm at the time instant $t = 0.020$ s.

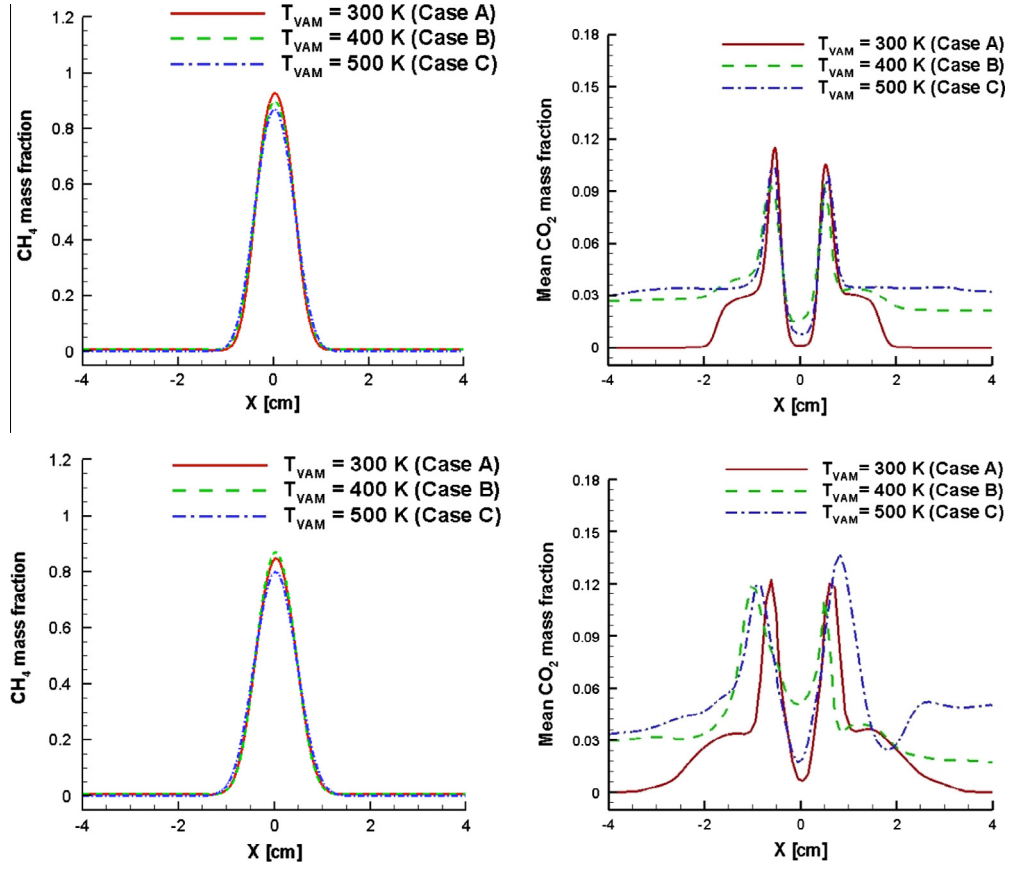

Fig. 10. Time-averaged species mass fraction profiles ($\overline{Y}_{CH_4}$ and $\overline{Y}_{CO_2}$) at two axial locations $Z = 2.0$ cm (top) and $Z = 4.0$ cm (bottom).

can be seen in Fig. 6 where a zoomed view of the profiles of methane mass fraction is shown at two axial locations. It indicates that the methane contained in the VAM of Cases A and B did not interact with the primary flame, while it was mostly consumed in the other cases. The primary flame tends to push the cold VAM mixture radially, although as the preheating increases, the two streams become closer until the oxidation takes place.

Time series analysis of data for temperature located at selected monitoring points near the flame core in the reacting zone can be used to investigate the ignition timing of the mixtures. Table 3 describes the location of the monitoring points. The time evolution of temperature at two locations (P1 and P2) close to the VAM inlet for the given mixtures is presented in Fig. 7. Cases A and B show that there is no reaction of the VAM mixture with the primary reaction zone, although the VAM stream in Case B is slightly heated. The temperature evolution for Case C indicates a low temperature oxidation after a delay for which the temperature of the VAM rises up to 800 K. Case D shows a similar evolution to Case C, but with a larger reaction initiation at a lower temperature due to the lower methane concentration. Finally, Case E is characterised by some oscillatory behaviour of temperature with time, which is caused by the increase of the oxidation reaction rate at the boundary of the primary reacting zone and throughout the VAM flow. This oscillatory behaviour is mainly induced by the local rapid burning of methane and the replacement of the fluid parcel by air.

Profiles of temperature and species mass fractions also provide some important information about the dynamics of these flames. These are presented in Figs. 8 and 9 by means of radial profiles at two different streamwise locations. Upstream (see Fig. 8), it is observed that the temperature peaks are found in the shear layer of the primary flame and no substantial differences can be found among the mixtures. The effects of preheating and methane concentration in the VAM have shown to have a low impact on the dynamics of the primary flame, except in Case E. This case shows an increase in flame thickness that is not observed in the other cases, which is caused by the enlargement of the reacting shear layer of the flame by the fuel content of the oxidizer.

The carbon dioxide mass fraction profile shows that its concentration is highly influenced by the initial methane concentration. This demonstrates that small differences in the methane concentration in the VAM mixture have a strong impact on the production of carbon dioxide and act as a good confirmation that the desired methane oxidation reaction occurs. At downstream locations, the radial temperature distribution at $Z = 4.0$ cm contains several peaks caused by the fast oxidation of the VAM mixture. These peaks are associated with the enlarged flame shear zone and correspond to the unsteady flames as seen for Case E.

4.2. Time-averaged results

The time-averaged results presented in this section are obtained after two flow through calculations and time-integrated for another two flow through times. These data are used to statistically determine the mean values of the flow fields. The results are

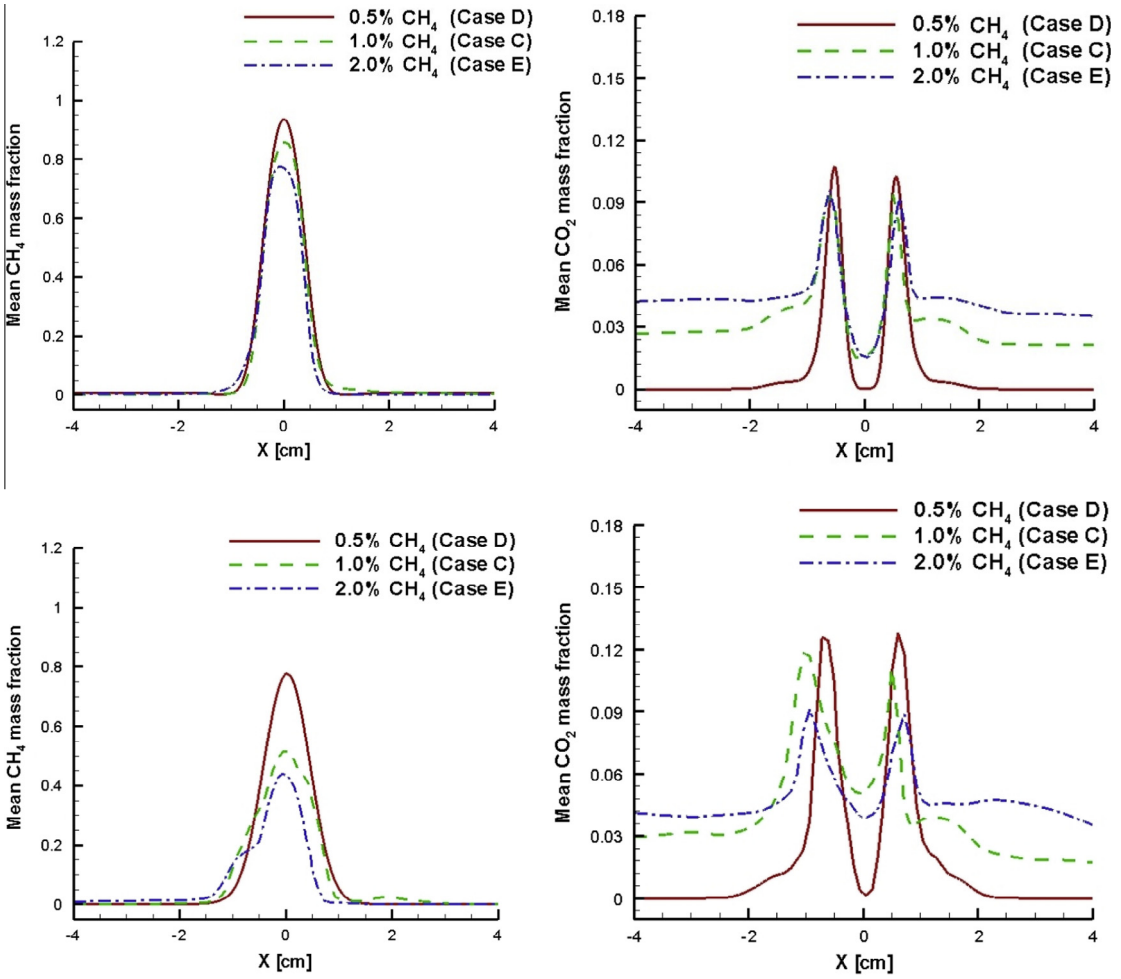

Fig. 11. Time-averaged species mass fraction profiles ($\overline{Y}_{CH_4}$ and $\overline{Y}_{CO_2}$) at two axial locations $Z = 2.0$ cm (top) and $Z = 4.0$ cm (bottom).

separated in two categories in order to study independently the effects of preheating and methane concentration on the burning characteristics of VAM mixtures.

The effects of preheating the mixture can be observed in Fig. 10 for Cases A–C. The profiles show that the preheating enhances the oxidation process because the energy level of the mixture is close to its activation energy; thus the heat required to oxidize the mixture is substantially reduced. It is observed that higher preheating temperatures lead to increased burning rates, since the flame becomes larger and the reaction zone enlarges.

The flame length is shorter and the flame spreading increases for high preheating temperatures due to the oxidation of the co-flowing VAM. The plot showing the combustion product CO_2 clearly indicates the location of the flame front and shows the large spreading experienced by the flame in Case C. Note that the plots on the right-hand side of Fig. 10 shows asymmetric results indicating that the time integration might need to be extended to achieve statistically fully converged results, although it would not affect the trends described here.

The effects of methane concentration at the fixed preheating temperature of 500 K can be examined by considering Cases C–E as shown in Fig. 11. For the higher concentration VAM mixtures, the flame length reduces substantially. Above a concentration of 1% methane, most of the methane contained in the co-flow mixture burns producing large amounts of carbon dioxide. Combustion of the high methane concentrated flow also provides more heat by conduction, which assists the burning of the incoming VAM. The peak values of CO_2 production by the flames seem to be rather similar in all cases with methane concentration above 1%. This difference, observed in the bottom-right plot of Fig. 11, is caused by the flame shortening experienced by Case E, where a large unsteady and vortical flame is formed after the VAM oxidation.

4.3. Study of the mixing process

In this section, the concept of unmixedness is introduced and examined for the mixtures under investigation. The temporal unmixedness is a factor used to describe the degree of mixing between fluid streams [38,39] and is obtained following Fric et al. [40] as:

$$Z_{unmix} = \frac{Y_f'^2}{\overline{Y}_f(1-\overline{Y}_f)} \tag{13}$$

where $Y_f'^2$ represents the standard deviation obtained from the instantaneous fuel concentration field and $\overline{Y}_f$ is the average fuel concentration at that location. Note when Z_{unmix} is zero, the fuel is completely mixed and homogeneously distributed, while there is

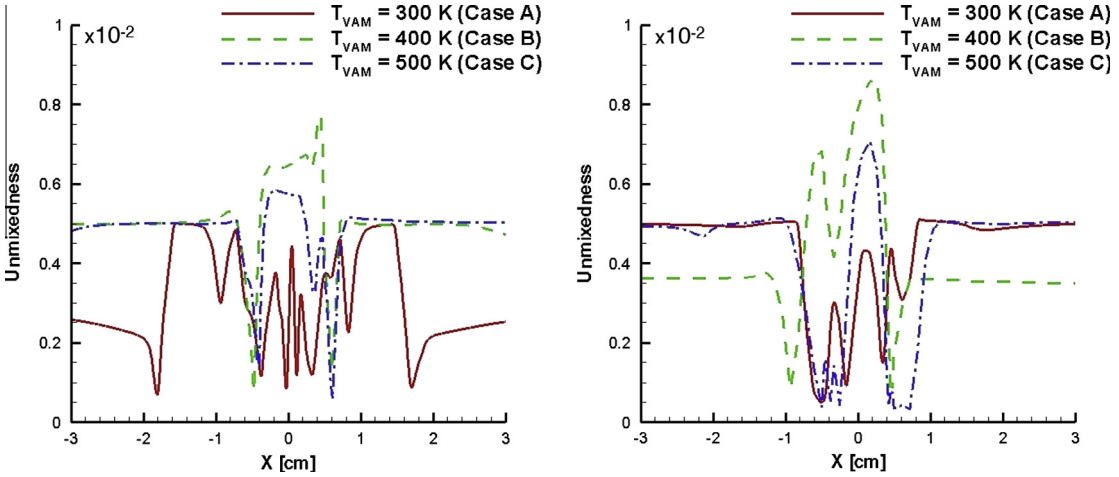

Fig. 12. Radial profiles of the unmixedness at two axial locations $Z = 2.0$ cm (left) and $Z = 4.0$ cm (right).

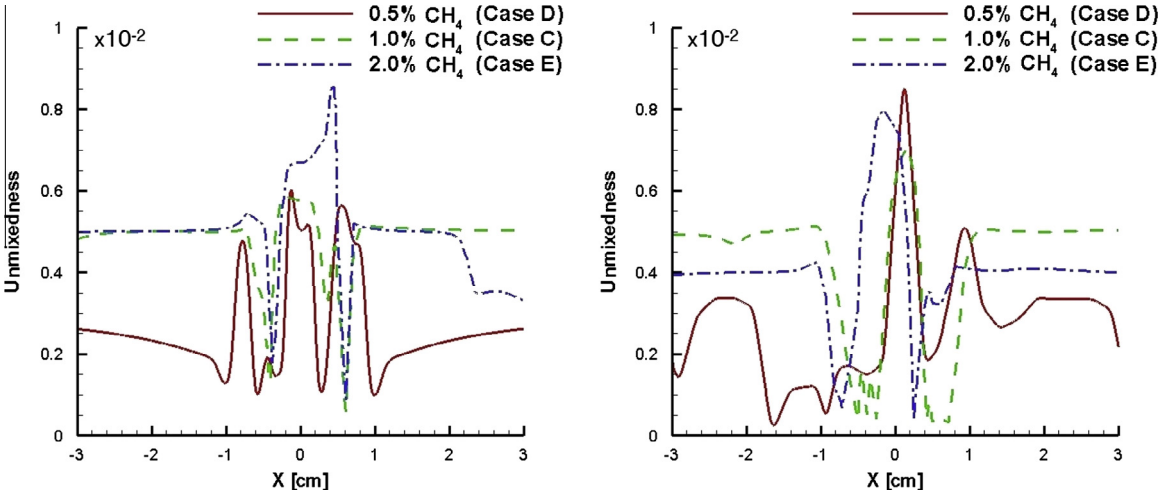

Fig. 13. Radial profiles of the unmixedness at two axial locations $Z = 2.0$ cm (left) and $Z = 4.0$ cm (right).

no mixing when Z_{unmix} is equal to unity. Values of Z_{unmix} close to unity would indicate large fluctuations of fuel mass fraction and shear mixing. The examination of the unmixedness factor at different axial locations shown in Figs. 12 and 13 provide some information concerning the mixing process between the primary flame and the VAM mixture.

The results corresponding to the cases with preheating temperature variation are shown in Fig. 12. Case A shows high degree of mixing between the primary fuel and the VAM stream with strong oscillations in the jet core. This high level of shear mixing is caused by the interaction of the injection of the primary fuel with its surroundings leading to large peaks in the unmixedness profile. As the preheating temperature increases and the VAM stream approaches to ignition, the oscillations of the unmixedness become smaller, accordingly the mixing by fluctuations becomes less effective. The profiles of Case C indicate that the heat release after combustion smoothes out the fluctuations and therefore the peaks for Case C become smaller than for Case B as observed downstream (right-hand side plot of Fig. 12). The preheating temperature enhances the mixing process by reducing the unmixedness oscillations and facilitating the chemical reactions.

The effects of methane concentration on the mixing process are presented in Fig. 13 by means of profiles of the unmixedness factor Z_{unmix} at two axial locations. As already described, the largest mixing oscillations are found in the jet core region where the mixing of the primary flame takes place. The case with lower methane concentration of the VAM mixture (Case D) shows the largest variations. At upstream locations, no major differences are found between Cases C and E, and it is downstream where the differences become more evident. At $Z = 4.0$ cm, the flow field in Case E is more vortical and dynamic leading to large variations of unmixedness. The concentration of methane in the VAM stream has an influence on the magnitude of the unmixedness factor, but its effects on the distribution along the flame are rather low.

5. Conclusions

A numerical investigation, using large-eddy simulation, of a key process in a proposed VAM mitigation system to reduce methane emissions from mining activities has been performed. The mitigation device is based on the oxidation of a preheated VAM mixture by means of a primary fuel injection acting as a pilot or primary flame. The VAM mixture is supplied as a co-flowing stream and after the interaction with the heat release of the primary flame, it is oxidized provided certain conditions are achieved. The effects of preheating temperature and methane concentration are examined in five computational cases. It was found that the preheating temperature has a significant influence on the oxidation process of VAM mixtures. For a relatively low methane concentration stream, combustion only takes place when the temperature of the mixture is as high as 500 K. In this case, the oxidation of the mixture takes place homogeneously at low temperatures surrounding the primary flame and a reaction zone over a large volume can be distinguished. At the higher methane concentration of 2.0%, the heat released by the VAM oxidation tends to induce instabilities leading to strong oscillations. Preheating of the incoming VAM allows oxidation at methane concentrations as low as 0.5%. Ignition timings are described and discussed for the different mixtures providing some insight into the flame dynamics in each case. Discussions of the flame structure and mixing evolution are also presented based on time-averaged results for the main reactants and products as well as the unmixedness parameter.

This study shows that the ventilation air methane flow oxidizes under certain conditions and motivates further analysis of the combustion characteristics of such mixtures for power generation. Mitigation systems to reduce greenhouse gas releases are extremely important from a global climate change perspective and further efforts from combustion researchers are required for the development of these systems.

Acknowledgements

The authors would like to thank the European Union's Research Programme of the Research Fund for Coal and Steel (RFCS) research programme under Grant agreement Number RFCR-CT-2010-00004 and EPSRC Grant EP/G062714/2 for funding the activities undertaken for this study.

References

[1] Shine KP, Fuglestvedt JS, Hailemariam K, Stuber N. Alternatives to the global warming potential for comparing climate impacts of emissions of greenhouse gases. Climatic Change 2005;68:281–302.
[2] Shakhova N, Semiletov I. Methane release and coastal environment in the East Siberian Arctic shelf. J Marine Syst 2007;66:227–43.
[3] Isaksen ISA, Gauss M, Myhre G, Walter Anthony KM, Ruppel C. Strong atmospheric chemistry feedback to climate warming from Arctic methane emissions. Global Biogeochem Cycles 2011:25,GB2002.
[4] Wickland KP, Striegl RC, Neff JC, Sachs T. Effects of permafrost melting on CO_2 and CH_4 exchange of a poorly drained black spruce lowland. J Geophys Res 2006;111:2156–202.
[5] Whiteman G, Hope C, Wadhams P. Vast costs of Arctic change. Nature 2013;499:401–3.
[6] Kirchgessner DA, Piccot SD, Masemore SS. An improved inventory of methane emissions from coal mining in the United States. J Air Waste Manage Assoc 2000;50:1904–19.
[7] Cluff DL, Kennedy GA, Bennett JG. Capturing energy from ventilation air methane. World mining congress, Montreal, Canada; 2013.
[8] Su S, Jenny A. Catalytic combustion of coal mine ventilation air methane. Fuel 2006;85:1201–10.
[9] Su S, Beath A, Guo H, Mallett C. An assessment of mine methane mitigation and utilisation technologies. Prog Energy Combust 2005;31:123170.
[10] Wilson DG, Korakianitis T. The design of high-efficiency turbomachinery and gas turbines. 2nd ed. Springer; 1998.
[11] Su S, Pohl JH, Holcombe D, Hart JA. A comparison of thermal condition between pilot- and full-scale furnaces for studying slagging and fouling propensity in PF boilers. Combust Sci Technol 2001;165:12950.
[12] Danell R, Nunn J, Kallstrand A. Demonstration of MEGTEC Vocsidizer for methane utilisation. ACARP report C9065, Brisbane; 2002.
[13] Cimino S, Pirone R, Russo G. Thermal stability of perovskite based monolithic reactors in the catalytic combustion of methane. Ind Chem Res 2001;40:805.
[14] Yin J, Li M, Zhu A, Zhu J. Part-load performance characteristics of a lean burn catalytic combustion gas turbine system. J Therm Sci 2013;22:159–67.
[15] Wang Y, Liu Y, Cao Q, Wang Q, Che D. Homogeneous combustion of fuel ultra-lean methane air mixtures: experimental study and simplified reaction mechanism. Energy Fuel 2011;25:3437–45.
[16] Michael J, Miles R. Ultra-lean combustion sustained by pulsed subcritical microwaves. In: 42nd AIAA plasma dynamics and lasers conference; 2011.
[17] Yahagi Y, Nihei H. Extinction and flame front behavior of ultra lean premixed flame formed in opposite flow. Transact Jpn Soc Mech Eng Ser B 2002;68:1287–94.
[18] Hamatsu K, Yahagi Y, Takeuchi M, Nakahara S. Effects of oxidizer preheating and dilution on the extinction and structure of CH_4–O_2–Ar diffusion flames. Transact Jpn Soc Mech Eng Ser B 2006;72:1052–9.
[19] Cheng Z, Wehrmeyer JA, Pitz RW. Lean or ultra-lean stretched planar methane/air flames. Proc Combust Inst 2005;30:59–66.
[20] Law CK. Proc Combust Inst 1988;22:13811402.
[21] Barlow RS, Karpetis AN, Frank JH, Chen J-Y. Combust Flame 2001;127:21022118.
[22] Duwig C, Stankovic D, Fuchs L, Li G, Gutmar E. Experimental and numerical study of flameless combustion in a model gas turbine combustor. Combust Sci Technol 2008;180:279295.
[23] Coelho PJ, Peters N. Numerical simulation of a mild combustion burner. Combust Flame 2001;124:503–18.
[24] Pitsch H. Large-eddy simulation of turbulent combustion. Annu Rev Fluid Mech 2006;38:45382.
[25] Poinsot T, Veynante D. Theoretical and numerical combustion. 2nd ed. R.T. Edwards; 2005.
[26] Menon S, Calhoon W. Subgrid mixing and molecular transport modeling for large-eddy simulation of turbulent reacting flows. Proc Combust Inst 1996;26:59–66.
[27] Law CK. Combustion physics. Cambridge University Press; 2006.
[28] Mira Martinez D, Jiang X, Moulinec C, Emerson DR. Numerical simulations of turbulent jet flames with non-premixed combustion of hydrogen-enriched fuels. Comput Fluids 2013;88:688–701.

[29] Menon S, Yeung P-K, Kim W-W. Effect of subgrid models on the computed interscale energy transfer in isotropic turbulence. Comput Fluids 1996;25:165–80.
[30] Jones WP, Lindstedt RP. Global reaction schemes for hydrocarbon combustion. Combust Flame 1988;73:233–49.
[31] Abani N, Ghoniem AF. Large eddy simulations of coal gasification in an entrained flow gasifier. Fuel 2013;104:664–80.
[32] Ridhaa E, Mohamedb H, Rachida S. Comparison of different chemical kinetic mechanisms of methane combustion in an internal combustion engine configuration. Therm Sci 2008;12:43–51.
[33] Smith GP, Golden DM, Frenklach M, Moriarty NW, Eiteneer B, Goldenberg M, Bowman CT, Hanson RK, Song S, Gardiner WC, Lissianski Jr VV, Qin Z., 2000 <http://www.me.berkeley.edu/gri_mech/>.
[34] Kee RJ, Dixon-Lewis G, Warnatz J, Coltrin ME, Miller JA. A Fortran computer code package for the evaluation of gas-phase multicomponent transport properties. Sandia National Laboratories, report SAND86-8246; 1986.
[35] Torres DJ, Trujillo MF. KIVA-4: an unstructured ALE code for compressible gas flow with sprays. J Comput Phys 2006;219:943–75.
[36] Jiang X, Luo KH, de Goey LPH, Bastiaans RJM, van Oijen JA. Swirling and impinging effects in an annular nonpremixed jet flame. Flow Turbul Combust 2010;86:63–88.
[37] Mira Martinez D, Jiang X. Large-eddy simulations of unsteady hydrogen annular flames. Comput Fluids 2013;80:429–40.
[38] Kang DM, Culick FEC., Ratner A. An experimental study of coupling between combustor pressure, fuel/air mixing, and the flame. In: 4th Joint meeting of the US Sections of the Combustion Institute; 2005.
[39] Zheng Y, Zhu M, Mira Martinez D, Jiang X. Large-eddy simulation of mixing and combustion in a premixed swirling combustor with synthesis gases. Comput Fluids 2013;88:702–14.
[40] Fric TH. Effects of fuel–air unmixedness on NOx emissions. J Propul Power 1993;9:708–13.

THE VAMTURBURNER© CAPTURING ENERGY FROM VENTILATION AIR METHANE

*D.L Cluff, G.A Kennedy, J.G Bennett and P.J. Foster

University of Exeter,
College of Engineering, Mathematics and Physical Sciences,
Camborne School of Mines
Tremough Campus,
Penryn, Cornwall, UK
TR10 9EZ
**(Corresponding author: D.L.Cluff@exeter.ac.uk)*

CAPTURING ENERGY FROM VENTILATION AIR METHANE

ABSTRACT

Ventilation Air Methane (VAM) is a high volume low concentration methane source. The capture or use of methane from VAM is challenging, which results in the routine discharge of methane into the atmosphere. Mitigating VAM has the benefits of providing an energy source and reducing the atmospheric Greenhouse Gas (GHG) burden. The GHG radiative forcing effect of methane is 17–23 times as potent as carbon dioxide on a 100-year time horizon. Thus, any reduction in atmospheric methane would be beneficial. The calorific value of methane is 55.5 MJ/Kg; therefore, a 100 m^3/s flow with VAM concentrations from 0.1–1% can provide 3.8–38 MW of exploitable power.

Strategies to mitigate VAM such as: Thermal Flow Reverse Reactors (TFRR), Catalytic Flow Reverse Reactors (CFRR), Lean Burn and Catalytic Gas Turbines, Biothermica Vamox®, Megtec VOCSIDIZER©, and Vamcat™ are briefly reviewed. The review of VAM mitigation technologies reveals disadvantages such as the need to maintain a minimum internal heat capable of oxidizing the methane. This requirement uses all of the available methane up to the point of reaction sustainability and up to half at the highest methane concentration in VAM. Some systems may introduce a pressure drop to the ventilation system, which would impinge on the existing ventilation system design. These impediments necessitate the development of a more amenable technology.

In the proposed VamTurBurner© system, gas turbines (GT), coupled to a combustion chamber with an external fuel supply, assist the combustion of the VAM. The combustion-chamber coupled system provides electricity, while the heat contained in the GT exhaust gases increases the temperature of the VAM, encouraging the development of a flame inside a combustion chamber. The flow from the combustion chamber streams through a primary air/fluid heat exchanger capable of producing steam of a high enough quality to generate electricity using conventional steam turbines. The residual heat after primary extraction, directed through other equipment, provides additional heat based products such as industrial scale dry air, chilling by an absorption chiller or hot water. The overall design of the system is scalable for low to high VAM flows or variations in concentrations and is capable of providing the company or community with heating, chilling, hot water, electricity or motive force as needed by the particular site or community.

The Multi-generation system uses heat from three sources to provide clean efficient energy while mitigating the atmospheric emissions of methane. These sources are heat from the GT, often considered waste heat, heat from fuel injected into the igniters and heat from the VAM. The opportunity to collect carbon credits may improve the economics. In order to design a system with this capacity, a detailed analysis of the combustion characteristics of three separate flows is required. VAM is the main airflow, having the highest volumetric effect, while the GT exhaust and the additional fuel added to the hot exhaust flow of the gas turbine are lower flows, but have a higher velocity and temperature. The aim of the modeling undertaken in this work is to establish the combustion dynamics, degree of pre-heating required and the geometry essential to the design of combustion based VAM mitigation multi-generation systems.

KEYWORDS

Ventilation air methane (VAM), Combustion, Coal mining, Ventilation, Gas turbine, Greenhouse gas (GHG), Methane mitigation, Carbon credits, Energy capture, Coalmine methane (CMM), Coal seam methane

1 INTRODUCTION

Methane is a greenhouse gas (GHG), with a global warming potential of 56, 21, and 6.5 over 20, 100, and 500 years, respectively, where the reference of unity is used for carbon dioxide (IPCC, Technical Summary; Table 4). Methane has a high radiative forcing factor second only to that of carbon dioxide (2). These two attributes exacerbate the impact of methane emissions on the near term global temperature. According to the long-term modeling of global temperature rise due to carbon dioxide forcing, the temperature increases are not globally uniform. Northern regions are more inclined to experience higher marginal increases in temperature than the southern hemisphere, due to the global redistribution of heat from the equator to the poles and the moderating influence of the oceans in the south. This expected increase of temperature in the northern region has the potential to create a strong methane feedback effect if the methane contained in the permafrost is released into the atmosphere as the permafrost melts (3).

Since the dawn of the industrial age, carbon dioxide and methane have increased by 31 and 149%, respectively. Human activity accounts for more than two-thirds of the increase in methane (5). The present atmospheric concentration of methane is an average of about 1800 ppb, which is quite abundant in the atmosphere (6) compared to the values a few centuries ago. An escalation of methane in the atmosphere corroborated by (7), confirmed an increase of 12.5% over 33 years, but the increase in the polar region is about 200 ppb greater than at the equator. Arctic methane levels during August ranged from 1840–1860 ppb in 2012 compared to 1830–1850 ppb in 2011 and 1820–1840 ppb in 2003 (8, 9). In the year from Aug 2011–Aug 2012, the average Arctic methane levels increased by about 10 ppb (8, 9) compared to an increase of 10 ppb over the previous 8 years since 2003 (Figure 1). The effect of the rate of methane increase in the Arctic for 2011 to 2012 is equivalent to the radiative forcing that an increase in carbon dioxide of about 250–1,000 ppb, or 12–50%, would have for that single year (8). This recent and rapid increase in Arctic methane concentration may be an early indicator of an Arctic methane radiative forcing feedback loop. The result of such a feedback loop leads to accelerated permafrost melting, an increase of the Arctic ice-melting rate and both effects influence the global temperature upward.

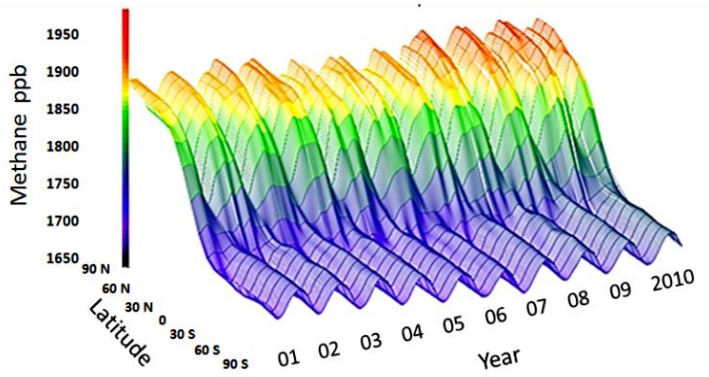

Figure 1 – Three dimensional plot of the Global Distribution of Atmospheric Methane NOAA ESPL Carbon Cycle over the last decade from the equator to the North Pole (42)

Other effects such as the increase in exposed land or decrease in the albedo due to a loss of ice cover compounds the problem adding to the potential for warmer temperatures. This could result in greatly increased Arctic heating along with more extreme weather events and glacial melting effects far exceeding the impacts we see today.

"Scientific climate projections do not currently account for carbon emissions from permafrost, but the study concludes that the effect is "strong enough to warrant inclusion in all projections of future climate."(12).

Figure 2 shows the distribution of carbon dioxide, methane, and nitrous oxide the three top GHG's by their sector source. The GHG effect of methane, which accounts for 9% of the total GHG emissions, is not discussed as frequently as carbon dioxide. Methane is a higher radiative forcer over a shorter term; thus, a small amount of methane has a large effect on the global thermal horizon over a shorter period. Upon consideration of the effect of methane releases in the Arctic, the urgency of methane mitigation programs becomes self-evident.

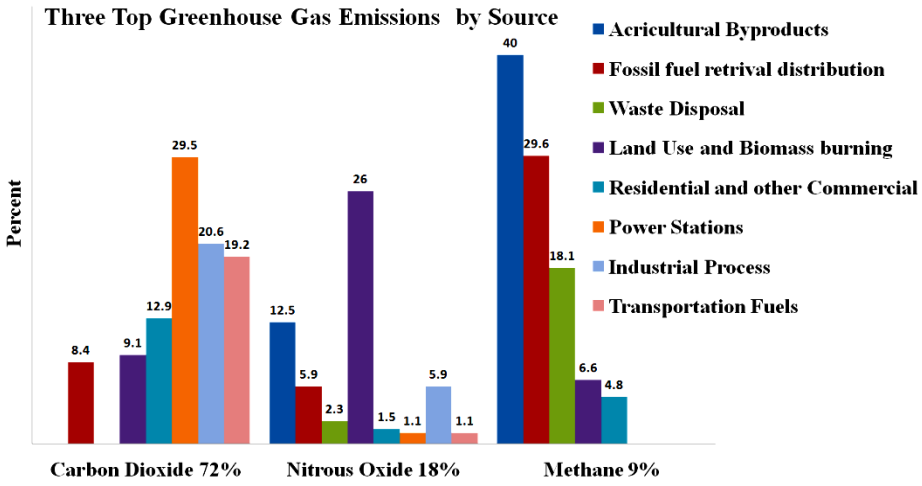

Figure 2 –Annual greenhouse gas emissions by sector (5, 19)

2 ATMOSPHERIC METHANE EMISSIONS FROM COAL MINES

Table 1Global anthropogenic methane by sector in 2000; total methane emissions were 282.6 Tg.

Agency/ Source	IEA CCC 2005 (%)	M2M 2006 (%)	US EPA 2006 (%)
Natural Gas	15	16	17
Coal	8	8	6
Oil	1	1	1
Solid Waste	13	14	12
Waste Water	10	11	9
Fuel	1	1	1
Biofuel	4	4	
Other Agriculture			7
Biomass	5		3
Fermentation	28	29	30
Manure	4	4	4
Rice	11	12	10

The atmospheric concentration of methane, associated with coal mining (Table 1), is estimated to be about 8% of the total anthropogenic methane produced (5). The largest fraction of atmospheric methane from coal mining activities is due to VAM release. Methods to mitigate VAM are desirable from a global climate perspective and could be economical if the generated heat is captured. Since methane is a GHG targeted for mitigation, VAM from coal mining operations or abandoned mines is an obvious candidate.

A typical gassy coalmine has five sources of methane (16):

1. Degasification or drainage systems at underground coalmines. Vertical and/or horizontal holes are used to recover methane in pre-mining or after mining from the gob or goaf.
2. Ventilation air containing dilute methane concentrations or VAM.
3. Nonoperational mines from vent holes or through fissures.
4. Open pits directly exposed to the atmosphere.
5. Post-mining operations where the coal emits methane during storage or transportation.

VAM stands out as the low methane concentration high volumetric flow case, while the other methane sources are typically higher concentrations at lower flow rates, correspondingly VAM is the most difficult to capture and exploit. The US data presented in Table 2 are representative of the typical emissions of global mines. The VAM emissions from US coalmine ventilation systems are 61% of the total coalmine related methane emissions. Some estimates for the global VAM emissions are as high as 70% (17) while other researchers set the value at 64% (18).

Table 2 – USA Methane emissions by coal mining activity source (U.S. Emissions Inventory)

	Average 1990–2009		2010	
Mining activity	bcf	%	bcf	%
Post mining	19	10.06	18.87	9.86
Surface mines	31.9	16.90	32.64	17.06
Abandoned mines	13.6	7.20	12.32	6.44
Drained gas			9.49	4.96
Degasification vented from UG	9.4	4.98		
VAM	114.9	60.86	118	61.68
Total bcf	188.8		191.32	

Typical methane percentages in VAM are in the neighborhood of 0.2–1% v/v, but vary in concentration as the atmospheric pressure changes, the underground operations change, the mining proceeds deeper or in the event of seismic activity. The concentration of methane in ventilation air is kept low, mainly for safety reasons (18). The flow rates needed to keep the methane from a coalmine at low concentrations in ventilation air can typically be 100 m^3/s, but can reach as high as 300 m^3/s. The comparison of anthropogenic methane sources in Table 1 shows that coal mining is responsible for about 8% of all emissions, which are broken into the various mining activities in Table 2. From the values in Tables 1 and 2, VAM accounts for 5% of the total anthropogenic methane.

It is clear from the calculations presented in Table 3, that the economic benefit of converting the fugitive methane emissions contained in VAM could provide a significant enhancement to any engineering project undertaken to mitigate the VAM. Essentially the VAM is a free energy source and according to the current climate models, mitigating a GHG with a carbon dioxide equivalence of 21 would be beneficial.

Table 3 – Power available and carbon dioxide equivalents for mitigation of various typical methane concentrations in typical ventilation flows of a coal mine (D.L. Cluff)

Ventilation flow rate (m^3/s)	Methane concentration (%)	Methane mass flow kg/s	Methane tonnes/yr	Conversion to carbon dioxide tonnes/yr	21 times equivalent carbon dioxide tonnes/yr	Power (MW)
50	0.2	0.068	2144	5897	39136	3.77
150	0.5	0.51	16083	44289	293521	28.30
300	1.0	2.04	64333	176917	1174085	113.22

All projections suggest an increase in energy demand and coal is expected to play a major role in the future energy supply of China, India, and the US. Regardless of whether technologies evolve to provide a cleaner coal burning plant, it is inevitable that more coal will have to be mined. China currently produces 71% of its energy from coal (41). The US, China, India, Australia, and Indonesia are the 5 countries (Figure 3) that account for > 75% of global coal production (19).

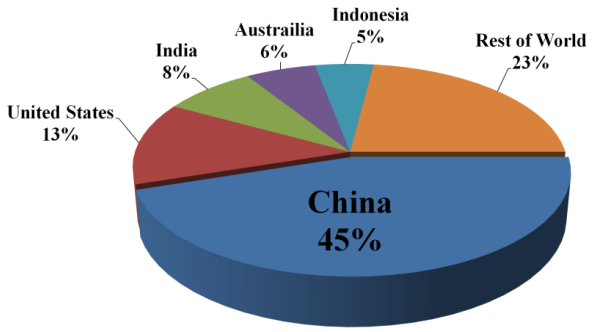

Figure 3 – Percent distribution of coal production for the top 5 producers and the rest of the world

The estimated quantities of VAM emissions (Figure 4) associated with these production quantities suggest the world market for VAM destruction technologies has a potential value of several billion dollars (20). Over the last decade, China and Indonesia have nearly doubled their production and although the US has reduced coal production somewhat, India has recently started to grow at a more rapid pace, which carries the expectation that their coal use will also increase. The VAM has clearly been increasing in the countries where the coal production has increased.

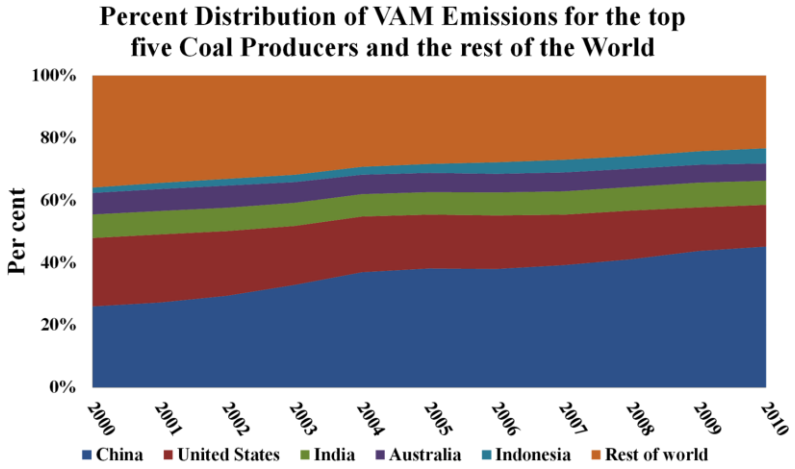

Figure 4 – Percent distribution of VAM emissions for the top five producers and the rest of the world.

3 A REVIEW OF VAM MITIGATION TECHNOLOGIES

A number of technologies have been developed to mitigate VAM, but there are essentially two basic methods. VAM is a primary fuel when used in Thermal Flow Reverse Reactors (TFRR), Catalytic Flow Reverse Reactors (CFRR), lean burn GT's, recuperative GT or Regenerative Thermal Oxidation (RTO) (22). When the VAM replaces air in a combustion process, such as GT, internal combustion engines, rotary kilns or even a coal fired power station, it is a secondary fuel residing in the intake air. Higher concentration sources of methane, such as drained sources, can be flared, mixed with the VAM to boost the calorific value of the VAM when it is used as a secondary fuel or sold to market.

The Commonwealth Scientific and Industrial Research Organization (CSIRO) built a 1.2 MW rotary kiln system, where waste coal and VAM are burned in a rotating kiln to generate electricity by using an externally fired steam turbine system (21, 23, 33). The VAMCAT™ is a lean burn catalytic gas turbine custom-built for VAM that operates on 0.8% methane using an innovative catalytic combustion gas turbine system to oxidize methane while generating electricity (11, 26, 40). A 25kWe power generation

demonstration operated at an underground coalmine of the Huainan Coal Mining Group, China during November 2011.

The VOCSIDIZER© was first established as a viable option to mitigate VAM in 1994 at the Thoresby Mine in Nottinghamshire, UK (23, 27). The result of that demonstration proved the VOCSIDIZER's© capability to maintain an oxidation reaction at the low and varying concentrations of methane found in a typical coalmine ventilation system.

Subsequent to the positive results from the Thoresby Mine, scaled-up testing was performed in 2001-2002 at the Appin Colliery in New South Wales, which included an internal heat exchanger to capture the heat of combustion. The project operated over a one-year trial period; a robust demonstration of the technology (23, 28). This project confirmed that a TFRR with a heat exchanger can provide energy for an assortment of potential applications such as: hot water for the company or the community, hot air for space heating, industrial drying, cooling using low grade heat with an absorption chiller or electricity generation. Consequently, MEGTEC and BHP Billiton installed a large-scale electrical power generation project at the West Cliff Colliery in New South Wales (29).

The West Cliff VAM Project (WestVAMP), the world's first commercial-scale VAM project, began operation in Windsor Mine in April 2007. WestVAMP oxidizes 70 m^3/s of 0.9% methane. The concentration is maintained at a constant flow rate by mixing drainage gas with the ventilation exhaust airflow. The 6 MWe generated is used by the West Cliff colliery. The heat collected from the VOCSIDIZER© units is used to provide superheated steam to conventional steam turbines producing electrical power (23, 30).

Apart from the UK and Australian projects, MEGTEC has also demonstrated their VOCSIDIZER© technology in the US at the CONSOL Energy Windsor Coal Mine, a closed mine in West Liberty, West Virginia (31, 32). The project operated for 20 months to demonstrate the reliability of VAM conversion, using drained methane from the closed workings, simulated at a 0.6% concentration and a 14 m^3/s flow rate. The project determined the available energy that can be extracted from the system (23).

The Zheng Zhou Coal Mining Group in China operates a system, based on the MEGTEC VOCSIDIZER©, that they use for VAM abatement and energy recovery to produce hot water for local use. The system was commissioned in October 2008. It has an 18 m^3/s system capacity while operating on a nominal VAM concentration of 0.3–0.7%. The VOCSIDIZER© was the first project to mitigate VAM to be officially approved by the UNFCCC for allocation of Kyoto related Carbon Credits (26, 33). The system requires a minimum of about 0.2% VAM to maintain the oxidation reaction.

Diesel engines are routinely used to provide electricity to mines in remote locations and are a well understood low capital cost option which can be used to reduce the VAM emissions provided the installation is designed to avoid costs associated with transportation of the VAM (29, Karakurt, Gokhan & Kerim, 2011, 35). The 54 internal combustion engines that are powering the electricity generation project at the Appin Colliery in New South Wales, comprise one MW unit. The VAM/coalmine methane (CMM) driven internal combustion engines can produce up to 55.6 MW of electricity for the mine (36). Forty more units at the Tower location provide a combined output of 97 MW from 94 Caterpillar 3516LE generators. In this case, VAM represents a supplemental fuel, which contributes a portion of the fuel input through the normal air intake to the IC engines. All of the drained gas from the mine is used, accounting for 4% to 10% of the required engine fuel, but only about 20% of the VAM emissions are mitigated (24, 29, 35, 37).

A pilot-scale study, performed at the Vales Point Power Station, determined the feasibility of using VAM as combustion airflow when the coalmine and power station are conveniently proximal. A full-scale demonstration, with the support of an Australian federal government program in 2003, directed a VAM flow rate of about 220 m^3/s to the intake of the power station. Total air consumption for the two 660 MW pulverized coal fired boilers at the power station is approximately 1200 m^3/s. Using ventilation

exhaust as combustion air in large boilers requires that the power plant and the mine be located within reasonable proximity to limit transportation issues. These possibilities are limited, while the more flexible internal combustion engines are routinely installed at remote locations.

A demonstration project undertaken in 2004 at the Appin Colliery mine, employed a 2.5 MW Solar Centaur 3000R GT modified to use an airflow containing about 1.6% methane (29, 35, 37). The trials were suspended when the contamination of the mine air had an adverse effect on the operation and stability of the gas turbine, which caused the combustor heat exchange tubing to over-heat and fail (37, 39).

The FlexEnergy Micro turbine was adapted, with a catalytic combustor, to operate on a wide range of fuels including VAM. The FlexEnergy unit can achieve full power with fuel as low as 1.5% methane. The compressor and combustor are contained within a compact turbine module and the hot compressed gases are allowed to expand in the turbine to power the generator (26). A FlexEnergy turbine has been installed at the DCOR oilfield near Santa Barbara, California to consume oilfield gas at concentrations ranging from 1.5–4.2%. Another Flex turbine is running on coal process waste gas at the Western Research Institute in Laramie, Wyoming.

Fluidized beds operate on the terminal velocity principle, such that the upward flow suspends solid particles in the flow. The resultant turbulent mixing of gas and solids provides a bubbling action which affords for a high chemical reaction rate and heat transfer. The technology is still a proposed concept, with no development to date (26).

Catalytic monolith reactor technology comprises a honeycomb shaped monolithic reactor. By virtue of the geometry, exceptional flow profiles at a low pressure drop due to low resistance and high mechanical strength are realized. Monoliths consist of a structure of parallel channels with walls coated by a porous support containing catalytically active particles. The methane in the flow is oxidized as it comes in contact with the catalyst on the substrate of the monolith.

Sindicatum acquired the global rights except for Japan until 2019 to use the “CH4MIN” catalytic oxidation technology that has been developed by the Centre for Mineral and Energy Technology (CANMET), a Canadian government energy research organization that is part of Natural Resources Canada. Sindicatum performed full-scale testing of this technology during 2008 and 2009 at a location in the US to facilitate the design of a commercial regenerative catalytic oxidizer the first one of which will be installed at Duerping coalmine, Shanxi Province, China.

4 THE VAMTURBURNER©

The current systems capable of VAM mitigation, while using the VAM as a primary fuel, such as the TFRR and CFRR, generally do not use all the VAM to produce an energy product because some of the energy is required to sustain the oxidation reaction (Figure 5). The plots in Figure 5 are typical for a typical TFRR and CFRR requiring VAM concentrations of 0.12 and 0.45%, respectively, simply to provide enough heat to sustain the reaction. The cutoff of 1.3% represents the assumed VAM concentration at which heat would have to be discarded due to the high temperatures that would damage the reactors. At a VAM concentration of 0.7%, the heat recovery is only 34% and 75% for the CFRR and TFRR, respectively. These systems may also introduce a pressure drop across the ventilation system and often require supplemental booster fans to overcome the pressure drop or to force the VAM through the system. Many other systems have proven to be subject to intractable problems, such as the catalytic GT, so further development has ceased. The projects using VAM as a secondary fuel are quite viable; however, the amount of VAM used as a secondary fuel depends on the normal air-intake flow rate. The number of units needed to accommodate the VAM in place of normal airflow is prohibitive, which prevents the full amount of the VAM available at the mine from being used in a given project. Improved economics may be realized by the installation of a system capable of converting all of the VAM to a useable energy product. An alternative to the existing systems, based on a gas turbine cogeneration system, is proposed.

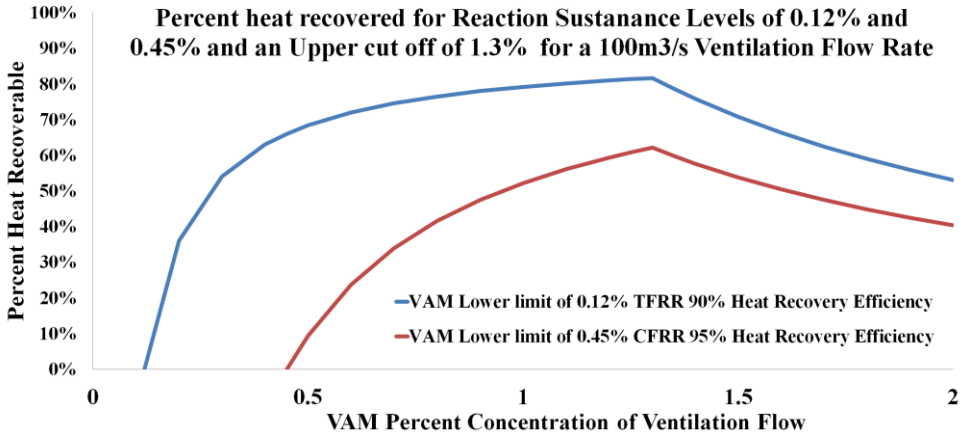

Figure 5 – Recoverable energy after reaction sustenance (D.L Cluff, 2012)

The VamTurBurner© system depends on the design of a combustion chamber to burn the VAM, which integrates the heat from both the exhaust gas of the electricity generating GT's and a pre-heating stage before the flow encounters an igniter connected to a supplemental fuel system. This VAM mitigation solution uses all of the VAM energy and is scalable to the various sizes of mine ventilation systems. The system uses staged heat exchange for the production of electricity, hot water, chilling or industrial drying as needed to meet the future demand for coal mining activities in a carbon conscious atmosphere.

Figure 6 presents a diagram of the VamTurBurner© VAM mitigation system, which includes the multi-generation heat exchange system. The fan motors at the upcast ventilation shaft of the mine ventilation system are located at the inlet of the VamTurBurner©. The fan motors are prime candidates for the energy produced through the gear driven generators connected directly to the GT's. A key feature of the design is a separate air intake system for the GT's protruding from the ventilation system ducting. The decision to keep the ventilation air from entering the GT ensures the operating conditions expected by the GT. The changes in VAM concentration would cause the GT to compensate by adjusting the fuel flow. The mine air may contain noxious fumes and dust that can potentially reduce the GT lifetime, as was experienced during the Solar Centaur 3000R trials. The GT's operate on natural gas or an appropriate separate jet fuel source as shown in the diagram. This guarantees the smooth operation of the gas turbine due to fresh air intake and properly regulated fuel as inputs. The exhaust gases from the GT are hot, in the neighborhood of 700-800K and exit the GT at a high velocity (50^{+} m/s). The hot, high velocity gas mixes with the incoming VAM in the pre-heating zone. The mixture of VAM and exhaust gases encounters a pre-heater and as the gas flows through the pre-heater; the temperatures are elevated to the pre-ignition temperatures.

The pre-heated VAM exits the pre-heater unit at temperatures high enough to allow for oxidization. The oxidization temperature depends on the VAM concentration; thus, the amount of pre-heating required is a critical variable. The pre-heated flow continues downstream and encounters the igniters, which are fueled by natural gas combined with any other CMM sources available at the site. The heat transferred to the airflow at the pre-heater is derived from steam created from heat produced in the combustion zone. Since this heat is transferred to the airflow internally, losses are minimal because it is either recycled at the higher temperature zones or proceeds to the multi-generation system.

Typically, a cogeneration system uses a single fuel to produce both electrical and thermal energy. The use of the thermal energy increases the overall efficiency of the system to 90% or more. Tri-generation generally refers to the addition of cooling to a cogeneration system. We propose the term "*multi-generation system*" to describe an extension of tri-generation to include additional products such as hot water, industrial drying, space heating or more electricity. Steam generators, absorption chillers, or compression chillers are routinely coupled to a variety of energy sources for instance: geothermal, methane from waste disposal sites, solar heating, agriculturally produced methane, or VAM.

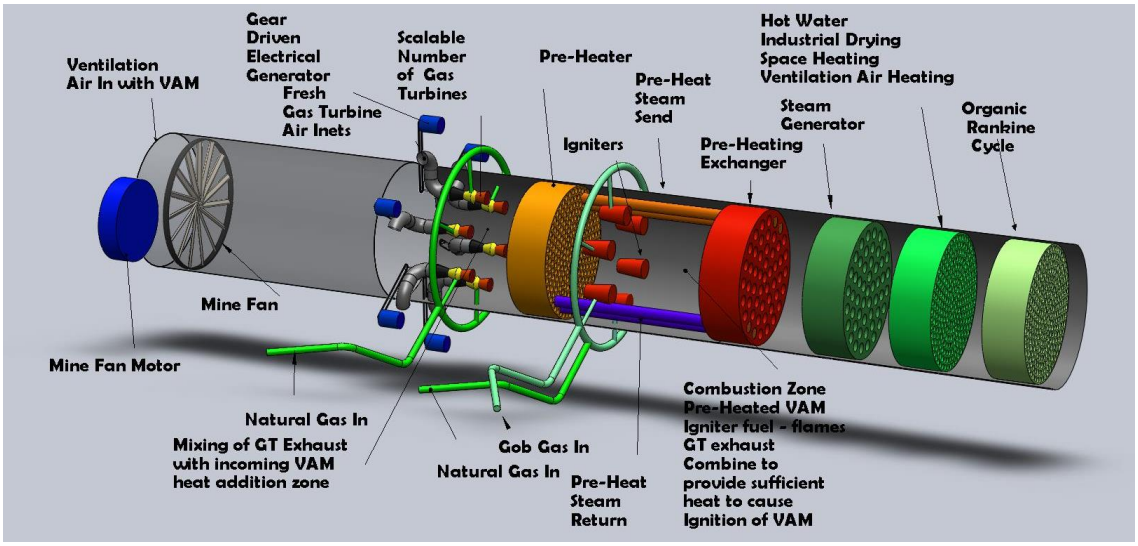

Figure 6 – The VamTurBurner©, a multi-generation system for the mitigation of VAM (D.L Cluff, 2013)

The mining company could use the various energy products to alleviate costs at their site or they may choose to sell electricity back to the grid, hot water to a community or provide services to an industrial site, essentially acting as a distributed energy node. It is clear that mining operations in different climates require different configurations of the multi-generation system. The adaptability of this system to provide heat or cooling in equal measure or switching outputs during different seasons is an attractive feature.

The benefits of this robust design are that it uses an external fuel source to balance the combustion chamber. This induces oxidization of the VAM while none of the energy is consumed to sustain the reaction. The energy contained in the VAM, considered as a free energy source, improves the overall efficiency of the system. The efficiency of any system is defined as the (work out)/(energy in). The energy input to the VamTurBurner© arises from three separate fuel sources: a co-generation system, which produces electricity plus exhaust heat, the igniters and the VAM, both of which only produce heat. The igniter fuel may contain CMM or any other fuel available from the mine to supplement the natural gas, which is a further reduction in overall cost to the company. Since the VAM energy is not considered as one of the input sources, but appears as part of the output, the overall system efficiency is increased.

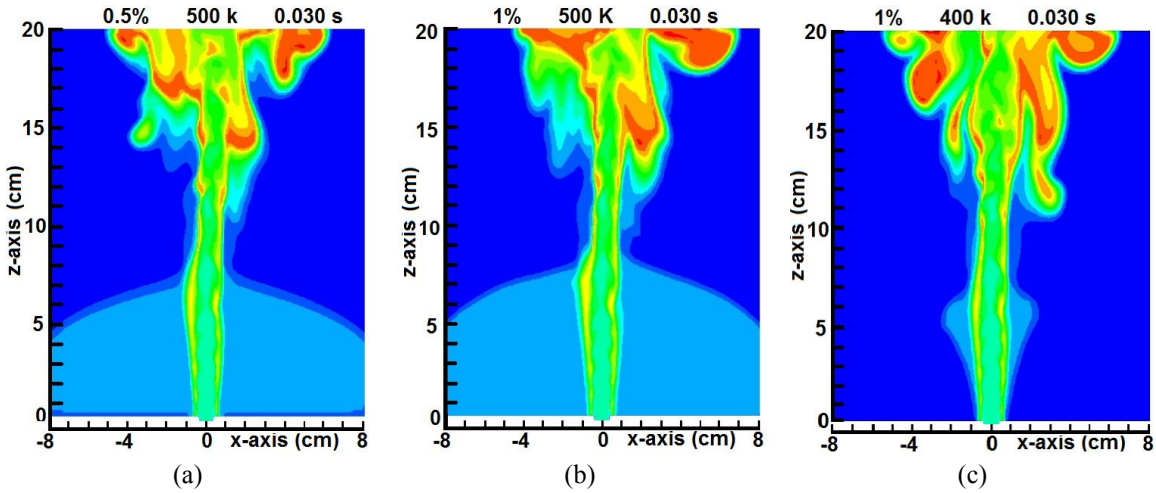

(a) (b) (c)

Figure – 7(a, b, c) shows the ignition of methane in a co-flow stream of an igniter flame and a ventilation flow containing 0.5% at 500K, 1% at 500K and 1% at 400K respectively (Martinez, Cluff, & Jiang, 2014).

The intractable problem associated with mitigating VAM to collect energy is the high volume of the ventilation flow with too low a methane content to be readily oxidized. Modeling the combustion dynamics of pre-heated VAM has shown that a 0.5% methane concentration in a ventilation flow will ignite and readily oxidize (42). Using the concepts of Large Eddy Simulation numerical modeling and supercomputing facilities, they have shown that pre-heating the VAM to 500 K allows for flameless burning of a 0.5% VAM concentration. Figure 7 shows the oxidization of methane at a 0.5% and 1% concentration at 500K, while the 1% concentration does not readily oxidize at an initial temperature of 400K. As the concentration of methane increases, the initial temperature required to allow oxidization of the methane reduces correspondingly.

Figure 8 is a representation of the computational flow dynamics modeling undertaken to establish the characteristics GT -VAM flow interactions and the design parameters of a heat exchanger to deliver the pre-heating prior to the combustion chamber. We model each stage of the system separately so the combustion chamber follows this section and the primary heat exchanger stage follows the combustion chamber. For each subsequent stage, the initial conditions shown as arrows on Figure 8 are derived from the output of the previous simulation.

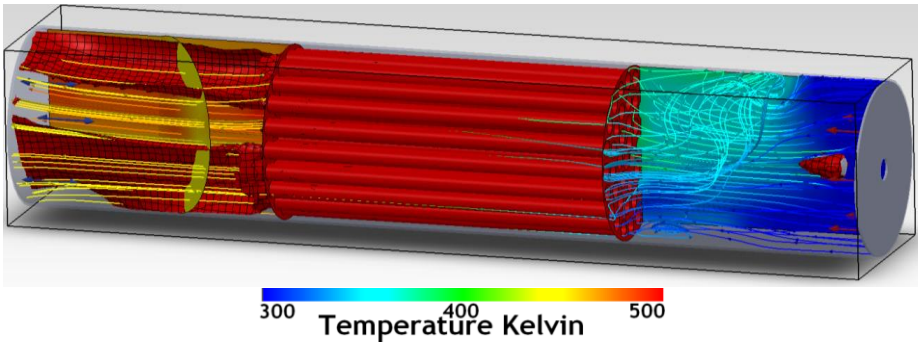

Figure 8 – Simulation of the flow from a gas turbine interacting with a typical VAM flow. The flow of the VAM is 2 m/s at 300 K and the flow of the exhaust gas from the GT is 50 m/s at 700 K. Flow trajectories display the temperature as well as the vorticity. The temperature profiles are fixed on a plane. The temperature scale, blue to red for this diagram, is 300–500 K (D.L. Cluff 2013).

An isosurface of 500 K, displayed as a red grid pattern in Figure 8, is shown for the GT exhaust and the same isosurface appears at the far left where the flow exits the pre-heater stage. The VAM flow trajectories begin on the right side; the dark blue hue of the trajectories signifies the VAM is at 300K. The interaction between the VAM and the GT exhaust yields a product gas with an increased temperature and turbulence length as seen by the increase in vorticity and temperature displayed on the flow trajectories. The exit temperature from the pre-heater is near 500 K, was previously suggested as an appropriate value for the purposes of creating a mixture in a state ready to undergo auto-ignition upon encountering the igniters. We will publish ongoing computational flow dynamics, combustion dynamics and engineering calculations required to integrate the various systems as they become available.

Since the design of the pre-heating section is an essential element of the VamTurBurner©; a comparison of heat exchange system designs to preheating has shown that a recirculation of the hot air from the combustion zone to the preheating zone is a more economical design for the preheating of the incoming ventilation air containing the methane than a heat exchange system operating between the two airflows. Heat exchange systems are employed for the conversion of heat to produce steam or hot water for the generation of electricity or other thermal products (43). A recirculation scenario is shown in Figure 9, several iterations of the model have resulted in a system with baffles and dispersion discs, which serve to mix the hot combustion air with the cool incoming ventilation air sufficiently and over a short traversal.

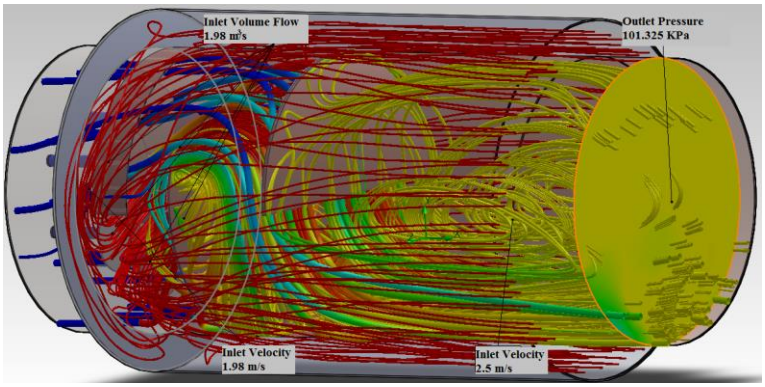

Figure 9 – Flow trajectories and temperature distribution of the preheating section of the VamTurBurner© (D.L Cluff, 2014).

5 CONCLUSIONS

Distributed energy systems may compete with the large-scale power plants in the not too distant future. When industry, communities, government institutions, medical facilities or universities take advantage of small-scale power systems such as GT CHP systems they can realize considerable savings if the systems are properly scaled. Mine sites are at an ideal scale, in terms of energy demand, for the implementation of scaled power systems, especially in cases where the deposit is conveniently located near a power grid. In the case of the multi-generation system, we allocate some of the energy to electricity then the various sections are serially connected to take advantage of the lower quality heat as the system exports power at each segment. The multiplicity of configurations makes a multi-generation system amenable to the inclusion of power storage systems. Combining power storage systems, such as liquid air as an energy storage vector, with scaled multi-generation systems may very well make the distributed power system more competitive than large-scale power plants. The advantages of having liquid air available at a mine site are: the opportunity to offset auto-compression as the depth increases; rapid rock skin temperature conditioning as ventilation on demand is implemented; production of compressed air and electricity using modular systems and the opportunity to employ renewable energy systems such as wind or solar with the smoothing of energy availability by storage during high availability.

ACKNOWLEDGMENTS

The European Union Research Program's Research Fund for Coal and Steel supported this research under grant agreement RFCR-CT-2010-00004.

REFERENCES

1. IPCC (1996). Inter-Governmental Panel on Climate Change. Second assessment – climate change. Retrieved from IPC website: www.ipcc.ch/pdf/climate-changes-1995/ipcc-2nd-assessment
2. Forster, P., et al. (2007). Chapter 2, Changes in Atmospheric Constituents and in Radiative Forcing, Cambridge University Press, Cambridge, United Kingdom and New York, NY, USA.
3. Methane Bubbles Climate Troubles. (2006). Retrieved from: http://news.bbc.co.uk/1/hi/sci/tech/5321046.stm
4. Rohde R.A., (2006). Global Warming Predictions. Retrieved from: http://www.globalwarmingart.com/wiki/File:Global_Warming_Predictions_Map_jpg
5. Blake D.R, Meinardi S, Rowland F.S, & Simpson I.J. (2006). *Geophysical Research Letters*. Retrieved from: http://oceanlink.island.net/ONews/ONews7/methane.html
6. Atmospheric Methane. (2005). Retrieved from: http://earthobservatory.nasa.gov/IOTD/view.php?id=5270
7. Cavanagh L.A, Robinson E., Shadt C.F. (1969). Atmospheric hydrocarbon and carbon monoxide measurements at point barrow, Alaska. *Environmental Science Technology, 3(3),* 251. doi: 10.1021/es60026a002

8. Scribbler S. (2012). Arctic methane concentrations for August 2012 shows jump from August 2011, part of larger arctic trend. Retrieved from robertscribbler wordpress: http://robertscribbler.wordpress.com/2012/09/13/arctic-methane-concentration-for-august-2012-much-higher-than-august-2011/
9. AIRS weather and climate from space. (2003). Retrieved from NASA AIRS: http://airs.jpl.nasa.gov/mission/description/
10. Coalbed methane outreach program. (2009). Retrieved from EPA: http://www.epa.gov/cmop/
11. Scribbler S. (2012) Arctic sea ice melt, methane release shows amplifying feedbacks from human caused climate change. Retrieved from: http://robertscribbler.wordpress.com/2012/03/18/arctic-sea-ice-melt-methane-release-shows-amplifying-feedbacks-from-human-caused-climate-change/
12. NOAA hot on methane's trail: scientists sniff around frozen ground. (2011). Retrieved from NOAA website: http://www.noaa.gov/features/02_monitoring/methane.html
13. Gunning P.M. (2008-2009). Methane: mitigation technologies, options, and policies. Presentation to arctic council task force on short-lived climate forcers, climate change division.
14. What is coal seam methane?. (2006). Retrieve from: http://www.worldcoal.org/coal/coal-seam-methane/
15. Methane: sources and emissions. (2011). Retrieved from EPA: http://www.epa.gov/methane/sources.html
16. Coalbed Methane Outreach Program. (2011). Retrieved from: EPA. http://www.epa.gov/cmop/basic.html
17. Warmuzinski K. (2008). Harnessing methane emissions from coal mining. *Process safety and environmental protection, 86(5)*, 44-100. doi: 10.1016/j.psep.2008.04.003
18. Mallett C.W, Su S. (2003). Progress in developing ventilation air methane mitigation and utilisation technologies. *Proceedings of the 3rd international methane & nitrous oxide mitigation conference*
19. Burklin C., Somers J. (2012). A 2012 update on the world VAM oxidizer technology market. In Calizaya & Nelson, *14th United States/North American Mine Ventilation Symposium* (pp. 262). University of Utah, Dept. of Mining Engineering.
20. China dominates global coal production. (2011). Retrieved from U.S Energy Information Administration Website: http://www.eia.gov/todayinenergy/detail.cfm?id=3350
21. Pyper, W. (2003). Hybrid turbine mines power from waste. ECOS, Vol 114, 9. (no DOI)
22. Air pollution control. (2009). Retrieved from: http://www.biothermica.com/2_1_1_operating.html
23. Schultz H.L., Somers J.M. (2010). Coalmine ventilation air emissions: project development planning and mitigation technologies. In Hardcastle & McKinnon, *13th United States/North American Mine Ventilation Symposium (118)*
24. Schultz, K. (2003). Coal mine – ventilation air methane mitigation: technologies to harness an energy and environmental resource. *Energia, Vol 14*.
25. VAMCAT generating energy from mine drainage gas. (2012). Retrieved from: http://www.csiro.au/en/Outcomes/Energy/Energy-from-coal/Advanced-coal-mining-technologies/VAMCAT.aspx
26. Coal mine methane mitigation and utilization technologies and project profiles. (2011). *Global Methane Initiative* (pp 6).
27. Basics on technologies for utilization of CMM. Retrieved from CoMeth website: http://wiki.umsicht.fraunhofer.de/cometh-wiki/images/8/8b/Vocsidizer.pdf
28. Schultz, H.L, Somers J.M. (2009). Coal mine methane ventilation air emissions: New mitigation technologies. *Coalbed Methane Outreach Program*, BCS Incorporated.
29. Using ventilation air methane (VAM) as combustion air in reciprocating engines and turbines. (2004). *EPA coalbed methane outreach program technical options series*. United States environmental protection agency.
30. Schultz H.L, Somers J.M. (2008). Thermal oxidation of coal mine ventilation air methane. *12th U.S/North American Mine Ventilation Symposium*.
31. Coalbed methane outreach program. Retrieved from Environmental Protection Agency website: http://www.epa.gov/cmop/basic.html
32. Kosmack D.A, Winschel R.A, Zak K.P. (2007). First U.S field trial of oxidation technology for ventilation air methane. *1st Annual US Coal Mine Methane Conference*.
33. Mattus R., Zhou Z. (2008). Abatement of VAM emissions and generating hot water from the energy released in VAM oxidation. Project Identification Business Operation. Retrieved from setatwork website:

http://www.setatwork.eu/downloads/SPI1_Sweden_Megtec_in_China.pdf and CDM website: http://cdm.unfccc.int/Projects/DB/DNV-CUK1201793890.37/view
34. Karakurt I, Gokhan A, Kerim A. (2011). Mine ventilation air methane as a sustainable energy source, *Renewable and Sustainable Energy Reviews, Vol 15, 2* (pp 1042-1049)
35. Canyon R., Kennedy C. (2012). Methane mitigation at underground coal mines: overview of technologies and early action incentives. *National Mining Association. (pp. 9-23)*. Las Vegas, Nevada
36. Bibler, C., Carothers, P. Overview of coal mine gas use technologies.
37. Mallet C. (2004). Coal mine methane activities in Australia. In CSRIO Exploration and Mining Technology Court, Ad Hoc Group of Experts on Coal Mine Methane (pp. 1-9). Pullenvale, Australia
38. Cummings D.R. Use and elimination of methane in coalmine ventilation air. DUT Pty Ltd, Retrieved from coalinfo website: http://www.coalinfo.net.cn/coalbed/meeting/2203/papers/coal-mining/CM046.pdf
39. Cummings D.R. (2006). Submission to the senate alternative fuels inquiry. DUT Pty Ltd.
40. Kiehl, J. T. and Trenberth, K. E. (1997). Earth's annual global mean energy budget. Bulletin of the American Meteorological Society, Vol 78, 197-208. doi: 10.1175/1520-0477(1997)078<0197:EAGMEB>2.0.CO;2
41. Badkar, M. (2012) The ultimate guide to china's voracious energy use. Retrieved from business insider website: http://www.businessinsider.com/china-energy-use-2012-8?op=1
42. D. Mira Martinez, D. Cluff and Xi Jiang (submitted to Fuel December, 2013, accepted May, 2014) Numerical investigation of the burning characteristics of ventilation air methane in a combustion based mitigation system.
43. Daniel L. Cluff, Concepts in Coalmine Ventilation; Development of the VamTurBurner© for Extraction of thermal Energy from Underground Ventilation Air Methane, PhD thesis, University of Exeter, 2014

FIGURES

Figure 2. Adapted from Globalwarmingart website: www.globalwarmingart.com/wiki/File:Greenhouse_Gas_by_Sector_png
Table 1. (2000–2006). Adapted from IEA CCC 2005, M2M 2006 and US EPA.
Table 2. (1990–2009). U.S emissions inventory.
Figure 3. (2011). Adapted from Adapted from U.S energy information administration, international energy statistics, 2000–2010. Retrieved from EIA website: www.eia.gov/todayinenergy/detail.cfm?id=3350
Figure 4. (2011). Adapted from U.S energy information administration, international energy statistics, 2000-2010. Retieved from website: www.eia.gov/todayinenergy/detail.cfm?id=3350
Figure 5. Recoverable energy after reaction sustenance D.L Cluff (2012)
Figure 6. The VamTurBurner©, a multi-generation system for the mitigation of VAM D.L Cluff (2013)
Figure – 7(a, b, c) shows the ignition of methane in a co-flow stream of an igniter flame and a ventilation flow containing 0.5% at 500K, 1% at 500K and 1% at 400K respectively (Martinez, Cluff, & Jiang, 2014).
Figure 8 – Simulation of the flow from a gas turbine interacting with a typical VAM flow. The flow of the VAM is 2 m/s at 300 K and the flow of the exhaust gas from the GT is 50 m/s at 700 K. Flow trajectories display the temperature as well as the vorticity. The temperature profiles are fixed on a plane. The temperature scale, blue to red for this diagram, is 300–500 K (D.L. Cluff 2013).
Figure 9 – Flow trajectories and temperature distribution of the preheating section of the VamTurBurner© (D.L Cluff, 2014).

Prototype development of the VamTurBurner© design concept.

A field trial based on the initial VamTurBurner© concept was formulated and carried out at the Holman's Test mine, a research facility operated by the Camborne School of Mines. A laboratory scale gas turbine engine, the AMT Netherlands Mercury HP Gas Turbine, was use as the main component.

This engine is a single radial compressor axial flow turbine designed, which provides excellent performance and power to weight ratio. The low mass of the axial turbine wheel allows the turbojet to ramp up to full 151,900 RPM in 4 seconds and back down idle 47,600 RPM in 3 seconds. The annular combustion chamber is fitted with a unique low-pressure fuel system; the Engine Control Unit (ECU) regulates the maximum performance with fully automatic proprietary software. The maximum thrust this engine produces is 88N

Parameter	E-start		Air-start
Diameter	100 mm		100 mm
Length	292 mm		220 mm
Turbine weight	1550 gram		1400 gram
System weight *	2235 gram		2005 gram
Thrust @ max. rpm	88 N		88 N
Thrust @ min. rpm	4 N		4 N
Maximum RPM	151,900		151,900
Idle RPM	47,600	47,600	
Pressure ratio max. rpm	2.8 :1		2.8 :1
Mass flow max. rpm gr/sec.	250 gr/sec.		250
Normal EGT	650 C		650 C
Maximum	EGT 750 C		750 C
Fuel rate max. rpm gr/min.	295 gr/min.		295
Fuel JP-4/petroleum/Jet A1			

Figure 1 AMT Mercury Gas Turbine

Figure 2 Operating system for the gas turbine, fuel pump, gas solenoid, fuel solenoid, Servo Control Board and Engine Control Unit.

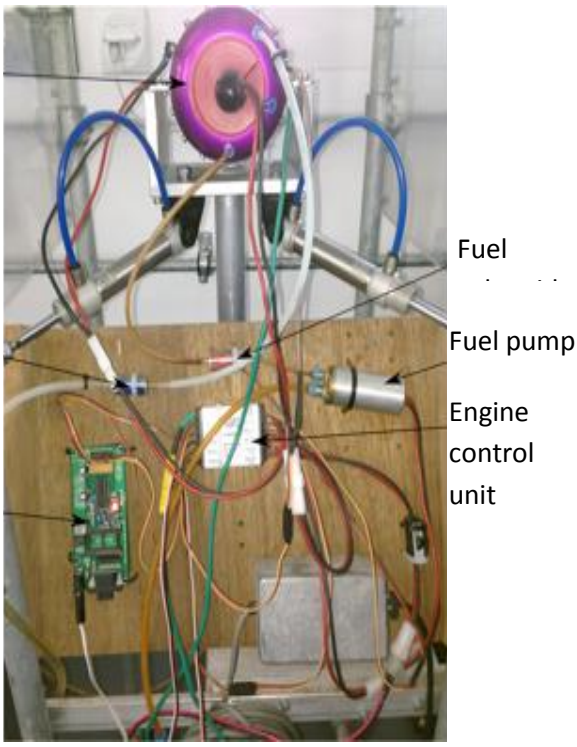

Figure 5 Control panel components

Figure 3 Tecpel digital anemometer - AVM-702

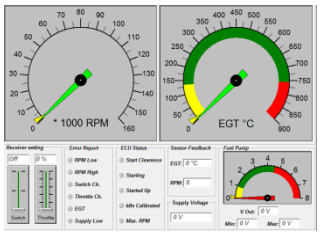

Figure 4 Gas Turbine control software

Figure 6 Ducting with gas turbine setup at test mine

The gas turbine system uses a standard RS232 connector, which was converted to USB to allow the use of newer computers. The connection to the ECU is through the TMC software with a servo control driver board required to operate the servos, a 1-904 Servo 8 driver board manufactured by Milford Instruments Ltd. Was found to be suitable for this purpose. Once the telemetry set up procedure has been carried out the engine is run by the speed bar, which is initially slid to the mid position, this governs at what speed the servos operate and mid position was found to the most effective during the start-up procedure. The “Switch” servo is slid fully to the left and when the counter registers zero the slider is then moved fully to the right and the starting sequence

initiates. Indication of the correct starting sequence is given by a series of five beeps from the engine and on the terminal display the ECU status moves from Start Clearance to Starting. The home button is used for a failed start to return the engine to its safe shut down settings.

Each test run followed the following sequence:

1. On moving the servo drive board controller 'switch' full over to the right the switch display on the terminal tab on the telemetry display moved from "Off" to mid-way then "On". At this point the engine gives 5 sharp beeps indicating it's about to start.
2. Power is drawn to the starter motor and the intake impeller winds up.
3. The gas solenoid open and starter gas is released into the combustion chamber where the glow plug is now hot enough to ignite the gas.
4. Once the impeller attains 14,000 RPM and the EGT (Exhaust Gas Temperature) exceeds138^{o}C the ECU opens the fuel solenoid valve and starts the fuel pump.
5. At this stage on each run the RPM climbs to 18,500 and remains there, with fuel still entering the combustion chamber the EGT rapidly climbs.
6. The test run is aborted, by activating the "Home'' button on the drive board controller display, as the EGT reaches 600$_{0}$C, to stop the engine from overheating.
7. The engine then performs a controlled shut down.

Figure 7 The exhaust gas was directed through the side of the vent chamber to allow for the input of the simulated ventilation air and preheating system to be attached from the end. The two gas flows merge prior to interaction with the igniters.

According to AMT Netherlands the exit velocity of the hot exhaust gasses at max RPM is approximately 350 m/s, which is a sufficient exit velocity to cause turbulent mixing of the co-flows. The mixing is further improved by a Tee-junction dead end in the connecting pipework and a baffle box was designed to fit in the ducting at the entry point of the hot gasses.

Figure 8 View of the hot exhaust gas inlet and the baffling act as diffusers to promote turbulent mixing

Figure 9 The preheating was simulated by an industrial heater (The Master BV 170 E Indirect Heater), which can be seen connected to the simulated mine ventilation tubing in Fig. 7.

Once The Master BV 170 E Indirect Heater was fitted and running the Tecpel Digital Anemometer - AVM-702 was used to ascertain the air speed down the ducting. The average air speed of 3 m/s gives a flow rate of 0.306 m^3/s, the manufactures output flow rate of 1,800 m^3/hr equates to 0.5 m^3/s.

Temperature measurements were taken with a wireless system, which allows the logging system to be placed further away from the heat sources without the complications of wires. The Wireless Thermocouple Connector Series features stand-alone, compact, battery powered wireless connectors that transmit their readings back to a host receiver up to a distance of 90m. The thermocouple units feature a programmable set of calibrations for J, K, T, E, R, S, B, N or C type thermocouples. Once remotely activated the wireless unit will transmit readings continuously at a pre-set time interval from seconds to hours depending on that decided on by the operator. The transmitted data includes the temperature at the thermocouple, ambient temperature, RF signal strength and battery condition to the host and are all displayed on the PC screen in real time. When used with host receiver UWTC- REC1 data from up to 48 wireless connectors can be received and displayed. The data logger readings can be saved and later printed or exported to a spreadsheet file.

Figure 10 Wireless transmitters and receivers from OMEGA

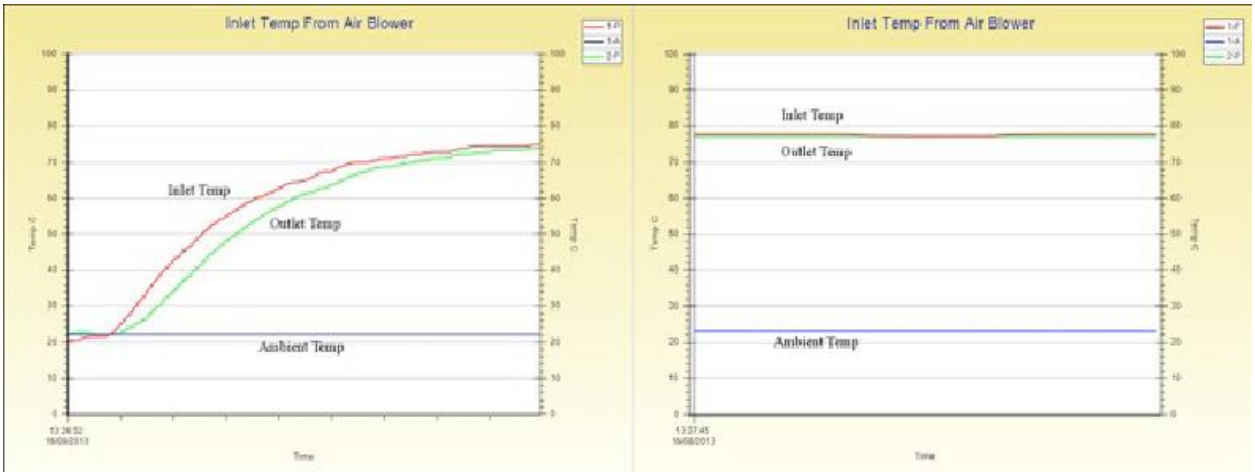

Figure 11 Temperature measurements from the inlet and outlet of the Master BV 170 E Indirect Heater, left shows the ramp up and right shows the steady state.

The igniters were simulated using a simple method that would provide an even distribution of heat across the ducting to ensure the methane flow would encounter the igniters. The Paella Company UK, retails Garcima paella gas burners of various diameters for use in outdoor cooking. Their range includes a 300 mm diameter burner, which compares favourably with the 36 cm ducting being used for the project to give an even flame distribution of heat across the ducting.

Figure 12 Left, the gas supply, center the Garcima paella gas burner used to simulate the igniters and right the burner fitted into the ventilation tube.

The burner test was performed by using an entry port in the side of the tubing, covered with aluminium tape, to access the burner for ignition with a long wick inserted through the port through a hole in the aluminum tape. A pitot tube stand was placed in the flow region and also serves to hold the thermocouple to record the temperature from the burner. The gas bottle was attached and removed to a safe distance of 2.5 m protected behind a sturdy container.

Figure 13 Burner gas supply left and ignited burner right.

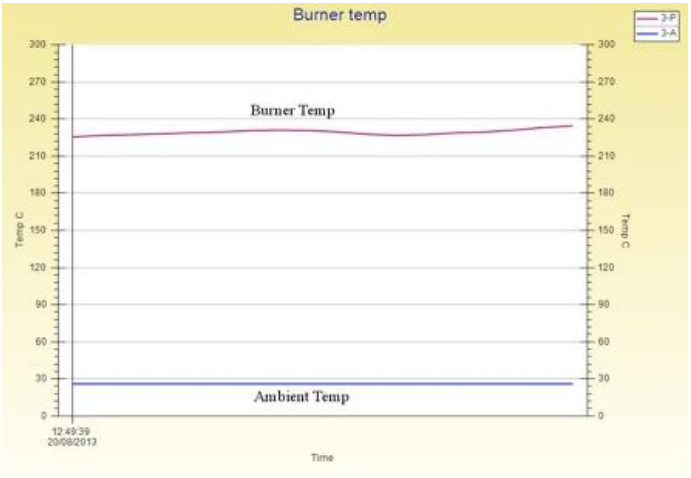

Figure 14 The burner gas flow temperature increase compared to ambient temperature of the air supplied to the burner

The steady state burner temperature of about 220 ^{o}C (493 K) is consistent with the modeling of the system parameter for preheating using the Large Eddy Simulation method, which showed that a preheating temperature of about 500 K for AM concentrations of 0.5% and higher.

Figure 15 Final experimental setup for the VamTurBurner© prototype test, upper, set up of all equipment, lower, aerial view of risk assessment.

During a full test the operations bench has been withdrawn to over 2.5 m from the exhaust of the gas turbine, this is over the recommended safe distance of 1 m stipulated by AMT Netherlands, to further reduce the risk to the operator and assistant in the event of any incident. During any test the assistant will act as a fire safety rating and attire in the appropriate PPE (hard hat, overalls, steel toe caped boots, gloves, eye and ear protection) with a foam fire extinguisher readily at hand. The operator will be required to wear protective footwear and eye and ear protection.

The test build being assembled and safety tested appears to be functional and consistent with the VamTurBurner© design concept.

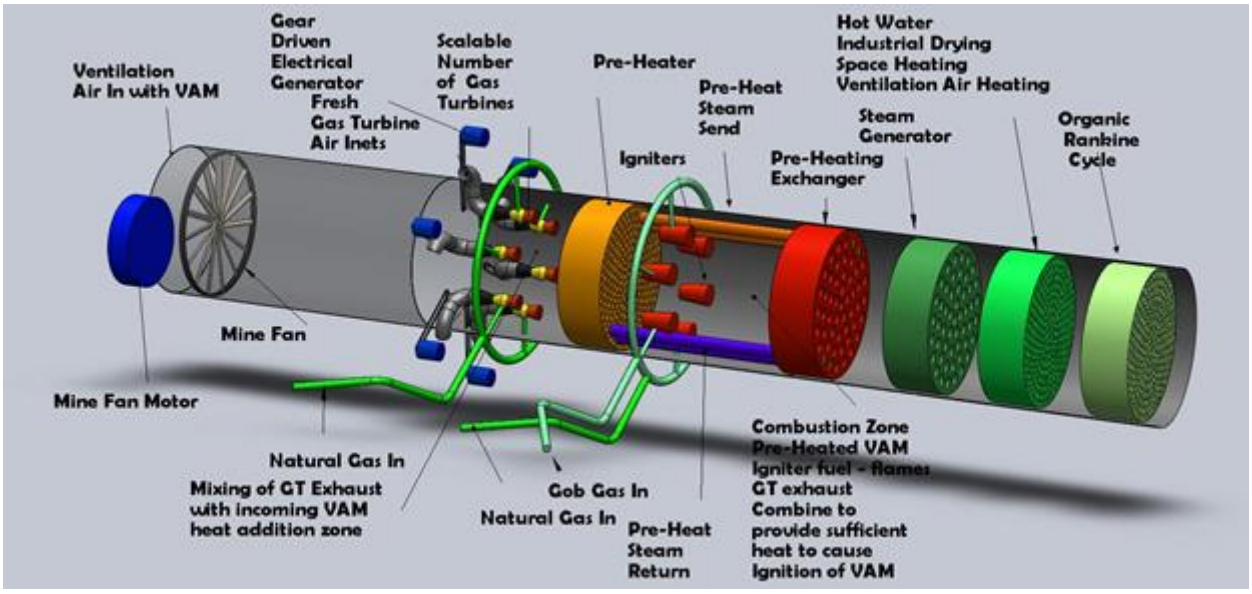

Figure 16 VamTurBurner(C) design concept, (D. L. Cluff 2013)

Although considerable effort to assemble an operational system was spent, the gas turbine failed at the most inopportune time, which prevented further testing within the timeframe of the project. Nonetheless, valuable design data has been obtained from the prototype process. The scale of the operation allowed for rapid prototyping; thus, continued research will not be an onerous task should the funding for new gas turbine equipment or a cogeneration plant come available. The measurement of temperatures and flow rate methodology is established and found to be robust. Equipment such as the temperature logging, thermocouples, ventilation tubing and software remain available. The construction methods are sound and rapid so provide a suitable template for further design builds.

A list of recommendations based on the prototype experience gained in these trials is provided below for the improvement of any future undertaking of this project given an appropriate budget.

.

RECOMMENDATIONS

1. **Ducting:** The 36 cm diameter ducting was adequate but a larger diameter +50 cm would be more representative of the scale between the volume of exhaust gasses and the VAM. This would also enable a larger air flow at a more representative flow rate to that of a mine exhaust ventilation system.
2. **Fan System:** The indirect heater fan used in this project provided a sufficient volume of air for the size of ventilation ducting; however, there are available purpose built ventilation fans, of various diameters, designed specifically as ventilation fans that would be a better option should the size of the system be increased.
3. **Baffling:** Numerical modeling has shown that a simple diffusion disc is sufficient for the creation of turbulent mixing of the co-flows.
4. **Burner Section:** It was proved in this project that commercially available gas cooking equipment is inadequate for the task. A series of remote blow torch type burners arrayed radially or possibly linearly in the burner section would ensure flaming of the VAM mixture with sufficient heat.
5. **Anemometers:** No instrumentation was available to measure the velocities or volumes of the hot section following the igniters (>2000 K) of this project. In a more comprehensive test, these measurements would be required if varying the output of the gas turbine and to confirm combustion.
6. **Exhaust gas analysis:** Exhaust gas analysis equipment to measure the CO_2 levels should also be used to characterize the VAM to confirm that it was oxidised by determining if the appropriate rise in CO_2 levels expected is attained.
7. **Gas Flow Meters:** In a more comprehensive study the amount of gasses being used in the burner section would enable further studies into how much energy is being added to the system to obtain a result.
8. **Insulation:** It became apparent on build that a certain amount of insulation would aid the project and protect equipment and personnel, unfortunately it did not get that far. If appropriate insulation (Mineral Wool, Ceramic fiber, Annex H), was used heat losses around the mixing and burner sections would be reduced and protect the instrumentation, personnel post run, the work bench and securing equipment.
9. **Securing Equipment:** Cable or chain securing straps to be used for ducting and a more permanent method for securing the gas turbine gas transfer pipework.
10. **Location:** For this type of project, the location was ideal.